ACTA TECHNICA

ACADEMIAE SCIENTIARUM HUNGARICAE

EDITOR-IN-CHIEF: P. MICHELBERGER

VOLUME 103
NUMBER 1

MATERIAL SCIENCES AND TECHNOLOGY–T/2

AKADÉMIAI KIADÓ, BUDAPEST 1990

ACTA TECHNICA

A JOURNAL OF THE HUNGARIAN ACADEMY OF SCIENCES

CENTRAL EDITORIAL BOARD

T. CZIBERE, K. GÉHER, L. KOLLÁR, P. MICHELBERGER (EDITOR-IN-CHIEF),
A. LÉVAI, J. PROHÁSZKA, K. REMÉNYI, J. SZABÓ,
GY. CZEGLÉDI (MANAGING EDITOR)

EDITORIAL COMMITTEE FOR MATERIAL SCIENCES AND TECHNOLOGY (SERIES T.)

M. HORVÁTH, Z. HORVÁTH,
J. PROHÁSZKA (CHAIRMAN), J. TALABÉR

Acta Technica publishes original papers, preliminary reports and reviews in English, which contribute to the advancement of engineering sciences.
Acta Technica is published by

AKADÉMIAI KIADÓ
Publishing House of the Hungarian Academy of Sciences
H-1117 Budapest, Prielle K. u. 19—35.

Subscription information

Orders should be addressed to

KULTURA Foreign Trading Company
H-1389 Budapest P.O. Box 149

or to its representatives abroad

Acta Technica is abstracted/indexed in Applied Mechanics Reviews, Current Contents–Engineering, Technology and Applied Sciences, GeoRef Information System, Science Abstracts.

© *Akadémiai Kiadó, Budapest*

ACTA TECHNICA

Volume 103 Nos 1-4

CONTENTS

Bakondi, K. - Buza, G.: Surface finish by means of high-power laser 15

Berke, P. - Galambosi, F.: Effect of rapid heat treatment on fatique 27

Bertóti, E.: Investigation of thick cylindrical shells under axisymmetric loads by asymptotic integration of the dual system of equations 61

Besze, J. - Mrs. Sándor, Gy.: Coupling elements of audio-frequency central control systems 225

Ecsedi, I.: Bounds for the deflection of beams of variable cross-section 91

Hegedűs, I.: Analytical solutions for discrete boundary value problems of macroscopically isotropical Hrennikoff-type grids 103

Jankó, L. - Nagy, Z.: The influence of the displacement spring rigidity on the critical load of bars 115

Káldor, M. - Mrs. Tranta, F.: Evaluation of the results of transformation measurements. 49

Keshava Murthy, K. - Jayaram, M.: A new investigation on parabolic weirs - proportional parabolic weirs 143

Kollár, L.P.: Buckling of generally anisotropic (aeolotropic) shallow shells 171

Kollár, P.W.: Determination of the erection shape for a single-mast rotationally symmetrical cable net in case of a specific variation of the tensile force 191

Michelberger, P.: J. Prohászka of seventy 7

Paláncz, B.: Simulation of power plant circuits and equipment state estimation I. - Simulation 249

Paláncz, B.. Simulation of power plant circuits and equipment state estimation II. - State estimation 263

Reményi, K.: Development of fluidized-bed firing technology in the Institute for Electric Power Research 279

Sharaf, A.: New aspects of drip irrigation hydraulics 203

Somosi, I. - Vitéz, J.: Dissolution of aluminium in gallium 33

Szergényi, I.: The bases of the prognosis of energy demand within the renewing Hungarian economy in the mirror of the 14th Energy World Congress 299

Tersztyánszky, T.: Probability distribution of random load of electric power system inter-ties 319

BOOK REVIEW

Frigyes, I. - Szabó, Z. - Várnyai, P.: Digital microwave transmission (Berczeli, T.) ... 329

CONTENTS

J. Prohászka of seventy 7

Bakondi, K. - Buza, G.: Surface finish by means of high-power laser 15

Berke, P. - Galambosi, F.: Effect of rapid heat treatment on fatigue 27

Somosi, I. - Vitéz, J.: Dissolution of aluminium in gallium 33

Mrs. Iranta, F. - Káldor, M.: Evaluation of the results of transformation measurements. 49

PRINTED IN HUNGARY

Akadémiai Kiadó és Nyomda Vállalat, Budapest

ACTA TECHNICA

ACADEMIAE SCIENTIARUM HUNGARICAE

EDITOR-IN-CHIEF: P. MICHELBERGER

VOLUME 103
NUMBERS 1—4

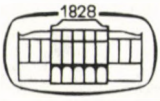

AKADÉMIAI KIADÓ, BUDAPEST 1990

Dedicated

to

Professor

János PROHÁSZKA

on his

70th birthday

Prof. Prohászka, János

Acta Technica Acad.Sci.Hung., 103(1), pp. 7-14 (1990)

J. PROHÁSZKA OF SEVENTY

MICHELBERGER, P.*

János Prohászka, member of the editorial board of our periodical, general editor of the technological series, has turned 70 in 1990. This special edition is intended to direct the readers' attention to the scientific achievement of János Prohászka, to the school based on his work, first of all because, in our view, his special line - research in material science - is one of the most important factors of the economic development of our time.

János Prohászka was born in Budapest, 1920. He graduated as a mechanical engineer at the Technical University of Budapest in 1950. He added theoretical studies to the earlier industrial experience when he was lecturer teaching mechanics and mathematics at the Economical and Technical Academy, an institution to stop the temporary gap in the education of engineers, for a year.

In 1953, he joined the research staff of Professor László Gillemot in the Research Institute of Iron Industry. The field of his research activities included investigation of the effect Ti as an alloying element on the cementation of steels as well as on the diffusion rate of C in low-carbon steels. He had written a thesis on the results of his research work and became candidate for Ph.D. in technical sciences in 1957.

From the year 1954 on, János Prohászka investigated the changes in the mechanical properties of tungsten at high temperatures, and the conditions of recrystallization of tungsten, first in the Research Institute of Telecommunication, a division of TUNGSRAM Corporation and then after 1957, in the Research Institute of Applied Physics of the Hungarian Academy of Sciences, founded in the same year.

*Michelberger, Pál, H-1111 Budapest, Egry J. u. 19-21, Hungary

Akadémiai Kiadó, Budapest

Prohászka's research work has been focussed on the relationship between the structure and macroproperties of metals and alloys (first of all steels) to discover, understand and define these properties and then to take this knowledge as a basis for the development of technological processes - heat treatment and plastic deformation - permitting the structure of metals to be changed either locally or globally as required.

János Prohászka was appointed professor of the Department of Materials Engineering in Electrical Industry, Technical University of Budapest, in 1964. In 1967, he became professor and head of department. The Institute of Mechanical Technology and Materials Science was organized at BME in 1972. Professor Prohászka was deputy director then, between 1977 and 1985, director of the Institute.

In 1966-1967, Professor Prohászka spent two semesters at Harvard, USA. During this period, he continued research and as a result, he developed (and patented) a high-speed annealing process for the heat treatment of low-carbon nonalloy steels with a view to improve not only the properties of HSLA and dual-phase steels but also the thermal efficiency (above 90%) of steelmaking without the use of expensive alloying elements.

Professor Prohászka's achievement in the field of research, education and school founding has been appreciated both in the country and internationally. He was the first in Hungary to write an up-to-date scientifically established textbook on physical metal science published in Hungarian language which had been written at that time for postgraduate students but it has become part of the regular educational program for the students of mechanical and electric engineering. This book is a summary of Professor Prohászka's ideas and philosophy.

In addition to orders awarded by the government, János Prohászka got President's reward from the Hungarian Academy of Sciences in 1962. In 1970, he became corresponding member while in 1982, regular member of the Hungarian Academy of Sciences. Throughout two terms, he was member of the presidium of the Academy. He was member, executive or head of Academy and engineers' committees of quite a number. At present, he is deputy president of the Department of Technical Sciences of the Hungarian Academy of Sciences, co-president of the Committee of Materials Science and Technology and president of the Technology of the Scientific Association of Mechanical Engineering.

As a result of his international reputation, he had been included among the members of CIRP in 1984 and awarded Rockwell Prize by the Inter-

national Technological Institute in 1986. As a State Prize winner in 1988, he was rewarded for his life's work.

However, greatest regard and respect for Professor Prohászka have come, and are still coming, from his students and collagues, many of them being candidates for Ph.D. or holders of Ph.D. His scientific achievement is multiplied in the students' and colleagues' activities still controlled by the advices and critiques of Professor Prohászka. We wish Professor Prohászka long years in good health and stamina to continue his work successfully for the sake of progress in the technical world.

LIST OF PROHÁSZKA PUBLICATIONS

1. Prohászka, J.: Diffusion in foundry practice (in Hungarian), Kohászati Lapok, 1954
2. Effect of titanium content of iron on the diffusion rate of carbon and cementation of steel (in Hungarian), Thesis (candidate for Ph.D.), 1956
3. Millner, T. - Prohászka, J. - Horváth, A.: Der Einfluss von Fremdsubstanzspuren auf die sekundäre Rekristallisation von Wolframdrähten, Acta Technica, Tom. XVIII. (1957), 289
4. Millner, T. - Bartha, L. - Prohászka, J.: Autoradiographische Untersuchungen über die Ortsänderung von Verunreinigungen während des Rekristallisationsvorganges, Zeitscrift für Metallkunde (BRD) 11. (1960), 639
5. Prohászka, J. - Horváth, A. - Millner, T.: Über die Wachstumgeschwindigkeit der Kristallite während der sekundären Rekristallisation von Wolframdrähten, Festkörperphysik, Akademie-Verlag, Berlin (DDR), 1961
6. Millner, T. - Prohászka, J. - Neugebauer, J.: Über den sekundären Rekristallisationsvorgang vom mit Zusatzstoffen bereiteten Wolframdrähten, Festkörperphysik, Akademie-Verlag, Berlin (DDR), 1961
7. Bartha, L. - Prohászka, J. - Millner, T.: Autoradiographische Untersuchungen über die Besiegungsart geringer Fremdsubstanzen während der sekundären Rektistallisation von Metallen, Festkörperphysik, Akademie-Verlag, Berlin (DDR), 1961
8. Millner, T. - Prohászka, J. - Bartha, L.: Autoradiographische Untersuchungen über die örtliche Verteilung von Silber in Zinn bei weit unterhalb der Löslichkeitsgrenze liegenden Ag-Konzentrationen, Chemie-Ing-Technik (BRD) 33. 1961, 224
9. Prohászka, J.: Change of the coefficient of thermal expansion of cold-formed metals in the course of annealing (in Hungarian), Kohászati Lapok, 1962. 6, 248
10. Bartha, L. - Millner, T. - Prohászka, J.: Autoradiographic testing of the changes in position of impurities in the course of recrystallization. (In Hungarian), Published by the Special Committee of Isotope Applications of the National Nuclear Energy Board. 3, 1962. I/1, I/1 IIr. 1-8
11. Prohászka, J.: Anderungen des Wärmeausdehnungskoeffizienten von kaltverformten Metallen im Verlauf des Weichglühens, Acta Technica, Tom. XXXIX. (1962). 349
12. Prohászka, J. - Wadewitz, H.: Zum Gelitsystem von Wolfram, Reinstoffe in Wissenschaft und Technik, Akademie-Verlag, Berlin (DDR), 1963
13. Millner, T. - Bartha, L. - Prohászka, J.: Untersuchungen über Wanderung kleiner Silbermengen in reinem Zinn bei Verwendung von radioaktiven Silber, Zeitschrift für Metallkunde (BRD), 54. (1963), 17

14. Prohászka, J.: Über einen Mechanismus der Versetzungsbildung während der dendritischen Kristallisation, Acta Metallurgica (USA), Vol. 11, (1963), 125

15. Gillemot, L. - Prohászka, J. - Kator, L.: Addendum to Textbook "Metallography and Materials Testing", Tankönyvkiadó, Budapest 1963. J4-366

16. Prohászka, J.: Dislocations in the course of dendritic crystallization (in Hungarian), Thesis for D.Sc. degree, Budapest, 1963

17. Prohászka, J.: Reply to comment by Hamilton on the origin of dislocations in dendrites, Acta Metallurgica (USA) 12. (1964), 11094

18. Prohászka, J.: Material Structure Theory (in Hungarian), Institute of Postgraduate Education for Engineers, Budapest, 1964 (p. 340)

19. Prohászka, J. - Tóth, Gy.: High-temperature techniques in precision mechanics (In Hungarian), Textbook, 1966, (p. 230)

20. Prohászka, J. - Ashby, M.F.: An experiment to determine the nature of work hardening in dispersion-hardened alloys, Research Report, Harward University (USA),1966

21. Prohászka, J.: Relationship between plastic strain of metals and real crystal structure (In Hungarian), Published by the Scientific Association of Mechanical Engineering (GTE), 2nd International Conference on Cold Forming, 1967

22. Prohászka, J. - Kovács, Á. - Ágoston, A.: Cold Forming, Textbook, 1968, (p. 223)

23. Prohászka, J.: Plastic stability during tensile test, Submitted for publication to the Academy of Sciences of the Soviet Union (Dokladi, A.N.), January 28, 1969

24. Prohászka, J. - Tóth, I.: Brittle fracture in alnico-type cast hard magnets having body centred cubic crystal structure, Acta Technica, Tom 64 (3-4) 443, (1969)

25. Prohászka, J.: Solution of problems in relation to stereographic projection of cubic crystals without plotting (in Hungarian), Bányászati és Kohászati Lapok - KOHÁSZAT, Vol. 103 (1970), No. 2

26. Prohászka, J.: Hrupkosty magnetich materialo tipa alnico, Metallowedenie, Isdatjeljstvo Nauka, Moscow, 1971

27. Prohászka, J.: Expectable development of the mechanical properties of metallic structural materials under medium temperature load (in Hungarian), Inaugural address, Hungarian Academy of Sciences, November 11, 1970. Published in Magyar Tudomány, 44, (1971)

28. (Expectable trends of development of solid state physics) Expectable development of the mechanical properties of metals (in Hungarian), Hungarian Journal of Physics (Magyar Fizikai Folyóirat), Vol. XIX, No. 5, Akadémiai Kiadó, Budapest, 1971

29. Prohászka, J.: Possible methods to increase strength and limits of the methods as reflected by up-to-date research in the field of metallurgy (in Hungarian), Bányászati és Kohászati Lapok - KOHÁSZAT, Vol. 105, No. 5, 1972.

30. Prohászka, J.: Determination of stereographic pole diagrams of hexagonal crystals without plotting (in Hungarian), Bányászati és Kohászati Lapok - KOHÁSZAT, Vol. 105, No. 2, 1972

31. Prohászka, J.: Structure of metals (in Hungarian), Természet Világa, Budapest, 1972

32. Prohászka, J.: Extension of heat treatment possibilities for steel by setting metastable states, International Conference on the Heat Treatment of Steels, Torino, 1972

33. Prohászka, J.: Determining orientations in metals of hexagonal crystal structure by etch pit figures, Periodica Polytechnica, Vol. 16, No. 2, Budapest, 1972

34. Prohászka, J. - Müller, L.: Schnellausglühen von Aluminium, Periodica Polytechnica, Vol. 15, No. 2, Budapest, 1972, 219-231

35. Prohászka, J.: Determining of the stereographic pole figures of hexagonal crystals without plotting, Acta Technica, Tom. 73(3-4), 279-291, (1972)

36. Prohászka, J. - Bánki, T.: Über den Einfluss der Värmungsgeschwindigkeit auf die Sprödbruchtemperature von Wolframdrähten, (Eingegangen am 1. April 1966). Offprint from TUNGSRAM Scientific Publications, No.23, September 1973

37. Prohászka, J.: Nuove possibilità nel campo dei trattamenti termici degli acciai per mezzo del controllo dello stato metastabile, Notiziario Tecnico Amma, No. 7-8, 1973

38. Prohászka, J.: Problems of increasing yield stress of metals and alloys used in engineering industries, ECE adhoc Meeting of Experts on Engineering Industries Symposium on Application of Metal and Non-Metal Materials in Engineering, Varna, 28 May - 2 June 1973, 1-14

39. Prohászka, J.: A general problem of metal research, Acta Technica, Tom. 75(1-4), 321-330, (1973)

40. Prohászka, J. and Department Team: Material technology (textbook), (In Hungarian), Egyetemi Tankönyvkiadó, Budapest, 1974 (p. 1-498)

41. Tassy-Betz, Eva - Prohászka, J.: A general method of determining orientation in the cubic crystal system on the basis of geometrical evaluation of etch figures, American Elsevier Publishing Company, Inc. 1974, Metallography, 189-226, (1974)

42. Prohászka, J. - Hidasi, B. - Varga, L.: Stress reduction without heat treatment (in Hungarian), Bányászati és Kohászati Lapok - KOHÁSZAT, Vol. 107, No. 9, 1974, 363-367

43. Prohászka, J.: New method of heat treatment of cold rolled and drawn products (in Hungarian), Bányászati és Kohászati Lapok - KOHÁSZAT, Vol. 108, No. 2, 1975, 61-67

44. Prohászka, J. - Hidasi, B. - Varga, L.: Vibration-induced internal stress relief, Periodica Polytechnica, Vol. 19, No. 1, 1975, 69-78

45. Prohászka, J. - Tassy-Betz, Eva: General metallographical method to determine the orientation of cubis crystals (in Hungarian), Műszaki Tudomány, 1976, 79-92

46. Verő, J. - Prohászka, J.: State diagrams of two-component alloys (in Hungarian), Műszaki Tudomány, 1976, 1-25

47. Prohászka, J.: On thermodynamic causes of the variation in the results of materials testing (in Hungarian), 9th Materials Testing Days, Balatonaliga (Hungary), May 2-5, 1977 (published among abstracts)

48. Prohászka, J.: Theoretische und praktische Probleme der Beschleunigung von Wärmebehandlungsprozessen, Neue Nütte, June 1977

49. Prohászka, J.: Life and career of László Gillemot (in Hungarian), Műszaki Tudomány, 1977, 283-292

50. Prohászka, J.: Reflections on technology (in Hungarian), Természet Világa, No. 8, 1978, 341-345

51. Prohászka, J.: Prof. Dr. László Gillemot. Periodica Polytechnica, Vol. 22, No. 1, 1987

52. Tardy, P. - Verő, B. - Prohászka, J.: Untersuchung des Korngefüges von Metallen mit kfz. Gitter unter dem Emissionselektronenmikroskop, Neue Hütte, Vol. 23, No. 8, August 1978, 303-308

53. Prohászka, J.: Importance of technology (in Hungarian), Kohászat, Vol. 111, No. 11, 1978

54. Prohászka, J.: Crystallographic calculations in metallurgy (in Hungarian), KOHÁSZAT, Vol. 111, No. 12, 1978

55. Prohászka, J. - Ginsztler, J. - Gangli, P. - Komáromi, M.: Tochnost Opredelesia raspredelenia temperatury na obrazcah pri termicheskoe ustalosty, Fizika i himia obrabotki materialov 6. 1978. 16-20

56. Prohászka, J. - Müller, L.: Some theoretical and technological problems of high-speed heat treatment (in Hungarian), Műszaki Tudomány, 55. 1978. 1-17

57. Prohászka, J.: Scientific basis of improvement of the quality of castings (in Hungarian), Műszaki Tudomány, 56. 1978. 412-430.

58. Prohászka, J.: Materials science, technology, properties (in Hungarian), Műszaki Tudomány, 56. 1978. 270-293

59. Prohászka, J. - Gangli, P. - Komáromi, M.: Wärmeverteilung in schnellerwärmten Stangen mit konstantem Querschnitt, Neue Hütte, No. 1, 1979

60. Prohászka, J.: Some problems of metallic materials for toolmaking (in Hungarian), Gép, Vol. XXXI, 1979. 1

61. Prohászka, J.: Technology: definitions and classification (in Hungarian), Gépgyártástechnológia, No. 6, 1979

62. Prohászka, J. - Berzy, J. - Dévényi, L. - Müller, L. - Szalai, I.: Erfahrungen mit der Schnellwärmebehandlung doppelgeschichteter (Cu-FeNi42) Metalle, 7th International Conference on Metallurgy and Heat Treatment, Bucharest, 24-26 September, 1979

63. Prohászka, J. - Varga, L.: The Effect of the Rapid Heat Treatment on the Strain Aging Behaviour of Unkilled Deep-drawing Steel by Means of Artificial Aging, 7th International Conference on Metallurgy and Heat Treatment, Bucharest, 24-26 September, 1979

64. Prohászka, J.: Characteristic features of technology and its relation to other sciences (in Hungarian), Műszaki Tudomány, 57, 1979

65. Prohászka, J.: Fulfilment of the plan - economy - technology (in Hungarian), Magyar Tudomány, No. 7-8, 1981. 558-564

66. Prohászka, J. - Varga, F.: Scientific basis of improvement of the quality of castings (in Hungarian), Part I, Part II, Bányászati és Kohászati Lapok - ÖNTÖDE, Vol. 32, No. 5, 1981

67. Prohászka, J. - Ginsztler, J.: Nianie formy obrazca na lokalizacie razrussnia lociklovom nagruzenie, VI. Mezdunarodny Kollokvium Mechanicheskova Ustalost Metallov, June 8-13. 1981. Kiew, Izd. Naukova Dumka, 12-13

68. Abd Elhady, M.A. - Prohászka, J.: Effect of rapid heat treatment on the microstructure and tensile properties of cold drawn boron-treated steel (ZF), Acta Technica, Budapest, 92, 1981. 23-32.

69. Prohászka, J.: Metallurgy with plasma (in Hungarian), Természet Világa, Vol. 112, No. 11, 1981. 482-485

70. Prohászka, J. - Ginsztler, J.: Some characteristics of low-cycle fatigue process. 8th Conference on Materials Testing, Budapest, 28 September - 1 October, 1982. MTESZ publications, Vol. I. 239-243

71. Prohászka, J. - Varga, F.: Wissenschaftliche Grundlagen der Güteverbesserung der Gussstücke und Entwicklungscrichtungen der hochfesten Gusslegierungen, 49th International Conference on Foundry Practice, Chicago, 14-17 April, 1988. 1-11

72. Prohászka, J.: On the fracture of Fe-Si single crystals, Akadémiai Kiadó, 1982

73. Prohászka, J.: New developments in rapid heat treatment of steel, 2nd International Congress on Heat Treatment of Materials of IFHT, Florence, Italy, 20-24 September, 1982, 791

74. Prohászka, J.: Reflections on graphite crystallization (in Hungarian), Bányászati és Kohászati Lapok - ÖNTÖDE - Vol. 34 (116), No. 3, March 1983

75. Prohászka, J.: The Relationship between the Strain-Hardening Coefficient and Machinability, Annuals of the CIRP, Vol. 32, No. 1, 1983. 105-107

76. Prohászka, J.: Die Rolle der Technologie in der wissenschaftlich-technischen Revolution, Academy of Sciences of DDR For Theorie, History and Organisation of Science, Socialism and Scientific-technical Revolution. Part I, 1983. 232-238

77. Prohászka, J. - Répási, G.: Possibilities to increase the strength of low-carbon steels (in Hung.), Technical-economic Publications of DUNAI VASMŰ (DUNA IRON WORKS), No. 4, 1983. 1-10

78. Prohászka, J.: Thermodynamic Instability of Solid Bodies, Periodica Polytechnica, 1983. 325-329

79. Prohászka, J.: Material quality and thermodynamic instability (in Hung.), Bányászati és Kohászati Lapok, Vol. 117, No. 4, April 1984. 145-153

80. Prohászka, J.: Relationship between a strain-hardening coefficient and machinability (in Hung.), GÉP, Vol. XXXVI, No. 5, May 1984. 175-178

81. Prohászka, J.: Studies, remembrance, Inaugural address, Hungarian Academy of Sciences, April 20, 1983. Material quality and thermodynamic instability, Akadémiai Kiadó, Budapest, 1984

82. Prohászka, J. - Baranyi, Z.: Diffusion processes in fire aluminizing accompanied with phase transformation (in Hung.), Bányászati és Kohászati Lapok - KOHÁSZAT, Vol. 117, No. 6, 1984. 256-261

83. Prohászka, J.: Importance of technology. PÁRTÉLET, Vol. XXIX, No. 7. 24-28

84. Prohászka, J.: Role of plastic forming in increase of the strength or rolled stock (in Hung.), Bányászati és Kohászati Lapok - KOHÁSZAT, Vol. 118, No. 2, 1985. 49-55

85. Prohászka, J. - Mrs. Kristyák-Maróti, G.: Dual-phase (DP) steels: structure, properties and technology (in Hungarian), Bányászati és Kohászati Lapok - KOHÁSZAT, Vol. 118, No. 4, 1985. 145-150

86. Prohászka, J.: Neue Ergebnisse der Schnellwärmebehandlung von Metallen, Neue Hütte, October 1985, No. 10. 387-390

87. Prohászka, J.: Large-scale production and economic efficiency (in Hungarian), GÉP, Vol. XXXVII, No. 1, 1985. 436-440

88. Prohászka, J.: Materials science and plastic formability (in Hungarian), Gépgyártástechnológia, Vol. XXV, No. 12, 1985. 537-642

89. Prohászka, J.: Improvement of the quality of structural steels by means of a new heat-treatment technology (in Hungarian), Minőség és megbízhatóság (Quality and reliability), Vol. XX, No. 2, 1986. 107-112

90. Prohászka, J.: Microstructure and plastic formability. Technical University of Athens, April 21-28, 1986

91. Prohászka, J.: Role of technology in scientific-technical development. "Role of Hungarians in the world's scientific and technical progress", Conference at the Technical University of Budapest, August 4-9, 1986 (in Hungarian)

92. Prohászka, J.: Funkce vedy o materialech a technologie v VTR, "Socialismus a globalny problemy somasnosty", Materialy z mezdunarodny Konferencia, Praha 1986, (Proceedings), 90-96

93. Prohászka, J.: Improvement of the conductivity of metals (in Hungarian), 5th Metallurgical Days, Balatonaliga (Hungary), October 1-3, 1986. Proceedings: Vol. 1. 1-12

94. Prohászka, J.: On the Incubation Time of Isothermal TTT Diagrams, International Heat Treatment Conference, Budapest, October 20-24, 1986. Proceedings: Vol. 1. 17-20

95. Prohászka, J.: Development of materials science as reflected in the demand for metallurgical products (in Hungarian), Miskolc, June 12,13, 1987

96. Prohászka, J.: Role and importance of structural materials (in Hungarian), 9th National Conference on Rolling, Ózd (Hungary), October 7-10, 1987

97. Prohászka, J.: Technology and economic implications of rapid heat treatment (in Hungarian), 12th National Heat Treatment Seminar, Zalaegerszeg (Hungary), October 8-10, 1987

98. Mrs. Krsityák-Maróti, G. - Prohászka, J.: Determination of the orientation of austenite crystallites on the basis of the typical planes of martensite produced in it (in Hungarian), 12th National Heat Treatment Seminar, Zalaegerszeg (Hungary), October 8-10, 1987

99. Mamalis, A.G. - Visniakos, G.C. - Vaxevanidis, N.M. - Prohászka, J.: Macroscopic and microscopic phenomena of electrodischarge machined steel surfaces: an experimental investigation, Journal of Mechanical Working Technology, No. 15 (1987), 35-356

100. Prohászka, J. - Mrs. Kristyák-Maróti, G.: Radiation damage of structural materials (in Hungarian), Energia és Atomtechnika, Vol. XLI, No. 1, 1988. 27-32

101. Prohászka, J.: Atomic displacements in martensitic transformations (in Hungarian), Bányászati és Kohászati Lapok - KOHÁSZAT, Vol. 121, No. 4, 1988. 145-148

102. Prohászka, J.: Technology as reflected in economic development (in Hungarian), Társadalmi Szemle, Vol. XLIII, No. 8-9, 1988. 110-115

103. Prohászka, J. - Mrs. Kristyák-Maróti, G.: Geometry-memorizing alloys (in Hungarian), Bányászati és Kohászati Lapok - KOHÁSZAT - Vol. 121, No. 7, 1988. 290-301

104. Prohászka, J.: Introduction into materials science I (for electric engineers), (in Hungarian), Tankönyvkiadó, Budapest, 1988, (p. 346)

105. Prohászka, J.: Phase transformations in steel during rapid heat treatment, Periodica Polytechnica - Mechanical Engineering , Vol. 32, No. 2, 1988

106. Prohászka, J.: Rapid heat treatment of unalloyed low-carbon steel, Symposium on Rapid Heat Treatment of Metals at the ASM World Materials Congress, Chicago, Illinois, September 24-30, 1988

107. Prohászka, J. - Mrs. Kristyák-Maróti, G.: On up-to-date alloys of excellent creep even at high temperatures (in Hungarian), Bányászati és Kohászati Lapok - KOHÁSZAT, Vol. 122, No. 6, 1988

108. Prohászka, J. - Mrs. Kristyák-Maróti, G.: Changes in the structure of steels in the course of rapid heat treatment (in Hungarian), "Role of Hungarians in the world's scientific and technical progress", Second scientific meeting, August 1989

109. Prohászka, J. - Mrs. Kristyák-Maróti, G.: Materials science and technology (in Hung.), GÉP, Vol. XLI, No. 10, 1989

110. Prohászka, J. - Mrs. K. Maróti, G.: In situ observations of plastic deformation on single crystals in SEM, International Symposium on Electron Microscopy in Plasticity and Fracture Research of Materials, Holzhau, October 8-13, 1989

111. Prohászka, J.: Economy - where to go? (in Hungarian), HITEL, Vol. 3, No. 6, March 27, 1990

Acta Technica Acad.Sci.Hung., 103(1), pp. 15-26 (1990)

SURFACE FINISH BY MEANS OF HIGH POWER LASER

BAKONDI, K.*, BUZA, G.**

(Received: 5 May 1990)

Within the wide range of industrial applications of CO_2 gas lasers of high power density, methods to modify the surface quality of components have been investigated by the authors. Special emphasis is laid on methods resulting in martensitic transformation of steels. In evaluation of the results of experiments with cast iron components, it was found that a structure other than the conventional cast iron structure could be obtained as a result of heat treatment with high power density. Methods like light microscopy, scanning electromicroscopy, X-ray diffraction and DTA were used as test methods in the experiments.

In the recent decades, conventional metalworking techniques like casting, forging, rolling, machining, welding, heat treatment etc. have lost their earlier monopolistic position. New, never used technological processes have been finding wide use in industry, among them metalworking by electron beam, plasma or laser, manufacture of metalglass, microcrystalline and sintered materials, monocrystals, geometry-memorizing alloys etc. /1/, /5/, /7/. However, in the colourful picture of what is new and latest in technology, some trends can be distinctly recognized along which these new technological processes are developing, perhaps most dynamically the processes of high power density including first of all electron beam, plasma and laser techniques. Discussed below are some of the results of investigations in relation to laser metalworking.

From among lasers of different wavelength and power, CO_2 gas lasers are most widely used in the field of materials science. Today CO_2 gas lasers have a power range of several kilowatts and thus the field of application includes a wide range of industrial uses from precision mechanic to structural steel production.

---

*Bakondi, Károly, H-1026 Budapest, Trombitás u. 26, Hungary

**Buza, Gábor, H-1028 Budapest, Kazinczy u. 14-16, Hungary

Akadémiai Kiadó, Budapest

A TUNGSRAM CO_2 gas laser of a power of 1 kW is operated by the Department of Machine Industry Technology, Faculty Transport Engineering, Technical University of Budapest. Research workers of the Department have been dealing with development of power lasers and their increased industrial application in the country. In addition to many other technological problems (such as cutting, boring, welding, marking etc.), investigated are the possibilities to change and improve the surface quality of structural elements and components.

Laser techniques are used to harden, refine or coat the surface of structural elements and components exposed to stress, first of all with a view to improve the tribological behaviour.

As compared with the conventional hardening techniques, short-time local surface finishing techniques by means of laser beam have advantages of quite a number in respect of manufacturing technology. The local heat input allows of pointlike hardening, or hardening along a line, without exposure of the surrounding material to heat resulting in significant changes. In this way, the specific energy consumption of heat treatment of the components reduces and the process becomes economically more efficient. By use of mirror systems, local hardening of otherwise inaccessible points becomes also possible. Reproducibility, automatization, minimum load to the workpiece and as a result, minimum buckling are additional factors explaining the increasing importance of laser application in this field.

It is first of all the good dimensional stability that allows of the surface finishing of components which could not have been worked so far by means of the conventional techniques.

CO_2 gas mixture is used for hardening and coating of the surface of components in case improvement of the tribological characteristics is necessary. Two types of laser surface finishing of workpieces can be used: martensitic hardening and fusion hardening.

Martensitic hardening

The surface of the workpiece is heated by the laser beam to a temperature lying below the solidus point.

As soon as the rear edge of the focal spot reaches the surface, the heating phase of the process is completed. As a result of heating, the surface of the workpiece becomes austenitic and goes into carbon solution.

Then cooling of the surface starts immediately as a result of heat transport taking place in the material treated and/or between the surface and the atmosphere and, in case of a sufficiently high rate of cooling, martensite is produced in the material parts that have been austenitic earlier. As a result of this structural change, the surface of the workpiece becomes hard.

The thermal process will be successful if the critical cooling rate is reached. Dissipation of heat will take place within a short time as a result of the temperature gradient if heat extraction by the surrounding material is appropriate and the heat capacity and thermal conductivity of the workpiece are sufficiently high. In this case, cooling results in self-hardening without the need for an external coolant.

Fusion hardening

The power density of the laser beam is increased until the melting point of the workpiece is reached (10^5 - 10^7 W/cm^2) and fusion of the surface takes place for a short time. Cooling and/or solidification starts soon after fusion.

The same process can be used also for purification of the surface containing volatile impurities (metallurgical processes). Inclusions that can not be removed from the melt are distributed more uniformly because of the rapid thermal processes and they separate as fine particles in the course of solidification.

Coating

Coating is a process similar to fusion hardening. The workpiece can be made in this case of an inexpensive but though material while the coat applied to the surface e.g. by thermal dispersion is an expensive material resulting in favourable properties. In this way, not only the tribological behaviour but also the optical characteristics, corrosion resistance and heat resistance of the component can be improved.

The parameters of the process shall be selected so as to result in fusion of the coat and the surface layer of the basic material. A metallurgically sufficient metallic bond can be produced only in this way. Should the power density of the laser beam used for heating be insufficient-

ly low, the coat, although molten, will separate from the carrier material immediately after the laser beam has been removed. On the other hand, a higher than desirable heat input stirs up the melt of basic material because of the significant convection and thus the unfavourable mechanical properties can act throughout the melt up to the surface. Therefore, the process shall be controlled in such a way that the intermediate zone will be stirred up only slightly.

The originally porous disperse coat will become compact after fusion. Optimum result can be achieved if the laser beam intensity and feed rate are adjusted to the properties and thickness of the coat, material quality and degree of porosity. Surface roughness, porosity and inclination to crack formation shall be minimum. Reproducibility of the coat production is a condition for repeatability of the results.

In another version of the surface finishing process, the alloying element is introduced directly (e.g. in the form of powder or gas) into the melt. In contrast to the coating process, intensive agitation of the melt due to convection is utilized to admix the alloying element with the basic material. Hence, the melt shall be stirred up thoroughly. This method is advantageous in that no uncertainty in manufacture resulting from the instability of the layer thickness of the porous coat applied to the surface by thermal dispersion shall be reckoned with.

An experiment series run by the Department demonstrates the wide range of applicability of power lasers and their special effects. The workpiece used in the experiments was a modular cast iron camshaft. This example has been selected from among experiments of a large number to demonstrate both versions of surface hardening mentioned above for the same workpiece, permitting thus a comparison of the effects of both mechanisms. Composition of the test material: C = 3.55, Si = 2.5, Mn = 0.35, Ni = 1.5, Mg = 0.055% by weight. Mechanical characteristics of the typically pearlitic modular cast iron material of the workpiece: R_m = 650 N/mm^2, R_e = 480 N/mm^2, A_5 = 5%, HB = 230-285.

The optical microphotograph of the metallographic specimen of part of the basic material is shown in Fig. 1. The photograph in Fig. 2 shows a sectional metallographic specimen of the environment of the surface treated by laser beam of a power of 500 W. As seen in the photograph, the graphite nodules are surrounded by a "halo" not eroded or, if indeed at all, only slightly eroded especially near the surface. This can be clearly seen in the photograph of 500 fold magnification given in Fig. 3. Otherwise the structure of the layer is martensitic or shows austenitic residues.

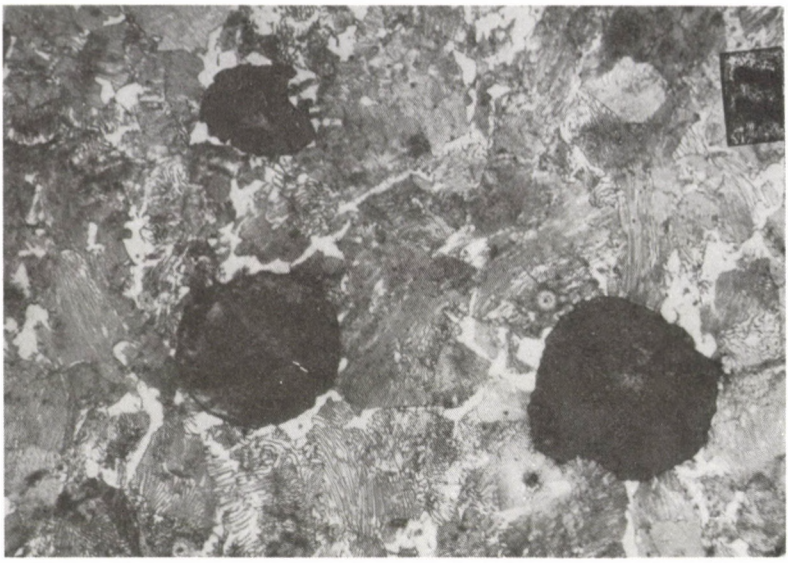

Fig. 1. Optical microphotograph of the metallographic specimen of the modular cast iron camshaft investigated (M = 500x, 3% Nital)

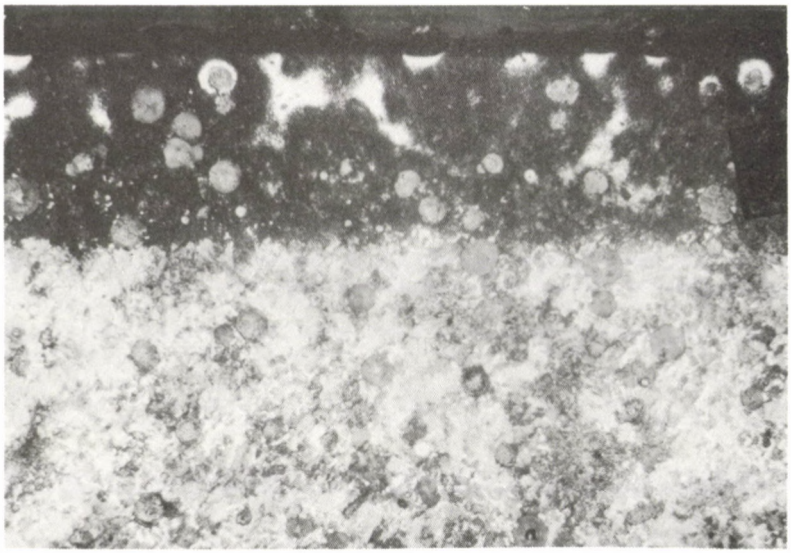

Fig. 2. Effect of 500 W laser light beam on the surface layer (M = 500x, 3% Nital)

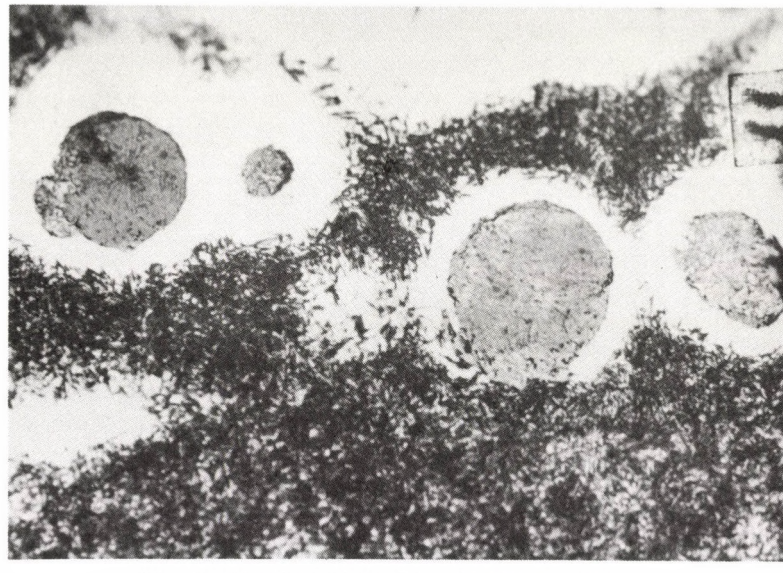

Fig. 3. Structure of the layer treated by laser
(M = 500x, 3% Nital)

The white, non-eroded parts between the martensite, the austenitic matrix and the graphite nodes remind us in their nature of the so-called ferrite ghosts of the ferritic-pearlitic nodular cast iron. However, white parts like these can not be seen in parts of the material that have not been heat-treated (Figs 1 and 2). Hence, these white parts must have been brought about in the course of heat treatment. Further experiments were run therefore to detect how these white parts had been produced and what they are at all.

It is necessary to make clear that the material of these white parts can not be ferrite because

(1) In the course of surface finishing with high power density, the material was exposed for too short a time (< 1 sec) to temperatures where diffusion of the carbon or other alloying elements could have taken place at a significant rate. Therefore, dissolved carbon present in austenite could not have separated onto graphite nodes, resulting thus in reduction of the carbon concentration as it would do in case of a ferritic-pearlitic nodular cast iron.

(2) Decarbonization could not have been responsible for the development of ferrite ghosts either, partly because also decarbonization is a diffusion process and partly since the material had not been decarobnized in the immediate vicinity of the surface. Last but no least, there is no thermodynamical explanation of this process either.

(3) The values of microhardness measured in the white parts using a load of 1-5 g range between 400 and 700 MHV, a hardness well over the usual hardness of ferrite in spite of the considerable variation.

In investigating the nature and way of production of the white parts, a phenomenon clarly visible even in the optical microphotograph of an 500 fold magnification shall be taken into consideration, namely that the martensite needles protrude into the white area i.e. there is no sharp boundary between the white area and the martensitic matrix.

The lattice structure of the material of the surface layer was investigated by means of X-ray diffraction analysis in an angular range of ϑ = 8 - 24 degrees using Mo $K_{\alpha 1}$ of a wavelength of 0.709261 Å as a line-focus test ray. The change of the reflected radiation intensity as a function of angle ϑ is shown in Fig. 4. Indicated in the Figure are also the most important data from pages 6-696 and 23-298 of the ASTM catalogue. The X-ray diffraction analysis detected a significant amount of γ-Fe in the skin of the casting.

On the basis of a comparison of the relative intensity maxima, the γ-Fe content is estimated to lie well above 10%, this quantity exceeding the possible quantity of rest austenite between the martensite needles. Hence, also the material of the white parts around the graphite nodes according to Figs 2 and 3 is most likely γ-Fe.

To make sure, the specimen had been deep-frozen in liquid nitrogen and then the structure developed in the course of deep-freezing was analyzed metallographically, using now scanning-electronmicroscopy to

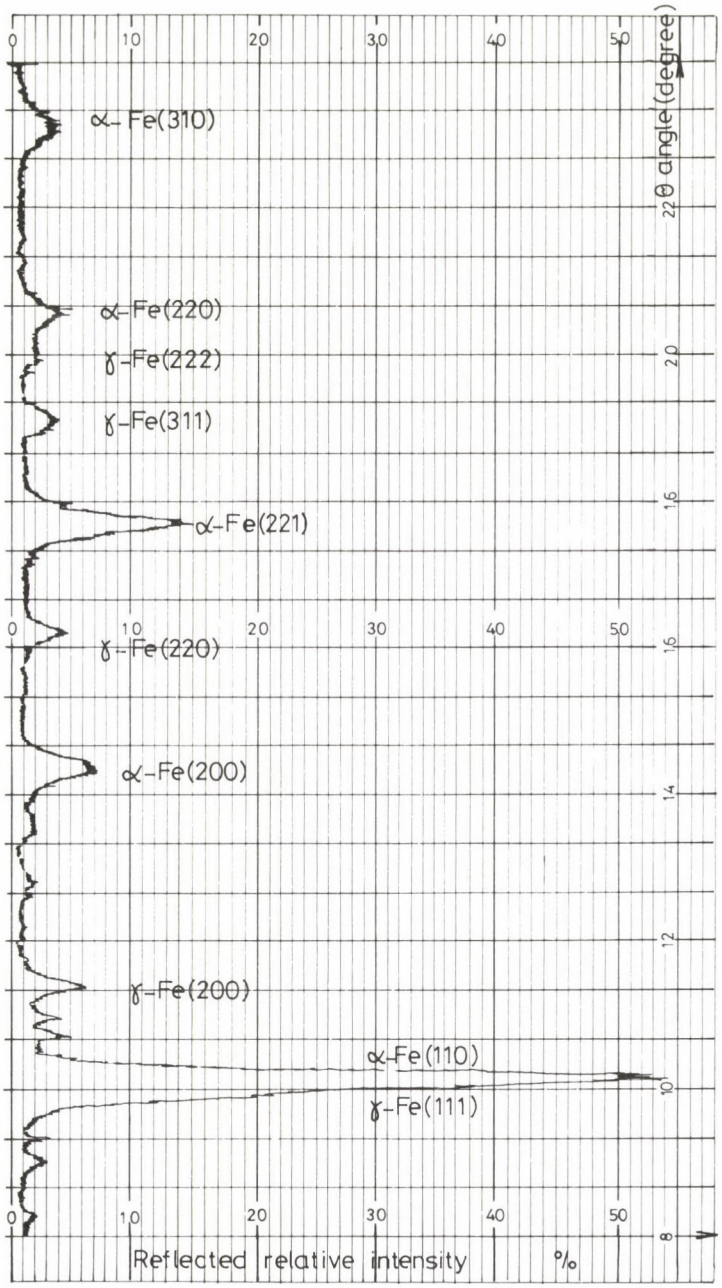

Fig. 4. X-ray diffractogramm of the layer treated by laser (Mo-K$_\alpha$, 50 kV, 44 mA)

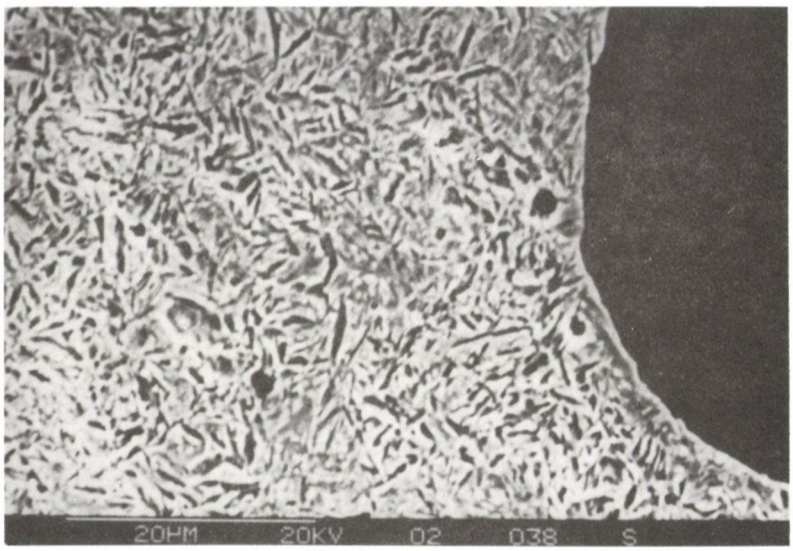

Fig. 5. SEM photograph of the layer treated by laser, taken after deep-freezing by nitrogen (3% Nital)

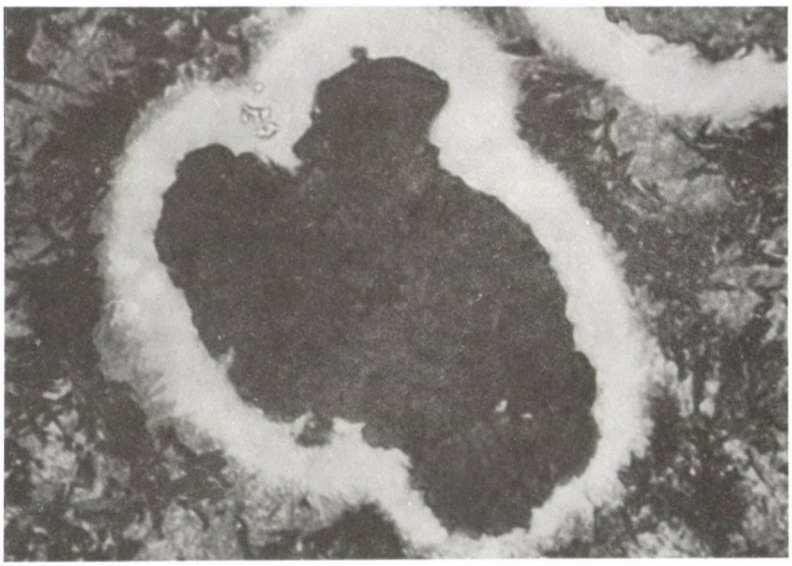

Fig. 6. Optical microphotograph of the metallographic specimen used for checking (M = 1000x, 3% Nital)

increase the resolution (Fig. 5). As seen in the Figure, also the material in the immediate vicinity of the graphite nodes consists of needled martensite.

Since, according to the results of scanning-electronmicroscopy, the white parts free from erosion earlier transformed into needled martensite as a result of deep-freezing, they must have been austenitic before quenching /4/. And this result raises additional questions to be answered:

- What is the difference between the austenite in the environment of the graphite nodes, non-transformed in the course of heat treatment by laser and the austenite in other parts of the skin, transformed in majority into martensite as a result of cooling after heating?

- What explains the phenomenon that rest austenite appears in every case in the environment of graphite nodes?

A possible answer to the above questions is that the austenite in material parts non-eroded earlier has been produced of melt by primary crystallization while in other parts of pearlite by solid phase transformation.

This explains at the same time the typical coexistence of these parts and graphite nodes. Namely, in the course of heat treatment of hypoeutectic alloys, the carbon content of the immediate environment of the graphite nodes is, due to diffusion, higher than that of the distant parts and thus the liquidus temperature of the microenvironment is lowest at these places (see curve B-C' of the state diagram of Fe-C alloy system). Accordingly, the temperature of the heat-treated layer exceeded the overall solidus temperature of the alloy in the course of heat treatment but the material melted only partially, indicating that the liquidus temperature had not been reached /6/.

This explanation is in line with the observation that the "halo" around the graphite nodes near the surface of the heat-treated layer is larger than that in deeper parts because, due to the limited thermal conductivity of the basic material, the deeper parts could not reach temperature as high as the temperature of parts near the surface /2/, /3/.

Since only a fraction of the basic material has molten that is its temperature exceeded only slightly the overall solidus temperature of the material, it is possible to determine maximum achievable layer temperature, measurable otherwise only rather circumstantially in the course of heat treatment by laser, indirectly on the basis of the solidus temperature.

A solidus temperature of 1135 ^{O}C has been measured for the basic material in the course of DTA (Differential Thermo Analysis).

Correctness of the DTA result was checked experimentally. In the experiment, a Ø 5x12 mm specimen of a wall thickness of 0.5 mm, made of non-treated basic material, had been heated to a temperature of 1140 ^{O}C within 1.8 sec (accuracy of PID-control: $\pm$ 2 K), then, without holding, it was cooled from 1140 ^{O}C to 500 ^{O}C within 2.5 sec. A radio-frequency inductor was used for heating while argon gas stream for cooling. White parts identical with those in Fig. 3 can be seen around the graphite nodes in the etched sectional metallographic specimen (Fig. 6). Hence, also the surface layer heated by laser reached a temperature of about 1140 ^{O}C in all probability.

Summary

CO_2 gas lasers are expected to find wide use in industry in the near future although so far only laser-beam cutting and welding have been widely known from among the processes of high power density representing high-tech. Introduction of surface treatment by laser is not likely to take a long time either. An explanation of these expectations is the typically low specific energy consumption of laser techniques in spite of the high power density.

Further advantage offered by power lasers are the good reproducibility, easy automatization, flexibility, environment-friendly nature etc.

As has been observed in the course of analysis of nodular cast iron, phenomena differing from those experienced in the course of conventional heat treatment processes are inherent in laser techniques. Similar phenomena will certainly contribute to a wide industrial use of lasers. The tests detected unambiguously a structural feature of the material according to which the process of martensite transformation is affected by the previous austenitic state of the material. Namely, different results are obtained for the martensite transformation properties of austenite depending on whether the austenite resulted from pearlite by phase transformation or from the melt by rapid cooling.

REFERENCES

1. Prohászka, J. - Müller, L.: Some theoretical and technological problems of rapid heating (in Hungarian), Műszaki Tudomány, 55, (1978), 1-17

2. Prohászka, J. - Gangli, P. - Komáromi, M.: Wärmeverteilung in schnellerwärmten Stangen mit konstantem Querschnitt, Neue Hütte, No. 1, (January 1979)

3. Prohászka, J.: Neue Ergebnisse der Schnellwärmebehandlung von Metallen, Neue Hütte, October 10, 1985, 387-390

4. Prohászka, J.: Atomic motions in martensite transformations (in Hung.), Bányászati és Kohászati Lapok, Kohászat, 121/1988/4, 145-148

5. Prohászka, J. - Mrs. Kristyák-Maróti, G.: Geometry-memorizing alloys (in Hungarian), Bányászati és Kohászati Lapok, Kohászat, 121(1988/7, 290-301

6. Prohászka, J.: Introduction into materials science, Vol. I (in Hung.), Tankönyvkiadó, Budapest, 1988

7. Prohászka, J. - Mrs. Kristyák-Maróti, G.: Alloys of excellent creep even at high temperatures (in Hungarian), Bányászati és Kohászati Lapok, Kohászat, 122/1989/6

Acta Technica Acad.Sci.Hung., 103(1), pp. 27-31 (1990)

EFFECT OF RAPID HEAT TREATMENT ON FATIGUE

BERKE, P.[*] - GALAMBOSI, F.[**]

(Received: 13 May 1990)

The properties of non-alloy low-carbon steels resulting from rapid heat treatment increase the field of application of steel. The increased strength of such steels permits the material to be utilized more economically.

Introduction

Materials and processes where minimum expenditure of energy results in significant changes in the material properties have increasingly come to the front recently.

Different methods are known to change the properties of steel /1/, /2/. Professor János Prohászka has an international reputation in the field of heat treatment. Mentioned here are only two basic works of Professor Prohászka from among those of quite a number contributing to the international literature, one dealing with the fundamentals of so-called rapid heat treatment /3/ while the other investigates the structure of steel resulting from the transformation mechanism in the course of heat treatment /4/.

The economically more efficient utilization of materials and the load analysis of vehicles have points in common which can be taken as a basis for the design of competitive products. In this field, significant results have been achieved by the Department of Mechanics, Faculty Transport Engineering, Technical University of Budapest /5/, /6/, /7/. In effort to extend theoretical work to the practical field, the first step was to start fatigue experiments of steels after rapid heat treatment with a view

[*]Berke, Péter, H-1119 Budapest, Nándorfehérvári u. 7, Hungary

[**]Galambosi, Frigyes, H-1037 Budapest, Erdőalja u. 110/b, Hungary

Akadémiai Kiadó, Budapest

to find the possibilities of practical application in vehicle production (IKARUS, GANZ-MÁVAG). The experiments described below were run to decide whether a more detailed test series, taking into consideration a wide range of technological possibilities, would be necessary and worth of the trouble or not.

Test materials, test procedure, test results

The test specimens were made of Grade RSt 27/2 C 0.1 Mn 0.3 Si 0.11 P 0.015 S 0.021 steel wire of a diameter of 5.5 mm according to DIN 17100 with and without heat treatment.

The purpose of the test series was, on the one hand,

- to compare the fatigue strength of specimens with and without heat treatment and, on the other hand,

- to investigate the effect of different material combinations and heat treatment of the weld (that is joining of heat-treated and non-treated materials by welding, followed by repeated heat treatment of the weld or omission of heat treatment) on the service life.

The test section of the Ø 5.5 mm specimens was 4 mm. (Specimens of this type were available when the test series was started. Now we have quite a choice of heat-treated specimens.)

It was found that the specimens made of heat-treated and non-treated material could not be subjected to the same load in the fatigue test because the test had resulted in extremely high or extremely low number of cycles (or even elongation in the latter case), depending on whether the load had been selected for non-treated or heat-treated material, respectively.

The specimens were subjected to the following loads in the fatigue test:

1. Non-treated specimens: $\sigma_{min} = 155.25\ N/mm^2$
   $\sigma_{max} = 390.68\ N/mm^2$
2. Heat-treated specimens: $\sigma_{min} = 176.43\ N/mm^2$
   $\sigma_{max} = 444.74\ N/mm^2$

In spite of the increased fatigue test load applied to heat-treated specimens as compared with non-treated specimens (the difference being about 14%), 3 of the 10 specimens of the heat-treated test sample endured the test without fracture (after a number of cycles of 6, 8, 10 x 10^6, the

test was discontinued). As demonstrated by the test, the fatigue strength of heat-treated materials is higher. The results are tabulated in Table 1.

Table 1

Fatigue test results for specimens made of heat-treated and non-treated material

Non-treated: Load: 155.25 N/mm^2 390.68 N/mm^2		Heat-treated Load: 176.43 N/mm^2 444.74 N/mm^2	
1	205 300	1	1 362 600
2	170 600	2	2 532 300
3	355 300	3	6 156 700 Nt
4	167 000	4	1 827 600
5	242 300	5	2 190 800
6	112 000	6	8 535 900 Nt
7	242 000	7	10 611 000 Nt
8	396 600	8	2 057 100
9	97 600	9	612 200
10	101 300	10	995 600

Heat-treated and non-treated specimens - Ø 5.5 mm wires - were welded together under CO_2 using VIH2 welding electrode (VIH2 electrode and CO_2 welding were chosen for the test for practical reasons only although this electrode and this process are most widely used in the vehicle industry).

Possible material combinations:

- joining of heat-treated specimens by welding with and without subsequent heat-treatment of the weld,
- joining of non-treated specimens as well as
- non-treated and heat-treated specimens by welding with and without subsequent heat treatment of the weld.

On the basis of the test results - because of the significant differences in the number of cycles at different loads - further investigation of the different material combinations described above seemed not to be reasonable.

In case of non-treated combinations, the service life which is expected to be shorter than the service life of the basic material is determined by the quality of the weld and its environment. In case of non-treated-heat treated combinations with repeated heat-treatment of the weld, it is again the weld that affects the service life predominantly. In this

case, the service life of the weld might be longer than that of the non-treated material but this could not have been determined numerically because of fracture of the non-treated material. The same was found for non-treated material combinations with repeated heat-treatment of the weld. These theoretical considerations had been backed up by preliminary experiments and thus only heat-treated specimens with and without repeated heat-treatment of the weld were subjected to fatigue tests.

A load of 155.24 N/mm^2 or 390.68 N/mm^2 was selected for the fatigue test. The welds were X-rayed. Aware of the fact that, because of the cylindric shape of the specimen and the expectable location of the fault, answer to the question whether it is worth to subject the specimens to fatigue tests or not can be obtained only in case of very coarse defects, we decided to evaluate every case where no welding defect could be detected in the fracture surface instead of preliminary sorting.

Table 2

Fatigue test results for specimens made of heat-treated and non-treated material

Load: 155.25 N/mm^2 390.68 N/mm^2			
Non-treated weld		Heat-treated weld	
1	406 000	1	1 329 300
2	317 900	2	183 500
3	370 400	3	376 200
4	160 900	4	18 500 00 Nt
5	187 000	5	447 100 H
6	75 300 H	6	12 058 800 Nt
7	1 010 500	7	1 442 700
8	115 600	8	10 871 400 Nt
9	613 900	9	13 521 500 Nt
10	556 300	10	146 300 H
11	10 568 700		
12	68 000		
13	4 110 700		
14	704 300		

The test results are tabulated in Table 2 where Nt denotes the discontinued fatigue test that is specimens that survived the test without fracture while the welding defects detected in the fracture surface are denoted by H. According to the Table, 4 of 10 specimens of the sample of heat-treated material with repeated heat-treatment of the weld survived

while in case of heat-treated material without repeated heat-treatment of the weld, only 1 of 14 specimens endured fatigue loading without fracture. Obviously, some statistical test could certainly have been used if the optimum load equally suited for both cases had been found. However, according to experience, it is rather difficult to find such a test load. At the same time, the number of loading cycles is conspicuously larger for specimens with heat-treated weld, due to heat-treatment among other reasons, which was a rather simple process in this case, dipping in cold water after welding, considering that the simplest the technology, the greater the success under operating conditions.

Summary

- As compared with specimens made of the same material without heat-treatment, specimens made of heat-treated material endure higher fatigue load (the difference being about 14%),

- from among welded specimens made of heat-treated material, specimens with heat-treated weld show a higher fatigue endurance, in particular, 4 of 10 specimens endured the test without fracture while only 1 of 14 specimens without heat-treatment of the weld, subjected to the same fatigue test load. (Of course, the number of loading cycles for specimens with heat-treated weld is larger than in case of specimens without heat-treatment of the weld as a result of the 4 specimens surviving the test.)

REFERENCES

1. Prohászka, J.: Theoretische und praktische Probleme der Beschleunigung von Wärmebehandlungsprozessen, Neue Hütte 1977/6

2. Prohászka, J.: Neue Ergebnisse der Schnellwärmebehandlung von Metallen, Neue Hütte 1985/10

3. Prohászka, J. - Müller, L.: Some problems of rapid heat treatment (in Hungarian), Műszaki Tudomány 55, 1978

4. Prohászka, J.: Phase transformations in steel during rapid heat treatment, Periodica Polytechnica - Mechanical Engineering, Vol. 32, No. 2, 1988

5. Michelberger, P. - Keresztes, A. - Várlaki, P. - Ginsztler, J.: Modelling of the fatigue damage processes of bus frames, Int. J. Fatigue 6 (1984), No. 2, 107-112

6. Michelberger, P.: On the Dual Exponentiality of the Stress Level Cross Intersection Numbers in Road Vehicle Vibration Systems, Acta Technica Acad. Sci. Hung. 94(1-2), 3-17

7. Michelberger, P.: Loading analysis under operational condition for the design of commercial road vehicles, Acta Technica Acad. Sci. Hung. 100, No. 1-2, 127-140

Acta Technica Acad.Sci.Hung, 103(1), pp. 33-48 (1990)

DISSOLUTION OF ALUMINIUM IN GALLIUM

SOMOSI, I.*- VITÉZ, J.**

(Received: 15 May 1990)

The authors investigate the development of the gallium-aluminium system that is the kinetics and mechanism of aluminium dissolution in liquid gallium.

Dissolution of aluminium in gallium was found to be a heterogeneous reaction. The rate of reaction and the value of aluminium concentration can be described using the appropriate equation. The process depends on the maximum achieavable concentration and constant of dissolution rate of aluminium and thus on temperature, size of the surface in contact with gallium and on time. First the gallium enters at the grain boundaries of the aluminium by diffusion and, breaking the coincident lattice bindings, it decomposes the aluminium into crystallites, then dissolves it. Hence, this diffusion process is also a function of the aluminium structure. The liquid gallium-aluminium alloy is a homogeneous system.

As is well known, the gallium content of some thousandth % in bauxite dissolves in the aluminate liquor of the Bayer process and it reaches equilibrium concentration in the system, depending on the gallium content of the bauxite and on the extraction and mixing parameters /1/.

Nowadays, the earlier mercury and/or amalgam cathode processes are increasingly replaced with the different cementation and extraction processes for environmental considerations and to protect health.

Included among cementation processes are methods where metallic aluminium is used to reduce the gallium concentration of 0.2 - 0.3 g/dm^3 in aluminate liquor. As an example, and at the same time for the sake of comparison, two processes are presented which seem to differ from each other only in the way of introduction of metallic aluminium into the system but, at least as far as the kinetics and the mechanism of aluminium dissolution are concerned, the difference between them is still considerable.

---

*Somosi, István, H-8400 Ajka, Semmelweis u. 14, Hungary

**Vitéz, János, H-8400 Ajka, Semmelweis u. 5, Hungary

Akadémiai Kiadó, Budapest

In the first process, granular aluminium is introduced into the cementator or more precisely, to the surface of the liquid gallium bath at the bottom of the cementator through the aluminate liquor /2/.

Since the dissolution of aluminium in gallium is a process depending also on time as will be explained later, the gallium-aluminium system developing under the circumstances of the process is a priori a chemically and electro-chemically inhomogeneous two phase system (Ga and Al) and thus it can not be considered as a polyelectrode.

In the second process, granular aluminium is dissolved in isolation from the cementator that is in the aliquot part of the gallium bath with the aluminate liquor excluded, in the so-called gallam-producer, and the aluminium concentration of the gallium bath is ensured by circulation between the gallam-producer and the cementator /3/.

The gallium-aluminium system called gallam, brought about in the gallam-producer and cementator, is a chemically and electro-chemically homogeneous system, essentially a polyelectrode where the electrode potential is determined by the less noble metal of more negative potential that is by aluminium or aluminium concentration. In a system like this, the gallium acts both as a solvent and as a diluent, permitting the uniform aluminium concentration and thus the required value of the electrode potential to be adjusted and stabilized.

Reactions taking place in cementation by aluminium

The gross process taking place in recovery of the gallium content of aluminium liquor by metallic aluminium cementation is described by the following formula (with the secondary reactions left out of consideration):

$$Al + (Ga/OH/_4)^- \longrightarrow Ga + (Al/OH/_4)^- \quad .$$

Investigation of cementation from a technological point of view requires that the gross process be theoretically decomposed with, however, the practical implications taken into consideration. In this case, the process is described by the following partial reactions (Ga being the gallium bath):

$$Al + /Ga/ \longrightarrow Al\ /Ga/ \qquad (1)$$

$$Al/Ga/ + 4\ OH^- \longrightarrow /Ga/ + (Al/OH/_4)^- + 3\ e^- \qquad (2)$$

$$/Ga/ + (Ga/OH/_4)^- + 3\ e^- \rightleftharpoons /Ga/ + Ga + 4\ OH^- \qquad (3)$$

In the cementation process, the succession of the partial reactions is fixed, reactions (1) and (2) being irreversible while reaction (3) is reversible. In case of too low an aluminium concentration, not only a reduction of the gallate ion may fail to occur but also a dissolution of the gallium charge may take place, depending on the value of the electrode potential.

Investigated in this work is reaction (1) under the conditions according to /3/ where, dissimilarly to the other cementation process, reaction (1) takes place in isolation from reactions (2) and (3) both in space and time.

Dissolution of aluminium in gallium

Dissolution of aluminium in liquid gallium has been investigated by several authors. The percentage of maximum soluble aluminium or, briefly, solubility is 3% according to Schreiter /4/, measured under conditions not disclosed by the author while Gusarova et al. measured a percentage of 0.52% at 40 °C 0.90% at 45 °C and 1.28% at 60 °C indirectly, on the basis of change of the value of the potential of gallam becoming poor in aluminium. Hence, the solubility of aluminium was found to be a function of temperature /5/. At the same time, no information on the rate of dissolution of gallium, the parameters affecting it and mechanism of dissolution was found in the literature.

1. Kinetics of aluminium dissolution

Visual observation in earlier experiments suggested that the dissolution of aluminium granulate was speeded up by introduction of the granulate under the surface of the gallium bath that is by increase of the surface of contact and by increase of the temperature. However, the effect of the quality of aluminium on dissolution has not been investigated earlier.

1.1. Dependence of dissolution on surface size

To investigate dependence on surface size, hard (tensile strength: 140-150 N/mm^2) Ø 12 x 10, 8, 4.5 mm aluminium wires (99.5% Al) were dipped

in gallium of 1000 g each to a depth of 6 cm, at a temperature of 40 °C for 3 hours. The mass of dissolved aluminium was measured by weighing of the aluminium wires after removal of gallium adhered to the surfaces by means of hot water. The average values are tabulated in Table 1.

Table 1

Relationship between the mass and surface of soluble Al

Wire diameter, mm	12	10	8	4.5
Wire surface in Ga bath, cm^2	22.6	18.8	15.1	8.4
Al-dissolution, g/h	1.33	1.13	0.90	0.51
Al-dissolution, $mg/h/cm^2$	58.8	60.1	59.6	60.7

On the basis of the results of the investigation, the extent of dissolution of aluminium in proportion to the surface is constant, its value being 0.06 g/h . cm^2 in case of given parameters and characteristics definitely representing hard wires (to be discussed later). It follows at the same time from the value obtained as a rate of dissolution (g/h) that at given temperature, the mass of dissolved aluminium in proportion to time can be increased proportionally as the surface in contact with gallium increases.

1.2. Dependence of dissolution on aluminium quality

The experiment was repeated under conditions according to part 1.1 but with a different (99.99% Al) aluminium quality. Practically identical results have been obtained for the values of both g/h and g/h . cm^2 of aluminium dissolution. Hence, the rate of dissolution is not affected by the quality of aluminium at least as far as the range of 99.5 to 99.99% Al is concerned.

1.3. Temperature dependence of dissolution

A Ø 6 mm soft (tensile strength: 40-50 N/mm^2) aluminium wire (99.99% Al) of a surface of 12 cm^2 was dipped in gallium of 1000 g at temperature of 40 °C, 60 °C and 100 °C. The change of the mass of the aluminium wire was measured at definite intervals and at the same time, the aluminium concentration in gallium was determined. The values of aluminium concentration in percentage by weight as a function of the product of reaction time and surface size - t . A (h . cm^2) are tabulated in Table 2 and illustrated in Fig. 1.

Table 2

Percentage of Al dissolved in gallium as a function of t . A at different temperatures

t . A / h . cm^2	40 °C	60 °C	100 °C
	Al mass, %		
12	-	-	0.58
13.3	-	0.42	-
18	0.25	-	-
24	0.32	-	1.06
36	-	-	1.45
42	0.50	-	-
48	-	-	1.79
60	-	1.01	2.01
66	0.65	-	-
72	-	-	2.28
84	0.73	-	-
108	0.83	-	-
160	-	1.40	3.05
174	1.00	-	-
198	1.04	-	-
240	-	1.50	-
264	-	-	3.24
320	-	1.59	-

On the basis of the values in Table 2 and Fig. 1, both the maximum concentration ie solubility and the rate of dissolution of aluminium in gallium depends on temperature.

Accordingly, the dissolution of aluminium in liquid gallium can be considered as a heterogeneous reaction of a rate described by equation

$$\frac{dC_{Al}}{dt} = k \cdot A(C_{Al,max} - C_{Al}) \qquad (4)$$

where

A dissolved surface, cm^2

$C_{Al,max}$ maximum Al concentration in gallium at given temperature ie solubility, %

t reaction time, h

k dissolution rate constant.

After integration of equation (4), the instantaneous percentage of aluminium is obtained as

$$C_{Al} = C_{Al,max}(1 - e^{-k \cdot A \cdot t}) \quad . \qquad (5)$$

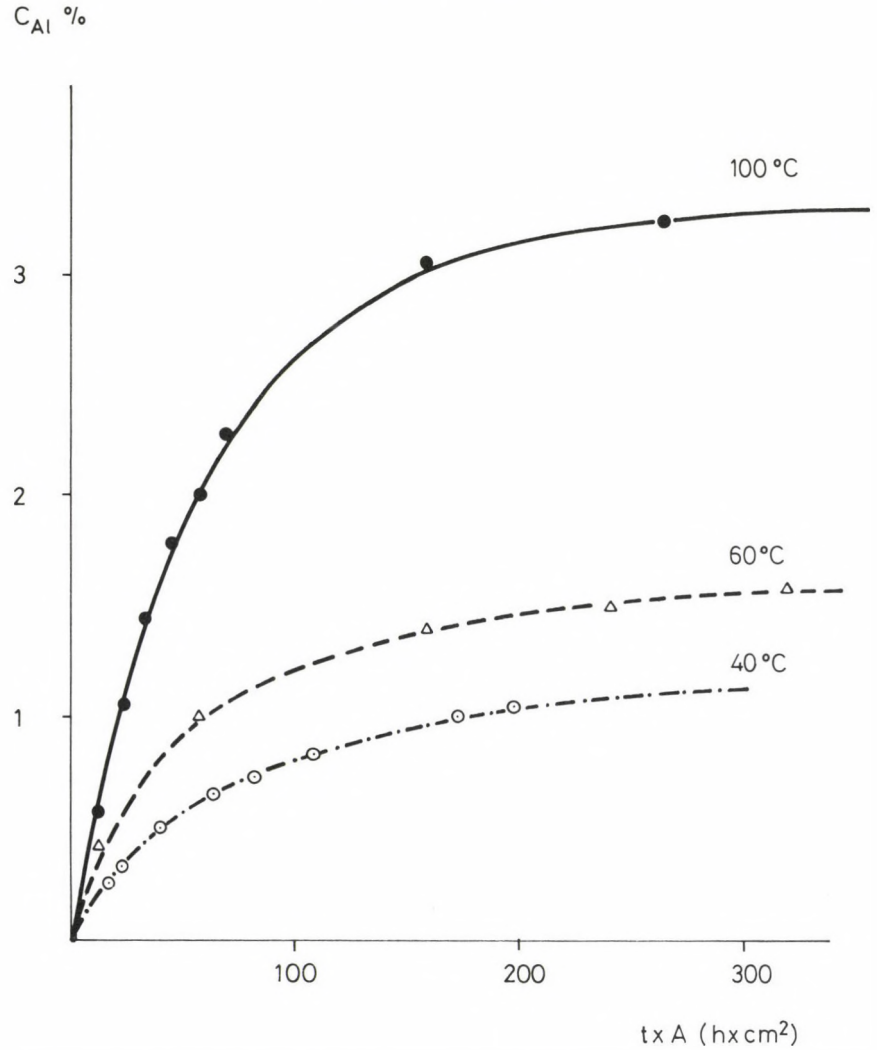

Fig. 1. Percentage of Al dissolved in gallium as a function of t · A at different temperatures

On the basis of equations (4) and (5), the rate of dissolution and the concentration of aluminium at constant temperature is a function of the aluminium surface in contact with gallium. The values obtained for the constants in equation (5) after regression calculation with the data of Table 2 are tabulated in Table 3.

Table 3

Maximum values of Al and k_{eff} at different temperatures

Temperature ^{o}C	$C_{Al,max}$ %	k_{eff} $h^{-1} cm^{-2}$
40	1.11	$1.3 \cdot 10^{-2}$
60	1.62	$1.4 \cdot 10^{-2}$
100	3.29	$1.6 \cdot 10^{-2}$

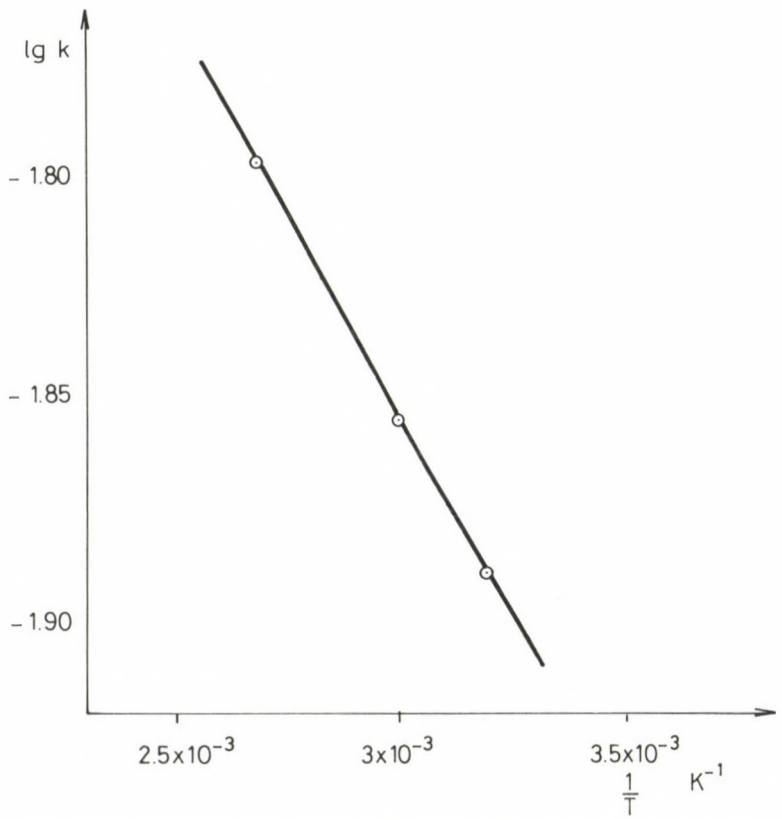

Fig. 2. Reaction rate constant as a function of the reciprocal of temperature

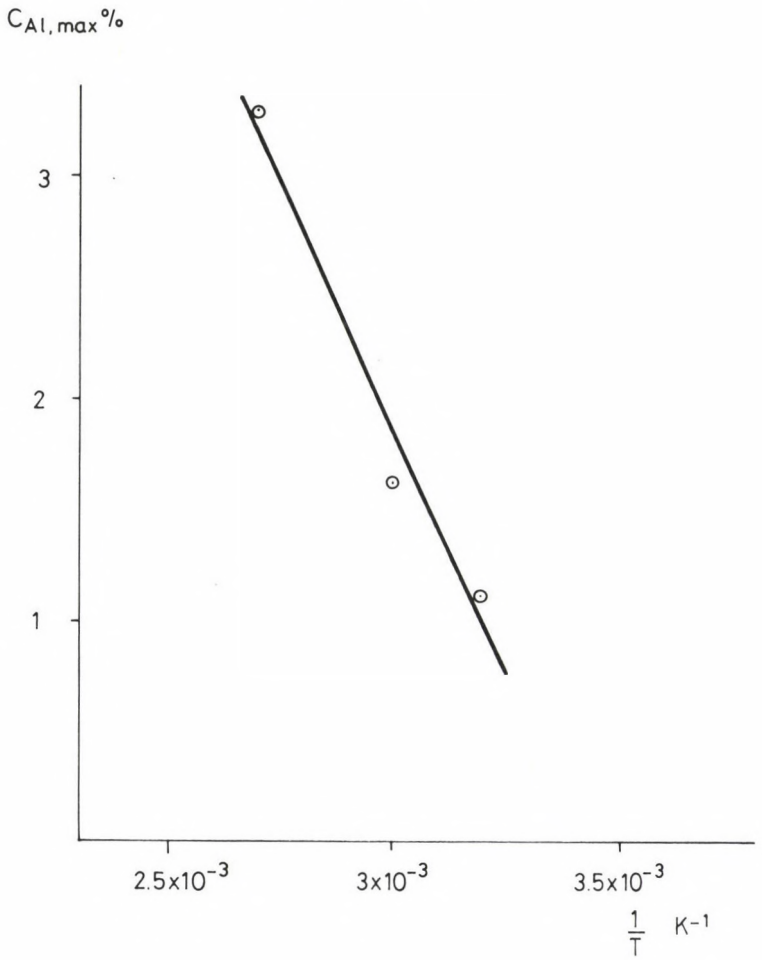

Fig. 3. Maximum possible aluminium concentration as a function of the reciprocal of temperature

As is well known, the reaction rate constant is a function of temperature that is

$$k = k_{max} \cdot e^{-\frac{A}{RT}} .$$

Considering the data of Fig. 2 and with the constants determined, relationship

$$k = 4.9 \cdot 10^{-2} \cdot e^{-4.17 \cdot 10^2/T}$$

Also the maximum possible aluminium concentration depends on temperature. According to Fig. 3, the function of the reciprocal of the temperature can be linearly approximated in the investigated temperature range of 40 - 100 ^{o}C:

$$C_{Al,max} = 14.9 - \frac{4.37 \cdot 10^3}{T} \quad . \tag{6}$$

As follows from the equation, there are two possibilities of increasing the percentage of aluminium to be dissolved in proportion to time that is the rate of dissolution: increase of the value of $\underline{k}$ or $C_{al,max}$ by increase of the dissolution surface and the temperature, respectively.

2. Mechanism of aluminium dissolution

Hard aluminium wires were used in the experiments described in parts 1.1 and 1.2 while the aluminium wire used in the experiment according to part 1.3 was soft. The value of dissolution of aluminium in proportion to the surface was, on the basis of Table 1, at a temperature of 40^{o}C and within a time of 3 hours 0.18 g/cm^2 for hard wires while, on the basis of Fig. 1, at the same temperature and within the same time 0.37 g/cm^2 for the soft wire. That means that the rate of dissolution is about twofold in the latter case with the value of $C_{Al,max}$ remaining unchanged. The anomaly was supposed to result from the difference in structure between the hard and the soft aluminium wire, each resulting from a different technology. This seems to be quite reasonable when the processes taking place in the course of crystallization and plastic forming of aluminium as well as the mechanism of aluminium dissolution in gallium are investigated in combination.

Crystallization of aluminium takes place in a regular cubic system. The atoms forming the elementary cell are located at the apexes of a cube and in the centers of the side diagonals. The distance is largest between the planes of a system parallel to the planes passing through the diagonal of three adjacent sides of the elementary cell while the linkage force acting between them is least. Thus displacement takes place along these planes in case of plastic forming (Fig. 4/a).

Crystal nuclei are formed first and then their growth of different orientation takes place also in case of solidification of liquid aluminium. The crystal (crystallite) growth discontinues at the point of concidence. The grain boundaries develop and a structure consisting of smaller or

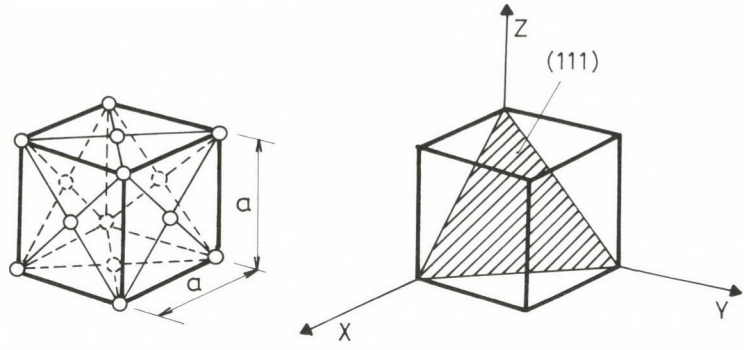

Fig. 4/a. Elementary cell of aluminium lattice
(a - Size of elementary cell,
(111) - Index of plane of minimum binding force in the lattice)

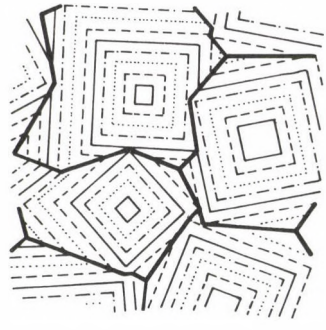

Fig. 4/b. Polyhedral development and boundary formation of crystallites

larger crystallites, depending on the rate of nuclei formation and growth as compared with each other, is built up (Fig. 4/b).

Plastic forming of aluminium and any additional deformation mean that the atomic planes mentioned are displaced as compared with each other, accompanied with dislocations and lattice distortions. In addition to dislocations of increased number, also the grain structure changes considerably. The grains become longer in the direction of metalworking, they disintegrate and a typical structure resulting from metalworking is brought about. However, in case of annealing, a recrystallization process takes place with the dislocations displacing and/or disappearing, new crystal grains are formed and as a result, a new structure is built up /6/.

2.1. Investigation of the morphology of aluminium dissolved in gallium

In the knowledge of what has been said above, the difference in the rate of dissolution in gallium between soft and hard aluminium wires is assumed to result from the different structures.

To prove this assumption, photomicrographic pictures were taken from the surface, ground and polished but chemically not etched, of the cross section of a soft aluminium wire (tensile strength: 40-50 N/mm^2) previously dipped in gallium and partly dissolved, using a Neophot-21 metallurgical microscope and a magnification hundred times natural size (Fig. 5).

The pictures clearly show the geometry of the aluminium structure and the arrangement of gallium, the light area being aluminium while the dark area gallium and spots of crystallite imperfection below the plane of exposure, falling beyond the focal range of the metallurgical microscope.

Figure 5/a shows the initial phase of dissolution that is penetration of gallium at the grain boundaries of aluminium. In fact, the grain boundaries have become perceptible (they could be developed) as a result of the effect of gallium because no chemical etching resulting in perceptibility of the structural details, among them grain boundaries, had been used in preparation for the experiment.

Picutres 5/b and 5/c show the progress of dissolution with time as illustrated by the increasing number of the spots of crystallite imperfection (dark spots).

On the basis of the photomicrographic pictures, the gallium seems to penetrate by intergranular diffusion at the grain boundaries - so-called coincident boundaries - into aluminium, breaking the lattice binding between the grains to decompose the aluminium into crystallites and then dissolving them.

To back up this statement, microstructural tests were carried out by Tatiana Tshurbakova, PhD and Imre Móricz (Central Laboratory of the Székesfehérvár Light-metal Works) upon the authors' request. The test specimens were soft and hard aluminium wires partly dissolved in gallium like those mentioned above. Both specimens had been mechanically ground and polished, then etched in 0.5% HF and/or electro-polished and photomicrographic pictures were taken from them using a Neophot-32 metallurgical microscope. Thanks are epxressed for the effort also at this place.

Also the pictures given in Fig. 6 show unambigously a structure of the soft aluminium wire consisting of crystallites. The increasing diffusion of gallium into aluminium can be clearly observed. The grain structure

a)

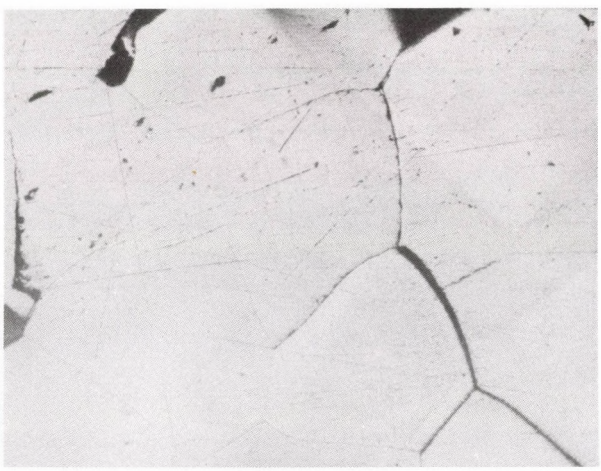

b)

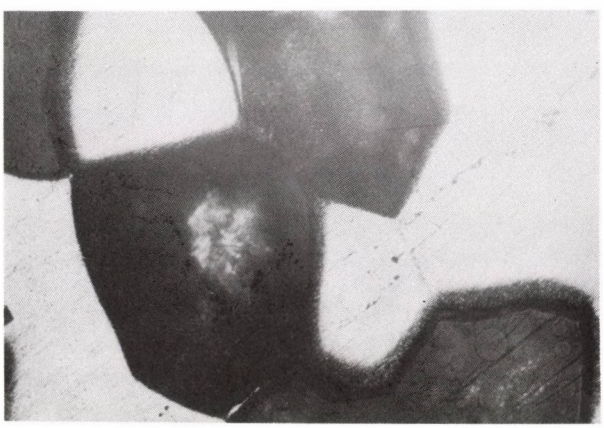

c)

Fig. 5. Grain structure of ground and polished but not etched soft aluminium wire
Magnification: 100x

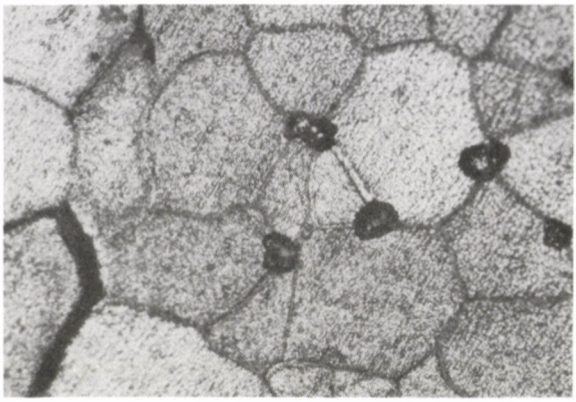

a)

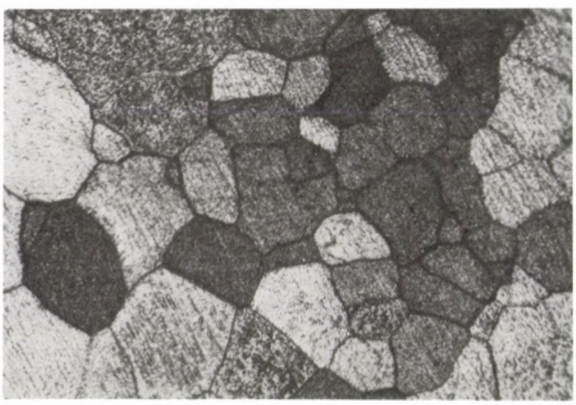

b)

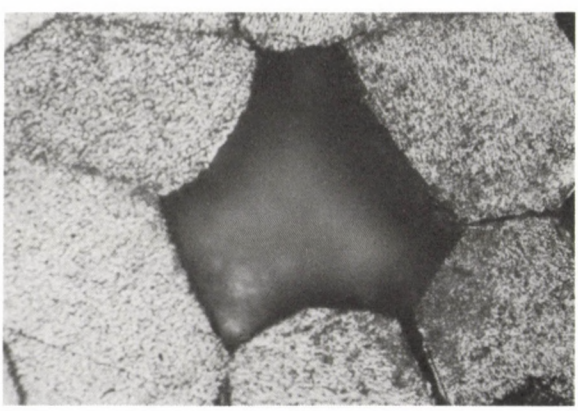

c)

Fig. 6. Grain structure of ground, polished and etched soft aluminium wire (Magnification: a) 200x; b) 100x; c) 200x)

a)

b)

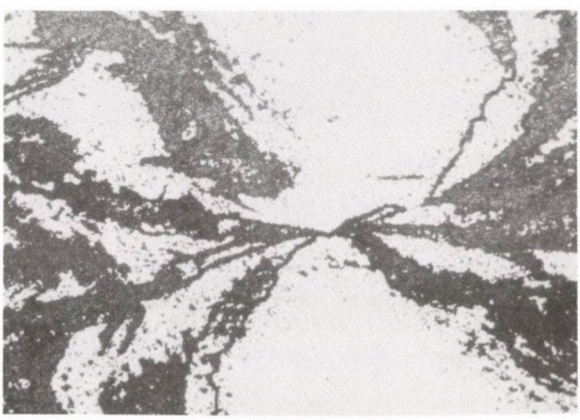

c)

Fig. 7. Grain structure of (a) electro-polished and (b, c) ground, polished and etched hard aluminium wire
(Magnification: a) 250x; b) 10x; c) 100x)

developing as a result of (surface) diffusion along the grain boundaries (Fig. 6/a,b) and later also the crystallite imperfections - dark spots - (Fig. 6/b,c) become increasingly perceptible.

At the same time, in addition to surface diffusion, also volume diffusion can be clearly recognized, especially in Fig. 6/c, as proved on the one hand by the completely different erosion of the grains as compared with pure aluminium and, on the other hand, by the small-size (pointlike) segregations ($GaAl_2$ phases). The effect of volume diffusion of gallium has been investigated also by microhardness measurement. Microhardness measurements of more grains from one to the other end of the specimen (dark spots in Fig. 6/a) detected no systematic change whereas a value of 20-22 HV was obtained as an average. As compared with soft Al of technical quality with a typical hardness of 18 HV, this value represents an increase of 10-20% in hardness and such an increase can be attributed to the volume diffusion of gallium only.

The structure of hard, electro-polished, aluminium wire can be seen in the photographs of Fig. 7, Fig. 7/a showing the surface of the longitudinal section, parallel to the direction of tension, of the specimen while the surface of the cross section of the specimen is shown in Figs 7/b,c. The pictures show a dislocation-type structure of the aluminium wire like structures typically resulting from cold forming. Penetration of gallium into a structure like this (dark strips and spots) takes place slowly and less evenly. All this suggests at the same time that gallium penetration resulted from diffusion along dislocations. However, this remains to be proved electron-microscopically /7/.

Thus our earlier assumption according to which the differences in the rate of dissolution of aluminium resulting from the differences in structure depending on the metalworking techniques is proved.

REFERENCES

1. Somosi, I.: Intensification of home production and refinement of gallium (in Hungarian), Postdoctorate thesis, 1978

2. Hungarian Patent, Budapest 1984, Registration No. 173 340

3. Hungarian Patent, Budapest, Registration No. 1512/86/71

4. Schreiter, W.: Seltene Metalle, Band I (p 207), Leipzig, 1960

5. Gusarowa, T.D. - Salavina, E.L. - Ponomarjev, V.D.: Elektrohimicheskoe isledovanie gallama aluminia. Tr. Inst. i Obog. AN. Kaz. S.S.R. 1967, No. 25. 21-24

6. Aluminium Industry II (MAT Bp, 1980)

7. Tschurbakova, T. - Móricz, I.: Testing of aluminium wire dipped in gallium (Székesfehérvár Light-metal Works, Central Laboratory, Test Report No. 78-88, 1988)

Acta Technica Acad.Sci.Hung., 103(1), pp. 49-59 (1990)

EVALUATION OF THE RESULTS OF TRANSFORMATION MEASUREMENTS

KÁLDOR, M.* - TRANTA, M.**

(Received: 10 May 1990)

There is a distinct relationship between the phase or phases constituting a metallic material. The transformations can be followed on the basis of the change of properties of the phase(s). Dilatometry is a method widely used to follow the changes in specific volume. The austenite transformation of steels can be defined both qualitatively and quantitatively on the basis of the dilatometric cooling curves. Changes of the heat content as a result of segregation and relaxation can be determined by differential analysis.

Introduction

The properties of metallic materials depend on the material composition as well as on the quality, quantity, size and arrangement of the crystals constituting the material.

Although, after all, responsibility for so to say everything falls upon composition, some material properties are still determined by the crystal structure, the phases of the material and some properties depend on the size and arrangement of the crystals constituting the phase that is on the texture of the metal.

Like every classification, also the above classification is somewhat arbitrary and inflexible. However, e.g., the specific volume is a property of the phase without doubt. The A_3 allotropic transformation of pure iron, called ferrite, into austenite is accompanied with a reduction of the specific volume. The grain size important in respect of deep-drawing capacity is essentially an anisotropic property of the texture, which can not

*Káldor, Mihály, H-1118 Budapest, Törökugrató u. 10, Hungary

**Tranta, Márta, H-3529 Miskolc, Desseffy u. 12, Hungary

Akadémiai Kiadó, Budapest

be evaluated in itself, in the knowledge of the material composition and phases constituting the material.

On the other hand, the phase is an equilibrium category and as such, independent of time and of what has happened before the phase is developing. (In this respect, a theoretical compromise is necessary at most in case of oversaturation.)

Texture as a concept implies no criteria in relation to equilibrium. Once determined, the texture reveals the complete history of the alloy.

The quality and quantity of the phases resulting in the alloy is illustrated by the equilibrium diagram of the phases.

Hence, to know the properties of metallic materials, it is necessary that the development and transformation of the phases be known.

Discussed below are the most important methods to investigate the development of phases and the texture of pure metal and alloys, namely, thermal analysis and dilatometry.

Heat content and specific volume

To follow transformations taking place in metals and alloys (including crystallization as a classic example of the transformation process controlled by long-term diffusion), measurement of the change of any property characteristic of the phases of transformation, changing as transformation advances, measurable and resulting in negligible error of measurement as compared with the extent of change, can be used as a suitable method.

Such properties are the heat content and the specific volume and, in case one of the phases is ferromagnetic, the magnetic properties that is properties which are typically "phase properties".

Time dependence shall be taken into consideration in the investigations and measurements since the processes take place as a function of time.

In accordance with the laws of nature in general, equilibrium is a ultimate state independent of time and history. The history can thus be determined only approximately in metals and alloys, especially in the course of measurements. Deviation from equilibrium is a matter of consideration in any case. Hence, the parameters belonging together shall be investigated under two aspects: relationship between the physical property and given

parameter independently of time, with respect to equilibrium and extent of deviation from equilibrium in case of given measurement.

In the course of transformation, both the quantity and the quality of the phases may change. In case of isothermal phase change, the number of degrees of freedom is zero and the composition remains unchanged in the phases taking part in the process. If the number of degrees of freedom of phase change is one, the temperature will change in the course of the process and at the same time the composition of the phases may change as well.

Accordingly, the relationship between physical characteristics and ratio of phases included in the process can be easily and unambiguously determined in case of an isothermal process. In case of a monovariant process, the parameter investigated is the temperature at the beginning and end of the process. At the same time, information can be obtained about the quality and ratio of the phases taking part in the process.

Nonvariant process are crystallization and allotropic transformation of pure metal and crystallization and eutectic or eutectoid formation of the binary process.

Isotherm indicates a nonvariant process in any diagram where the temperature is one of the variable independently of the nature of the other parameter.

The other parameter is time,e.g.,in thermal analysis or the physical property to be measured, e.g.,expansion in dilatometry (the time being here a measurement parameter, insignificant in respect of equilibrium).

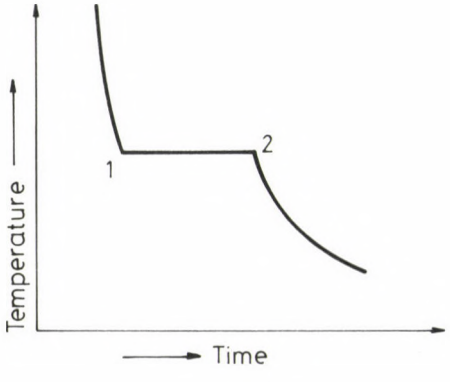

Fig. 1.

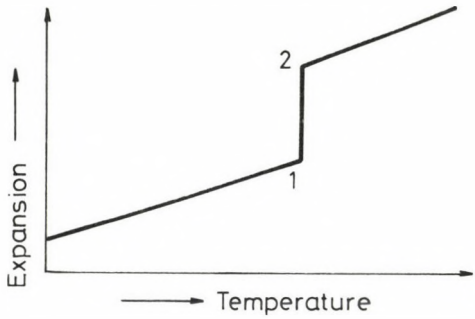

Fig. 2.

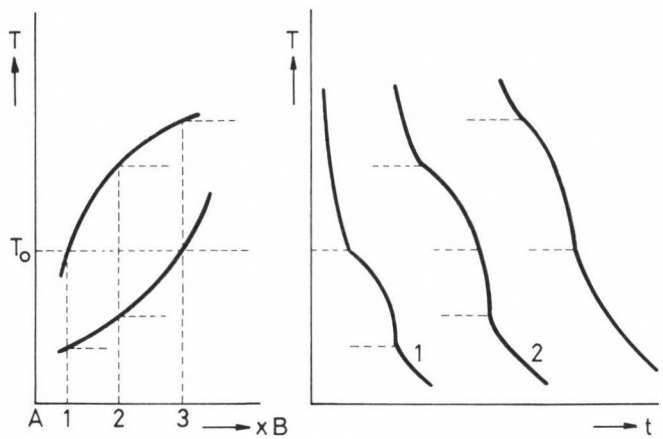

Fig. 3.

Fig. 1 shows the temperature as a function of time in the course of crystallization, allotropic transformation, eutectic crystallization and eutectoid formation in case of pure metals. On the basis of the simple additive nature of the heat content, each point of the isotherm between point 1 and 2 belongs to a definite ratio between the matrix and the product.

Hence, a definite state of the pure metal or binary alloy belongs to each point of the isotherm denoted by 1 and 2.

Fig. 2 shows the change of the specific volume in the course of the nonvariant process. Each point of the isotherm between points 1 and 2 gives, and belongs to, the specific volume corresponding to the ratio of the matrix and the product.

The changes can be defined also in case of monovariant processes.

Crystallization of the melt of a binary alloy takes place at different temperatures that is the temperature changes in the course of the process. That means at the same time that the composition of the two phases in equilibrium, the liquid phase and the crystalline phase, is different.

In an alloy crystallizing into a solid solution at a temperature T_0, a reduction in temperature results in a shift of the state of the alloy towards quantitative growth of the solid phase. Hence, the composition of the solid phase is equal to the composition of alloy No. 3 because temperature T_0 of this alloy is the solidus temperature. Similarly, the liquid phase of alloy No. 2 corresponds at this temperature to the composition of alloy No. 1 (Fig. 3). Hence, in the course of monovariant crystallization of a binary alloy, the composition of the melt corresponds to the composition of an alloy which would just start crystallizing at this temperature while the composition of the crystalline phase is equivalent to a composition which would just start melting at this temperature. Hence, the composition of the liquid phase can be found along the liquidus curve while that of the crystalline phase along the solid curve, by means of isotherm in both cases.

Accordingly, each point of the cooling curve corresponds to the presence of liquid phase and crystalline phase in combination, with a different composition each. If the composition of the melt and crystalline phases is identical, crystallization will take place at invariable temperature like in case of pure metal, eutectic or alloys where the liquidus and solidus curves are in contact. In the latter case, the degree of freedom of one, characteristic of the crystallization of binary alloys, is further reduced as a result of the identical composition of the liquid phase and crystalline phase in equilibrium.

If a nonvariant process, e.g., the allotropic transformation of pure metal, is accompanied with a change in specific volume, the two phases, the curve indicating expansion of the matrix and product and the rapid change in length, indicating change in specific volume will appear in the dilatometric diagram. The two curves are almost straight, the angular coefficient being the coefficient of linear expansion. The coefficient of expansion is a basic property of the phase as suggested by the fact that the coefficient of expansion of the austenite is only slightly affected, if indeed at all, by the composition. There is little difference between the coefficients of expansion of the austenite in case of pure metal and stainless steel. Also the coefficient of expansion of ferrite changes only slightly while its

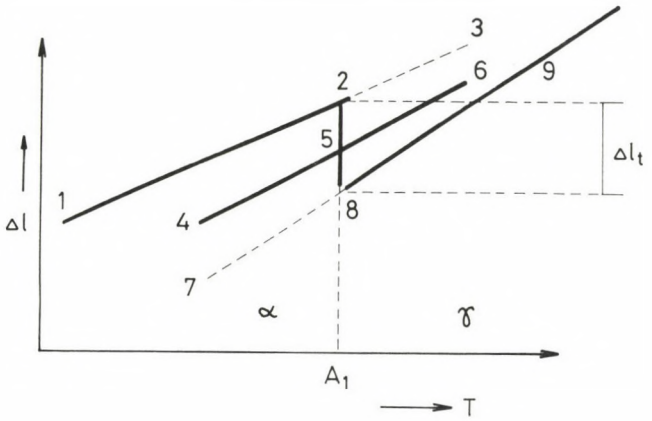

Fig. 4.

value is approximately identical for unalloyed steel, pure metal or chromium steel.

In the course of transformation taking place in metals or alloys, the phase change is accompanied with a change Δl_t in the length of the specimen (Fig. 4).

As has been mentioned earlier, the ratio of phases α and γ changes between points 2 and 8, the phase of the material being α at point 2 while γ at point 8 and each point corresponds to a definite ratio of phases α and γ between 2 and 8.

Any of the three sections of the diagram can be considered as a reference curve as well.

This means that the relationship between change in the length of the specimen and temperature is shown by curves 1, 2, 8 and 9.

A certain ratio of phases α and γ belongs to point 5.

If the workpiece is heated or cooled from this temprature in such a way that the allotropic transformation can be suppressed or hindered, expansion of the workpiece will be described by coefficient of expansion

$$\beta = m\beta_\alpha + n\beta_\gamma ,$$

where

m ratio of phase α,

n ratio of phase γ,

(m+n21),

β coefficients of expansion of the different phases.

Hence, the change in length upon heating will be described by curves 1, 2, 5, 6 if the transformation is interrupted at the transformation temperature to which point 5 belongs.

In case of cooling, the change in length can be described by points 9, 8, 5 and 4 provided the transformation takes place only partially (over the section before point 5).

Hence, the expansion curves can be lengthened by extrapolation in the direction of points 1, 2, 3 and 9, 8, 7, respectively.

This assumption certainly holds within certain limits.

Evaluation of curves 4, 5, 6 of the diagram outlined above assumes, in addition to suppressibility of the allotropic transformation, that the coefficient of expansion is an additive quantity. Obviously, this can be an approximation only as it depends e.g. on the arrangement of the crystals constituting the phase. Changes in length resulting from stresses due to the different expansion contribute to the effect.

Dilatometry and thermal analysis

Supercooling or superheating always necessary for an allotropic transformation is the driving force of phase change. The change in length accompanying the phase change in supercooled or superheated state is different from that in the state of equilibrium, it depends on the value of the coefficient of expansion of the two phases and on whether the transformation takes place at a temperature higher or lower than the equilibrium temperature that is in the course of heating or cooling.

Dilatometry has become most significant in investigation of the conditions of transformation of steels. The change in specific volume accompanying transformations is measurable and permits the temperature of the transformation process to be determined as a function of the way and rate of heating or cooling.

The specific volume of iron-carbon alloys increases monotonously with increasing temperatures up to temperature A_{c1} where the specific volume reduces as a result of austenitic transformation of pearlite. At temperatures above A_{c1} but below A_{c3}, the specific volume is rather diversified. The specific volume of ferrite and austenite equally increases whereas the specific volume reduces with increasing quantities of austenite and reducing quantities of ferrite.

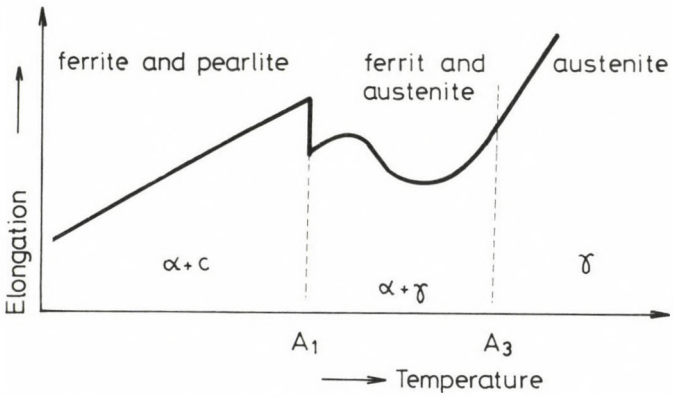

Fig. 5.

The change in specific volume of low-carbon alloys - in the length of the specimen - as a function of time is illustrated in Fig. 5.

Isothermally, the pearlite undergoes an austenitic transformation at temperature A_{c1}. In practice, the linear contraction takes place rather within narrow temperature limits than isothermally considering that, on the one hand, steel is a multicomponent alloy and, on the other hand, the driving force of austenitic transformation is a gradual superheating.

In an alloy of higher carbon content, the austenitic transformation of the pearlite results in an austenite-ferrite ratio in the texture which would develop in case of an alloy of lower carbon content at higher temperatures only. Hence, the change in specific volume is similar in character while, because of the lower temperature, the same ratio corresponds to a different specific volume.

Steel is typically an alloy where the allotropic transformation can be retarted in case of cooling. As a result, a bainitic, martensitic, residual-austenitic structure is brought about instead of a ferritic-pearlitic structure.

In case of given steel, the rate of cooling determines the hysteresis of the transformation that is essentially the temperature or temperature interval where the transformation takes place while the temperature determines the structural element or phase developing, the properties of which (first of all the mechanical properties) being essentially the characteristics of the steel. The possible extent of the hysteresis is determined, in addition to the rate of cooling, by the composition of the austenite, the size of the austenite crystals.

As a result of transformation of the austenite, the steel texture becomes ferritic-pearlitic, bainitic or martensitic. The fundamental phase of bainite is ferrite with cementite appearing in it but also non-transformed austenite may occur in bainite. Essentially, the martensite shall be considered ferrite strongly supersaturated with carbon. In the martensitic structure, residual austenite is necessarily present in any case.

Concerning coefficient of expansion of the different structural components or phases, there is little difference between martensite, bainite and ferrite. The coefficient of expansion of a material of martensitic structure is increased by residual austenite present in an amount depending mainly on the carbon content, the extent of increase depending on the quantity of residual austenite. The value of the coefficient of expansion of bainite also lies near the value for ferrite. Cementite present in the ferrite and the residual austenite mentioned changes the value of the coefficient, the effect of cementite being negligible and that of the residual austenite is similarly insignificant as the quantity of residual austenite itself is insignificant.

Of course, austenite transformation is always accompanied with an increase in specific volume. According to what has been said, the lower the temperature of transformation, the higher the increase in specific volume. Hence, martensitic transformation is accompanied with maximum, bainitic transformation with medium while ferritic-pearlitic transformation with minimum increase in the specific volume.

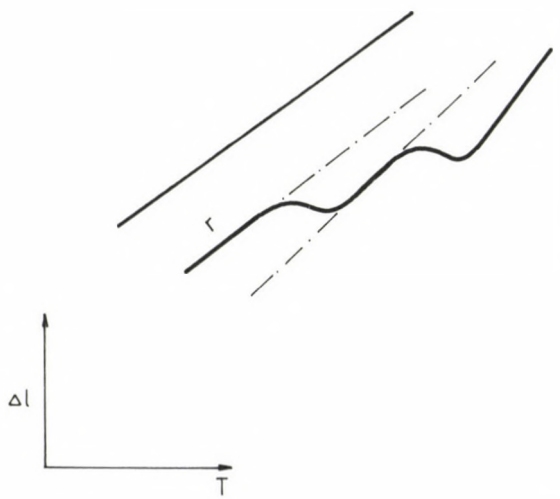

Fig. 6.

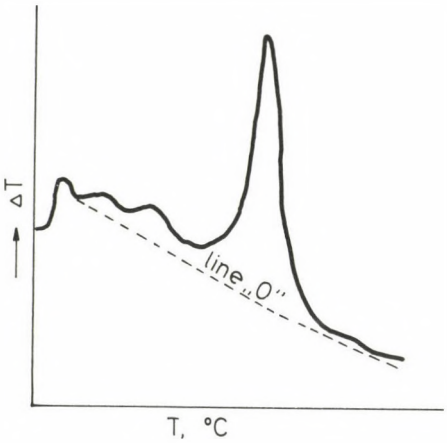

Fig. 7.

The expansion and the temperature of transformation are a priori an indicator of the quality of the transformation product.

The distance between tangents drawn to the starting point and end point of the expansion curve, measured parallel to the axis of expansion, is a good approximation to the quantity of austenite undergoing transformation (Fig. 6).

The accurate value can not be specified because of the changes in composition and the stresses arising.

In case of more transformations taking place one after the other, more straights can be drawn as tangents towards the same point. The transformations can be distinguished, the temperature is unambiguously characteristic of the way of transformation while the quantity of the texture developed can be estimated.

There is a difference of an order of magnitude between the change in heat content accompanying the transformations and the change in crystallization heat, the latter being 0.1 eV/atom while the former 0.01 eV/atom. Temperatures typical of crystallization can be measured by thermal analysis while differential thermal analysis shall be used to investigate the conditions of transformations.

The difference between the specimen temperature and reference temperature is a function of reference temperature in case the process resulting in heat release or absorption fails to take place in the specimen in the course of heating. The change in heat content resulting from segregation and relaxation appears as a deviation from the reference line and the temperature of the process can be unambiguously determined.

REFERENCES

1. Reed, R.E. - Hill: Physical Metallurgy Principles, D. van Nostrand Co., 1973
2. Prohászka, J.: Introduction into materials science (in Hungarian), Tankönyvkiadó, 1988, Budapest
3. Verő, J. - Káldor, M.: Science of Metal, Tankönyvkiadó, 1977, Budapest

ENGINEERING

Proceedings of the Ninth Danube-European Conference on Soil Mechanics and Foundation Engineering

Budapest, October 2-5, 1990

edited by

PETRASOVITS, G.

The Ninth Danube-European Conference on Soil Mechanics and Foundation Engineering was held in Budapest from 2nd to 5th of October 1990.

The idea of this Regional Conference was initiated more than twenty years ago and the first Danube-European Conference was jointly organized by the Austrian and Hungarian National Committees of ISSMFE. Since this time practically all of the Danube Countries have been hosts to these Regional Conferences and the good cooperation between the member Societies stimulated keeping this good ideal alive.

The main topic of this Ninth Danube-European Conference on Soil Mechanics and Foundation Engineering:

"Deep Geotechnical Works in Urban Areas"

was chosen by the representatives of the ISSMFE National Committees of the Danubian Countries.

The Proceedings contains 70 papers contributed by authors from 18 countries. These papers were selected from more than 120 abstracts submitted to the Organizing Committee.

Readership: specialists in soil mechanics and foundation engineering

Studies in English and German. 1190. XII + 555 pages. Numerous figures and tables. 17x25 cm. Hardbound $66.00
ISBN 963 05 5898 X

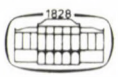

Akadémiai Kiadó, Budapest

Emil MOSONYI

WATER POWER DEVELOPMENT

In two volumes

Third, enlarged and completely revised edition

Volume 1: **Low-Head Power Plants**

1074 pages. 320 photos. 430 figures. 7 supplements
17x25 cm. Hardbound $99.00 ISBN 963 05 4271 4

Volume 2: **High-Head Power Plants**

In two parts
Forthcoming. Approx. 1280 pages. 750 figures. 4 supplements
17x25 cm. Hardbound Approx. $135.00 ISBN 963 05 5885 8

After a few decades' decline in water power utilization, this type of electric power generation is receiving renewed interest all over the world. This fact encouraged both author and publisherto produce a completely updated third edition of this book.

The book reflects the author's vast experience in research, modelling techniques, planning, construction and concerning various types of power projects and multipurpose hydroelectric master plans.

Volume I presents all types of hydropower resources and a classification of plant types, including the possibilities of the utilization of tidal potentials and wave power conversion. It covers the procedures of planning the station of low-head development as power estimate, selection of plant arrangement, civil structures, machinery, aesthetic and environmental aspects.

Volume II presents all new achievements in classical high-head utilization.The chapters dealing with the procedures of preliminary planning and of selecting the turbine are largely extended, including a detailed interpretation of the performance diagrams. The technical descriptions and illustrations of numerous projects completed since the publication of the first two editions have been included.

This reference book is written especially for experts engaged in the overall planning and design of hydroelectric projects.

ORDER FORM

Please send to your bookseller or to KULTURA Hungarian Foreign Trading Co.
P.O. Box 149, H-1389 Budapest, Hungary

Please send me/us

..... copy(ies) of
Water Power Development
Vol. I. Low-Head Power Plants

..... copy(ies) of
Water Power Development
Vol. II. High-Head Power Plants

by Emil MOSONYI

Price: $99.00
ISBN 963 05 4271 4

Price: Approx. $135.00
ISBN 963 05 5885 8

Name:
Address:
Date, signature:
(Postage and packing: charged as per weight)

O Check enclosed
O Please send invoice (for institutions only)

Akadémiai Kiadó, Budapest

NOTICE TO CONTRIBUTORS

Papers in English* are accepted condition that they have not been previously published or accepted for publication.

Manuscripts in two copies (the original type-written copy plus a clear duplicate one) complete with figures, tables, and references should be sent to

Acta Technica
Nádor u. 7. I. 118
Budapest, Hungary
H-1051

Although every effort will be made to guard against loss, it is advised that authors retain copies of all material which they submit. The editorial board reserves the right to make editorial changes.

Manuscripts should be typed double-spaced on one side of good quality paper with proper margins and bear the title of the paper and the name(s) of the author(s). The full postal address(es) of the author(s) should be given in a footnote on the first page. An abstract of 50 to 100 words should precede the text of the paper. The approximate locations of the tables and figures should be indicated on the margin. An additional copy of the abstract is needed. Russian words and names should be transliterated into English.

References. Only papers closely related to the author's work should be referred to. The citations should include the name of the author and/or the reference number in brackets. A list of numbered references should follow the end of the manuscript.

References to periodicals should mention: (1) name(s) and initials of the author(s); (2) title of the paper; (3) name of the periodical; (4) volume; (5) year of publication in parentheses; (6) numbers of the first and last pages. Thus: 5. Winokur, A., Gluck, J.: Ultimate strength analysis of coupled shear walls. American Concrete Institute Journal 65 (1968) 1029-1035

References to books should include: (1) author(s)' name; (2) title; (3) publisher; (4) place and year of publication. Thus: Timoshenko, S., Gere, J.: Theory of Elastic Stability. McGraw-Hill Company, New York, London 1961.

Illustrations should be selected carefully and only up to the necessary quantity. Black-and-white photographs should be in the form of glossy prints. The author's name and the title of the paper together with the serial number of the figure should be written on the back of each print. Legends should be brief and attached on a separate sheet. Tables, each bearing a title, should be self-explanatory and numbered consecutively.

Authors will receive proofs which must be sent back by return mail.

Authors will receive 50 reprints free of charge.

*Hungarian authors can submit their papers also in Hungarian.

Periodicals of the Hungarian Academy of Sciences are obtainable at the following addresses:

AUSTRALIA
C.B.D. LIBRARY AND SUBSCRIPTION SERVICE
39 East Splanade
P.O. Box 1001, Manly N.S.W. 2095

AUSTRIA
GLOBUS, Höchstädtplatz 3, *1206 Wien XX*

BELGIUM
OFFICE INTERNATIONAL DES PERIODIQUES
Avenue Louise, 485, *1050 Bruxelles*
E. STORY-SCIENTIA P.V.B.A.
P. van Duyseplein 8, *9000 Gent*

BULGARIA
HEMUS, Bulvar Ruszki 6, *Sofia*

CANADA
PANNONIA BOOKS, P.O. Box 1017
Postal Station "B", *Toronto, Ont. M5T 2T8*

CHINA
CNPICOR, Periodical Department, P.O. Box 50
Peking

CZECH AND SLOVAK FEDERAL REPUBLIC
MAD'ARSKA KULTURA, Národni třida 22
11566 Praha
PNS DOVOZ TISKU, Vinohradská 46, *Praha 2*
PNS DOVOZ TLAČE, *Bratislava 2*

DENMARK
EJNAR MUNKSGAARD, 35, Nørre Søgade
1370 Copenhagen K

FEDERAL REPUBLIC OF GERMANY
KUNST UND WISSEN ERICH BIEBER
Postfach 10 28 44
7000 Stuttgart 10

FINLAND
AKATEEMINEN KIRJAKAUPPA, P.O. Box 128
00101 Helsinki 10

FRANCE
DAWSON-FRANCE S.A., B.P. 40, *91121 Palaiseau*
OFFICE INTERNATIONAL DE DOCUMENTATION ET LIBRAIRIE, 48 rue Gay-Lussac
75240 Paris, Cedex 05

GREAT BRITAIN
BLACKWELL'S PERIODICALS DIVISION
Hythe Bridge Street, *Oxford OX1 2ET*
BUMPUS, HALDANE AND MAXWELL LTD.
Cowper Works, *Olney, Bucks MK46 4BN*
COLLET'S HOLDINGS LTD., Denington Estate,
Wellingborough, Northants NN8 2QT
WM DAWSON AND SONS LTD., Cannon House
Folkstone, Kent CT19 5EE

GREECE
KOSTARAKIS BROTHERS INTERNATIONAL BOOKSELLERS, 2 Hippokratous Street, *Athens-143*

HOLLAND
FAXON EUROPE, P.O. Box 167
1000 AD Amsterdam
MARTINUS NIJHOFF B. V.
Lange Voorhout 9–11, *Den Haag*
SWETS SUBSCRIPTION SERVICE
P.O. Box 830, 2160 Sz Lisse

INDIA
ALLIED PUBLISHING PVT. LTD.
750 Mount Road, *Madras 600002*
CENTRAL NEWS AGENCY PVT. LTD.
Connaught Circus, *New Delhi 110001*
INTERNATIONAL BOOK HOUSE PVT. LTD.
Madame Cama Road, *Bombay 400039*

ITALY
D. E. A., Via Lima 28, *00198 Roma*
INTERSCIENTIA, Via Mazzé 28, *10149 Torino*
LIBRERIA COMMISSIONARIA SANSONI
Via Lamarmora 45, *50121 Firenze*

JAPAN
KINOKUNIYA COMPANY LTD.
Journal Department, P.O. Box 55
Chitose, *Tokyo 156*
MARUZEN COMPANY LTD., Book Department
P.O. Box 5050 Tokyo International, *Tokyo 100-31*
NAUKA LTD., Import Department
2-30-19 Minami Ikebukuro, Toshima-ku, *Tokyo 171*

KOREA
CHULPANMUL, *Phenjan*

NORWAY
S.A. Narvesens Litteraturjeneste
Box 6125, Etterstad
1000 Oslo

POLAND
WĘGIERSKI INSTYTUT KULTURY
Marszalkowska 80, *00-517 Warszawa*
CKP I W, ul. Towarowa 28, *00-958 Warszawa*

ROUMANIA
D. E. P., *Bucuresti*
ILEXIM, Calea Grivitei 64–66, *Bucuresti*

SOVIET UNION
SOYUZPECHAT — IMPORT, *Moscow*
and the post offices in each town
MEZHDUNARODNAYA KNIGA, *Moscow G-200*

SPAIN
DIAZ DE SANTOS Lagasca 95, *Madrid 6*

SWEDEN
ESSELTE TIDSKRIFTSCENTRALEN
Box 62, *101 20 Stockholm*

SWITZERLAND
KARGER LIBRI AG, Petersgraben 31, *4011 Basel*

USA
EBSCO SUBSCRIPTION SERVICES
P.O. Box 1943, *Birmingham, Alabama 35201*
F. W. FAXON COMPANY, INC.
15 Southwest Park, *Westwood Mass. 02090*
MAJOR SCIENTIFIC SUBSCRIPTIONS
1851 Diplomat, P.O. Box 819074,
Pallas, Tx. 75381-9074
REDMORE PUBLICATIONS, Inc.
22 Cortlandt Street, New York, N.Y. 1007

YUGOSLAVIA
JUGOSLOVENSKA KNJIGA, Terazije 27, *Beograd*
FORUM, Vojvode Mišića 1. *21000 Novi Sad*

HU ISSN 0865-7440

Index: 26.025

ACTA TECHNICA

ACADEMIAE SCIENTIARUM HUNGARICAE

EDITOR-IN-CHIEF: P. MICHELBERGER

VOLUME 103
NUMBERS 2—3

CIVIL ENGINEERING — C/4

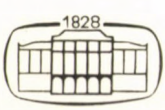

AKADÉMIAI KIADÓ, BUDAPEST 1990

ACTA TECHNICA

A JOURNAL OF THE HUNGARIAN ACADEMY OF SCIENCES

CENTRAL EDITORIAL BOARD

T. CZIBERE, K. GÉHER, L. KOLLÁR, P. MICHELBERGER (EDITOR-IN-CHIEF),
A. LÉVAI, J. PROHÁSZKA, K. REMÉNYI, J. SZABÓ,
GY. CZEGLÉDI (MANAGING EDITOR)

EDITORIAL COMMITTEE FOR MATERIAL SCIENCES AND TECHNOLOGY (SERIES T.)

M. HORVÁTH, Z. HORVÁTH,
J. PROHÁSZKA (CHAIRMAN), J. TALABÉR

Acta Technica publishes original papers, preliminary reports and reviews in English, which contribute to the advancement of engineering sciences.
Acta Technica is published by

AKADÉMIAI KIADÓ
Publishing House of the Hungarian Academy of Sciences
H-1117 Budapest, Prielle K. u. 19—35.

Subscription information

Orders should be addressed to

KULTURA Foreign Trading Company
H-1389 Budapest P.O. Box 149

or to its representatives abroad

Acta Technica is abstracted/indexed in Applied Mechanics Reviews, Current Contents–Engineering, Technology and Applied Sciences, GeoRef Information System, Science Abstracts.

© *Akadémiai Kiadó, Budapest*

CONTENTS

Bertóti, E.: Investigation of thick cylindrical shells under axisymmetric loads by asymptotic integration of the dual system of equations 61

Ecsedi, I.: Bounds for the deflection of beams of variable cross-section 91

Hegedűs, I.: Analytical solutions for discrete boundary value problems of macroscopically isotropical Hrennikoff-type grids 103

Jankó, L. - Nagy, Z.: The influence of the displacement spring rigidity on the critical load of bars 115

Keshava Murthy, K. - Jayaram, N.: A new investigation on parabolic weirs - proportional parabolic weirs 143

Kollár, L.P.: Buckling of generally anisotropic (aeolotropic) shallow shells 171

Kollár, P.W.: Determination of the erection shape for a single-mast rotationally symmetrical cable net in case of a specific variation of the tensile force 191

Sharaf, A.: New aspects of drip irrigation hydraulics 203

Acta Technica Acad. Sci. Hung., 103(2-3), pp. 61-89 (1990)

INVESTIGATION OF THICK CYLINDRICAL SHELLS UNDER AXISYMMETRIC LOADS BY ASYMPTOTIC INTEGRATION OF THE DUAL SYSTEM OF EQUATIONS

BERTÓTI, E.*

(Received: 20 November 1989)

A three-dimensional, linear shell theory with stresses as configuration variables is applied to determine axisymmetric deformations of circular cylindrical shells. Asymptotic integration of the dual equation system is used as a numerical method. Using a computer program developed by the author for calculation, some numerical problems with typical loads are presented. The solutions obtained by asymptotic integration of the dual equation system are compared with those obtained by use of the technical theory of shells. Since the asymptotic shell theory can be applied to both thin and thick shells, it is possible to investigate how the error of the technical theory of shells increases with increasing shell thickness and whether approximation of the distribution of variables along the thickness of the shell by linear functions is acceptable or not.

1. Introduction

In dual system of elasticity stress functions or stresses are the configuration variables /10/. A three-dimensional, linear shell theory with stresses as configuration variables and the asymptotic integration of its equations are presented in /6/, /7/ and /2/. No particular assumptions have been introduced into this shell theory and therefore the stresses and strains can be determined at any point of the shell to arbitrary accuracy by asymptotic integration of the dual system of equations (equilibrium equations, Hooke's law, independent compatibility equations) for both thin and thick shells. Displacements can be calculated from strains by integration.

Application of the above-mentioned theory to axisymmetric deformation of cylindrical shells has been presented in a previous paper /1/. After a brief review of previous results, this paper presents the equations ob-

*Bertóti, Edgár, H-3535 Miskolc, Hegyalja út 215, Hungary

Akadémiai Kiadó, Budapest

tained in /1/ in a numerically integrable form. Then the dual form for stress and displacement boundary conditions are given and the process of asymptotic integration is presented.

Considering the asymptotic method as a numerical method, a computer program has been developed and numerical examples have been tested by the author. The results obtained by asymptotic integration of the dual system of equations are compared with those obtained by the technical theory of shells based on the Kirchhoff-Love hypothesis. Since the asymptotic method can be applied also to thick shells the examples show how the error of the technical theory of shells increases with increasing shell thickness and whether approximations of stresses, strains and displacements by linear functions along the thickness of the shell is acceptable or not.

2. Summary of results obtained for cylindrical shells in /1/

2.1. Geometry

Let A^+ and A^- denote the faces while A_1^* and A_2^* the lateral surfaces of the cylindrical shell of thickness 2b and of length ℓ. Let S denote the middle surface of radius R_0 and let h_1^* and h_2^* denote the boundary curves of S (Fig. 1). The shell middle surface S with a system of cylindrical coordinates $x^1 = s$, $x^2 = \varphi$, $x^3 = z$ on it is shown in Fig. 2.

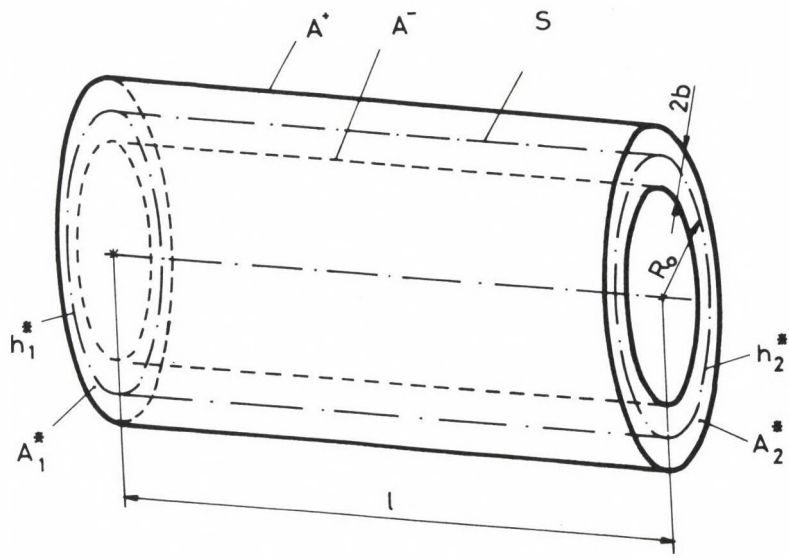

Fig. 1. Cylindrical shell, notation

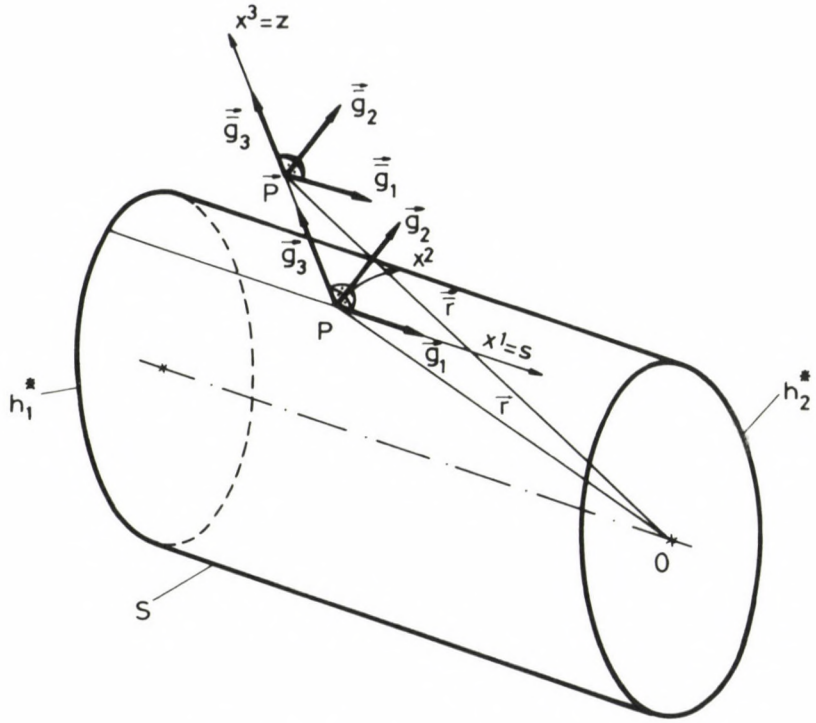

Fig. 2. Middle surface, coordinate systems

Let us introduce the non-dimensional coordinate

$$\zeta = \frac{x^3}{b} \tag{2.1}$$

measured along the normal to the middle surface and the non-dimensional parameter

$$\lambda = \frac{R_0}{b} \quad . \tag{2.2}$$

Let so-called shifted tensors defined at points P of the middle surface S be used to describe the three-dimensional deformation of the cylindrical shell. Dependence of an arbitrary shifted tensor $\overline{h}^k{}_\ell$ on coordinate ζ (on x^3) can be expressed by a polynomial with terms of finite number:

$$\overline{h}^k{}_\ell\,(x^1, x^2, x^3) = \sum_{i=0}^{n} (h_i)^k{}_\ell(x^1, x^2)\,\zeta^i \quad , \tag{2.3}$$

where the three-dimensional tensors $(h_i)^k{}_\ell\,(x^1, x^2)$; (i = 0,1,2,...,n) are the surface factors of the tensor h^k_ℓ (see /2/, /7/).

2.2. Shell problems in dual system

Configuration variables of the linear, dual shell theory (/6/, /7/) applied in this paper are the stress surface factors $(\sigma_i)^{k\ell}$. The shell is considered to be a homogeneous, isotropic, three-dimensional continuum and the following dual system of equations should be fulfilled on the shell's middle surface S:

- equilibrium equations,
- Hooke's law,
- independent compatibility equations and
- equations of compatibility in the large.

Appearing as additional variables in the above equations are the strain surface factors $(\varepsilon_i)_{k\ell}$; (i = 0,1,2,...) and the incompatibility surface factors $(\eta_i)^{ab}$; (i = 0,1,2,...).

If the number of two-dimensional equations in terms of surface factors is sufficiently large then also the three-dimensional equations and boundary conditions will be satisfied to any desirable accuracy.

Displacement surface factors $(u_i)_k$; (i = 0,1,2,...) are not appearing as variables in the dual system of equations. Displacements can be calculated by integration of strains (Cesaro's formula /2/).

To solve the above dual system of equations, stress boundary conditions are prescribed on faces A^+ and A^- while stress or/and displacement boundary conditions on lateral surfaces A_1^* and A_2^* of the shell (for details see Section 4). Stress boundary conditions prescribed on the faces are considered as field equations (see /7/, /1/).

2.3. Asymptotic integration of the dual system of equations

In accordance with the number of surface factors also the number of equations and boundary conditions in terms of surface factors may be infinitely large. Asymptotic integration of the system of equations means determination of the approximations denoted by I, II, III,... .

Approximation is started any time with calculation of the basic solution of equations of finite number. In the knowledge of the basic solution, surface factors of higher order can be calculated to arbitrary order number.

In approximation I, the stress boundary conditions on the faces are not accurately satisfied. They shall therefore be modified using the results of approximation I. In this way, we have the equation system of approximation II. After determination of the surface factors of lower and higher order for approximation II and modification of the boundary conditions on the faces, approximation III can be calculated, and so on.

Main iteration of the asymptotic method is the series of approximations I, II, III, ..., while determination of the basic solution and surface factors of higher order are the subiteration of the method. The number of both the main iteration and subiteration steps can be determined by investigation of the order of magnitude of the surface factors (see /7/, /1/).

As a result of asymptotic integration of the dual equation system, the three-dimensional deformation of the shell can be determined to any desirable accuracy.

2.4. Dual system of equations in terms of surface factors for cylindrical shells

Considered now are cylindrical shells under axisymmetric loads, using the physical components of the tensors. The surface factors depend only on coordinate $x^1 = s$. Differentiation with respect to $x^1 = s$ is denoted by a comma in superscript.

The physical components of the stress and strain tensors are

$$(\sigma_i)_s,\ (\sigma_i)_\varphi,\ (\tau_i)_{sz},\ (\sigma_i)_z;\quad i = 1,2,2,\ldots,$$

and

$$(\varepsilon_i)_s,\ (\varepsilon_i),\ (\varepsilon_i)_{sz},\ (\varepsilon_i)_z;\ i = 0,1,2,\ldots,$$

respectively. The surface factors of mass forces are denoted by $(q_i)_s$ and $(q_i)_z$; $(i = 0,1,2,\ldots)$. The components of surface loads on the faces $\underline{A}^+$ and $\underline{A}^-$ are denoted by $(p^+)_s$, $(p^+)_z$ and $(p^-)_s$, $(p^-)_z$, respectively.

2.4.1. Equations of approximation I

The basic solution of approximation I is obtained as a solution of the differential equation system written with stress surface factors

$$(\sigma_0)_s,\ (\sigma_0)_\varphi,\ (\tau_0)_{sz},\ (\sigma_0)_z,$$

$$(\sigma_1)_s,\ (\sigma_1)_\varphi,\ (\tau_1)_{sz},\ (\sigma_1)_z, \tag{2.4}$$

$$(\tau_2)_{sz},\ (\sigma_2)_z\ .$$

The system of ordinary differential equations /1/:

$$(E_0)_s = R_0(\sigma_0)'_s + (\tau_0)_{sz} + \lambda(\tau_1)_{sz} + R_0(q_0)_s = 0\ , \tag{2.5}_1$$

$$(E_0)_z = R_0(\tau_0)'_{sz} + (\sigma_0)_z - (\sigma_0)_\varphi + \lambda(\sigma_1)_z + R_0(q_0)_z = 0, \tag{2.5}_2$$

$$(E_1)_s = R_0(\sigma_1)'_s + (\tau_1)_{sz} - \frac{1}{\lambda}(\tau_0)_{sz} + 2\lambda(\tau_2)_{sz} + R_0(q_1)_s = 0\ , \tag{2.5}_3$$

$$(E_1)_z = R_0(\tau_1)'_{sz} + (\sigma_1)_z - \frac{1}{\lambda}(\sigma_0)_z - (\sigma_1)_\varphi + \frac{1}{\lambda}(\sigma_0)_\varphi +$$

$$+ 2\lambda(\sigma_2)_z + R_0(q_1)_z = 0\ , \tag{2.5}_4$$

$$(\tilde{\eta}_0)_{sz} = (1+\nu)\left[(\sigma_0)_z - (\sigma_0)_\varphi\right] +$$

$$+\lambda\left[\nu(\sigma_1)_s + \nu(\sigma_1)_z - (\sigma_1)_\varphi\right] = 0\ , \tag{2.5}_5$$

$$(\eta_0)_z = R_0^2\left[(\sigma_0)''_{\varphi} - \nu(\sigma_0)''_z - \nu(\sigma_0)''_s\right] - 2R_0(1+\nu)(\tau_0)'_{sz} +$$

$$+\lambda\left[(\sigma_1)_s - \nu(\sigma_1)_\varphi - \nu(\sigma_1)_z\right] = 0\ , \tag{2.5}_6$$

$$(\tau_0)_{sz} + (\tau_2)_{sz} = \frac{1}{2}\left[(p^+)_s - (p^-)_s\right] = p_1\ , \tag{2.5}_7$$

$$(\sigma_0)_z + (\sigma_2)_z = \frac{1}{2}\left[(p^+)_z - (p^-)_z\right] = p_2\ , \tag{2.5}_8$$

$$(\tau_1)_{sz} = \frac{1}{2}\left[(p^+)_s + (p^-)_s\right] = p_3\ , \tag{2.5}_9$$

$$(\sigma_1)_z = \frac{1}{2}\left[(p^+)_z + (p^-)_z\right] = p_4\ . \tag{2.5}_{10}$$

Sign $\sim$ above η on the left-hand side of the equation $(2.5)_5$ indicates that $(2.5)_5$ is obtained from the independent compatibility equation $(\eta_0)_{sz} = 0$ after integration with respect to s. According to /1/, this equation is the so-called equation of compatibility in the large.

In the knowledge of the basic solution obtained by integration of $(2.5)_{1-10}$, the surface factors of higher order can be calculated by means of equations not used so far, that is equilibrium equations

$$(E_{i+2})_s = R_0(\sigma_{i+2})'_s + \sum_{j=0}^{i+2} (-\frac{1}{\lambda})^{i+2-j} (\tau_j)_{sz} + \\ + (i+3)\lambda(\tau_{i+3})_{sz} + R_0(q_{i+2})_s = 0 \quad , \qquad (2.6)_1$$

$$(E_{i+2})_z = R_0(\tau_{i+2})'_{sz} + \sum_{j=0}^{i+2} (-\frac{1}{\lambda})^{i+2-j} \left[(\sigma_j)_z - (\sigma_j)_\varphi\right] + \\ + (i+3)\lambda(\sigma_{i+3})_z + R_0(q_{i+2})_z = 0 \quad ; \qquad i = 0,1,2,\ldots, \qquad (2.6)_2$$

and independent compatibility equations

$$(\eta_i)_s = (i+1)(i+2)\lambda^{i+1}(\varepsilon_{i+2})_\varphi + \\ + (-1)^i \sum_{j=0}^{i} (-\lambda)^j (j+1)\left[2(\varepsilon_{j+1})_\varphi - (\varepsilon_{j+1})_z\right] = 0 \quad , \qquad (2.7)_1$$

$$(\eta_i)_\varphi = (i+1)(i+2)\lambda^2(\varepsilon_{i+2})_s + R_0^2(\varepsilon_i)''_z - \\ - 2(i+1)\lambda R_0(\varepsilon_{i+1})'_{sz} = 0 \quad ; \qquad i = 0,1,2,\ldots \quad . \qquad (2.7)_2$$

The relationship between the strain and stress surface factors is given by Hooke's law

$$(\varepsilon_i)_s = \frac{1}{2G}\frac{1}{1+\nu}\left[(\sigma_i)_s - \nu(\sigma_i)_\varphi - \nu(\sigma_i)_z\right] \quad , \qquad (2.8)_1$$

$$(\varepsilon_i)_\varphi = \frac{1}{2G}\frac{1}{1+\nu}\left[(\sigma_i)_\varphi - \nu(\sigma_i)_z - \nu(\sigma_i)_s\right] \quad , \qquad (2.8)_2$$

$$(\varepsilon_i)_z = \frac{1}{2G}\frac{1}{1+\nu}\left[(\sigma_i)_z - \nu(\sigma_i)_s - \nu(\sigma_i)_\varphi\right] \quad , \qquad (2.8)_3$$

$$(\varepsilon_i)_{sz} = (\varepsilon_i)_{zs} = \frac{1}{2G}(\tau_i)_{sz} = \frac{1}{2G}(\tau_i)_{zs} \quad ; \quad i = 0,1,2,\ldots, \qquad (2.8)_4$$

where ν is Poisson's ration and G is the shear modulus.

2.4.2 Determination of approximation II, III, ... etc.

Using the results of approximation I, stress boundary conditions satisfied approximately on the faces of the shell with equations $(2.5)_{7-10}$ are modified as follows:

$$(\tau_0)_{sz} + (\tau_2)_{sz} = p_1 - (\tau_4^I)_{sz} - (\tau_6^I)_{sz} - \dots \quad , \tag{2.9}_1$$

$$(\sigma_0)_z + (\sigma_2)_z = p_2 - (\sigma_4^I)_z - (\sigma_6^I)_z - \dots \quad , \tag{2.9}_2$$

$$(\tau_1)_{sz} = p_3 - (\tau_3^I)_{sz} - (\tau_5^I)_{sz} - \dots \quad , \tag{2.9}_3$$

$$(\sigma_1)_z = p_4 - (\sigma_3^I)_z - (\sigma_5^I)_z - \dots \quad . \tag{2.9}_4$$

The basic solution of approximation II can be obtained from $(2.5)_{1-6}$ and $(2.9)_{1-4}$. Using equations $(2.6)_{1,2}$, $(2.7)_{1,2}$ and $(2.8)_{1-4}$ we can get surface factors of higher order.

Having the results of approximation II, we can modify stress boundary conditions on the faces in the same way i.e. by using equations $(2.9)_{1-4}$. Approximation III, etc. can then be calculated accordingly.

3. Numerical solution of the dual system of equations

3.1. Calculation of the basic solution

Let new variable

$$(\tilde{\sigma}_0)_\varphi = R_0(\sigma_0)_\varphi \tag{3.1}$$

and column matrices

$$\underline{\sigma}_1^T = \left[(\sigma_0)_s \; (\sigma_0)_\varphi \; (\tau_0)_{sz} \; (\sigma_1)_s \; (\tilde{\sigma}_0)_\varphi\right] \quad , \tag{3.2}$$

and

$$\underline{\sigma}_2^T = \left[(\sigma_0)_z \; (\sigma_1)_\varphi\right] \tag{3.3}$$

be introduced, where T indicates the transposed matrix. Let equations $(2.5)_{1-10}$ be transformed as follows:

Substitute first surface factors

$$(\tau_2)_{sz} = p_1 - (\tau_0)_{sz} \quad , \tag{3.4}_1$$

$$(\sigma_2)_z = p_2 - (\sigma_0)_z \quad , \tag{3.4}_2$$

$$(\tau_1)_{sz} = p_3 \quad , \tag{3.4}_3$$

$$(\sigma_1)_z = p_4 \tag{3.4}_4$$

obtained from $(2.5)_{7-10}$ into $(2.5)_{1-6}$. Then, surface factors $(\sigma_0)_z$ and $(\sigma_1)_z$ can be expressed from $(2.5)_4$ and $(2.5)_5$ as a function of variables (3.2) to find that

$$\underline{\sigma}_2 = \underline{\underline{A}}\, \underline{\sigma}_1 + \underline{b} \quad , \tag{3.5}_1$$

where

$$\left[\underline{\underline{A}}\right] = \frac{1}{2\lambda^2 + 2+\nu} \begin{bmatrix} 0 & 2+\nu & 0 & -\lambda\nu & 0 \\ 0 & -2\lambda(1+\nu) & 0 & \nu(2\lambda^2+1) & 0 \end{bmatrix} , \tag{3.5}_2$$

$$\left[\underline{b}\right] = \frac{1}{2\lambda^2 + 2+\nu} \begin{bmatrix} 2\lambda^2 p_2 + \lambda(1-\nu)p_4 + \lambda R_0 \left[p_3' + (q_1)_z\right] \\ 2\lambda(1+\nu)p_2 + (2\lambda^2\nu + 2\nu + 1)p_4 + (1+\nu)R_0 \left[p_3' + (q_1)_z\right] \end{bmatrix} . \tag{3.5}_3$$

Taking into consideration also equations $(3.4)_{1-4}$ and $(3.5)_{1-3}$, the remaining equations $(2.5)_{1-3}$ and $(2.5)_6$ form a system of differential equations in terms of variables (3.2). Second order differential equation $(2.5)_6$ can be replaced with two first order equations. The steps are, as follows:

(a) first we calculate the derivatives with respect to $\underline{s}$ for surface factors $(\sigma_0)_s''$, $(\sigma_0)_z''$ and $(\sigma_1)_s''$ obtained from equations $(2.5)_1$, $(3.5)_1$ and $(2.5)_3$, respectively;

(b) next we substitute both the mentioned surface factors and $(\tau_0)_{sz}'$ expressed from $(2.5)_2$ into $(2.5)_6$;

(c) making use of the new variable (3.1), the two first order differential equations can be obtained from equation $(2.5)_6$.
The latter two equations, together with equations $(2.5)_{1-3}$, form an inhomogeneous differential equation system for variables (3.2). This system of equation can be written as

$$R_0 \underline{\sigma}_1' = \underline{\underline{D}}\, \underline{\sigma}_1 + \underline{f} \quad , \tag{3.6}_1$$

where

$$\left[\underline{\underline{D}}\right] = \begin{bmatrix} 0 & 0 & -1 & 0 & 0 \\ 0 & 0 & 0 & 0 & 1 \\ 0 & 1 & 0 & 0 & 0 \\ 0 & 0 & d_{43} & 0 & 0 \\ 0 & d_{52} & 0 & d_{54} & 0 \end{bmatrix} , \tag{3.6}_2$$

$$d_{43} = 2\lambda + \frac{1}{\lambda} \quad , \tag{3.6}_3$$

$$d_{52} = \frac{2\lambda^2(1+\nu)\left[(4\lambda^2+3+\nu)(1-\nu)+1\right]}{(2\lambda^2+2+\nu)\left[2\lambda^2+2-\nu(1+\nu)\right]} \quad , \tag{3.6}_4$$

$$d_{54} = \frac{\lambda\nu(1+\nu)\left[4\lambda^4(1-\nu)-2\lambda^2(\nu^2+3\nu-6)+8-\nu^2\right]}{(2\lambda^2+2+\nu)\left[2\lambda^2+2-\nu(1+\nu)\right]} \quad , \tag{3.6}_5$$

$$\left[\underline{f}\right] = \begin{bmatrix} -\lambda p_3 - R_0 (q_0)_s \\ 0 \\ -\lambda p_4 - R_0 (q_0)_z \\ -2\lambda p_1 - p_3 - R_0 (q_1)_s \\ f_5 \end{bmatrix} , \tag{3.6}_6$$

$$f_5 = \frac{1}{2\lambda^2+2-\nu(1+\nu)} \left\{ \left[(2\lambda^2+1)(\nu^2-\nu-2)-(1+\nu)(2+\nu) \right] b_1 - \right.$$

$$- \lambda\nu(2\lambda^2+2+\nu)b_2 + \left[(2\lambda^2+1)(\nu^2-2)-2(2+\nu) \right] p_4 + 2\lambda^2\nu^2 R_0^2 p_1' -$$

$$- \lambda\nu(2\lambda^2+2)R_0 p_3' + 2\lambda^2\nu R_0^2 p_2'' + \lambda\nu(1-\nu)R_0^2 p_4'' + \lambda\nu R_0^3 p_3''' +$$

$$+ \left[(2\lambda^2+1)(\nu^2-\nu-2)-(2+\nu)(1+\nu) \right] R_0 (q_0)_z - \nu(2\lambda^2+2+\nu)R_0^2 (q_0)'_s +$$

$$\left. + \lambda\nu^2 R_0^2 (q_1)'_s + \lambda\nu R_0^3 (q_1)''_z \right\} . \qquad (3.6)_7$$

Now, the basic solution of approximation I can be calculated as follows:

(a) taking into consideration the boundary conditions on the lateral surfaces we can solve the differential equation system $(3.6)_1$ (for example by Runge-Kutta method);

(b) using formulae $(3.5)_{1-3}$ and $(3.4)_{1-4}$, the other stress surface factors of the basic solution can be calculated;

(c) finally, using $(2.8)_{1-4}$, we get the strain surface factors.

Determination of the basic solution of approximation II is similar to that of approximation I with, however, modified values p_1, p_2, p_3, p_4 on the right-hand side of $(2.9)_{1-4}$ substituted here into equations $(3.4)_{1-4}$, $(3.5)_{1-3}$ and $(3.6)_{1-7}$.

3.2. Calculation of surface factors of higher order

In the knowledge of the basic solution, surface factors of higher order can be calculated step by step from equations $(2.6)_{1,2}$ and $(2.7)_{1,2}$, taking into consideration Hooke's law $(2.8)_{1-4}$ as well.

3.2.1. Calculation of the first approximation

From independent compatibility equations $(2.7)_{1,2}$ we obtain strain surface factors

$$(\varepsilon_{i+2})_s = \frac{1}{(i+1)(i+2)\lambda^2} R_0^2 (\varepsilon_i)''_z + \frac{2}{(i+2)\lambda} R_0 (\varepsilon_{i+1})'_{sz} \quad , \qquad (3.7)_1$$

$$(\varepsilon_{i+2})_\varphi = -\frac{1}{\lambda}(\varepsilon_{i+1})_\varphi + \frac{1}{(i+2)\lambda}(\varepsilon_{i+1})_z \quad ; \quad i=0,1,2,\ldots \quad . \qquad (3.7)_2$$

From Hooke's law $(2.8)_{1-2}$, substituting i+2 for i, surface factors

$$(\sigma_{i+2})_s = \frac{\nu}{1-\nu}(\sigma_{i+2})_z + \frac{2G}{1-\nu}\left[(\varepsilon_{i+2})_s + \nu(\varepsilon_{i+2})_\varphi\right] \quad , \qquad (3.8)_1$$

$$(\sigma_{i+2})_\varphi = \frac{\nu}{1-\nu}(\sigma_{i+2})_z + \frac{2G}{1-\nu}\left[\nu(\varepsilon_{i+2})_s + (\varepsilon_{i+2})_\varphi\right] \quad ; \qquad (3.8)_2$$

$$i = 0,1,2,\ldots$$

can be expressed. From equilibrium equations $(2.6)_{1,2}$ stress surface factors

$$(\tau_{i+3})_{sz} = -\frac{1}{(i+3)\lambda}\left[R_0(\sigma_{i+2})'_s + \sum_{j=0}^{i+2}(-\frac{1}{\lambda})^{i+2-j}(\tau_j)_{sz} + R_0(q_{i+2})_s\right] \quad , \qquad (3.9)_1$$

$$(\sigma_{i+3})_z = -\frac{1}{(i+3)\lambda}\left\{R_0(\tau_{i+2})'_{sz} + \sum_{j=0}^{i+2}(-\frac{1}{\lambda})^{i+2-j}\left[(\sigma_j)_z - (\sigma_j)_\varphi\right] + R_0(q_{i+2})_z\right\} \quad ; \qquad (3.9)_2$$

$$i = 0,1,2,\ldots$$

are obtained.

Thus, in accordance with the above equations, surface factors of higher order for approximation I can be calculated as follows:

(a) i = 0: using $(3.7)_{1,2}$ we get $(\varepsilon_2)_s$ and $(\varepsilon_2)_\varphi$. Then, from $(3.8)_{1,2}$ we get $(\sigma_2)_s$ and $(\sigma_2)_\varphi$. Finally, using $(3.9)_{1,2}$ we obtain surface factors $(\tau_3)_{sz}$ and $(\sigma_3)_z$.

(b) i = 1: using formulae $(3.7)_{1,2}$, $(3.8)_{1,2}$, $(3.9)_{1,2}$ and the values previously computed, surface factors $(\varepsilon_3)_s$ and $(\varepsilon_3)_\varphi$, $(\sigma_3)_s$ and $(\sigma_3)_\varphi$, $(\tau_4)_{sz}$ as well as $(\sigma_4)_z$ can be obtained, respectively.

With this procedure repeated in steps of arbitrary number i, stress and strain surface factors of arbitrary number can be determined.

Calculation of the derivatives in formulae $(3.7)_{1,2}$ and $(3.9)_{1,2}$ is based on earlier equations and therefore a numerical differentiation is not necessary. For example in the knowledge of the basic solution, equation $(3.6)_1$ gives the first derivative of $\underline{\sigma}_1$ with respect to s. After differentiation of $(3.6)_1$ with respect to s, we get the second derivative of $\underline{\sigma}_1$:

$$R_0 \underline{\sigma}_1'' = \underline{\underline{D}} \underline{\sigma}_1' + \underline{f}' \quad . \tag{3.10}$$

Thus, taking the basic solution as a starting point, the n-th derivative of $\underline{\sigma}_1$ can be calculated by formula

$$R_0 \underline{\sigma}_1^{(n)} = \underline{\underline{D}} \underline{\sigma}_1^{(n-1)} + \underline{f}^{(n-1)} \quad ; \tag{3.11}$$

$$n = 1,2,3,\ldots \quad .$$

Similarly, the n-th derivative of $\underline{\sigma}_2$ can be calculated from $(3.5)_1$ as

$$\underline{\sigma}_2^{(n)} = \underline{\underline{A}} \underline{\sigma}_1^{(n)} + \underline{b}^{(n)} \quad ; \tag{3.12}$$

$$n = 0,1,2,\ldots,$$

where $\underline{\sigma}_1^{(n)}$ is given by (3.11). The derivatives of column matrices $\underline{f}$ and $\underline{b}$ on the right-hand side of (3.11) and (3.12) contain the derivatives of external (given) loads.

It is true also in general that the formulae obtained earlier for the surface factors enable us to calculate the n-th derivative of the appropriate surface factors.

3.2.2. Calculation of the second, third, etc. approximations

In approximation I only boundary conditions for surface factors giving the basic solution have been taken into consideration (by integration of differential equation system $(3.6)_1$ from among those prescribed on lateral surfaces. Boundary conditions for surface factors of higher order are satisfied in approximations II, III, ..., in particular, by rearrangement of equations $(3.8)_{1,2}$ and $(3.9)_{1,2}$ to calculate surface factors $(\sigma_{i+2})_s$, $(\tau_{i+3})_{sz}$; (i = 0,1,2,...) by integration.

What follows now applies to approximation II. Approximation III, etc. can be calculated in a similar way.

Subtract $(3.8)_1$ from $(3.8)_2$. After rearrangement we obtain

$$(\sigma_{i+2})_\varphi = (\sigma_{i+2})_s + 2G\left[(\varepsilon_{i+2})_\varphi - (\varepsilon_{i+2})_s\right] ; \qquad (3.13)$$

$$i = 0,1,2,\ldots \quad .$$

By substituting i+1 for i in $(3.9)_2$, we find for $(\tau_{i+3})'_{sz}$ that

$$R_0(\tau_{i+3})'_{sz} = -\frac{1}{\lambda}(\sigma_{i+2})_\varphi + \frac{1}{\lambda}(\sigma_{i+2})_z + (\sigma_{i+3})_\varphi - (\sigma_{i+3})_z +$$

$$+ \sum_{j=0}^{i+1} (-\frac{1}{\lambda})^{i+1-j}\left[(\sigma_j)_\varphi - (\sigma_j)_z\right] - (i+4)\lambda(\sigma_{i+4})_z - R_0(q_{i+3})_z ; \qquad (3.14)$$

$$i = 0,1,2,\ldots \quad .$$

If we express $(\sigma_{i+2})'_s$ from $(3.9)_1$ and insert $(3.9)_1$ and (3.13) into (3.14), a system of two first order, linear, inhomogeneous differential equations will be obtained for variables $(\sigma_{i+2})_s$, $(\tau_{i+3})_{sz}$:

$$R_0(\sigma_{i+2})'_s = -(i+3)\lambda(\tau_{i+3})_{sz} - \sum_{j=0}^{i+2}(-\frac{1}{\lambda})^{i+2-j}(\tau_j)_{sz} - R_0(q_{i+1})_s , \quad (3.15)_1$$

$$R_0(\tau_{i+3})'_{sz} = -\frac{i+4}{(i+3)\lambda}(\sigma_{i+2})_s - 2G\frac{i+4}{(i+3)\lambda}\left[(\varepsilon_{i+2})_\varphi - (\varepsilon_{i+2})_s\right] +$$

$$+ \left[1 - \frac{1}{(i+3)\lambda}\right]\sum_{j=0}^{i+1}(-\frac{1}{\lambda})^{i+1-j}\left[(\sigma_j)_\varphi - (\sigma_j)_z\right] + \frac{i+4}{(i+3)\lambda}(\sigma_{i+2})_z +$$

$$+ \frac{1}{(i+3)\lambda}R_0(\tau_{i+2})'_{sz} + (\sigma_{i+3})^I_\varphi - (i+4)\lambda(\sigma_{i+4})^I_z +$$

$$+ \frac{1}{(i+3)\lambda}R_0(q_{i+2})_z - R_0(q_{i+3})_z ; \qquad i = 0,1,2,\ldots . \qquad (3.15)_2$$

All terms except for the first term on the right-hand side of $(3.15)_{1,2}$ are known from the basic solution of approximation II, or from approximation I. The latter terms are marked with I in upper subscripts.

Surface factors of higher order can be calculated then, as follows:

(a) i = 0: using $(3.7)_{1,2}$ we get $(\varepsilon_2)_s$ and $(\varepsilon_2)_\varphi$. Then, taking into account the boundary conditions prescribed on the lateral surfaces, the differential equation system $(3.15)_{1,2}$ for variables $(\sigma_2)_s$ and $(\tau_3)_{sz}$ can be solved. Making use of these surface factors, $(\sigma_2)_\varphi$ and $(\sigma_3)_z$ can be obtained from (3.13) and $(3.9)_2$, respectively.

(b) i = 1: using $(3.7)_{1,2}$ we get $(\varepsilon_3)_s$ and $(\varepsilon_3)_\varphi$. Then, by integrating $(3.15)_{1,2}$, $(\sigma_3)_s$ and $(\tau_4)_{sz}$ are obtained. Finally, using (3.13) and $(3.9)_2$ we get $(\sigma_3)_\varphi$ and $(\sigma_4)_z$.

With this procedure continued, surface factors of arbitrary number can be calculated.

Approximations III, IV, ... etc. are determined in a way similar to that in case of approximation II, but here I shall be replaced with II, III, ... etc. in subscript.

The required number of iteration steps for desirable accuracy can be selected in advance in the knowledge of the shell geometry (see /1/, /7/).

4. Boundary conditions prescribed on the lateral surfaces

4.1. Stress boundary conditions

Let $(p_i^*)^\ell$; (i = 0,1,2,...) denote the surface factors of loads acting on the lateral surfaces. Then, according to /2/ and /1/, the stress boundary conditions on boundary curves h_1^* and h_2^* of lateral surfaces A_1^* and A_2^*, respectively, are given by equation

$$\frac{1}{\bar{\chi}}\ \bar{n}_1^*\sum_{i=0}\ (\sigma_i)^{1\ell}\ \zeta^i = \sum_{i=0}\ (p_i^*)^\ell\ \zeta^i\ , \tag{4.1}$$

where

$$\underline{\bar{n}}^* = -\bar{\chi}\underline{g}_1\ ; \qquad x \in A_1^*\ , \tag{4.2}_1$$

and

$$\underline{\bar{n}}^* = \bar{\chi}\underline{g}_1\ ; \qquad x \in A_2^* \tag{4.2}_2$$

are the outward normal vectors of the lateral surfaces, and

$$\bar{\chi} = \left|\underline{\bar{n}}^*\right| = 1 + \frac{\zeta}{\lambda}\ . \tag{4.2}_3$$

Coefficients of powers of on the left- and right-hand side of (4.1) must be equal. Then, using now physical components, stress boundary conditions

$$(\sigma_i)_s = \mp (p_i^*)_s \quad , \tag{4.3}_1$$

$$(\tau_i)_{sz} = \mp (p_i^*)_z \quad ; \qquad i = 1,2,3,... \tag{4.3}_2$$

can be prescribed in case of tension-compression, bending-shearing problems, respectively with negative sign for boundary A_1^* while positive sign for boundary A_2^*.

4.2. Displacement boundary conditions

Since in dual system of elasticity displacements are not appearing as variables, displacement boundary conditions should be replaced with appropriate boundary conditions in terms of strains or, through Hooke's law in terms of stresses. Let $(u_i^*)_\ell$; $(i = 0,1,2,...)$ denote the surface factors of displacements prescribed on the lateral surfaces. Then, according to /2/, /7/, the displacement boundary conditions on boundary curves h_1^* and h_2^* of lateral surfaces A_1^* and A_2^*, respectively, are given by

$$(\varepsilon_i)_{KL} = \frac{1}{2}\left[(u_i^*)_{K:L} + (u_i^*)_{L:K} \right] \quad , \tag{4.4}_1$$

$$(\varepsilon_i)_{KL:1} - (\varepsilon_i)_{1L:K} = (\varepsilon_i)_{1K:L} - (u_i^*)_{1:KL} \quad , \tag{4.4}_2$$

$$i = 0,1,2,...$$

where indices K and L may only have the range 2,3, a colon followed by an index denotes the surface factors of the corresponding covariant derivative. For example:

$$(\varepsilon_1)_{12:2} = -\frac{1}{\lambda} R_0 (\varepsilon_0)_{13} + R_0 (\varepsilon_1)_{13} \quad .$$

When changing over to physical components and differentiating in formulae $(4.4)_{1,2}$, we obtain displacement boundary conditions in terms of strains. From $(4.4)_1$ we arrive at

$$(\varepsilon_i)_\varphi = \sum_{j=0}^{i} \left(-\frac{1}{\lambda}\right)^{i-j} \frac{1}{R_0} (u_j^*)_z \quad , \tag{4.5}_1$$

$$(\varepsilon_i)_z = \frac{i+1}{b}(u^*_{i+1})_z \quad ; \qquad i = 0,1,2,... \qquad (4.5)_2$$

from $(4.4)_2$ equations

$$R_0(\varepsilon_i)'_\varphi - 2\sum_{j=0}^{i}(-\frac{1}{\lambda})^{i-j}(\varepsilon_j)_{sz} + \frac{1}{b}\sum_{j=1}^{i+1} j(-\frac{1}{\lambda})^{i+1-j}(u^*_j)_s = 0, \qquad (4.5)_3$$

$$R_0(\varepsilon_i)'_z - 2(i+1)\lambda(\varepsilon_{i+1})_{sz} + \frac{(i+1)(i+2)}{b}\lambda(u^*_{i+2})_s = 0 \quad ; \qquad (4.5)_4$$

$$i = 0,1,2,...$$

are obtained.

In case of stress surface factors, it is necessary that the following be taken into consideration:

(a) boundary conditions associated with differential equation system $(3.6)_{1-7}$ should be given in terms of stress surface factors (3.2);

(b) boundary conditions associated with differential equation system $(3.15)_{1,2}$ should be given in terms of stress surface factors $(\sigma_{i+2})_s$, $(\tau_{i+3})_{sz}$; $(i = 0,1,2,...)$.

E.g. to calculate the basic solution, substitute Hooke's law $(2.8)_{1-4}$ into $(4.5)_3$ and into $(4.5)_4$, the latter multiplied with ν, and add. Then, using (3.1), relationship

$$(1-\nu)(\tilde{\sigma}_0)_\varphi - \nu R_0(\sigma_0)'_s - 2(\tau_0)_{sz} - 2\lambda\nu(\tau_1)_{sz} =$$

$$= -\frac{2G}{b}\left[(u^*_1)_s + 2\lambda\nu(u^*_2)_s\right] \qquad (4.6)$$

exists between the prescribed displacements and stress surface factors. Remark: Displacement surface factor $(u^*_0)_s$ is not included in equations $(4.5)_{1-4}$. Thus, if the displacement of the middle surface in direction s is also prescribed, condition

$$(u^*_0)_s\Big|_{s=0}^{s=\ell} = \int_0^\ell (\varepsilon_0)_s\, ds \qquad (4.7)$$

should be taken into consideration as well.

5. Numerical results, comparisons

It is stressed again that stresses, strains and displacements at any point of the cylindrical shell (considered to be a three-dimensional continuum) can be determined to any desirable accuracy by asymptotic integration of the dual equation system. This is also true to numerical calculation of the solution(disregarding errors resulting from the numerical method used and rounding errors).

To investigate different types of loads, a PASCAL program has been developed and used for problems of quite of number by the author. The primary objective has been a comparison of the technical theory of shells with the asymptotic method.

Based on the Kirchhoff-Love hypothesis, the technical theory of shells yields acceptable results for thin shells. Variables along the thickness of the shell are linearly distributed whereas transverse shears and normal strains are neglected (as a consequence of the Kirchhoff-Love hypothesis).

The asymptotic method satisfies the equations and boundary conditions exactly. The distribution of variables along the thickness of the shell are approximated by polynomials. The degrees of these polynomials equal to the number of the subiteration steps. It is therefore possible to investigate the accuracy of the solutions obtained for thick shells by applying the technical theory of shells. It can also be investigated whether approximation of distribution along the thickness by linear functions is acceptable or not.

Presented below are five numerical examples. The solutions that are based on the technical theory of shells have been obtained by means of the program /5/.

1. example: Cylindrical concrete container

The fundamental equation of cylindrical shells in terms of radial displacement is considered in /4/. Paper /4/ presents analytical solutions for different types of loads and finally, a cylindrical concrete container (Fig. 3a) is investigated as a numerical example. The height of this container is 5 m, the thickness 250 mm, the radius of the middle surface 10 m; $E = 16$ GPa and $\nu = 0.2$.

The inner face of the shell is subjected to radial pressure while the outer face to vertical line load. These loads are linearly distributed

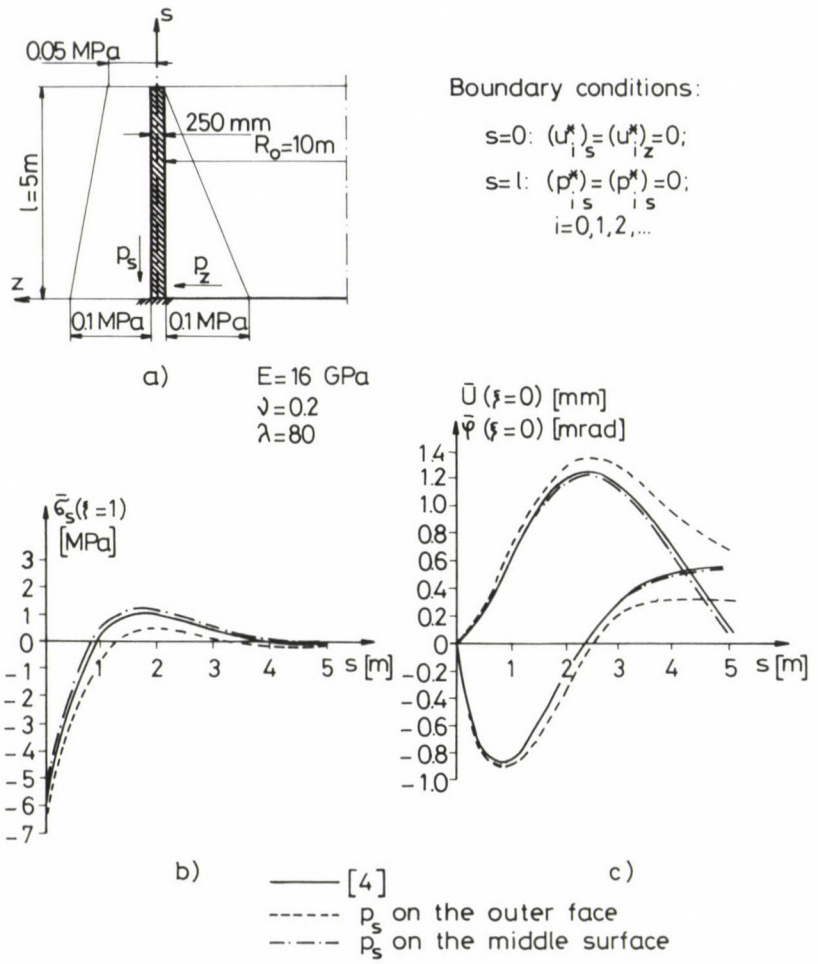

Fig. 3. Cylindrical concrete container

along the coordinate s (Fig. 3 a). At s = 0 the shell is clamped, so the displacement boundary conditions are:

$$(u_i^*)_s = (u_i^*)_z = 0 \quad ; \qquad i = 0,1,2,\ldots \quad . \tag{5.1}$$

The edge at s = ℓ is free, so here

$$(p_i^*)_s = (p_i^*)_z = 0 \quad ; \qquad i = 0,1,2,\ldots \tag{5.2}$$

stress boundary conditions should be prescribed.

From among the solutions obtained by means of the asymptotic method, there is a good agreement between stresses σ_φ and the results of /4/. For stress σ_s (its value on the outer face being shown in Fig. 3b), displacement u_z and rotation φ of the middle surface results different from /4/ have been obtained.

Full lines indicate the results obtained by asymptotic method. Responsibility for the difference lies mainly on the vertical line load p_s acting on the outer face. In /4/ this load is considered as a line load acting on the middle surface. For the sake of comparison we considered the load p_s to be body force $(q_0)_s$ acting on the middle surface. The solutions obtained in this case (dot- and dashed lines in Figs 3b, c) are in good agreement with those given in /4/. For instance, the maximum value of u_z is 1.23 mm in /4/ while 1.37 mm and 1.24 mm in the first and second case, respectively, in calculation with the asymptotic method.

Because the quotient $\lambda = R_0/b = 80$, the cylindrical container can be considered as a thin shell. Thus, the distribution of the values along the thickness is approximately linear.

2. example: Constant radial loads acting on the faces

The technical theory of shells makes no distinction between the loads acting on the outer and inner faces. In case of thick shells, the two different, statically equivalent loads may result different stresses in a shell. The differences are investigated in this example by asymptotic method.

Consider a cylindrical shell of length $\ell = 1$ m. The radius of the middle surface is $R_0 = 0.5$ m, the thickness of the shell $2b = 200$ mm. Since $\lambda = R_0/b = 5$, this is a thick shell. At $s = 0$, the shell edge is clamped while the edge at $s = \ell$ is free, so the boundary conditions (5.1) and (5.2) are valid. A constant radial load of $p_0 = -10$ MPa is acting on the faces (Figs 4a, b, c). The shell material is steel: $E = 205$ GPa and $\nu = 0.3$.

In Fig. 4, stress distributions along the thickness are shown and compared. In Figs 4d and 4e distributions for $\bar{\sigma}_s$ and $\bar{\sigma}_\varphi$ at $s = 0$ (at the clamped edge) are shown, respectively. Full lines indicate the solutions obtained by the technical theory of shells, —— o —— lines and —— + —— lines indicate the results obtained by the asymptotic method with p_0 acting on the outer and inner face, respectively.

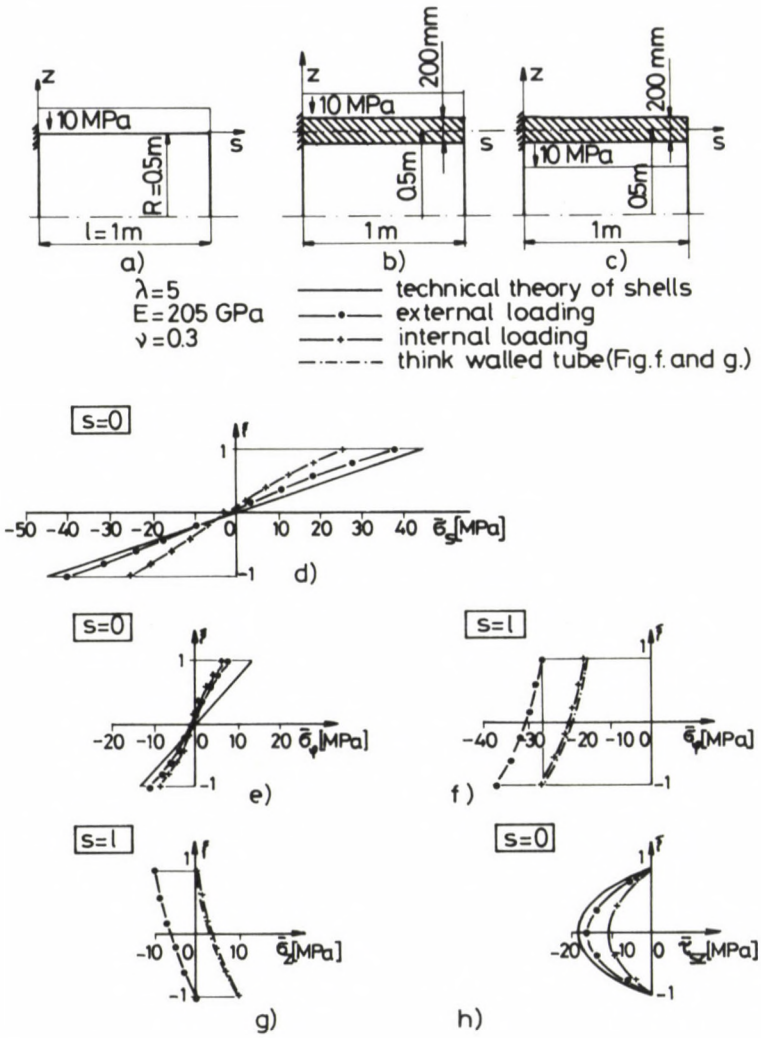

Fig. 4. Constant radial loads acting on the outer and inner faces of the shell. Comparison of stress distributions along the thickness of the shell

In Figs 4f and 4g, distributions of σ_φ and σ_z at $s = \ell$, in Fig. 4h, distributions of shear stresses τ_{sz} at $s = 0$ are shown. Stresses σ_z are neglected in the technical theory of shells. However, on the faces, σ_z is equal to the radial load. In Fig. 4h, the distribution of shear stress τ_{sz} obtained from shearing force Q of the technical theory of shells is considered as a quadratic function.

The maxima of displacement u_z for the three statically equivalent loads given in Figs 4a, b, c are -0.065 mm, -0.079 mm and -0.053 mm, respectively.

Since the influence of the edge $s = 0$ disappear at $s = \ell$, the solution for load acting on the inner face is comparable with the thick walled tube's solutions (see /8/, /1/). Dot- and dashed-line was used to plot the latter results in Figs 4f and 4g. The thick walled tube was found to be an ideal model to approximate the stressed state at points being far enough from the clamped edge.

This examples warns at the same time to calculate loads acting on the inner and outer faces of the shell simultaneously carefully.

3. example: Loads acting on a narrow strip of the outer face

According to Figs 5a, b, c, statically equivalent loads of constant, quadratic and linear distribution are acting on a narrow strip of the outer face. Both edges of the shell are clamped and thus displacement boundary conditions (5.1) are valid at both $s = 0$ and $s = \ell$. The shell is $\ell = 3$ m long, $2b = 400$ mm thick, the middle surface's radius is $R_0 = 1$ m, $\lambda = R_0/b = 5$ (thick shell), $E = 205$ GPa and $\nu = 0.3$.

In all three cases the loads are acting on a $\Delta s = 200$ mm wide strip in the middle of the shell. The intensity of the equivalent line load is 25.6 MN/m. Maximum values of the loads for constant, quadratic and linear distribution are 128 MPa, 192 MPa and 256 MPa, respectively.

In Figs 5a, b and c, the distribution of stresses σ_s, σ_φ and σ_z along the thickness at $s = \ell/2 = 1.5$ m are shown. Results of the technical theory of shells are illustrated with dashed-line while the results of the asymptotic method with full line. The distribution of shear stresses τ_{sz} along the thickness is approximately parabolic. The maximum values of τ_{sz} and radial displacement u_z are shown in Table 1.

Since stresses σ_z cannot be neglected and because of the thickness of the shell the differences between the stresses obtained by the two different methods are significant.

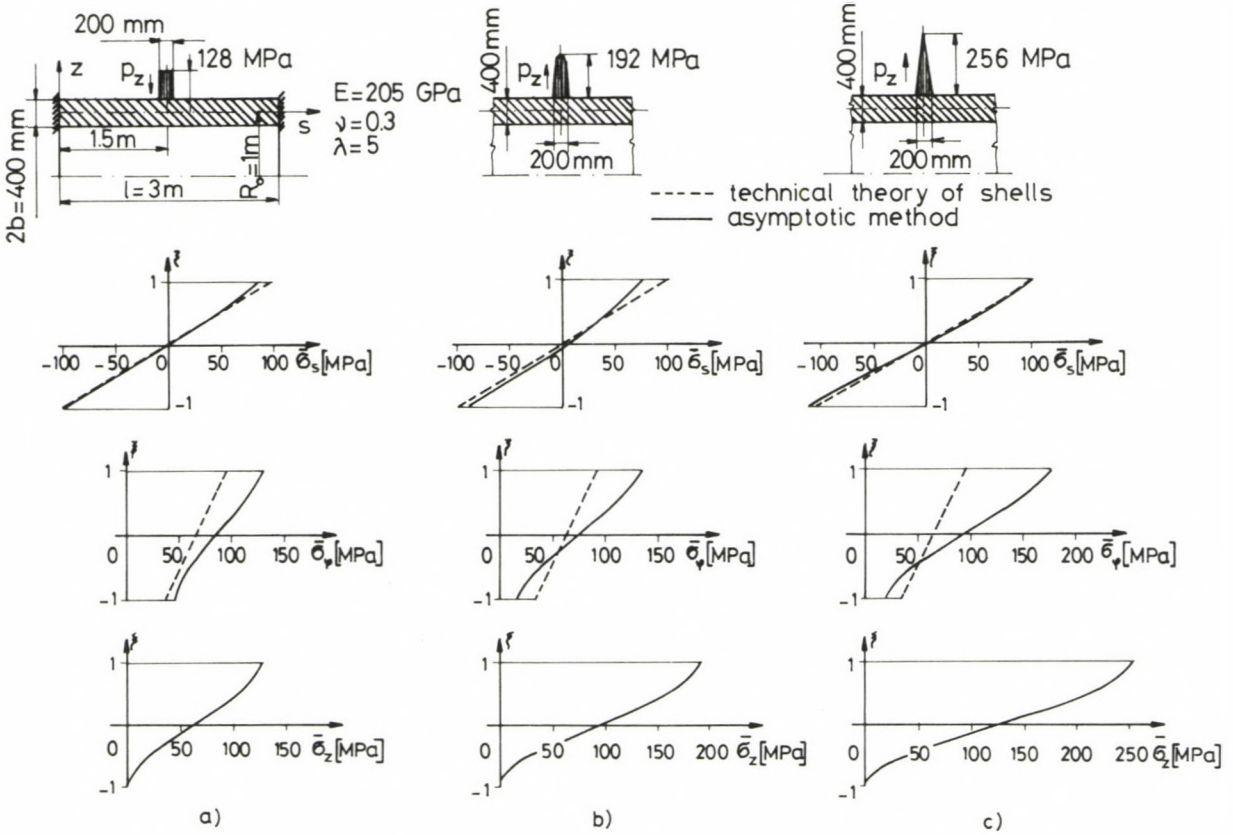

Fig. 5. Constant, quadratic and linear distribution of statically equal loads acting on a narrow strip of the outer face. Stress distributions along the thickness of the shell at $s = \ell/2$

Table 1

Maximum values for shear stresses $\bar{\tau}_{sz}$ and radial displacements $\bar{u}_z$ in example 3

	Constant		Quadratic		Linear	
	Techn. theory	Asympt. method	Techn. theory	Asmypt. method	Techn. theory	Asympt. method
$\bar{\tau}_{sz\ max}$ MPa	38.1	40.1	38.3	34.6	38.4	44.2
$\bar{u}_{z\ max}$ [mm]	0.32	0.47	0.32	0.48	0.32	0.61

4. example: Bending moment acting on the edge

As is well known, the thinner the shell, the higher the accuracy of the solution obtained on the basis of the technical theory of shells. To investigate the error caused by the technical theory of shells in case of thick shells, assume that pure bending is acting on one of the edges of the shell (Fig. 6a). At s = 0 the shell is clamped, thus the displacement boundary condition (5.1) is valid. The edge at $s = \ell$ is subjected to bending moment M_1 (Fig. 6a), which means that stress boundary conditions

$$(p_1^*)_s = \sigma_M \ , \qquad (p_i^*)_s = 0 \ ; \qquad i = 0,2,3,\ldots$$
$$(p_i^*)_z = 0 \ ; \qquad i = 0,1,2,\ldots \tag{5.3}$$

shall be prescribed together with the condition of equivalence

$$\int_{-b}^{b} (R_0 + x^3)\, \sigma_M\, \zeta\, \bar{\chi}(\zeta)\, dx^3 = M_1 \ ,$$

if the asymptotic method is used (Fig. 6b). Let the length of the shell be ℓ = 1 m, the middle surface's radius R_0 = 0.5 m; E = 208 GPa and ν = 0.3.

A series of shells of different thickness have been investigated (Fig. 6c).

According to the numerical results, the difference between the

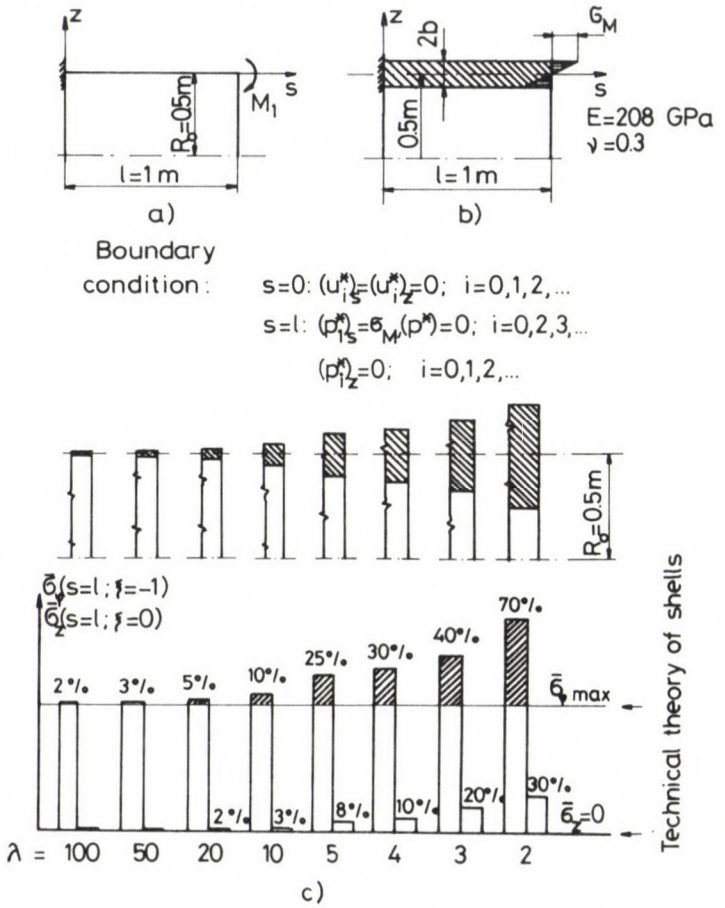

Fig. 6. Bending moment acting on one of the edges of the shells of different thickness. Comparison between the technical theory of shells and the asymptotic method

results of the technical theory of shells and the asymptotic method is greatest for stresses σ_φ and σ_z. The difference between both methods in per cents for maximum stresses at point $s = l$, $\zeta = -1$ are illustrated by column diagrams in Fig. 6 c, the higher columns representing stresses σ_φ while the lower columns stresses σ_z. The maximum value for σ_φ obtained on the basis of the technical theory of shells is denoted by a horizontal line. Heights of the columns are proportional to the maxima of stresses obtained by asymptotic method. Marked parts of the columns indicate the magnitude of the difference. Difference in per cents for σ_φ is calculated by means of formula

$$\sigma_{\varphi}\Big|_{\%\ \text{difference}} = \frac{\sigma\ \text{asympt} - \sigma\text{techn.}}{\sigma\ \text{techn.}} \cdot 100\ \% \ . \qquad (5.4)$$

Percentages σ_z are calculated as the quotient of σ_z and the maximum stress obtained by use of the technical theory of shells, multiplied by 100.

5. example: Shear force acting on the edge

The series of shells (series of λ) of different thickness investigated in the previous example are now subjected to shear force Q_1 at $s = \ell$ (Fig. 7.a). The stress boundary conditions at $S = \ell$ are:

$$(p_i^*)_s = 0 \ ; \qquad i = 0,1,2,\dots \ ,$$

$$(p_0^*)_z = \tau_Q \ , \qquad (p_2^*)_z = -\tau_Q \ ,$$

$$(p_i^*)_z = 0 \ ; \qquad i = 1,3,4,5,\dots \ ,$$

where the equivalence condition

$$\int_{-b}^{b} \overline{\chi}(\zeta)\,(\tau_Q - \tau_Q \zeta^2)\,dx^3 = Q_1$$

should also be satisfied. The values Q_1 and τ_Q have been selected in such a way that the maximum stresses obtained by the technical theory of shells will be identical (namely $\tau_Q\sqrt{\lambda} = \text{const.}$).

According to the numerical results, greatest difference between the results of the technical theory of shells and the asymptotic method has been obtained for stresses σ_φ and σ_z (the difference between stresses σ_s being 10% even for $\lambda = 2$). At point $s = \ell$, $\zeta = -1$ (at maximum stresses), the difference in per cents between the results of the two methods are illustrated as column diagrams in Fig. 7c, higher columns representing stresses σ_φ while lower columns stresses σ_z. Interpretation of Fig. 7c is the same as for Fig. 6x (in example 4.).

A comparison of Fig. 6c and Fig. 7c shows that the error of the technical theory of shells is greater when the edge is subjected to shear force.

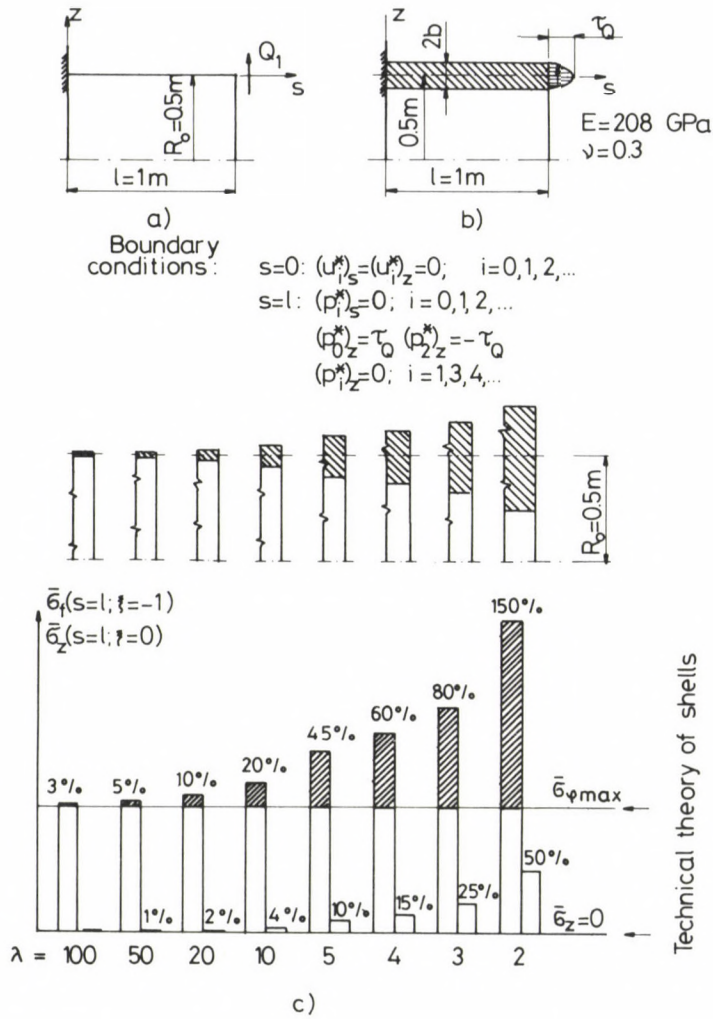

Fig. 7. Shear force acting on one of the edges of the shells of different thickness. Comparison between the technical theory of shells and the asymptotic method

Transverse shear deformations of the edge at s = 0 are shown for λ = 10 and λ = 4 in Figs 8a and 8b. According to the Kirchhoff-Love hypothesis, the normal of the middle surface remains normal to the deformed middle surface (dashed line). The actual deformation of the normal is illustrated with full lines. The equivalent loads are Q_1 = 32 MN/m, τ_Q = 475 MPa for λ = 10 and Q_1 = 125 MN/m, τ_Q = 750 MPa for λ = 4. Shell thickness: 100 mm and 250 mm for λ = 10 and λ = 4, respectively.

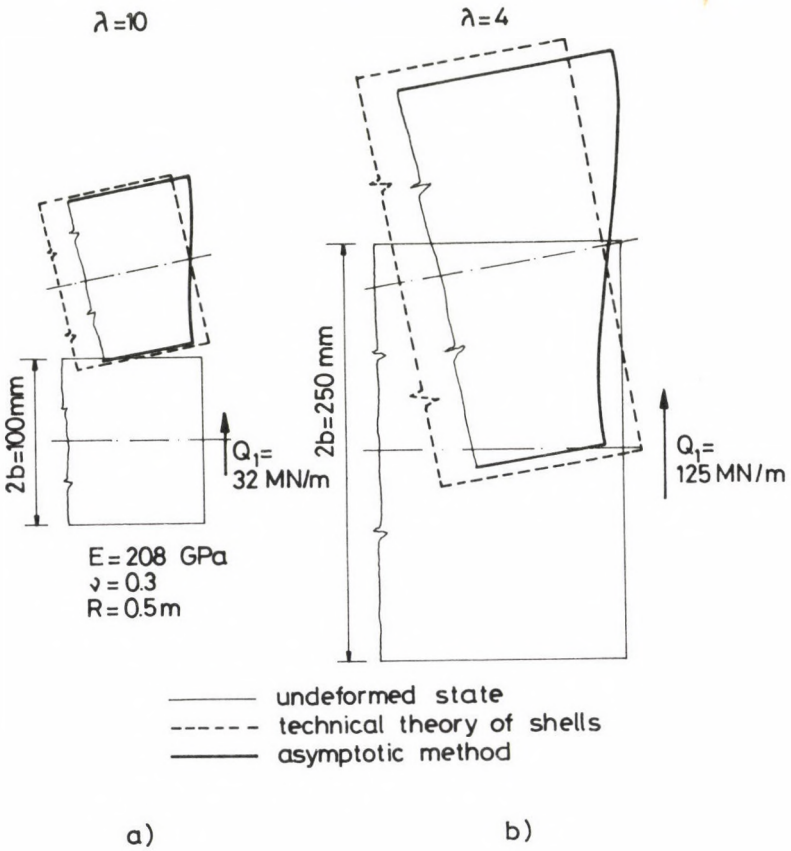

Fig. 8. Transverse shear deformations for $\lambda = 10$ and $\lambda = 4$

The difference in rotation between the middle surface normals is 0.4^{o} for $\lambda = 4$, a very small value while the difference between the stresses are significant (see Fig. 7c).

REFERENCES

1. Bertóti, E.: Application of a dual shell theory to axisymmetric deformations of cylindrical shells, Publication of the Technical University for Heavy Industry Series C, (in print)

2. Béda, Gy. - Kozák, I.: Mechanics of elastic bodies (in Hung.), Műszaki Könyvkiadó, Budapest, 1987

3. Béda, Gy. - Kozák, I. - Verhás, J.: Mechanics of solids (in Hung.), Műszaki Könyvkiadó, Budapest, 1986

4. Hemsley, J.A.: Elastic solutions for thin cylindrical shell walls under axisymmetric loading, Proc. Instn. Civ. Engrs, Part 2, 1987, 83, Mar., 91-114

5. KIMHER computer program for axisymmetrical deformations of shells, plates and disks and for plane structures, Software catalogue of NME, 1988. No. G-9-6

6. Kozák, I.: Theory of thin elastic shells in terms of stresses (in Hung.), Theses for degree D. Sc., Miskolc, 1980

7. Kozák, I.: Construction of an approximate linear shell theory by asymptotic integration of the equations of elasticity in terms of stresses, Advances in Mechanics, 6, 1-2, (1983), 91-110

8. Kozák, I.: Strength of materials III (in Hung.), Tankönyvkiadó, Budapest, 1981

9. Kozák, I.: Strength of materials V (in Hung.), Tankönyvkiadó, Budapest, 1979

10. Oden, J.T. - Reddy, J.N.: On dual complementary variational principles in mathematical physics, Int. J. Engng. Sci., 12, (1974), 1-29

Acta Technica Acad. Sci. Hung., 103(2-3), pp. 91-102 (1990)

BOUNDS FOR THE DEFLECTION OF BEAMS OF VARIABLE CROSS-SECTION

ECSEDI, I.*

(Received: 2 April 1990)

The objective of this paper is to give a method for obtaining the upper and lower bounds for the end deflection of a beam of variable cross section treated as a generalised plane stress state of a disk of variable thickness. The material of the beam is linearly elastic, isotropic and inhomogeneous. The bounding formulae are derived by means of application of the principles of minimum potential and complementary energy of the theory of elasticity.

1. The beam AB of length L and symmetrical cross-section with respect to axis y is subject at its end B to a concentrated load $\underline{F}_B = Q\,\underline{e}_y$. The other end of the beam is fixed. The shape of the beam is given by thickness function $h = h(x,y)$ (Fig. 1). Young's modulus E and Poisson's ratio ν are depending on coordinates x,y, i.e.

$$E = E(x,y) \quad , \qquad \nu = \nu(x,y) \quad . \tag{1.1}_{1,2}$$

As a consequence of Eqs $(1.1)_{1,2}$, shear modulus G is depending also on coordinates x,y. It is known that

$$G(x,y) = \frac{E(x,y)}{2(1+\nu(x,y))} \quad . \tag{1.1}_3$$

The middle firbre of the beam considered as a disk of variable thickness is plane xy. We investigate a rectangular region bounded by straight lines $\overline{A_1A_2}$, $\overline{A_2B_2}$, $\overline{A_1B_1}$, $\overline{B_1B_2}$ (Fig. 2). The cross-sections of the beam-ends are A and B, resp. Boundary section $\overline{B_1B_2}$ is loaded by force Q in positive direction y, boundary sections $\overline{A_1B_1}$ and $\overline{A_2B_2}$ are traction-free, boundary section $\overline{A_1A_2}$ is fixed.

*Ecsedi, István, H-3526 Miskolc, Klapka Gy. u. 36, IX/2, Hungary

Akadémiai Kiadó, Budapest

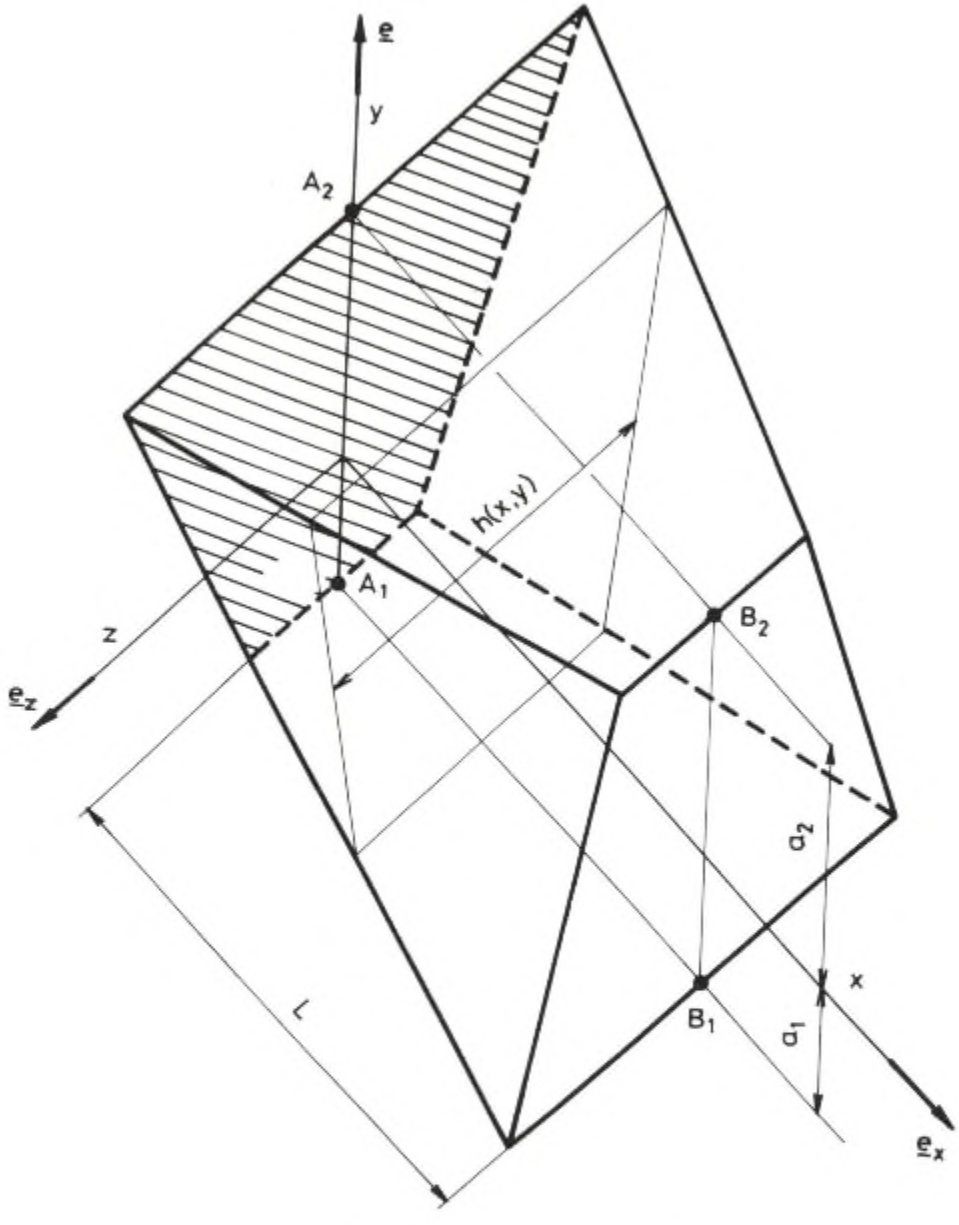

Fig. 1. Elastic beam of variable cross-section

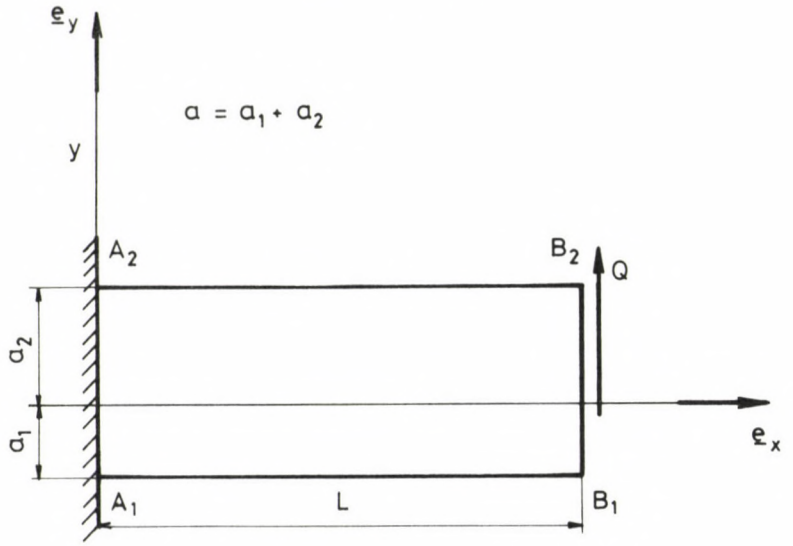

Fig. 2. Rectangular region

The governing equations of the disk of variable cross-section are as follows (/1/, /2/, /3/):

(a) Equations of equilibrium for the stress resultants:

$$\frac{\partial N_x}{\partial x} + \frac{\partial N_{xy}}{\partial y} = 0 \quad , \qquad 0 < x < L \quad , \quad -a_1 < y < a_2 \quad ; \ (1.2)_1$$

$$\frac{\partial N_{xy}}{\partial x} + \frac{\partial N_y}{\partial y} = 0 \quad , \qquad 0 < x < L \quad , \quad -a_1 < y < a_2 \quad ; \ (1.2)_2$$

$$N_{xy} = N_{yx} \quad , \qquad 0 \leq x \leq L \quad , \quad -a_1 \leq y \leq a_2 \quad . \ (1.2)_3$$

(b) Strain equations:

$$\varepsilon_x = \frac{\partial u}{\partial x} \quad , \quad \varepsilon_y = \frac{\partial v}{\partial y} \quad , \ 0 \leq x \leq L \quad , \quad -a_1 \leq y \leq a_2 \quad ; \ (1.3)_{1,2}$$

$$\gamma_{xy} = \frac{\partial u}{\partial y} + \frac{\partial v}{\partial x} \quad , \qquad 0 \leq x \leq L \quad , \quad -a_1 \leq y \leq a_2 \quad . \ (1.3)_3$$

(c) Relationships between the stress resultant and strain:

$$N_x = \frac{Eh}{1-\nu^2} \left(\varepsilon_x + \nu \varepsilon_y \right) \quad , \quad 0 \leq x \leq L \quad , \quad -a_1 \leq y \leq a_2 \quad ; \ (1.4)_1$$

$$N_y = \frac{Eh}{1-\nu^2}(\nu\varepsilon_x + \varepsilon_y) \quad , \qquad 0 \leq x \leq L \quad , \quad -a_1 \leq y \leq a_2 \quad ; (1.4)_2$$

$$N_{xy} = \frac{Eh}{2(1+\nu)} \gamma_{xy} \quad , \qquad 0 \leq x \leq L \quad , \quad -a_1 \leq y \leq a_2 \quad . (1.4)_3$$

In the present case, the following boundary conditions should be satisfied.

(a) Boundary conditions for traction:

$$N_x(L, y) = 0 \quad , \qquad -a_1 \leq y \leq a_2 \quad ; \qquad (1.5)_1$$

$$N_{xy}(x, -a_1) = 0 \quad , \quad N_y(x, a_2) = 0 \quad , \quad 0 < x < L \quad ; \qquad (1.5)_2$$

$$N_{xy}(x, a_2) = 0 \quad , \quad N_y(x, a_2) = 0 \quad , \quad 0 < x < L \quad . \qquad (1.5)_3$$

(b) Boundary conditions for displacement:

$$u(0, y) = 0 \quad , \qquad v(0, y) = 0 \quad , \quad -a_1 \leq y \leq a_2 \quad ; \qquad (1.6)_1$$

$$v(L, y) = f \quad , \qquad -a_1 \leq y \leq a_2 \quad . \qquad (1.6)_2$$

Deflection f of cross-section B is caused by vertical force Q. Q is given by the integral:

$$Q = \int_{-a_1}^{a_2} N_{yx}(L, y)\, dy \quad . \qquad (1.7)$$

There will be two formulae used with strain energy:

- strain energy U, which is a homogeneous quadratic function of the strain components, can be obtained from the formula:

$$U = \frac{1}{2} \int_{-a_1}^{a_2} \int_0^L \frac{Eh}{1+\nu} \left\{ \frac{1}{1-\nu} (\varepsilon_x^2 + \varepsilon_y^2 + 2\nu\varepsilon_x \varepsilon_y) + \right.$$

$$\left. + \frac{1}{2} \gamma_{xy}^2 \right\} dxdy \qquad (1.8)_1$$

- strain energy V, which is a homogeneous quadratic function of the stress resultants, can be obtained from the formula:

$$V = \frac{1}{2} \int_{-a_1}^{a_2} \int_{0}^{L} \frac{1}{Eh} \left\{ N_x^2 + N_y^2 - 2\nu N_x N_y + 2(1+\nu) N_{xy}^2 \right\} dxdy \quad . \qquad (1.8)_2$$

The work performed by the traction at boundary section B_1B_2 is equal to W. The magnitude of work W can be calculated as follows:

$$W = \frac{1}{2} \int_{-a_1}^{a_2} N_{yx}(L,y)\, v(L,y)\, dy = \frac{1}{2} f \int_{-a_1}^{a_2} N_{yx}(L,y)\, dy = \frac{1}{2} Qf \quad . \qquad (1.9)$$

From the equality of the eigenwork with the strain energy, we get formulae $(1.10)_{1,2}$

$$U = \frac{1}{2} Qf \quad , \qquad V = \frac{1}{2} Qf \quad . \qquad (1.10)_{1,2}$$

By using the principle of potential energy and the principle of complementary energy, we can establish a two-sided estimation for work W. The two-sided estimation is given by inequalities:

$$W \leq U(\tilde{\varepsilon}_x, \tilde{\varepsilon}_y, \tilde{\gamma}_{xy}) \quad , \qquad (1.11)_1$$

$$W \geq f\tilde{Q} - V(\tilde{N}_x, \tilde{N}_y, \tilde{N}_{xy}) \quad . \qquad (1.11)_2$$

In relationships $(1.11)_{1,2}$:

$$\tilde{\varepsilon}_x = \frac{\partial \tilde{u}}{\partial x} \quad , \qquad \tilde{\varepsilon}_y = \frac{\partial \tilde{v}}{\partial y} \qquad (1.12)_{1,2}$$

$$\tilde{\gamma}_{xy} = \frac{\partial \tilde{v}}{\partial x} + \frac{\partial \tilde{u}}{\partial y} \quad , \qquad (1.12)_3$$

where $\tilde{u} = \tilde{u}(x,y)$ and $\tilde{v} = \tilde{v}(x,y)$ are differentiable functions which satisfy displacement boundary conditions $(1.6)_{1,2}$, and $\tilde{N}_x$, $\tilde{N}_y$, $\tilde{N}_{xy} = \tilde{N}_{yx}$ are differentiable functions which satisfy differential equations of equilibrium $(1.2)_{1,2,3}$ and traction boundary conditions $(1.5)_{1,2,3}$, moreover Q is given by formula:

$$Q = \int_{-a_1}^{a_2} \tilde{N}_{yx}(L,y)\, dy \quad . \tag{1.13}$$

Functions $\tilde{u} = \tilde{u}(x,y)$, $\tilde{v} = \tilde{v}(x,y)$ are called kinematically admissible displacement functions, and functions $\tilde{N}_x = \tilde{N}_x(x,y)$, $\tilde{N}_y = \tilde{N}_y(x,y)$, $\tilde{N}_{xy} = \tilde{N}_{yx} = \tilde{N}_{xy}(x,y)$ are called statically admissible stress resultants /5/. Equal signs in relationships $(1.11)_{1,2}$ apply whenever $\tilde{u}$, $\tilde{v}$ and $\tilde{N}_x$, $\tilde{N}_y$, $\tilde{N}_{xy} = \tilde{N}_{yx}$, respectively, are the actual solution functions to the boundary value problem formulated in Eqs $(1,2)_{1,2,3}$, $(1.3)_{1,2,3}$, $(1.4)_{1,2,3}$, $(1.5)_{1,2,3}$, $(1.6)_{1,2}$.

2. Let inequality relationship $(1.11)_1$ be applied to kinematically admissible displacement functions:

$$\tilde{u} = -\frac{3}{2}(\lambda - 1) f \frac{y}{L} \left[\frac{(L-x)^2}{L^2} - 1 \right] , \tag{2.1}_1$$

$$\tilde{v} = \frac{\lambda - 1}{2} f \left[3\frac{L-x}{L} - \frac{(L-x)^3}{L^3} - 2 \right] - \lambda f \left(\frac{L-x}{L} - 1 \right) . \tag{2.1}_2$$

In $(2.1)_{1,2}$, λ is an arbitrary constant. By performing a simple calculation, we obtain upper bound relationship:

$$W \leq \overline{W}(\lambda) = \frac{f^2}{2} \left[9(\lambda - 1)^2 \frac{C}{L^6} + \frac{1}{2} \lambda^2 \frac{D}{L^2} \right] , \tag{2.2}$$

where

$$C = \int_{-a_1}^{a_2} \int_0^L \frac{E(x,y)h(x,y)}{1 - [\nu(x,y)]^2} (L-x)^2 y^2 \, dxdy , \tag{2.3}_1$$

$$D = \int_{-a_1}^{a_2} \int_0^L \frac{E(x,y)h(x,y)}{1+\nu(x,y)} \, dxdy . \tag{2.3}_2$$

The optimum value of λ is belonging to the minimum value of upper bound $\overline{W}$. From the necessary condition of optimum:

$$\frac{\partial \overline{W}(\lambda)}{\partial \lambda} = 0 \tag{2.4}$$

we obtain

$$\lambda = \frac{9\frac{C}{L^6}}{9\frac{C}{L^6} + \frac{1}{2}\frac{D}{L^2}} \quad . \tag{2.5}$$

With Eq. (2.5) substituted into relationship (2.2), the following upper bound relationship is yielded:

$$W \leq \frac{1}{2} f^2 \frac{1}{\frac{2L^2}{D} + \frac{L^6}{9C}} \quad . \tag{2.6}$$

From upper bound relationship (2.6) follows that

$$Q \leq f\,\overline{K} = f \frac{1}{\frac{2L^2}{D} + \frac{L^6}{9C}} \quad . \tag{2.7}$$

If Q is a prescribed value, then relationship (2.7) yields the lower bound for deflection f.

3. Starting from inequality relationship $(1.11)_2$, we obtain relationship:

$$f^2\left\{\int_{-a_1}^{a_2} T(y)dy - \int_{-a_1}^{a_2}\int_0^L \frac{(L-x)^2\,|T'(y)|^2}{2E(x,y)\,h(x,y)}\,dxdy - \right.$$

$$\left. - \int_{-a_1}^{a_2}\int_0^L \frac{|T(y)|^2}{2G(x,y)\,h(x,y)}\,dxdy \right\} \leq W \tag{3.1}$$

by choosing

$$\tilde{N}_x = f(L - x)T'(y) \quad , \tag{3.2}_1$$

$$\tilde{N}_y = 0 \quad , \tag{3.2}_2$$

$$\tilde{N}_{xy} = \tilde{N}_{yx} = fT(y) \quad . \tag{3.2}_3$$

In $(3.2)_{1,3}$, function $T = T(y)$ will satisfy boundary conditions:

$$T(-a_1) = 0 \quad , \qquad T(a_2) = 0 \quad . \tag{3.3}_{1,2}$$

From relationship (3.1), gives to us the upper bound for deflection f is yielded as follows:

$$f \left\{ 2 \int_{-a_1}^{a_2} T(y)dy - \int_{-a_1}^{a_2} \int_0^L \frac{(L-x)^2 |T'(y)|^2}{E(x,y)\, h\,(x,y)} \, dxdy - \right.$$

$$\left. - \int_{-a_1}^{a_2} \int_0^L \frac{|T(y)|^2}{G(x,y)h(x,y)} \, dxdy \right\} \leq Q \tag{3.4}$$

if load Q is a prescribed value.

4. We shall restrict our considerations to a special case of inhomogeneity and the non-uniform cross-section. The special case is characterised by the following form of thickness function:

$$h(x,y) = H_0 h_1(x)\, h_2(y) \tag{4.1}$$

and the elastic inhomogeneity is given by formulae:

$$E(x,y) = E_0\, e_1(x)\, e_2(y) \quad , \tag{4.2}_1$$

$$\nu(x,y) = \nu_0\, \nu_1(x)\, \nu_2(y) \quad . \tag{4.2}_2$$

Naturally, relationship:

$$G(x,y) = \frac{E_0 e_1(x)\, e_2(y)}{2(1+\nu_0\, \nu_1(x)\, \nu_2(y))} \tag{4.2}_3$$

holds. Quantities H_0, E_0, ν_0 are constants. Next, we choose the position of axis z so that equation:

$$\int_{-a_1}^{a_2} y e_2(y)\, h_2(y)\, dy = 0 \tag{4.3}$$

be satisfied. We define the following quantities:

$$N_1 = \int_0^L \frac{(L - x)^2}{e_1(x) h_1(x)}\, dx \quad , \tag{4.4}_1$$

$$P_1 = \int_0^L \frac{dx}{e_1(x) h_1(x)} \quad , \qquad R_1 = \int_0^L \frac{\nu_1(x) dx}{e_1(x) h_1(x)} \quad ; \tag{4.4}_{2,3}$$

$$I_2 = \int_{-a_1}^{a_2} y^2\, e_2(y)\, h_2(y)\, dy \quad , \tag{4.5}_1$$

$$S_2(y) = \int_{-a_1}^{y} \eta\, e_2(\eta)\, h_2(\eta)\, d\eta \quad , \tag{4.5}_2$$

$$P_2 = \int_{-a_1}^{a_2} \frac{|S_2(y)|^2}{e_2(y) h_2(y)}\, dy \quad , \tag{4.5}_3$$

$$R_2 = \int_{-a_1}^{a_2} \frac{|S_2(y)|^2\, \nu_2(y)}{e_2(y)\, h_2(y)}\, dy \quad . \tag{4.5}_4$$

From relationship (3.4), by using function:

$$T(y) = -cf \frac{E_0 H_0}{I_2} S_2(y) \tag{4.6}$$

the following bounding formula is obtained:

$$f\frac{E_0H_0}{I_2}\left\{-c^2\left[N_1+\frac{2}{I_2}(P_1P_2+\nu_0R_1R_2)\right]+2cI_2\right\}\leq Q \tag{4.7}$$

where c is an arbitrary constant. It may easily be pointed out that bounding formula (4.7) gives the best result if

$$c=\frac{I_2}{N_1+\frac{2}{I_2}(P_1P_2+\nu_0R_1R_2)} \quad . \tag{4.8}$$

Introduction of formula (4.8) into relationship (4.7) gives bounding formula:

$$Q\geq\underline{K}f=\frac{E_0H_0I_2}{N_1+\frac{2}{I_2}(P_1P_2+\nu_0R_1R_2)}\,f \quad . \tag{4.9}$$

5. Let us consider the case of a homogeneous beam of constant cross-section. In this case we have:

$$h_1(x)=1 \quad , \qquad h_2(y)=1 \quad , \tag{5.1}_{1,2}$$

$$e_1(x)=1 \quad , \qquad e_2(y)=1 \quad , \tag{5.1}_{3,4}$$

$$\nu_1(x)=1 \quad , \qquad \nu_2(y)=1 \quad . \tag{5.1}_{5,6}$$

It follows from Eqs $(5.1)_{1,2,3,4,5,6}$ that

$$H=H_0 \quad , \qquad E=E_0 \quad , \qquad \nu=\nu_0 \quad , \tag{5.2}_{1,2,3}$$

$$I_2=I_0=\frac{a^3}{12} \quad , \qquad (a=a_1+a_2) \quad , \tag{5.2}_4$$

$$N_1=\frac{L^3}{3} \quad , \qquad C=\frac{E_0H_0I_0L^3}{3(1-\nu_0^2)} \quad . \tag{5.2}_{5,6}$$

If we neglect the effect of shear on deflection f, then relationships:

$$\overline{K}=\frac{3E_0\,H_0\,I_0}{(1-\nu_0^2)\,L^3} \quad , \tag{5.3}_1$$

$$\underline{K} = 3\frac{E_0 H_0 I_0}{L^3} \qquad (5.3)_2$$

are obtained from bounding formulae (2.7) and (4.9). By the application of the theory of strength of materials formula:

$$Q = \frac{3E_0 H_0 I_0}{L^3} f \qquad (5.4)$$

can be derived in this special case. It can be read out from formulae $(5.3)_{1,2}$ and (5.4) that in case the effect of shear on the deformation is neglected and if $\nu_0 = 0$, then the results yielded by bounding formulae (2.7), and (4.9) will be identical in the case of a homogeneous beam of constant cross-section.

6. The basic idea of this paper is borrowed from Reissner's paper /4/, mainly to choose the suitable functions for obtaining the bounding formulae of end deflection. Reissner's work /4/ is concerning the laminated cantilever beam of constant cross-section. In /4/, Young's moduli and Poisson's ratio are independent from coordinate x, the material of the beam is anisotropic, and the elastic constants are even functions of coordinate y.

7. The results of this paper can be directly used to solve some simple practical problems of composite beams, sandwich beams, laminated beams of variable cross-section.

The theory of beams is widely used as a first approximation to numerous problems in practice. When the theory of composite beams is applied, the accuracy of the beam theory becomes problematic because several flexible couplings can occur that strongly influence the behaviour of composite beams. These coupling effects, and the effect of shear stress on deformation should be reckoned with if the beam problem is analysed as a disk of variable thickness. In this paper, a simple practical problem illustrates how we can use the governing equations of the disk of variable thickness to solve beam-like problems in a more exact form than that obtained by the application of the traditional theory of composite beams.

The flexibility and stiffness coefficient of the end-loaded composite beams of variable cross-section can be also calculated by using

bounding formulae (2.7), (4.9). It is important that these coefficents should be reckoned with in the solution of certain problems associated with materials and vibration.

REFERENCES

1. Sokolnikoff, I.S.: Mathematical theory of elasticity, 2nd edition McGraw-Hill, New York, 1956, 253-257

2. Vocke, W.: Der profil-ebene Spannungszustand, ZAMM. 4.1. 1961. Heft 6. 257-261

3. Trefftz, E.: Mathematische Elastizitästheorie, Handbuch der Physik. VI. Mechanik der Elastichen Körper, Springer Verlag, Berlin, 1928. 112-113

4. Reissner, E.: Upper and lower bounds for deflections of laminated cantilever beams including the effect of transverse shear deformation, Journ. Appl. Mech. December 1973, 988-991

5. Washizu, K.: Variational methods in elasticity and plasticity, New York, Pergamon Press, 1968. 27-31

Acta Technica Acad. Sci. Hung., 103(2-3), pp. 103-113 (1990)

ANALYTICAL SOLUTIONS FOR DISCRETE BOUNDARY VALUE PROBLEMS OF MACROSCOPICALLY ISOTROPIC HRENNIKOFF-TYPE GRIDS

HEGEDŰS, I.*

(Received: 25 January 1990)

The paper deals with an analytical method for solving discrete boundary value problems of partial difference equations for the stress functions of macroscopically isotropic Hrennikoff-type grids having two sets of analogous joints. This network property permits alternative ways of formulating the problem: one when a difference equation of variable coefficients is used for one stress function and another when a system of difference equations of constant coefficients is used for two stress functions. The paper shows that the two ways lead to the same solution and this solution differs from that obtained by the difference method for the analogue disc problem. It also presents an analysis for the same grid formulated in a rotated coordinate system. The illustrative example attached to this analysis shows the existence of boundary loads of a semi-infinite Hrennikoff-type grid which produce bar forces only inside a one mesh thick boundary strip.

1. Macroscopically isotropic Hrennikoff-type grids

Hrennikoff-type grids are plane grids with hinged joints and with a regular network shown in Fig. 1. The grid is called macroscopically homogeneous and isotropic if all the bars forming the squares and the diagonals, respectively, are of the same cross-sectional area and the ratio of the cross-sectional area of bars forming the squares to that of the diagonals is $\sqrt{2/2}$.

Isotropic Hrennikoff-type grids are useful tools in numerical analysis as discrete replacements for in-plane loaded isotropic plates, provided the mesh of the replacement grid is less by magnitude than the characteristic measures of the plate /1/. Actually, a detailed analysis can show that a one-to-one correspondence of connections between values characterizing the states of stress and strain of homogeneous isotropic plates and those of macroscopically isotropic Hrennikoff-type grids can

*Hegedűs, István, H-2083 Solymár, Váci Mihály u. 10, Hungary

Akadémiai Kiadó, Budapest

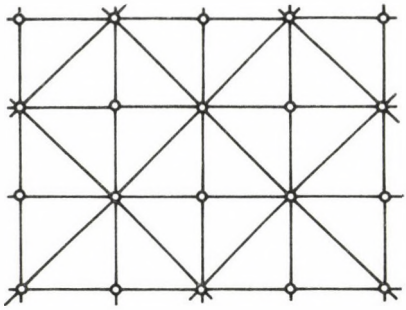

Fig. 1.

only found in cases of homogeneous states of stress and strain and only if Poisson's ratio of the plate equals with 1/3, /2/. Hence, in cases of varying states of stresses the accuracy of the results obtained by a replacement Hrennikoff-type grid somehow depends on this variation. The aim of the paper presented here is to show an analytical formulation which enables us to analyse this question with the aid of efficient mathematical methods.

2. Stress function of plane grids with hinged joints

For plane grids with hinged joints and with general triangular networks there exists a discrete analogue of Airy's stress function of in-plane loaded elastic plates /3/. It can be used to reduce the analysis of internal forces and deformations of plane grids to boundary value problems for a stress function in a way analogous to that in case of in-plane loaded plates, that is, if the boundary conditions of the grid permit to take the boundary values of the stress function.

Stress function of a plane grid with triangular network loaded by external forces at the boundary consists of linear functions of the coordinates of the plane of the grid which attach to each other at the netlines of the grid with discontinuites in the first derivatives. Hence, the diagram of the stress function is an open polyhedron of triangular faces and the problem can be reduced to the determination of the values of the stress function at the summits of this polyhedron. The diagram of the stress function visibly defines the bar forces of the grid in a way that the changes in slope of a broken surface line which has a projection perpendicular to the bar axis containing the projection of the kneeing point is proportional with the bar force acting at the bar in question.

Summit values of the stress function can be computed by solving the system of compatibility equation of the elastic bar extensions expressed in terms of the stress function. In case of grids with regular networks and homogeneous rigidities the way of the solution resembles very much to the finite difference technics. Compatibility equations can be written joint by joint, analogously to those for nodal values of a regular network of differences in finite difference method, applying star-shaped operator diagrams of the compatibility equations /3/.

Hrennikoff-type grids contain two analogous systems of joints, that is, in case of macroscopically homogeneous Hrennikoff-type grids two different compatibility operators are to use: one for joints connecting eight bars, and another for those connecting only four ones. The star-shaped diagrams of both operators are shown in Fig. 2.

Fig. 2.

Irrelevant constant multipliers have been omitted from the above operators. Both operators could also be divided by 2, however, their presented form refers better to the speciality of the two compatibility operators: the averages of the respective operator-weights obtain those of the well-known "biharmonic" difference operator.

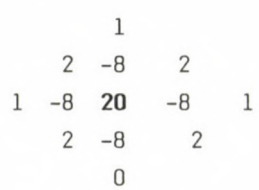

Fig. 3.

3. The difference equation of a Hrennikoff-type grid

There is an alternative way of defining compatibility conditions, using difference calculus for functions of discrete variables. Let serial numbers of rows and columns i and j, respectively, be integer variables, so that any paris of i and j refer to joints that lie in the i-th row at the j-th column. One system of analogous joints belongs to the even values another one belongs to the odd values of the sum i+j. The two different type compatibility equations defined by the star shaped operators in Fig. 2 can be written in an unified form of the following equation:

$$D^2[F] + (-1)^{i+j} D[F] = 0 \qquad (1)$$

where $F = F(i,j)$ is the stress function of discrete variabels i, and j and higher order partial difference operators $D[\ ]$, and $\tilde{D}[\ ]$ can be expressed as polynomials of first order difference operators $\delta_1[\ ]$, and $\delta_2[\ ]$ which refer to first central differences in variables i and j, respectively:

$$D^2[\ ] = (\delta_1^2 + \delta_2^2)^2[\ ],$$

$$\tilde{D}[\ ] = (\delta_1^4 + \delta_2^4)[\ ] + 4(\delta_1^2 + \delta_2^2)[\ ].$$

Advantages of using difference calculus become obvious by taking into account the analogies between analytical methods for solving linear differential, and difference equations /4/.

Despite of using difference calculus, Eq. 1 looks problematic in this respect because of variable coefficient $(-1)^{i+j}$. Variable coefficients do not permit to use in a simple way discrete analogues of Lagrange's method for solving linear differential equations of constant coefficients. However, these methods can again be used if a method is found which reduces the problem to another with a governing difference equation of constant coefficients.

3.1. Reducing the equation to that of constant coefficients

Eq. 1 can be reduced to another with constant coefficients in the way as follows.

First, a generator function H is introduced by the equation

$$M(H) = F \quad ,$$

where M is a difference operator not yet known. It has to be chosen in a way that by introducing Eq. 2 into Eq. 1

$$D^2 \left[M(H) \right] + (-1)^{i+j} \tilde{D} \left[M(H) \right] = 0 \qquad (3)$$

the difference operator of the equation becomes of constant coefficients.

Taking into account that for arbitrary functions X of discrete variables i, and j equations

$$D^2 \left[(-1)^{i+j} X \right] = (-1)^{i+j} \left\{ D^2 \left[X \right] + 16 D \left[X \right] + 64 X \right\} ,$$

$$\tilde{D} \left[(-1)^{i+j} X \right] = (-1)^{i+j} \tilde{D} \left[X \right] ,$$

identically hold, it is easy to prove that

$$M\left[\quad \right] = D^2\left[\quad \right] + 8 D\left[\quad \right] + (-1)^{i+j} \tilde{D}\left[\quad \right] \qquad (4)$$

meets this requirement. By introducing Eq. 4 into Eq. 3 difference equation of constant coefficients is obtained:

$$\left\{ D^2 (D+8)^2 - \tilde{D}^2 \right\} \left[H \right] = 0 \quad . \qquad (5)$$

The difference operator of Eq. 5 can be factorized into a product of two operators:

$$\left\{ D(D+8) + \tilde{D} \right\}\left[\quad \right] \times \left\{ D(D+8) - \tilde{D} \right\}\left[\quad \right] ,$$

that is, solutions for Eq. 5 can be constructed as linear combinations of the solutions of equations

$$D^2 \left[H \right] + 8 D \left[H \right] + \tilde{D} \left[H \right] = 0 \quad , \qquad (6a)$$

and

$$D^2 \left[H \right] + 8 D \left[H \right] - \tilde{D} \left[H \right] = 0 \quad . \qquad (6b)$$

Solving Eq. 5 of Eqs 6a, b needs boundary conditions for H. These can be obtained by expressing in terms of differences of H the boundary loads as bar forces acting at the fictitious continuation of the grid. However, in

most practical cases complete discrete boundary value problems are not of the form favourable for analytical solution.

Complete analytical solutions can be derived e.g. for grids of the shape of infinitely long strips, or for semi-infinite grids loaded by periodic boundary loads. Their importance is rather in the fact that available analytical solutions qualitatively show the behaviour of the structure in cases of different types of external loads.

3.2. An alternative method: using two stress functions

An alternative way of formulating the problem in difference equations with constant coefficients can be found by using two functions of discrete variables $F_1(i,j)$, and $F_2(i,j)$ to obtain the stress function of the grid. One which has to be interpreted only at joints where i+j is an even, number and another at joints where i+j is odd. By so doing, Eq. 1 can be replaced for a system of two simultaneous difference equations as follows:

$$D_{11}[F_1] + D_{12}[F_2] = 0 \quad , \tag{7a}$$

$$D_{21}[F_1] + D_{22}[F_2] = 0 \quad , \tag{7b}$$

where

$$D_{11}[\ ] = D^2[\ ] + \tilde{D}[\ ] + 8\,(\delta_1^2[\ ] + \delta_2^2[\ ] + 4) \quad ,$$

$$D_{12}[\ ] = D_{21}[\ ] = -8\,(\delta_1^2[\ ] + \delta_2^2[\ ] + 4) \quad , \tag{8a-c}$$

$$D_{22}[\ ] = D^2[\ ] - \tilde{D}[\ ] + 8\,(\delta_1^2[\ ] + \delta_2^2[\ ] + 4) \quad .$$

It may worth to mention that neither F_1 nor F_2 are stress functions in the original sense of the word, moreover, they are differentiable functions of two variables without discontinuities in the derivatives. Their diagrams are envelopes of that of the stress function of the grid, and only summits of the polyhedron diagram of the stress function lie on either envelopes. Eqs 7a, and 7b are physically interpreted only at joints belong to even and odd values of i+j, respectively, nevertheless, they can be met for any values of i, and j, if F_1 and F_2 are produced as analytical solutions of the difference equation system.

The way of producing analytical solutions is as follows /4/. First, the characteristic difference equation for a generator function H is

written as

$$\{D_{11}D_{22} - D_{12}D_{21}\}[H] = 0 \quad , \tag{9}$$

where the operator of the characteristic difference equation equals with the operator determinant of the linear difference equation system. Then, F_1, and F_2 are produced by using the generator function as

$$F_1 = a\, D_{22}[H] - b\, D_{12}[H] \quad , \tag{10a}$$

$$F_2 = b\, D_{11}[H] - a\, D_{21}[H] \quad , \tag{10b}$$

where a, and b are arbitrary numbers.

Taking into account the expressions for the difference operators given by Eqs 8a-c, Eq. 9 can be written as

$$\{D^2\,(D+8)^2 - \tilde{D}^2\}[H] = 0 \quad .$$

This equation is perfectly the same as Eq. 5, that is, the procedure of using of two functions to obtain the stress function of the grid arrives at the same characteristic difference equation as the alternative method presented in Sec. 3.1. despite of the different physical interpretations of the generator functions. Obviously, the boundary conditions for H can also be expressed in the same mathematical form.

There exists a general method of analysis based on the difference equation system for the displacements of joints. It can also be reduced to a discrete boundary value problem for a generator function that has to meet a characteristic difference equation and this equation is also the same as Eq. 5.

4. Hrennikoff-type grids in a rotated co-ordinate system

Isotropic Hrennikoff-type grids are mostly used in another co-ordinate system, where directions of i and j are parallel with the squares of the network as shown in Fig. 4.

In this case the simplest way of using discrete coordinates is that integer values of i, and j refer to the set of joints that connect eight bars and those of fractures 0.5 refer to points of intersection of diag-

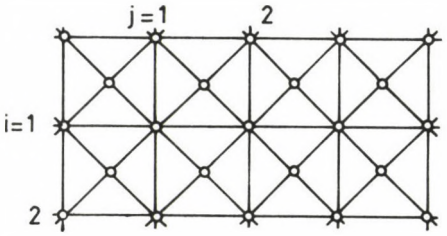

Fig. 4.

onals. Introducing functions F_1 and F_2 physically interpreted for values of i, and j of zero and of 0.5 fractures, respectively, compatibility conditions can again be epxressed by a system of partial linear difference equations of the form of Eqs 7a, b, where

$$D_{11}[\quad] = \{\delta_1^2 \quad \delta_2^2 + 3(\delta_1^2 + \delta_2^2) + 16\}[\quad],$$

$$D_{22}[\quad] = \{\delta_1^2 + \delta_2^2 + 16\}[\quad], \tag{11a-c}$$

$$D_{12}[\quad] = D_{21}[\quad] = \{-16\,\mu_1\mu_2\}[\quad].$$

$\mu_1[\ ]$ and $\mu_2[\ ]$ refer to average operators in variables i and j, respectively. The solution can again be reduced to that of a characteristic difference equation for a generator function H:

$$\{(\delta_1^2 + \delta_2^2)(\delta_1^2 + \delta_2^2 + \tfrac{1}{3}\delta_1^2 \quad \delta_2^2)\}[H] = 0 \quad . \tag{12}$$

The factorized form of the operator shows that the solutions can be found using those of the equations

$$(\delta_1^2 + \delta_2^2)[H] = 0 \quad ,$$

and

$$(\delta_1^2 + \delta_2^2 + \tfrac{1}{3}\delta_1^2\,\delta_2^2)[H] = 0 \quad .$$

It may worth to mention that the "biharmonic" difference operator can also be interpreted in the rotated co-ordinate system used in this section. It yields the characteristic difference equation as follows:

$$(\delta_1^2 + \delta_2^2 + \tfrac{1}{4}\delta_1^2\,\delta_2^2)^2[H] = 0 \quad , \tag{13}$$

that is, solutions of Eq. 12 and Eq. 13 may significantly differ from each other in the cases when the effect of operator term $\delta_1^2 \quad \delta_2^2$ is not negligible.

5. Illustrative example

Let us analyse the bar forces of the Hrennikoff-type grid shown in Fig. 5. The grid is supposed infinite in directions i and the positive values of j and its boundary is at j=0.

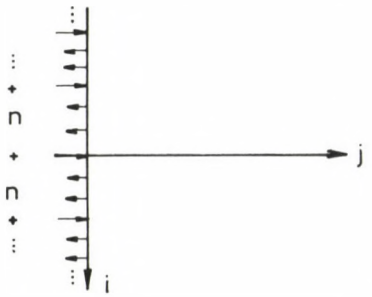

Fig. 5.

The boundary is subject at the joints to normal forces P(i) of the magnitudes periodically varying with a period n,

$$P(i) = P_0 \cos\left(\frac{2}{n}\pi i\right) \quad .$$

Boundary conditions for F_1, and F_2 are as follows:

$$\mu_1/\mu_2 \left[F_1\left(i, -\tfrac{1}{2}\right)\right] = F_2\left(i, -\tfrac{1}{2}\right) \quad ,$$

$$\mu_2\left[F_1\left(i, -\tfrac{1}{2}\right)\right] - \mu_1\left[F_2\left(i, -\tfrac{1}{2}\right)\right] = \frac{a}{4}\, p(i) \quad .$$

These boundary conditions refer to zero bar forces at the diagonals and bar forces equal to the external loads at the squares of the fictitious continuation of the grid over the boundary. We can also state as boundary conditions that both F_1, and F_2 have to tend to zero when j tends to the infinity, that is, bar forces are negligibly small outside a boundary zone. Generator function H for F_1 and F_2 can be supposed in the form

$$H = h(j)_n \cos\left(\frac{2}{n}\,\pi i\right) \quad , \tag{14}$$

where $h(j)_n$ does not depend on i.

Taking into account that

$$\delta_1^2 \left[\cos\left(\frac{2}{n}\pi i\right) = -4 \sin^2\left(\frac{\pi}{n}\right) \cos\left(\frac{2}{n}\pi i\right)\right] ,$$

and introducing Eq. 14 into Eq. 12, we obtain a common linear difference equation for $h(j)_n$ as follows:

$$\left\{\left(\delta_2^2 - \alpha\right)\left(\delta_2^2 - \alpha_n - \frac{1}{3}\alpha_n \delta_2^2\right)\right\}\left[h(j)_n\right] = 0 ,$$

where

$$\alpha_n = 4 \sin^2\left(\frac{\pi}{n}\right) .$$

Function $h(j)_n$ can be supposed in the form

$$h(j)_n = A_n \beta_n^j + B_n \gamma_n^j$$

where β_n, and γ_n are solutions of absolute values less than the unity for the algebraic equations

$$\beta_n^2 - (2 - \alpha_n)\beta_n + 1 = 0 ,$$

and

$$\gamma_n^2 - \left(2 + \alpha_n \frac{3}{3 - \alpha_n}\right)\gamma_n + 1 = 0 ,$$

respectively, and coefficients A_n, and B_n are to use for meeting boundary conditions.

Similarly to H, stress functions F_1, and F_2 also consist of two terms, one containing β_n and another containing γ_n. The two terms represent two different "spreadings" of periodic disturbances caused by the boundary loads.

This structure of the solution must basically change if $n = 3$, because in this case $\alpha_n = 3$ and the second factorized operator term of the difference equation for $h(j)_n$ becomes a constant multiplier. A detailed analysis can show that in this case there are components of the boundary loads which do not make rise "spreading" internal forces at all, that is, their effect is limited to a one-step thick boundary zone. This strange behaviour is absolutely unfamiliar among those of continuous elastic structures, however, it is also produced by the discrete substituting model for an isotropic disc represented by Eq. 13 in the case of $n = 2$.

6. Closing remarks

The outlined analysis has shown that stress functions of plane grids with triangular networks and hinged joints can also be used for obtaining analytical solutions in cases of regular networks when the number of sets of analogous joints differs from one. The alternative formulations presented in Secs 3.1 and 3.2 yield the same characteristic difference equation, hence, the two formulations are only different in interpreting the intermediate results.

Both Eqs 5, and 12 show that periodic boundary loads make rise only boundary disturbances, and the "spreadings" of the disturbances depend on the length of the period. This behaviour is analogous to that of isotropic plates, however, the analogy is not perfect. First, because the operator of Eq. 5 and also of Eq. 12 cannot be factorized into the square of an operator, thus, they define two different quotients for the "spreadings", while the operator of Airy's differential equation is the square of the Laplace operator, thus, it defines only one; secondly, because Eqs 5, and 12 define substantially different "spreadings" of the boundary disturbances in the cases of boundary loads with short periods, thus, the grid does not exhibit isotropy. Both discrepancies of the analogy asymptotically vanish if n tends to the infinity, that is, if the mesh of the grid is less by magnitudes than the characteristic length of the boundary load.

REFERENCES

1. Hrennikoff, A.: Solution of problems of elasticity by the framework method, Journ. Appl. Mech., 8, (1941), 169-175

2. Hegedűs, I.: The stress function of plane grids of a general triangular network, Acta Technica Acad. Sci. Hung. 98(3-4), (1985), 309-316

3. Hegedűs, I.: Continuous model analysis of plane trusses of four or more directed diagonals, Acta Technica Acad. Sci. Hung. 83, (1976), 213-228

4. Kollár, L. - Hegedűs, I.: Analysis and Design of Space Frames by the Continuum Method, Akadémiai Kiadó, Budapest, 1985

Acta Technica Acad. Sci. Hung., 103(2-3), pp. 115-141 (1990)

THE INFLUENCE OF THE DISPLACEMENT SPRING RIGIDITY ON THE CRITICAL LOAD OF BARS

JANKÓ, L.* - NAGY, Z.**

(Received: 3 March 1988)

When dimensioning frame-structure bars for buckling, we can proceed - in compliance with the relevant regulations - the way that we examine only one bar at a time while substituting the clamping effect of the rest of the bars by springs. These can be either displacement springs or rotation springs. Literature has so far only considered displacement springs of either zero or infinite rigidity, or rotation springs of finite rigidity. The present article takes a step forward by considering - besides rotation springs of finite rigidity - displacement springs of finite rigidity, too.

The present paper goes beyond theoretical solutions and provides tables which are of high practical value by giving data for determining the critical strength of the bar.

1. Introduction

Although the **linear** (and large deformation) stability theory of elastic bar-structures can already be thought of as a cleared subject, the widespread use of most of the solutions in practical design can only be expected sometime in the future. This delay is partly accounted for by the lack of proper software. But even until then, there is a need for a usable approximative method that meets the requirements of design.

With reinforced concrete structures, the principle on a regulational level /10/ is that - once a set of conditions are fulfilled - bars taken for **separate** ones are investigated individually instead of considering the whole frame in an approximate way. As it is commonly known, the regulation provides approximate formulae on the basis of Gábory's paper /4/ for the calculation of buckling wavelength of bars **fixed** against

*Jankó, László, H-1113 Budapest, Dávid F. u. 5, Hungary

**Nagy, Zoltán, H-1027 Budapest, Mártírok útja 64/A, Hungary

Akadémiai Kiadó, Budapest

displacement (Fig. 1, $c^y \longrightarrow \infty$) and bars that **sway** ($c^y = \emptyset$). For the above two cases of flexibly fixed bars (fixed and swaying) Nemestóthy published /7/, /13/ the precise relations about the calculation of swaying wavelength, and made up diagrams of high utility in design. These diagrams show well how precise the approximation is in /4/ and /10/.

The basic equations in /13/ set up for the extreme cases ($c^y \longrightarrow \infty$, $c^y = 0$) of c^y displacement-rigidity of springs (spring-constant) can also be obtained by way of limiting process (from the connection by Kollár /7/ (see further in (2.7) - (2.13)) which holds for optional values of c^y. Relations in /7/ refer to the case of the model in Fig. 1 where one of the joints has no lateral displacement (e.g. $c_i^y \longrightarrow \infty$).

Setting up a model which shows the buckling of a **frame column** more accurately would require a third spring for each column-end according to /7/ and /8/, since the φ rotation of the column-end creates an H^{φ} horizontal force as well. Further than this, Δy displacement of the column-end creates a bending moment of M^{Δ}. The model of Fig. 1 suggests that rotation φ only causes clamping moment, while displacement Δy, only causes horizontal force. Determining the critical force of the column supported by 3 springs at each column-end is possible on the basis of Lipták's article /8/. This method is especially recommended for taking into account **flexible** fixing effect of the **ground** on the column. The article includes diagrams fit for the purposes of designing columns with pinned upper end and flexibly fixed lower end on the ground.

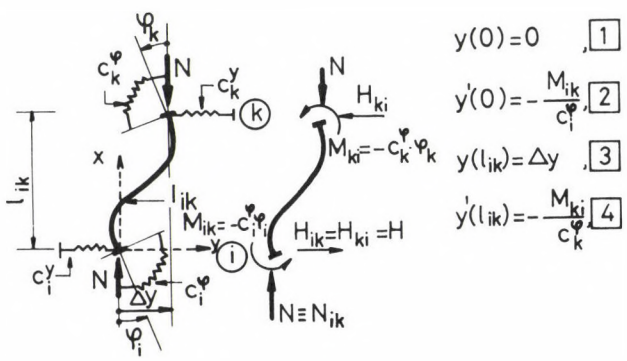

Fig. 1. The calculation model

The present paper is based on the model with 2 springs at both column-ends presented in /7/ and /13/.

The model provides us with the exact solution about the extreme cases of the spring constant against displacement ($c^y \longrightarrow \infty$, $c^y = 0$), as it is very easy to see by comparing equations in /13/ with those in /15/. Regarding the values between the extreme values of c^y, numerical investigations prove that the inaccuracy of the model as compared to /8/ does not exceed the limits of required exactitude in engineering.

If the model is not meant to refer to a frame column, but to **an individual bar supported by actual springs as shown in Fig. 1**, our solution is **accurate**; otherwise the extent of our approximation depends on how much the springs' rigidity values involved can realistically reflect the fixing effects represented by the environment of the frame column and some supporting structure.

Our aim in the following is to extend the procedure in /7/ on pp 7-12 to even **extreme values of the displacement spring constants** (c_i^y, c_k^y) at joints as it is shown by the model of Fig. 1. Besides this, we will also try to demonstrate the impact of the displacement spring constant on the critical load with the help of diagrams and tables.

2. Basic relations

Figure 1 also shows the boundary conditions of the eigenvalue problem. It is to be noted that the procedure in /7/ and /13/ taken as basis fulfils the boundary conditions connected to the curvatures at the end of the bar.

2.1. Auxiliary quantities

The ratio of the rotation spring constants:

$$\delta = \frac{c_k^\varphi}{c_i^\varphi} = \frac{\varrho_k}{\varrho_i} \quad . \tag{2.1}$$

The eigenvalue parameter ($N_{ik} = N_{cr}$):

$$\varepsilon = \varepsilon_{ik} = \frac{\pi}{\nu} = \ell_{ik} \sqrt{\frac{N_{cr}}{E \cdot I_{ik}}} \quad . \tag{2.2}$$

Auxiliary quantities:

$$\mu_a = \frac{1}{4}\ \varrho_i\ , \quad \mu_f = \frac{1}{4}\ \varrho_k\ , \tag{2.3a-b}$$

$$\nu = \frac{\pi}{\varepsilon} = \frac{\ell_o}{\ell_{ik}}\ . \tag{2.4}$$

The enlarged rotation spring constants:

$$\varrho_i = \frac{c_i^{\varphi}\ \cdot\ \ell_{ik}}{E\ \cdot I_{ik}}\ , \quad \varrho_k = \frac{c_k^{\varphi}\ \cdot\ \ell_{ik}}{E \cdot I_{ik}}\ . \tag{2.5a-b}$$

The enlarged displacement spring constant:

$$\varrho^y = \frac{c^y \cdot \ell_{ik}^3}{E \cdot I_{ik}} \tag{2.6}$$

Relations (2.3a-b) are shown so they demonstrate the connection between μ_a, μ_f as published in the regulation /10/, and our enlarged rotation spring constants ϱ_i, ϱ_k.

2.2. Basic relations

Conscious of the fact that the derivation of the buckling determinant (2-8) in /7/, p 11 is found in literature that is not easily available, we first publish the equations that fulfil the conditions in Fig. 1.

The differential equation of the problem (see also /6/ p 52):

$$EI_{ik}\ y'' + N_{cr} y + M_{ik} - H\ x = 0\ .$$

The eigenfunction:

$$y = A \cos \varepsilon\ \frac{x}{\ell_{ik}} + B \sin \varepsilon\ \frac{x}{\ell_{ik}} + \frac{H}{N_{cr}}\ x - \frac{M_{ik}}{N_{cr}}\ .$$

The conditional equations:

$$
\begin{bmatrix}
1 & 0 & 0 & -\frac{1}{N_{cr}} & 0 \\
0 & \frac{\varepsilon}{\ell_{ik}} & \frac{1}{N_{cr}} & \frac{1}{c_i^{\varphi}} & 0 \\
\cos\varepsilon & \sin\varepsilon & \frac{\ell_{ik}}{N_{cr}} - \frac{1}{c^{y}} & -\frac{1}{N_{cr}} & 0 \\
-\frac{\varepsilon}{\ell_{ik}}\sin\varepsilon & \frac{\varepsilon}{\ell_{ik}}\cos\varepsilon & \frac{1}{N_{cr}} & 0 & \frac{1}{c_k^{\varphi}} \\
-\frac{\varepsilon^2}{\ell_{ik}^2}\cos\varepsilon & \frac{-\varepsilon^2}{\ell_{ik}^2}\sin\varepsilon & 0 & 0 & -\frac{1}{EI_{ik}}
\end{bmatrix}
\begin{bmatrix} A \\ B \\ H \\ M_{ik} \\ M_{ki} \end{bmatrix}
= \underline{0} \, .
$$

It is easy to see that the four condition equations (Fig. 1) have been expanded by

$$y''(\ell_{ik}) = -\frac{M(\ell_{ik})}{E\,I_{ik}} = \frac{M_{ki}}{E\,I_{ik}}$$

curvature condition equation (fifth equation). Since the differential equation of the problem is in fact quadratic (/16/ p 51), the number of independent unknowns is four (A, B, H, M_{ik}). It seemed a sensible solution, however, to introduce parameter M_{ik} as an independent fifth unknown instead of writing the relation between M_{ik} and M_{ki} into the original equation system with four unknowns.

This is how the satisfaction of the curvature conditions becomes also obvious; the fulfilment of the local condition (x=0):

$$y''(0) = -\frac{M_{ik}}{EI_{ik}}$$

will be easily understood through applying the first line of the matrix.

From the buckling determinant being zero Kollár /7/ derived a transcendent equation, which we brought to the following form for the sake of our further investigations:

$$A_0 + A_1 \sin\varepsilon + A_2 \cos\varepsilon = 0 \quad , \tag{2.7}$$

where

$$A_0 = 2\,\varepsilon\,\varrho_k \quad , \tag{2.8}$$

$$A_1 = \varepsilon^2 (1+\delta) + \varepsilon^2 \left(\frac{\varepsilon^2}{\varrho_i} - \varrho_k \right) C_f \quad , \tag{2.9}$$

$$A_2 = -2 \varepsilon \varrho_k - \varepsilon^3 (1+\delta) C_f \quad , \tag{2.10}$$

$$C_f = 1 - \frac{\varepsilon^2}{\varrho^y} \quad . \tag{2.11}$$

In the basis equation (2.7) parameter ε according to (2.2) is unknown.

These formulae hold for the version of the model seen on Fig. 1, where one of the joints is not allowed lateral displacement, e.g. when the lower joint is of this type ($H = c^y \Delta y$):

$$c_i^y \longrightarrow \infty \quad , \tag{2.12}$$

$$c_k^y = c^y \quad . \tag{2.13}$$

of Fig. 2.2.

It can be shown that with the help of equations (2.7) - (2.11) any of the ways of support ever described in special literature /1/, /5/, /12/, /13/, /15/, /16/, /17/ can be obtained. In the case of joints with no displacement ($c^y \longrightarrow \infty$) and swaying joints ($c^y = 0$) the equations published by Pflüger /15/ (/15/ p.341, after /1/ and /9/) will result. The equations by Nemestóthy /13/ are identical with these.

3. Extension

First of all let us consider Fig. 2 which we made on the basis of /15/ and /16/.

Equations (2.7) - (2.11) suggest the possibility of extending the procedure to cover the general cases of displacement springs, according to Fig. 2.1 (i.e. the one presented in Fig. 1).

Equations (2.9) and (2.10) show that the size of the support **against displacement** depends on factor C_f /Eq.(2.11)/. This lets us conclude that if we apply the substitution

$$\varrho^y \longrightarrow \varrho_{ik}^y = \frac{\varrho_i^y \cdot \varrho_k^y}{\varrho_i^y + \varrho_k^y} \tag{3.1}$$

in the relation (2.11), then the set of formulae (2.7) - (2.11) will give us the linear (**branching**) critical load of the bar **supported at both ends** by springs of rigidity c_i^y and c_k^y. In this case

$$C_f \longrightarrow C_{ik} = 1 - \frac{\varepsilon^2}{\varrho_{ik}^y} \quad . \tag{3.2}$$

In the special case if $c_i^y = c_k^y = c^y$ ($H = \frac{1}{2} c^y \cdot \Delta y$):

$$\varrho^y \longrightarrow \varrho_{ik}^y = \frac{1}{2} \varrho^y \quad , \tag{3.3}$$

$$C_f \longrightarrow C_r = 1 - 2 \frac{\varepsilon^2}{\varrho^y} \quad . \tag{3.4}$$

The other special case characterized by (2.12) - (2.13) corresponds to the original solution of /7/, i.e. the unchanged form of (2.7) - (2.11).

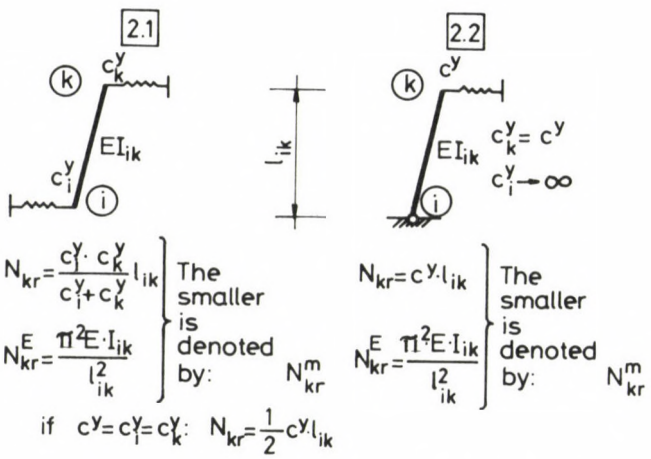

Fig. 2. Characteristic cases of support against displacement

4. The effect of the displacement spring constant

It is easy to see that the weaker is the spring effect against rotation (and the more the rotational spring effect of the two bar-ends diverge), the more strongly the c^y displacement spring constant influences the critical load and the ν parameter of ℓ_o buckling wavelength ((2.2), (2.4)). When this effect tends to zero, equations (2.7) - (2.11) give the buckling condition

$$C_f = 0 \tag{3.5}$$

through the limiting process $\varrho_i \rightarrow \varrho_k \rightarrow 0$ (C_f:Eq.(2.11)). By substituting parameter $\varrho^y = \varrho^y_{ik}$ (Eq. (3.1)) into (3.5), we get the buckling wavelength parameter ν (Eq. (2.2)). Of course we must be aware that in this case the value of ν should not be lower than value 1, corresponding to the buckling of the common two-hinged Euler-bar (Fig. 3, $\varrho_i = \varrho_k = 0$: $\varrho^y \geq 10$).

Figure 3 provides further information about the changes of the spring effect. The results of the calculations that follow the restrictions in (2.12), (2.13) are written in continuous lines. We equally produced the curve (broken line) that follows the restrictions in (3.3) for the enlarged spring constants against rotation $\varrho_i = \varrho_k = 1$. This line may be produced through simple **coordinate-transformation** as well: one of the ν ordinates of the continuous line belonging to ϱ^y has to be drawn to abscissa $2 \cdot \varrho^y$. The maximum difference between the continuous and the broken line in this case is approx. 25%. Fig. 3 shows the results of the solution referring to a swaying bar ($c^y = 0$) and a fix one ($c^y \rightarrow \infty$). These results precisely correspond to what we find in /13/.

The diagrams advise the designer on which ϱ^y, ϱ_i and ϱ_k domain it is sensible and worthwhile to make a more accurate calculation than the one referring to the swaying and to the fixed case involving the displacement spring constant.

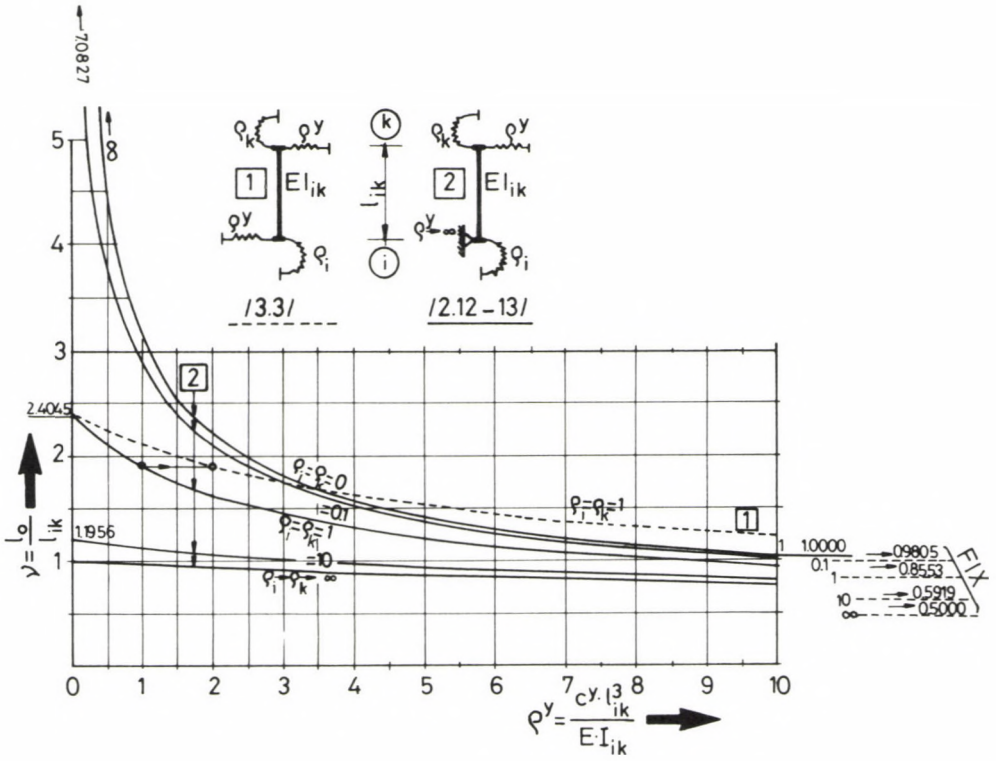

Fig. 3. The effect of the displacement spring rigidity

5. Tables

The tables in the Appendix provide the designer with useful information. Parameters ϱ_i, ϱ_k, ϱ^y(/2.5a-b/, /2.6/) refer to a relatively wide domain. However, the linear interpolation referring to ϱ^y is not always exact. Similar is the case within a certain ϱ_i, ϱ_k domain.

More tables would be needed to increase the accuracy of the interpolation. This, however, is outside the scope of this paper.

An important fact to point out about the use of the tables is that these refer to the unchanged form of the equations (2.7) - (2.13), i.e. to the form where one of the joints is fixed against displacement (Fig. 2.2 + rotation springs = Fig. 3 case 2).

Accordingly, if both joints develop lateral displacements, and e.g. $c_i^y = c_k^y = c^y$, then ν = (2.4) parameter will be found at $\frac{1}{2}\cdot\varrho^y$, not at ϱ^y corresponding to c^y. For instance, if $\varrho_i = \varrho_k = 1$ and $\varrho_i^y = \varrho_k^y = \varrho^y = 2$, then $\nu = 1.9110$, because it belongs to $\frac{1}{2}\cdot\varrho^y = 1$. The same is true for the use of Fig. 3.

6. Practical aspects

Checking stability first of all requires to find out the spring constant. If the bar to be measured is supported by actual springs of known resistance, no difficulty arises.

In the event, however, when the bar is part of a frame structure, and spring constants have to be calculated on the basis of the data of the rest of the bars, the task becomes fairly difficult. Since Dulácska and Kollár /2/, /7/ give a detailed analysis of the connected problems, let us, at this point merely recall briefly the essentials.

If enlarged rotation spring constants $\mu_a = \frac{1}{4}\cdot\varrho_i$, $\mu_f = \frac{1}{4}\varrho_k$ are calculated to standard /10/, the smaller part of the inaccuracy of insignificant size comes from neglecting the secondary effect that manifests itself in the change of the bending rigidity, which is accounted for by the presence of the compressive force. The major part of the inaccuracy is caused by the fact that only in special geometrical and load cases can one calculate rotational spring constants - using the approximation method to standard /10/ - on the basis of the data of the beams exerting restraint on the bar.

It is an advantageous circumstance in this respect that the extreme inaccuracy in the value of the parameters ϱ_i, ϱ_k (in certain cases amounting up to 50-100%) - as our numerical investigations witness the fact - affects the end result only to a very slight extent in some large ϱ_i, ϱ_k domains. This is especially true for domain $\varrho_i = \varrho_k = 10 \div \infty$ (Fig. 3).

It is worthwhile to mention that by supposing the fixing conditions of the other weaker end at the more rigidly fixed end of the bar is a plausible way of reducing the extent of the inaccuracy committed on the account of security.

Kollár /7/ provides detailed instructions for taking parameters μ_a, μ_f : (2.3a-b) in a more realistic way. Displacement spring constants originating from the **supporting effect** of columns placed alongside one another could only be determined by way of exact procedures examining the whole of the frame; that is why this effect cannot be taken into consideration at this approximative level. In the absence of a support system the frame must be considered as a sway-frame ($c^y = 0$).

In the event that either the frame or the column system is **supported by a wall**, we can arrive at the values of the **displacement spring constants** from the data of the wall in the usual way.

Dulácska's theorem in /3/, /7/ shows how rigid the **support walls** need to be for the loaded columns supported by them to be considered as having fixed joints ($c^y \longrightarrow \infty$). This theorem is found in the form of a prescription in point F2.3 of standard /11/. Its application makes the designing of e.g. the support system of an originally unstable (prefabricated) structure considerably easier.

All diagrams and tables published in this paper apply through the above limitations for investigating the stability of **frame columns**. Our results are, however, perfectly valid for the **model** seen in Fig. 1. Therefore the designer can use these not only for analysing quality or concept or to decide about the necessity of a (more) accurate calculation between the extreme cases of the swaying ($c^y = 0$) and the fixed ($c^y \longrightarrow \infty$), but also for actual quantity analyses.

The designer can all the more do so since the above-mentioned approximations connected to spring constants are included in the Code of Practice /10/, and, since with the same approximations our results can be taken for "interpolations" between /10/ and the extreme cases prescribed /13/ and /17/ (fixed and swaying), even though the method is more accurate than the one given in the Code of Practice.

To end it up we would like to recall the fact that prescription (/10/ F 4.1.3), which requires designers to calculate with an average substitute ν value in the case of swaying groups of columns aims at reducing the inaccuracy in parameters ν of the individual columns. This way one can take it roughly into consideration that the whole elastical frame structure can only buckle together, whereby the columns with less load will support those with more load /7/.

Appendix

Table 1

Values of ν in the function of ϱ^y, ϱ_i, ϱ_k

ϱ^y = 1.0000E-09

ϱ_i \ ϱ_k	1.0E-09	1.0E-06	1.0E-04	1.0E-03	1.0E-02	1.0E-01	1.0E+00	1.0E+01	1.0E+02	1.0E+03	1.0E+04	1.0E+06	1.0E+09
1.0E-09	∞			99.4476	31.4623	10.0996	3.6516	2.1987	2.0200	2.0020	2.0002	2.0001	2.0000
1.0E-06				99.4476	31.4623	10.0996	3.6516	2.1987	2.0200	2.0020	2.0002	1.9999	1.9999
1.0E-04				94.8423	31.3120	10.0933	3.6512	2.1985	2.0199	2.0019	2.0001	1.9999	1.9999
1.0E-03	99.4476	99.4476	94.8423	70.2422	29.9936	10.0469	3.6484	2.1976	2.0192	2.0012	1.9993	1.9992	1.9992
1.0E-02	31.4623	31.4623	31.3120	29.9936	22.2382	9.6023	3.6206	2.1890	2.0118	1.9940	1.9922	1.9919	1.9919
1.0E-01	10.0996	10.0996	10.0933	10.0469	9.6023	7.0827	3.3808	2.1086	1.9436	1.9269	1.9252	1.9250	1.9250
1.0E+00	3.6516	3.6516	3.6512	3.6484	3.6206	3.3808	2.4045	1.6752	1.5615	1.5498	1.5487	1.5485	1.5485
1.0E+01	2.1987	2.1987	2.1985	2.1976	2.1890	2.1086	1.6752	1.1956	1.1074	1.0984	1.0975	1.0974	1.0974
1.0E+02	2.0200	2.0200	2.0199	2.0192	2.0118	1.9436	1.5615	1.1074	1.0200	1.0110	1.0101	1.0100	1.0100
1.0E+03	2.0020	2.0020	2.0019	2.0012	1.9940	1.9269	1.5498	1.0984	1.0110	1.0020	1.0011	1.0010	1.0010
1.0E+04	2.0002	2.0002	2.0001	1.9993	1.9922	1.9252	1.5487	1.0975	1.0101	1.0011	1.0002	1.0001	1.0001
1.0E+06	2.0001	1.9999	1.9999	1.9992	1.9919	1.9250	1.5485	1.0974	1.0100	1.0010	1.0001	1.0000	1.0000
1.0E+09	2.0000	1.9999	1.9999	1.9992	1.9919	1.9250	1.5485	1.0974	1.0100	1.0010	1.0001	1.0000	1.0000

Table 2

Values of ν in the function of ϱ^y, ϱ_i, ϱ_k

ϱ^y = 1.0000E-03

ϱ_i \ ϱ_k	1.0E-09	1.0E-06	1.0E-04	1.0E-03	1.0E-02	1.0E-01	1.0E+00	1.0E+01	1.0E+02	1.0E+03	1.0E+04	1.0E+06	1.0E+09
1.0E-09	99.3458	99.2782	94.7223	70.2516	29.9987	10.0483	3.6492	2.1982	2.0197	2.0017	1.9999	1.9997	1.9997
1.0E-06	99.2782	99.2406	94.6881	70.2328	29.9987	10.0479	3.6492	2.1982	2.0197	2.0017	1.9999	1.9997	1.9997
1.0E-04	94.7223	94.6881	90.6916	68.5613	29.8620	10.0429	3.6489	2.1981	2.0196	2.0016	1.9998	1.9996	1.9996
1.0E-03	70.2516	70.2328	68.5613	57.3557	28.7139	9.9954	3.6460	2.1972	2.0188	2.0009	1.9990	1.9989	1.9989
1.0E-02	29.9987	29.9987	29.8620	28.7139	21.6962	9.5574	3.6184	2.1885	2.0115	1.9936	1.9918	1.9916	1.9916
1.0E-01	10.0483	10.0479	10.0429	9.9954	9.5574	7.0654	3.3788	2.1082	1.9432	1.9266	1.9249	1.9247	1.9247
1.0E+00	3.6492	3.6492	3.6489	3.6460	3.6184	3.3788	2.4038	1.6750	1.5613	1.5497	1.5485	1.5484	1.5484
1.0E+01	2.1982	2.1982	2.1981	2.1972	2.1885	2.1082	1.6750	1.1955	1.1074	1.0983	1.0974	1.0973	1.0973
1.0E+02	2.0197	2.0197	2.0196	2.0188	2.0115	1.9432	1.5613	1.1074	1.0199	1.0110	1.0101	1.0099	1.0100
1.0E+03	2.0017	2.0017	2.0016	2.0009	1.9936	1.9266	1.5497	1.0983	1.0110	1.0020	1.0011	1.0010	1.0010
1.0E+04	1.9999	1.9999	1.9998	1.9990	1.9918	1.9249	1.5485	1.0974	1.0101	1.0011	1.0002	1.0001	1.0001
1.0E+06	1.9997	1.9997	1.9996	1.9989	1.9916	1.9247	1.5484	1.0973	1.0099	1.0010	1.0001	1.0000	1.0000
1.0E+09	1.9997	1.9997	1.9996	1.9989	1.9916	1.9247	1.5484	1.0973	1.0100	1.0010	1.0001	1.0000	1.0000

Table 3

Values of ν in the function of ϱ^y, ϱ_i, ϱ_k

ϱ^y = 1.0000E-02

ϱ_i \ ϱ_k	1.0E-09	1.0E-06	1.0E-04	1.0E-03	1.0E-02	1.0E-01	1.0E+00	1.0E+01	1.0E+02	1.0E+03	1.0E+04	1.0E+06	1.0E+09
1.0E-09	31.4159	31.4152	31.2616	29.9542	22.2335	9.6152	3.6275	2.1940	2.0166	1.9987	1.9969	1.9967	1.9968
1.0E-06	31.4152	31.4114	31.2579	29.9542	22.2316	9.6152	3.6275	2.1940	2.0166	1.9987	1.9969	1.9967	1.9967
1.0E-04	31.2616	31.2579	31.1058	29.8179	22.1771	9.6106	3.6272	2.1939	2.0165	1.9986	1.9968	1.9966	1.9966
1.0E-03	29.9542	29.9542	29.8179	28.6794	21.6944	9.5692	3.6245	2.1930	2.0158	1.9979	1.9961	1.9959	1.9959
1.0E-02	22.2335	22.2316	22.1771	21.6944	18.1484	9.1827	3.5972	2.1843	2.0084	1.9907	1.9889	1.9887	1.9887
1.0E-01	9.6152	9.6152	9.6106	9.5692	9.1827	6.9099	3.3616	2.1044	1.9405	1.9239	1.9222	1.9221	1.9221
1.0E+00	3.6275	3.6275	3.6272	3.6245	3.5972	3.3616	2.3975	1.6731	1.5598	1.5482	1.5471	1.5470	1.5469
1.0E+01	2.1940	2.1940	2.1939	2.1930	2.1843	2.1044	1.6731	1.1948	1.1068	1.0978	1.0969	1.0968	1.0968
1.0E+02	2.0166	2.0166	2.0165	2.0158	2.0084	1.9405	1.5598	1.1068	1.0196	1.0106	1.0097	1.0096	1.0096
1.0E+03	1.9987	1.9987	1.9986	1.9979	1.9907	1.9239	1.5482	1.0978	1.0106	1.0016	1.0007	1.0006	1.0006
1.0E+04	1.9969	1.9969	1.9968	1.9961	1.9889	1.9222	1.5471	1.0969	1.0097	1.0007	0.9998	0.9997	0.9997
1.0E+06	1.9967	1.9967	1.9966	1.9959	1.9887	1.9221	1.5470	1.0968	1.0096	1.0006	0.9997	0.9996	0.9996
1.0E+09	1.9968	1.9967	1.9966	1.9959	1.9887	1.9221	1.5469	1.0968	1.0096	1.0006	0.9997	0.9996	0.9996

Table 4

Values of ν in the function of ϱ^y, ϱ_i, ϱ_k

ϱ^y = 1.0000E-01

ϱ_i \ ϱ_k	1.0E-09	1.0E-06	1.0E-04	1.0E-03	1.0E-02	1.0E-01	1.0E+00	1.0E+01	1.0E+02	1.0E+03	1.0E+04	1.0E+06	1.0E+09
1.0E-09	9.9346	9.9344	9.9295	9.8853	9.4738	7.0830	3.4303	2.1531	1.9867	1.9698	1.9681	1.9679	1.9680
1.0E-06	9.9344	9.9344	9.9295	9.8853	9.4738	7.0830	3.4303	2.1531	1.9867	1.9698	1.9681	1.9679	1.9679
1.0E-04	9.9295	9.9295	9.9246	9.8805	9.4693	7.0810	3.4300	2.1530	1.9866	1.9698	1.9681	1.9679	1.9679
1.0E-03	9.8853	9.8853	9.8805	9.8367	9.4308	7.0644	3.4277	2.1521	1.9859	1.9691	1.9674	1.9672	1.9672
1.0E-02	9.4738	9.4738	9.4693	9.4308	9.0703	6.9046	3.4046	2.1439	1.9789	1.9621	1.9605	1.9603	1.9603
1.0E-01	7.0830	7.0830	7.0810	7.0644	6.9046	5.7674	3.2024	2.0680	1.9137	1.8980	1.8964	1.8962	1.8962
1.0E+00	3.4303	3.4303	3.4300	3.4277	3.4046	3.2024	2.3373	1.6539	1.5453	1.5341	1.5330	1.5329	1.5329
1.0E+01	2.1531	2.1531	2.1530	2.1521	2.1439	2.0680	1.6539	1.1877	1.1015	1.0927	1.0918	1.0917	1.0917
1.0E+02	1.9867	1.9867	1.9866	1.9859	1.9789	1.9137	1.5453	1.1015	1.0156	1.0067	1.0058	1.0058	1.0058
1.0E+03	1.9698	1.9698	1.9698	1.9691	1.9621	1.8980	1.5341	1.0927	1.0067	0.9979	0.9970	0.9969	0.9969
1.0E+04	1.9681	1.9681	1.9681	1.9674	1.9605	1.8964	1.5330	1.0918	1.0058	0.9970	0.9961	0.9960	0.9960
1.0E+06	1.9679	1.9679	1.9679	1.9672	1.9603	1.8962	1.5329	1.0917	1.0058	0.9969	0.9960	0.9959	0.9959
1.0E+09	1.9680	1.9679	1.9679	1.9672	1.9603	1.8962	1.5329	1.0917	1.0058	0.9969	0.9960	0.9959	0.9959

Table 5

Values of ν in the function of ϱ^y, ϱ_i, ϱ_k

$\varrho^y = 0.5000$

ϱ_i \ ϱ_k	0.10	0.20	0.30	0.40	0.60	0.80	1.00	2.00	3.00	4.00	5.00	6.00	8.00
0.10	3.7639	3.5341	3.3532	3.2067	2.9833	2.8204	2.6962	2.3527	2.1961	2.1071	2.0500	2.0102	1.9587
0.20	3.5341	3.3359	3.1776	3.0480	2.8478	2.7002	2.5867	2.2685	2.1217	2.0379	1.9838	1.9462	1.8973
0.30	3.3532	2.1776	3.0358	2.9186	2.7360	2.6001	2.4948	2.1966	2.0577	1.9779	1.9264	1.8905	1.8438
0.40	3.2067	3.0480	2.9186	2.8111	2.6421	2.5153	2.4166	2.1345	2.0019	1.9254	1.8760	1.8415	1.7966
0.60	2.9833	2.8478	2.7360	2.6421	2.4929	2.3795	2.2904	2.0324	1.9094	1.8381	1.7918	1.7594	1.7173
0.80	2.8204	2.7002	2.6001	2.5153	2.3795	2.2754	2.1931	1.9520	1.8359	1.7682	1.7242	1.6934	1.6532
1.00	2.6962	2.5867	2.4948	2.4166	2.2904	2.1931	2.1157	1.8872	1.7761	1.7112	1.6688	1.6391	1.6004
2.00	2.3527	2.2685	2.1966	2.1345	2.0324	1.9520	1.8872	1.6905	1.5922	1.5339	1.4957	1.4688	1.4337
3.00	2.1961	2.1217	2.0577	2.0019	1.9094	1.8359	1.7761	1.5922	1.4988	1.4430	1.4062	1.3803	1.3463
4.00	2.1071	2.0379	1.9779	1.9254	1.8381	1.7682	1.7112	1.5339	1.4430	1.3884	1.3522	1.3267	1.2932
5.00	2.0500	1.9838	1.9264	1.8760	1.7918	1.7242	1.6688	1.4957	1.4062	1.3522	1.3165	1.2911	1.2578
6.00	2.0102	1.9462	1.8905	1.8415	1.7594	1.6934	1.6391	1.4688	1.3803	1.3267	1.2911	1.2659	1.2326
8.00	1.9587	1.8973	1.8438	1.7966	1.7173	1.6532	1.6004	1.4337	1.3463	1.2932	1.2578	1.2326	1.1995

Table 6

Values of ν in the function of ϱ^y, ϱ_i, ϱ_k

ϱ^y = 1.0000E+00

ϱ_i \ ϱ_k	1.0E-09	1.0E-06	1.0E-04	1.0E-03	1.0E-02	1.0E-01	1.0E+00	1.0E+01	1.0E+02	1.0E+03	1.0E+04	1.0E+06	1.0E+09
1.0E-09	3.1416	3.1416	3.1414	3.1400	3.1261	3.0001	2.3919	1.8414	1.7473	1.7375	1.7365	1.7364	1.7364
1.0E-06	3.1416	3.1416	3.1414	3.1400	3.1261	3.0001	2.3919	1.8414	1.7473	1.7375	1.7365	1.7364	1.7364
1.0E-04	3.1414	3.1414	3.1413	3.1399	3.1259	3.0000	2.3919	1.8413	1.7473	1.7374	1.7364	1.7363	1.7363
1.0E-03	3.1400	3.1400	3.1399	3.1385	3.1245	2.9987	2.3911	1.8408	1.7468	1.7369	1.7359	1.7358	1.7358
1.0E-02	3.1261	3.1261	3.1259	3.1245	3.1107	2.9861	2.3830	1.8355	1.7419	1.7321	1.7311	1.7310	1.7310
1.0E-01	3.0001	3.0001	3.0000	2.9987	2.9861	2.8719	2.3090	1.7860	1.6960	1.6865	1.6856	1.6855	1.6855
1.0E+00	2.3919	2.3919	2.3919	2.3911	2.3830	2.3090	1.9110	1.4934	1.4194	1.4117	1.4110	1.4109	1.4109
1.0E+01	1.8414	1.8414	1.8413	1.8408	1.8355	1.7860	1.4934	1.1237	1.0523	1.0449	1.0442	1.0441	1.0441
1.0E+02	1.7473	1.7473	1.7473	1.7468	1.7419	1.6960	1.4194	1.0523	0.9783	0.9707	0.9700	0.9699	0.9699
1.0E+03	1.7375	1.7375	1.7374	1.7369	1.7321	1.6865	1.4117	1.0449	0.9707	0.9631	0.9623	0.9622	0.9622
1.0E+04	1.7365	1.7365	0.7364	1.7359	1.7311	1.6856	1.4110	1.0442	0.9700	0.9623	0.9615	0.9614	0.9614
1.0E+06	1.7364	1.7364	1.7363	1.7358	1.7310	1.6855	1.4109	1.0441	0.9699	0.9622	0.9614	0.9614	0.9614
1.0E+09	1.7364	1.7364	1.7363	1.7358	1.7310	1.6855	1.4109	1.0441	0.9699	0.9622	0.9614	0.9614	0.9613

Table 7

Values of ν in the function of ϱ^y, ϱ_i, ϱ_k

$\varrho^y = 2.0000$

ϱ_i \ ϱ_k	0.10	0.20	0.30	0.40	0.60	0.80	1.00	2.00	3.00	4.00	5.00	6.00	8.00
0.10	2.1197	2.0762	2.0381	2.0045	1.9480	1.9026	1.8653	1.7495	1.6904	1.6550	1.6315	0.6149	1.5929
0.20	2.0762	2.0336	1.9963	1.9633	1.9079	1.8632	1.8265	1.7124	1.6540	1.6190	1.5959	1.5795	1.5578
0.30	2.0381	1.9963	1.9596	1.9272	1.8726	1.8286	1.7923	1.6795	1.6216	1.5870	1.5640	1.5478	1.5264
0.40	2.0045	1.9633	1.9272	1.8952	1.8414	1.7978	1.7619	1.6501	1.5926	1.5582	1.5355	1.5193	1.4981
0.60	1.9480	1.9079	1.8726	1.8414	1.7885	1.7457	1.7104	1.5998	1.5429	1.5088	1.4862	1.4703	1.4492
0.80	1.9026	1.8632	1.8286	1.7978	1.7457	1.7034	1.6684	1.5586	1.5019	1.4679	1.4454	1.4295	1.4086
1.00	1.8653	1.8265	1.7923	1.7619	1.7104	1.6684	1.6337	1.5243	1.4676	1.4336	1.4111	1.3952	1.3743
2.00	1.7495	1.7124	1.6795	1.6501	1.5998	1.5586	1.5243	1.4147	1.3571	1.3223	1.2993	1.2830	1.2615
3.00	1.6904	1.6540	1.6216	1.5926	1.5429	1.5019	1.4676	1.3571	1.2984	1.2627	1.2390	1.2222	1.2000
4.00	1.6550	1.6190	1.5870	1.5582	1.5088	1.4679	1.4336	1.3223	1.2627	1.2263	1.2020	1.1847	1.1620
5.00	1.6315	1.5959	1.5640	1.5355	1.4862	1.4454	1.4111	1.2993	1.2390	1.2020	1.1773	1.1597	1.1364
6.00	1.6149	1.5795	1.5478	1.5193	1.4703	1.4295	1.3952	1.2830	1.2222	1.1847	1.1597	1.1418	1.1182
8.00	1.5929	1.5578	1.5264	1.4981	1.4492	1.4086	1.3743	1.2615	1.2000	1.1620	1.1364	1.1182	1.0941

Table 8

Values of ν in the function of ϱ^y, ϱ_i, ϱ_k

$\varrho^y = 4.0000$

ϱ_i \ ϱ_k	0.10	0.20	0.30	0.40	0.60	0.80	1.00	2.00	3.00	4.00	5.00	6.00	8.00
0.10	1.5336	1.5170	1.5023	1.4893	1.4672	1.4492	1.4345	1.3886	1.3653	1.3515	1.3424	1.3359	1.3274
0.20	1.5170	1.5001	1.4851	1.4717	1.4490	1.4306	1.4154	1.3682	1.3443	1.3301	1.3207	1.3141	1.3054
0.30	1.5023	1.4851	1.4697	1.4560	1.4328	1.4139	1.3983	1.3498	1.3252	1.3107	1.3011	1.2943	1.2854
0.40	1.4893	1.4717	1.4560	1.4421	1.4183	1.3990	1.3830	1.3332	1.3080	1.2930	1.2832	1.2763	1.2672
0.60	1.4672	1.4490	1.4328	1.4183	1.3937	1.3735	1.3568	1.3045	1.2780	1.2622	1.2519	1.2447	1.2352
0.80	1.4492	1.4306	1.4139	1.3990	1.3735	1.3526	1.3352	1.2807	1.2529	1.2364	1.2256	1.2180	1.2081
1.00	1.4345	1.4154	1.3983	1.3830	1.3568	1.3352	1.3173	1.2606	1.2316	1.2144	1.2031	1.1952	1.1849
2.00	1.3886	1.3682	1.3498	1.3332	1.3045	1.2807	1.2606	1.1960	1.1621	1.1419	1.1286	1.1192	1.1071
3.00	1.3653	1.3443	1.3252	1.3080	1.2780	1.2529	1.2316	1.1621	1.1250	1.1026	1.0878	1.0774	1.0638
4.00	1.3515	1.3301	1.3107	1.2930	1.2622	1.2364	1.2144	1.1419	1.1026	1.0787	1.0629	1.0517	1.0370
5.00	1.3424	1.3207	1.3011	1.2832	1.2519	1.2256	1.2031	1.1286	1.0878	1.0629	1.0462	1.0344	1.0190
6.00	1.3359	1.3141	1.2943	1.2763	1.2447	1.2180	1.1952	1.1192	1.0774	1.0517	1.0344	1.0222	1.0062
8.00	1.3274	1.3054	1.2854	1.2672	1.2352	1.2081	1.1849	1.1071	1.0638	1.0370	1.0190	1.0062	0.9893

Table 9

Values of ν in the function of ϱ^y, ϱ_i, ϱ_k

$\varrho^y = 10.0000$

ϱ_i \ ϱ_k	0.10	0.20	0.30	0.40	0.60	0.80	1.00	2.00	3.00	4.00	5.00	6.00	8.00
0.10	0.9839	0.9829	0.9828	0.9828	0.9828	0.9828	0.9828	0.9828	0.9828	0.9828	0.9828	0.9828	0.9828
0.20	0.9829	0.9749	0.9726	0.9719	0.9714	0.9713	0.9712	0.9710	0.9710	0.9709	0.9709	0.9709	0.9709
0.30	0.9828	0.9726	0.9665	0.9638	0.9619	0.9612	0.9608	0.9603	0.9601	0.9601	0.9600	0.9600	0.9599
0.40	0.9828	0.9719	0.9638	0.9587	0.9542	0.9525	0.9517	0.9505	0.9502	0.9500	0.9499	0.9499	0.9498
0.60	0.9828	0.9714	0.9619	0.9542	0.9444	0.9396	0.9372	0.9336	0.9327	0.9323	0.9321	0.9319	0.9318
0.80	0.9828	0.9713	0.9612	0.9525	0.9396	0.9317	0.9271	0.9197	0.9180	0.9172	0.9168	0.9165	0.9162
1.00	0.9828	0.9712	0.9608	0.9517	0.9372	0.9271	0.9204	0.9085	0.9056	0.9044	0.9037	0.9033	0.9028
2.00	0.9828	0.9710	0.9603	0.9505	0.9336	0.9197	0.9085	0.8786	0.8682	0.8635	0.8609	0-8593	0.8574
3.00	0.9828	0.9710	0.9601	0.9502	0.9327	0.9180	0.9056	0.8682	0.8520	0.8441	0.8395	0.8367	0.8333
4.00	0.9828	0.9709	0.9601	0.9500	0.9323	0.9172	0.9044	0.8635	0.8441	0.8338	0.8278	0.8239	0.8192
5.00	0.9828	0.9709	0.9600	0.9499	0.9321	0.9168	0.9037	0.8609	0.8395	0.8278	0.8207	0.8160	0.8104
6.00	0.9828	0.9709	0.9600	0.9499	0.9319	0.9165	0.9033	0.8593	0.8367	0.8239	0.8160	0.8108	0.8044
8.00	0.9828	0.9709	0.9599	0.9498	0.9318	0.9162	0.9028	0.8574	0.8333	0.8192	0.8104	0.8044	0.7969

Table 10

Values of ν in the function of ϱ^y, ϱ_i, ϱ_k

ϱ^y = 1.0000E+01

ϱ_i \ ϱ_k	1.0E-09	1.0E-06	1.0E-04	1.0E-03	1.0E-02	1.0E-01	1.0E+00	1.0E+01	1.0E+02	1.0E+03	1.0E+04	1.0E+06	1.0E+09
1.0E-09	1.0000	1.0000	1.0000	0.9999	0.9991	0.9963	0.9957	0.9956	0.9956	0.9956	0.9956	0.9956	0.9956
1.0E-06	1.0000	1.0000	1.0000	0.9999	0.9991	0.9963	0.9957	0.9956	0.9956	0.9956	0.9956	0.9956	0.9956
1.0E-04	1.0000	1.0000	1.0000	0.9999	0.9991	0.9963	0.9957	0.9956	0.9956	0.9956	0.9956	0.9956	0.9956
1.0E-03	0.9999	0.9999	0.9999	0.9998	0.9990	0.9962	0.9956	0.9955	0.9955	0.9955	0.9955	0.9955	0.9955
1.0E-02	0.9991	0.9991	0.9991	0.9990	0.9980	0.9949	0.9943	0.9943	0.9943	0.9943	0.9943	0.9943	0.9943
1.0E-01	0.9963	0.9963	0.9963	0.9962	0.9949	0.9839	0.9828	0.9828	0.9828	0.9828	0.9828	0.9828	0.9828
1.0E+00	0.9957	0.9957	0.9957	0.9956	0.9943	0.9828	0.9204	0.9025	0.9015	0.9014	0.9014	0.9014	0.9014
1.0E+01	0.9956	0.9956	0.9956	0.9955	0.9943	0.9828	0.9025	0.7877	0.7714	0.7698	0.7697	0.7697	0.7697
1.0E+02	0.9956	0.9956	0.9956	0.9955	0.9943	0.9828	0.9015	0.7714	0.7484	0.7462	0.7460	0.7460	0.7460
1.0E+03	0.9956	0.9956	0.9956	0.9955	0.9943	0.9828	0.9014	0.7698	0.7462	0.7439	0.7437	0.7437	0.7437
1.0E+04	0.9956	0.9956	0.9956	0.9955	0.9943	0.9828	0.9014	0.7697	0.7460	0.7437	0.7434	0.7434	0.7434
1.0E+06	0.9956	0.9956	0.9956	0.9955	0.9943	0.9828	0.9014	0.7697	0.7460	0.7437	0.7434	0.7434	0.7434
1.0E+09	0.9956	0.9956	0.9956	0.9955	0.9943	0.9828	0.9014	0.7697	0.7460	0.7437	0.7434	0.7434	0.7434

Table 11

Values of ν in the function of ϱ^y, ϱ_i, ϱ_k

ϱ^y = 1.0000E+02

ϱ_i \ ϱ_k	1.0E-09	1.0E-06	1.0E-04	1.0E-03	1.0E-02	1.0E-01	1.0E+00	1.0E+01	1.0E+02	1.0E+03	1.0E+04	1.0E+06	1.0E+09
1.0E-09	1.0000	1.0000	1.0000	0.9999	0.9990	0.9902	0.9231	0.7663	0.7144	0.7084	0.7078	0.7078	0.7077
1.0E-06	1.0000	1.0000	1.0000	0.9999	0.9990	0.9902	0.9231	0.7663	0.7144	0.7084	0.7078	0.7078	0.7077
1.0E-04	1.0000	1.0000	1.0000	0.9999	0.9990	0.9902	0.9231	0.7663	0.7144	0.7084	0.7078	0.7077	0.7077
1.0E-03	0.9999	0.9999	0.9999	0.9998	0.9989	0.9901	0.9231	0.7663	0.7144	0.7084	0.7078	0.7077	0.7077
1.0E-02	0.9990	0.9990	0.9990	0.9989	0.9980	0.9892	0.9222	0.7657	0.7138	0.7078	0.7072	0.7072	0.7071
1.0E-01	0.9902	0.9902	0.9902	0.9901	0.9892	0.9805	0.9146	0.7598	0.7085	0.7026	0.7020	0.7019	0.7019
1.0E+00	0.9231	0.9231	0.9231	0.9231	0.9222	0.9146	0.8553	0.7131	0.6660	0.6607	0.6601	0.6600	0.6600
1.0E+01	0.7663	0.7663	0.7663	0.7663	0.7657	0.7598	0.7131	0.5919	0.5508	0.5462	0.5458	0.5457	0.5457
1.0E+02	0.7144	0.7144	0.7144	0.7144	0.7138	0.7085	0.6660	0.5508	0.5100	0.5055	0.5050	0.5050	0.5050
1.0E+03	0.7084	0.7084	0.7084	0.7084	0.7078	0.7026	0.6607	0.5462	0.5055	0.5010	0.5005	0.5005	0.5005
1.0E+04	0.7078	0.7078	0.7078	0.7078	0.7072	0.7020	0.6601	0.5458	0.5050	0.5005	0.5001	0.5000	0.5000
1.0E+06	0.7078	0.7078	0.7077	0.7077	0.7072	0.7019	0.6600	0.5457	0.5050	0.5005	0.5000	0.5000	0.5000
1.0E+09	0.7077	0.7077	0.7077	0.7077	0.7071	0.7019	0.6600	0.5457	0.5050	0.5005	0.5000	0.5000	0.5000

Table 12

Values of ν in the function of ϱ^y, ϱ_i, ϱ_k

ϱ^y = 1.0000E+03

ϱ_i \ ϱ_k	1.0E-09	1.0E-06	1.0E-04	1.0E-03	1.0E-02	1.0E-01	1.0E+00	1.0E+01	1.0E+02	1.0E+03	1.0E+04	1.0E+06	1.0E+09
1.0E-09	1.0000	1.0000	1.0000	0.9999	0.9990	0.9902	0.9225	0.7608	0.7068	0.7006	0.6999	0.6999	0.6999
1.0E-06	1.0000	1.0000	1.0000	0.9999	0.9990	0.9902	0.9225	0.7608	0.7068	0.7006	0.6999	0.6999	0.6999
1.0E-04	1.0000	1.0000	1.0000	0.9999	0.9990	0.9902	0.9225	0.7608	0.7068	0.7006	0.6999	0.6999	0.6999
1.0E-03	0.9999	0.9999	0.9999	0.9998	0.9989	0.9901	0.9225	0.7607	0.7067	0.7005	0.6999	0.6998	0.6998
1.0E-02	0.9990	0.9990	0.9990	0.9989	0.9980	0.9892	0.9217	0.7601	0.7062	0.7000	0.6994	0.6993	0.6993
1.0E-01	0.9902	0.9902	0.9902	0.9901	0.9892	0.9805	0.9141	0.7546	0.7014	0.6952	0.6946	0.6946	0.6946
1.0E+00	0.9225	0.9225	0.9225	0.9225	0.9217	0.9141	0.8553	0.7105	0.6620	0.6565	0.6559	0.6559	0.6559
1.0E+01	0.7608	0.7608	0.7608	0.7607	0.7601	0.7546	0.7105	0.5919	0.5507	0.5461	0.5457	0.5456	0.5456
1.0E+02	0.7068	0.7068	0.7068	0.7067	0.7062	0.7014	0.6620	0.5507	0.5100	0.5055	0.5050	0.5050	0.5050
1.0E+03	0.7006	0.7006	0.7006	0.7005	0.7000	0.6952	0.6565	0.5461	0.5055	0.5010	0.5005	0.5005	0.5005
1.0E+04	0.6999	0.6999	0.6999	0.6999	0.6994	0.6946	0.6559	0.5457	0.5050	0.5005	0.5001	0.5000	0.5000
1.0E+06	0.6999	0.6999	0.6999	0.6998	0.6993	0.6946	0.6559	0.5456	0.5050	0.5005	0.5000	0.5000	0.5000
1.0E+09	0.6999	0.6999	0.6999	0.6998	0.6993	0.6946	0.6559	0.5456	0.5050	0.5005	0.5000	0.5000	0.5000

Table 13

Values of ν in the function of ϱ^y, ϱ_i, ϱ_k

ϱ^y = 1.0000E+09

ϱ_i \ ϱ_k	1.0E-09	1.0E-06	1.0E-04	1.0E-03	1.0E-02	1.0E-01	1.0E+00	1.0E+01	1.0E+02	1.0E+03	1.0E+04	1.0E+06	1.0E+09
1.0E-09	1.0000	1.0000	1.0000	0.9999	0.9990	0.9902	0.9225	0.7603	0.7061	0.6998	0.6992	0.6992	0.6991
1.0E-06	1.0000	1.0000	1.0000	0.9999	0.9990	0.9902	0.9225	0.7603	0.7061	0.6998	0.6992	0.6992	0.6991
1.0E-04	1.0000	1.0000	1.0000	0.9999	0.9990	0.9902	0.9225	0.7602	0.7061	0.6998	0.6992	0.6991	0.6991
1.0E-03	0.9999	0.9999	0.9999	0.9998	0.9989	0.9901	0.9224	0.7602	0.7060	0.6998	0.6992	0.6991	0.6991
1.0E-02	0.9990	0.9990	0.9990	0.9989	0.9980	0.9892	0.9216	0.7596	0.7055	0.6993	0.6987	0.6986	0.6986
1.0E-01	0.9902	0.9902	0.9902	0.9901	0.9892	0.9805	0.9140	0.7541	0.7007	0.6946	0.6940	0.6939	0.6939
1.0E+00	0.9225	0.9225	0.9225	0.9224	0.9216	0.9140	0.8553	0.7103	0.6617	0.6561	0.6556	0.6555	0.6555
1.0E+01	0.7603	0.7603	0.7602	0.7602	0.7596	0.7541	0.7103	0.5919	0.5507	0.5461	0.5457	0.5456	0.5456
1.0E+02	0.7061	0.7061	0.7061	0.7060	0.7055	0.7007	0.6617	0.5507	0.5100	0.5055	0.5050	0.5050	0.5050
1.0E+03	0.6998	0.6998	0.6998	0.6998	0.6993	0.6946	0.6561	0.5461	0.5055	0.5010	0.5005	0.5005	0.5005
1.0E+04	0.6992	0.6992	0.6992	0.6992	0.6987	0.6940	0.6556	0.5457	0.5050	0.5005	0.5001	0.5000	0.5000
1.0E+06	0.6992	0.6992	0.6991	0.6991	0.6986	0.6939	0.6555	0.5456	0.5050	0.5005	0.5000	0.5000	0.5000
1.0E+09	0.6991	0.6991	0.6991	0.6991	0.6986	0.6939	0.6555	0.5456	0.5050	0.5005	0.5000	0.5000	0.5000

REFERENCES

1. Altenbach, J. - Garz, K.F.: Wissensch. Zeitschrift der Hochschule für Schwermasch., Magdeburg, III, (1959), 19
2. Dulácska, E. - Kollár, L.: Angenährte Berechnung des Momentenzuwachses und der Stabilität von gedrückten Rahmenstielen, Die Bautechnik, H.3, (1960), 98-108
3. Dulácska, E.: Design problems of reinforced concrete wall-beams, Mélyépítéstudományi Szemle (in Hungarian), 1966/10, 466-475
4. Gábory, P.: Dimensioning eccentrically compressed, elastically fixed reinforced concrete columns with a straight axis taking buckling into consideration (in Hungarian), ÉTI Tudományos Közlemények, 1951/5, 5-26
5. Handbook of Structural Stability, Corona Publishing Company, Tokyo, 1971
6. Horn, M.R. - Merchant, W.: The Stability of Frames. Pergamon Press, Oxford, 1965
7. Kollár, L.: Stability of frame structures and column systems (in Hungarian), BVTV Technical Dep. 1972, 8-12
8. Lipták, L.: Elastic buckling of prismatic straight-axis bars under optional fixing conditions (in Hungarian), Építés- és Közlekedéstudományi Közlemények 4, (1960), 621-626
9. Mayer, R.: Die Knickfestigkeit, Berlin, 1921, 5
10. MSZ 15022/1-86 Static design of load bearing structures of buildings. Reinforced Concrete Structures, Chapter F4 (in Hungarian)
11. MSZ 15022/4-86 Static design of load bearing structures of buildings. Concrete, reinforced concrete and prestressed concrete precast structures, Chapter F2 (in Hungarian)
12. Mudrak, W.: Die Knickbedingungen für den geraden Stab, Der Bauingenieur, 1941, 153
13. Nemestóthy, É.: Buckling lengths of elastically fixed columns (in Hungarian), Magyar Építőipar, 1972, 576-580
14. Petersen, Ch.: Statik und Stabilität der Baukonstruktionen. Vieweg u. Sohn, Braunschweig/Wiesbaden, 1982
15. Pflüger, A.: Stabilitätsprobleme der Elastostatik. 3. Aufl. Berlin-Göttingen-Heidelberg, Springer-V., (1975), 341, 371
16. Timoshenko, S.P.- Gere, J.M.: Theory of Elastic Stability, McGraw-Hill Book Company, New York-Toronto-London, (1961), 82
17. Wood, R.H.: Effective Lengths of Columns in Multistorey Buildings, Parts1-3, The Structural Engineer, 52, (1974)

Acta Technica Acad. Sci. Hung., 103(2-3), pp. 143-170 (1990)

A NEW INVESTIGATION ON PARABOLIC WEIRS - PROPORTIONAL PARABOLIC WEIRS

KESHAVA MURTHY, K.* - JAYARAM, N.**

(Received: 28 August 1989)

This paper is devoted to the consideration of the improved design of Parabolic Weirs. This is achieved by designing the weir as a "compensating weir" having a base. A detailed design is given for the parabolic weir having a rectangular base of width '2W' and depth 'a' over which a designed complimentary weir is fitted. It is shown that for this weir, the discharge is proportional to the square of the head measured above a datum line situated at (1/3) a below the crest of the weir. The design is further improved by incorporating additional advantages in the form of:

1. equal slope at the junction of the base weir and the complementary weir, and

2. constant indication accuracy (λ =1) i.e., reference plane coinciding with the crest.

The equal slope condition which provides a smooth transition of flow has been achieved for the weirs having the base in the form of $Y_1 = C_1 + C_2 X^{3/2}$ and $Y_1 = C_1 + C_2 X^2$. The second condition of constant indication accuracy has also been achieved for the above bases. In the third design both the above conditions have been incoroporated simultaneously by taking the base weir of the form $Y_1 = C_1 + C_2 X^{3/2} + C_3 X^2$.

It is shown that for all the weirs, the profile of the complementary weir retains the simplicity of the conventional parabolic weir in so far as it rapidly approaches the shape of the conventional parabolic weir. A theorem connected with the realizability of the parabolic weir (for all the bases) has been enunciated and proved. Also, it is shown that the width of the weir tends to infinity as the depth of flow increases without limit.

Experiments with five of the nine designed weirs show excellent agreement with the theory by giving a constant coefficient of discharge which varies for different weirs from 0.602 to 0.613.

*Keshava Murthy, K., Indian Institute of Sciences, Bangalore-560012, India

**Jayaram, N., Indian Institute of Sciences, Bangalore-560012, India

Akadémiai Kiadó, Budapest

NOTATIONS

a	depth of base weir
b	dimensional proportional constant
C_d	coefficient of discharge
c,d	dimensional constants
ee_Q	relative error in calculating flow
e_{hc}	relative error in measuring head over the weir
$f(h)$	function of h
$f(x)$	function of $x = y(x)$
g	acceleration due to gravity
H	head measured from reference plane
h_c	head measured from the weir crest
h	head from y-axis
K	$2C_d(2g)^{1/2}$ = dimensional constant
λ	datum parameter
m	exponent
P	parameter of parabola
Q	discharge
Q'_b	$dQ/dh = \sigma$
W	half width of the base weir
X_1, X_2	vertical coordinates
Y_1, Y_2	horizontal coordinates
$\phi(h)$	function of $h = \int_0^h \frac{f(x)dx}{\sqrt{h-x}}$
$\phi'(h)$	differential of $\phi(h)$ with respect to 'h'.

Introduction

Proportional weirs are well-known discharge measuring devices which find application in various fields like Hydraulic Engineering, Sanitary Engineering, Chemical Engineering and Irrigation Engineering. For the past two decades extensive work has been done on these weirs. A generalized theory for the design of weirs was given by Keshava Murthy and Seshagiri /11/. Based on this, a new classification was made by Keshava Murthy and Pillai /9/. Accordingly, the weirs are classified as 'Compen-

sating weirs' and 'noncompensating weirs' depending on the discharge head relationship $Q = bH^m$. When $m \geq 3/2$ the weirs are called as noncompensating weirs which essentially do not require a base weir for their deisgn; the conventional rectangular weir, V-notch and parabolic weirs are well known examples. Weirs for which $m < 3/2$ are called as compensating weirs, Sutro weir (Linear Proportional Weir) /2/, Quadratic Weir /5, 7, 10/, Logarithmic Weir /3/ are well-known examples of this category. These weirs invariably require a base weir for their design. It was pointed out that the non-compensating weirs can also be designed with bases with advantage. These are termed as "noncompensating base weirs". Recently, Keshava Murthy and Pillai have designed a new class of weirs called 'Proportional V-notch Weirs' /9/ having different bases which give the same discharge-head relationship as that of the conventional V-notch. These weirs are called as P-Vee weirs and the authors have shown that they have the advantages of both the V-notch, and the rectangular notch, in that they have higher indication accuracy besides having the advantage of horizontal crest.

Parabolic Weir which gives discharge proportional to the squre of the head is supposed to have been invented by Lauritson* /4/. Considerable experimental work was done in the early part of the nineteenth century by Poncelet in France, Francis at the Massachusetts Institute in U.S.A. and Bazin in Europe. Parabolic Weirs have two distinct features which mark it as superior for the accurate measurement of wide variations of flow namely, a relatively deeper section at small discharges and a relatively large section for a given depth, i.e. the area is small for low heads and increases faster than the depth. The coefficient of discharge is practically constant for a wide variations of head and the Parabolic Weir is adaptable as a simple and accurate meter for measuring the discharge. Further, the Parabolic Weir can be used as outlet weirs in grit chambers of triangular and trapezoidal cross-sections to maintain constant average velocity for all variations of depth.

In 1920, Greve /4/ did extensive work on both chamfered and unchamfered parabolic weirs at Purdue Univeristy. Since then, to the authors' knowledge, very little work has been done on Parabolic Weirs.

Parabolic Weir suffers from the major lacuna in that the fixing and finding the initial level of the weir is difficult as the vertex of the weir may not be so accurately defined in practice, particularly, as the

---

*However, questioned by many authors. (Please refer the discussions on this paper)

curvature of the parabola is changing so rapidly at that point and it would seem that errors in shaping the notch are more likely to occur here than at other parts of the outline. In this paper, the problem of parabolic weir is reconsidered. In the present design, this lacuna is removed by a providing horizontal crest for the weir. Incidentally, it is shown that the indication accuracy for the weir is greater than the conventional weir.

It is well known that for every weir, there is a minimum reliable depth /16/ below which the measurements are not to be made for a defined limit of accuracy. For an allowable error of 1% in the measurement of head and 2% in the measurement of discharge, it can be shown that the minimum reliable depth, $(h_c)_{min}$, for parabolic weir is 4" (10 cm) below which it is not advisable to make measurements. This minimum reliable depth can be utilised for providing a base for the parabolic weir.

Mathematical formulation

A Proportional Wier consists of a base weir and a complementary weir. It is required to design the complementary weir for a chosen base weir and for a given discharge-head relationship. For proportional parabolic weir $Q \propto H^2$, where Q = discharge and H = head measured above a datum. Fig. 1 shows the descriptions of the proportional parabolic weir.

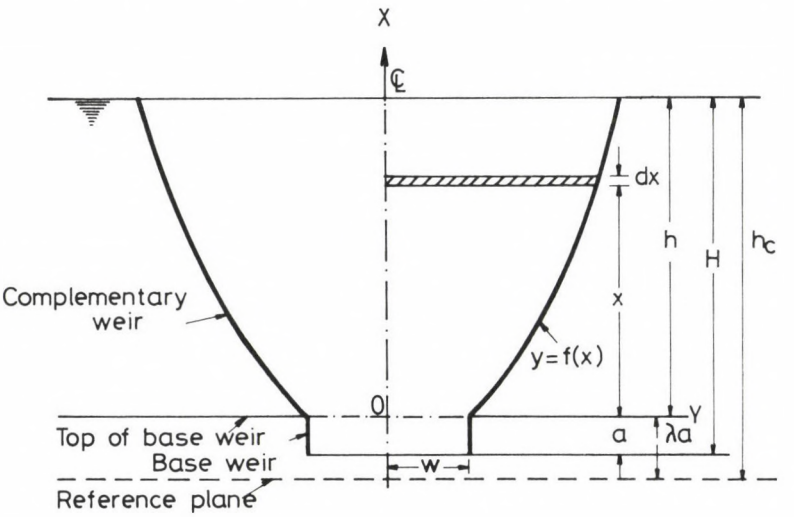

Fig. 1. Nomenclature of rectangular based proportional parabolic weir

For mathematical simplicity, a weir having a rectangular base of half width 'W' and depth 'a' is chosen over which a complementary weir $y = f(x)$, to be designed is fitted. The weir is assumed to be symmetrical and sharp crested. However, the symmetry is not necessary for the design. A common coefficient of discharge has been assumed for both base weir and complementary weir.

Referring to Fig. 1, the total discharge 'Q through the weir for flows above the base weir ($h \geq 0$) is given by

$$Q_b + Q_c = Q \tag{1}$$

where

Q_b = discharge through the base weir acting as an orifice.

$$= \frac{4}{3} W C_d \sqrt{2g} \left[(h+a)^{3/2} - h^{3/2}\right] \tag{2}$$

and Q_c = discharge through the complementary weir, above the base.

$$= 2 C_c \sqrt{2g} \int_0^h \sqrt{h-x}\, f(x)\, dx \tag{3}$$

in which,

h = depth of flow above the origin 'O';

C_d = coefficient of discharge;

and g = acceleration due to gravity.

For proportional parabolic weir, the total discharge for flows above the base is proportional to the square of the head measured above a reference plane, i.e., $Q \propto (h+\lambda a)^2$ where 'λ' is the datum constant /11/ which fixes the reference plane of the weir. Hence we write,

$$\frac{4}{3} WC_d \sqrt{2g} \left[(h+a)^{3/2} - h^{3/2}\right] + 2C_d \sqrt{2g} \int_0^h \sqrt{h-x}\, f(x)dx = b(h+\lambda a)^2, \; h \geq 0 \tag{4}$$

where, b = proportionality constant.

Evaluation of 'b' and 'λ'

Letting $2C_d \sqrt{2g} = K$ Eq. 4 may be written as

$$\frac{2}{3} WK \left[(h+a)^{3/2} - h^{3/2}\right] + K \int_0^h \sqrt{h-x}\, f(x)dx = b(h+\lambda a)^2 \quad , \; h \geq 0 \tag{5}$$

The constants 'b' and 'λ' are evaluated using the slope-discharge continuity theorem /11, 12/.

Differentiating Eq. 5 using Leibnitz's rule /13/ and rearranging we get,

$$WK\left[(h+a)^{1/2} - h^{1/2}\right] + \frac{K}{2}\int_0^h \frac{f(x)dx}{\sqrt{h-x}} = 2b\left[(h+\lambda a)\right]$$

i.e. $$\int_0^h \frac{f(x)dx}{\sqrt{h-x}} = \frac{4b}{K}\left[h+\lambda a\right] - W\left[(h+a)^{1/2} - h^{1/2}\right] = \phi(h), \text{ say} \qquad (6)$$

Letting h = 0, in equations 5 and 6 and solving for 'b' and 'λ' we get

$$b = \frac{3WK}{32\sqrt{a}} \qquad (7a)$$

and

$$\lambda = 8/3 \qquad (7b)$$

This means that the discharge is proportional to the square of the head measured above a reference plane or datum situated at $(\frac{1}{3})$ a below the crest of the weir. Eq. 6 is in the Abel's form of Volterrra's integral equation whose solution /6/ is

$$f(x) = \frac{1}{\pi}\int_0^x \frac{\phi'(h)dh}{\sqrt{x-h}}$$

Integrating after substituting for $\phi(h)$ we get,

$$f(x) = y = W\left[1 - \frac{2}{\pi}\tan^{-1}\sqrt{x/a} + \frac{3}{\pi}\sqrt{x/a}\right] \qquad (8)$$

It may be of interest to note that the first two terms of the above equation constitute the Sutro weir equation /2, 14/. Profile of the complementary weir given by the Eq. 8 is given in the Table 1, under the weir type number 1 and its coordinates are given in the column 2 of Table 2. Profile equations and the coordinates of different designed weirs are shown in the Tables 1 and 2, respectively. The profiles of the designed and experimented weirs are shown in Fig. 2 and Fig. 3, respectively. The profile equations of the experimented weirs are shown in Table 3.

Table 1 Details of the designed proportional parabolic weirs

Weir type (1)	Base weir equation (2)	C_1 (3)	C_2 (4)	C_3 (5)	b (6)	λ (7)	Complementary weir profile $y = f(x)$ (8)
1	$C_1 + C_2 x$	0	W	-	$\frac{3}{8}\frac{WK}{a^{1/2}}$	4/3	$W\left[1-\frac{2}{\pi}\tan^{-1}\sqrt{\frac{x}{a}}+\frac{3}{\pi}\sqrt{\frac{x}{a}}\right]$
2	$C_1 + C_2 x$	0	W/a	-	$\frac{5}{12}\frac{WK}{a^{1/2}}$	4/5	$W\left[(1+\frac{x}{a})(1-\frac{2}{\pi}\tan^{-1}\sqrt{\frac{x}{a}})+\frac{4}{3\pi}\sqrt{\frac{x}{a}}\right]$
3	$C_1 + C_2 x^{3/2}$	0	$W/a^{3/2}$	-	$\frac{9\pi}{64}\frac{WK}{a^{1/2}}$	2/3	$W\left[(1+\frac{x}{a})^{3/2}-(\frac{x}{a})^{3/2}-\frac{3}{8}(\frac{x}{a})^{1/2}\right]$
4	$C_1 + C_2 x^2$	0	W/a^2	-	$\frac{7}{15}\frac{WK}{a^{1/2}}$	4/7	$W\left[(1+\frac{x}{a})(1-\frac{2}{\pi}\tan^{-1}\sqrt{\frac{x}{a}})-\frac{2}{\pi}\sqrt{\frac{x}{a}}(\frac{x}{a}+\frac{5}{3})+\frac{56}{15\pi}\sqrt{\frac{x}{a}}\right]$
5	$C_1 + C_2 x^{1/2}$	W_1	$\frac{-8}{3}\frac{W_1}{a^{1/2}}$	-	$\frac{W_1 K}{12a^{1/2}}$	2	$W_1\left[(1-\frac{2}{\pi}\tan^{-1}\sqrt{\frac{x}{a}})-\frac{8}{3\pi}\left[(1+\frac{x}{a})^{1/2}-\frac{5}{4}(\frac{x}{a})^{1/2}\right]\right]$
6	$C_1 + C_2 x$	W_1	$\frac{-5W_1}{6a}$	-	$\frac{W_1 K}{9a^{1/2}}$	2	$W_1\left[(1-\frac{2}{\pi}\tan^{-1}\sqrt{\frac{x}{a}})(1-\frac{(1+\frac{x}{a})}{3})+\frac{23}{9\pi}\sqrt{\frac{x}{a}}\right]$
7	$C_1 + C_2 x^{3/2}$	W_1	$\frac{-8W_1}{3a^{3/2}}$	-	$\frac{W_1 K}{8a^{1/2}}$	2	$W_1\left[(1-\frac{2}{\pi}\tan^{-1}\sqrt{\frac{x}{a}})-\frac{8}{3\pi}\left[(1+\frac{x}{a})^{3/2}-(\frac{x}{a})^{3/2}\right]+\frac{5}{\pi}\sqrt{\frac{x}{a}}\right]$
8	$C_1 + C_2 x^2$	W_1	$\frac{-7W_1}{a^{3/2}}$	-	$\frac{2W_1 K}{15a^{1/2}}$	2	$W_1\left[(1-\frac{2}{\pi}\tan^{-1}\sqrt{\frac{x}{a}})\left[1-\frac{7}{8}(1+\frac{x}{a})^2\right]+\right.$ $\left.+\frac{7}{4\pi}\sqrt{\frac{x}{a}}(\frac{x}{a}+\frac{5}{3})+\frac{16}{15\pi}\sqrt{\frac{x}{a}}\right]$
9	$C_1 + C_2 x^{3/2} + C_3 x^2$	W_1	$\frac{-4.321W_1}{a^{3/2}}$	$\frac{3.58W_1}{a^2}$	$\frac{0.091W_1 K}{a^{1/2}}$	2	$W_1\left[1-\frac{2}{\pi}\tan^{-1}\sqrt{\frac{x}{a}}-4.321\left[(1+\frac{x}{a})^{3/2}-(\frac{x}{a})^{3/2}-\frac{3}{2}(\frac{x}{a})^{1/2}\right]+\right.$ $+3.58\left[(1+\frac{x}{a})^2(1-\frac{2}{\pi}\tan^{-1}\sqrt{\frac{x}{a}})-\frac{2}{\pi}\sqrt{\frac{x}{a}}(\frac{x}{a}+\frac{5}{3})\right]+$ $\left.+0.2315\sqrt{\frac{x}{a}}\right]$

Table 2 Coordinates of points on the proportional parabolic weirs

	Weir type number								
	1	2	3	4	5	6	7	8	9
x/a	Y/W	Y/W	Y/W	Y/W	Y/W_1	Y/W_1	Y/W_1	Y/W_1	Y/W_1
0.00	1.0000	1.0000	1.0000	1.0000	0.5117	0.1667	0.1512	0.1250	0.2583
0.10	1.1070	1.1539	1.0035	0.9942	0.2503	0.3243	0.3559	0.3713	0.2928
0.20	1.1593	1.2583	1.0574	1.0545	0.2770	0.3638	0.4042	0.4265	0.3129
0.30	1.2040	1.3502	1.1125	1.1160	0.2943	0.3888	0.4340	0.4600	0.3279
0.40	1.2449	1.4342	1.664	1.1758	0.3077	0.4077	0.4562	0.4845	0.3404
0.50	1.2834	1.5125	1.2184	1.2333	0.3188	0.4232	0.4743	0.5043	0.3513
0.60	1.3201	1.5862	1.2686	1.2887	0.3286	0.4366	0.4898	0.5213	0.3611
0.70	1.3554	1.6562	1.3171	1.3419	0.3374	0.4487	0.5037	0.5364	0.3702
0.80	1.3996	1.7230	1.3640	1.3932	0.3456	0.4599	0.5165	0.5501	0.3787
0.90	1.4227	1.7871	1.4049	1.4427	0.3533	0.4703	0.5283	0.5629	0.3868
1.00	1.4549	1.8488	1.4534	1.4907	0.3606	0.4801	0.5395	0.5750	0.3945
1.10	1.4864	1.9084	1.4962	1.5372	0.3676	0.4895	0.5502	0.5864	0.4020
1.20	1.5171	1.9661	1.5378	1.5824	0.3743	0.4986	0.5605	0.5974	0.4092
1.30	1.5472	2.0221	1.5783	1.6263	0.3808	0.5073	0.5704	0.6081	0.4161
1.40	1.5766	2.0764	1.6179	1.6691	0.3871	0.5158	0.5799	0.6183	0.4229
1.50	1.6054	2.1294	1.6564	1.7914	0.3933	0.5241	0.5893	0.6283	0.4296
2.00	1.7423	2.3759	1.8374	1.9059	0.4221	0.5627	0.6328	0.6749	0.4608
4.00	2.2050	3.1739	2.4306	2.5481	0.5192	0.6922	0.7787	0.8306	0.5665
6.00	2.5858	3.8064	2.9049	3.0464	0.5999	0.7999	0.8999	0.9599	0.6545
8.00	2.9173	4.3481	3.3120	3.4793	0.6709	0.8946	1.0064	1.0734	0.7319
12.00	3.4869	5.2664	4.0040	4.2105	0.7940	1.0586	1.1909	1.2703	0.8661

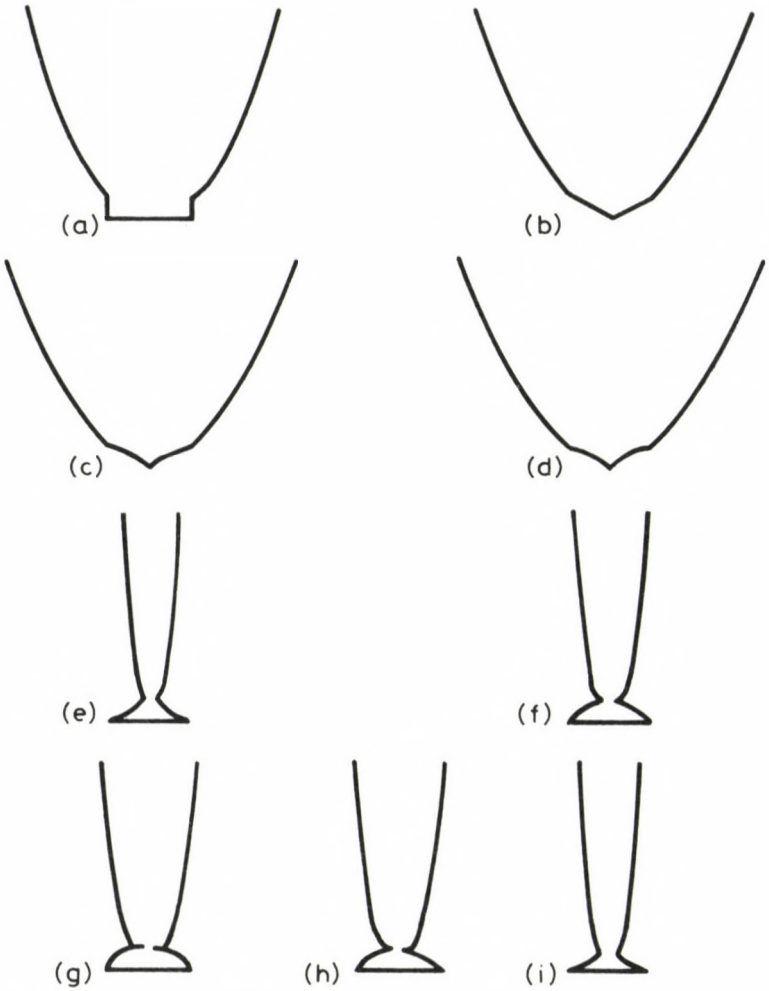

Fig. 2. Shapes of the designed parabolic weirs

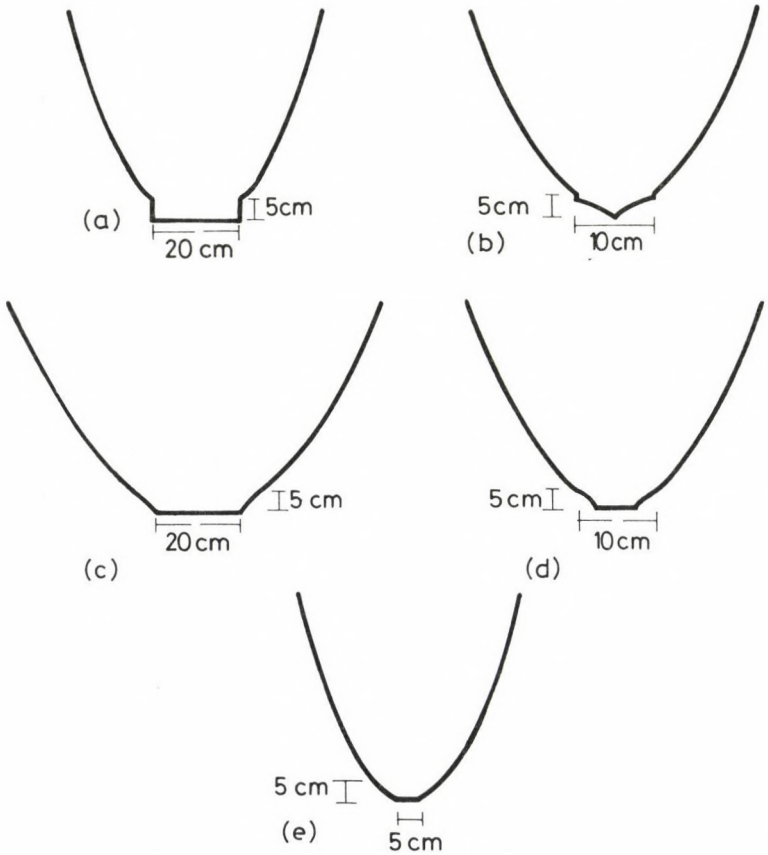

Fig. 3. Shapes of experimented parabolic weirs

Complementary Weir

An interesting and significant feature of all the designed weirs is that the profile of the complementary weir approaches the shape of the corresponding conventional parabolic weir after even a small value of $x/a = x_0$ (say), i.e. $(y/w) \alpha (x+\lambda a)^{1/2}$ or $y/w = p(x+\lambda a)^{1/2}$ (where 'p' is a constant) as could be seen from Table 4. Hence the width of the weir is very nearly proportional to the square root of the ordinates measured above the reference plane, for $X \geq X_0$ thus retaining the essential simplicity of the conventional weir. The apex of all these parabolae will be at the reference plane.

Table 3 Details of the experimented proportional parabolic weirs

Weir type	Base weir equation	C_1	C_2	C_3	b	λ	Complementary weir profile y = f(x)
1	$C_1 + C_2 x^0$	0	W	-	$\frac{3}{8}\frac{WK}{a^{1/2}}$	4/3	$W\left[1-\frac{2}{\pi}\tan^{-1}\sqrt{\frac{x}{a}}+\frac{3}{\pi}\sqrt{\frac{x}{a}}\right]$
2	$C_1 + C_2 x^{3/2}$	0	$\frac{W}{a^{3/2}}$	-	$\frac{9}{64}\frac{WK}{a^{1/2}}$	2/3	$W\left[(1+\frac{x}{a})^{3/2}-(\frac{x}{a})^{3/2}-\frac{3}{8}(\frac{x}{a})^{1/2}\right]$
3	$C_1 + C_2 x^{3/2}$	W_1	$\frac{16}{3}\frac{W_1}{a^{3/2}}$	-	$\frac{W_1 K}{a^{1/2}}$	1.178	$W_1\left[1-\frac{2}{\pi}\tan^{-1}\sqrt{\frac{x}{a}}-0.51422\left[(1+\frac{x}{a})^{3/2}-(\frac{x}{a})^{3/2}-(\frac{x}{a})^{1/2}\right]+1.40783\sqrt{\frac{x}{a}}\right]$
4	$C_1 + C_2 x^2$	W_1	$\frac{35}{24}\frac{W_1}{a^2}$	-	$\frac{8}{9}\frac{W_1 K}{a^{1/2}}$	1	$W_1\left[1-\frac{2}{\pi}\tan^{-1}\sqrt{\frac{x}{a}}+\frac{35}{9}\left[(1+\frac{x}{a})^2(1-\frac{2}{\pi}\tan^{-1}\sqrt{\frac{x}{a}}-\frac{2}{\pi}\sqrt{\frac{x}{a}}(\frac{x}{a}+\frac{5}{3})\right]+\frac{64}{9\pi}\sqrt{\frac{x}{a}}\right]$
5	$C_1 + C_2 x^{3/2} + C_3 x^2$	W_1	$\frac{64}{3}\frac{W_1}{a^{3/2}}$	$\frac{-35}{8}\frac{W}{a^2}$	$\frac{4WK}{a^{1/2}}$	1	$W_1\left[1-\frac{2}{\pi}\tan^{-1}\sqrt{\frac{x}{a}}+\frac{64}{3\pi}\left[(1+\frac{x}{a})^{3/2}-(\frac{x}{a})^{3/2}-\frac{2}{3}(\frac{x}{a})^{1/2}\right]-\frac{35}{8}\left[(1+\frac{x}{a})^2(1-\frac{2}{\pi}\tan^{-1}\sqrt{\frac{x}{a}})-\frac{2}{\pi}\sqrt{\frac{x}{a}}(\frac{x}{a}+\frac{5}{3})\right]+\frac{32}{\pi}\sqrt{\frac{x}{a}}\right]$

Realizability

For a given base weir it may not be always possible to obtain a physically realizable proportional weir. As in the case of Logarithmic weir /1, 3, 13/ with rectangular base or Quadratic weir with V-notch base, the function defining the complementary weir assumes negative values after a certain height thus limiting the range of applicability. However, it can be proved that the proportional parabolic weir is always realizable and the value of the function and hence the width of the weir approaches infinity when the height increases without limit. These are expressed in the following theorem:

Statement

"For any physically realizable base weir $Y_1 = F_1(X_1)$, defined in $-a \leq x_1 \leq 0$, the function $y = f(x)$ defining the complementary weir of the proportional parabolic weir is always positive in $0 \leq x \leq \infty$ and $f(x) \rightarrow \infty$ as $x \rightarrow \infty$".

Proof

1. f(x) is realizable:

Let the proportional parabolic weir have the base in the form of $Y_1 = F(X_1)$ referred to the origin O_1 (Fig. 4) to a depth 'a' over which the complementary weir $y = f(x)$ is fitted to produce the discharge-head relationship $Q = b(h+\lambda a)^2$ where 'b' is the proportionality constant and 'λ' the datum constant.

The discharge equation for the weir can be written as:

$$2C_{d1}\sqrt{2g}\int_0^a \sqrt{h+a-x_1}\, F_1(X_1)dX_1 + 2C_{d2}\sqrt{2g}\int_0^h h-x\, f(x)dx = b(h+\lambda a)^2, \qquad (9)$$

$$h \geq 0$$

For simplicity, assuming the coefficient of discharge to be the same for both the base weir and the complementary weir i.e., $C_{d1} = C_{d2} = C_d$ (this condition is not absolutely essential for the proof) the discharge equation for the proportional parabolic weir can be written as:

$$Q_b + K\int_0^h \sqrt{h-x}\, f(x)dx = b(h+\lambda a)^2$$

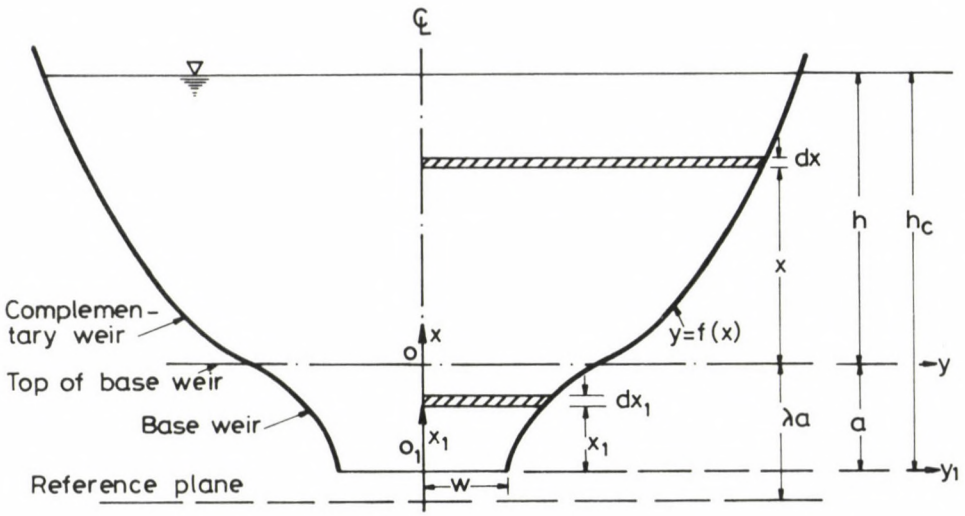

Fig. 4. Definition sketch

$$\int_0^h \sqrt{h-x}\, f(x)dx = \frac{b}{K}(h+\lambda a)^2 - \frac{Q_b}{K} \qquad (10)$$

where, Q_b = discharge through the base weir acting as an orifice.

Differentiating Eq. 10, with respect to 'h' using Leibnitz' rule (16), we have

$$\int_0^h \frac{f(x)dx}{(h-x)^{1/2}} = \frac{4b}{K}(h+\lambda a) - \frac{2}{K}\left(\frac{dQ_b}{dh}\right) = \phi(h) \text{ say} \qquad (11)$$

Applying the slope-discharge continuity theorem, Eq. 11 gives $O(O)=O$. Equation 11 is in the Abel's form of Volterra's Integral equation whose solution /6/ is

$$f(x) = \frac{1}{\pi}\int_0^x \frac{\phi'(h)dh}{\sqrt{x-h}}$$

$$= \frac{4}{K\pi}\frac{d}{dx}\int_0^x \sqrt{x-h}\left[2b - d^2Q_b/dh^2\right] dh \qquad (12)$$

Q_b representing the discharge through the base weir is a monotonically increasing single valued function of head defined by,

$$Q_b = K \int_0^a \sqrt{h_c - x_1}\; F_1(X_1)\, dX_1 \quad , \qquad h_c \geq a$$

$$= K h_c^{1/2} \int_0^a \left(1 - \frac{x_1}{h_c}\right)^{1/2} F_1(X_1)\, dX_1$$

$$= K h_c^{1/2} \int_0^a \left[1 - \frac{1}{2}\left(\frac{x_1}{h_c}\right) + \frac{1}{8}\left(\frac{x_1}{h_c}\right)^2 + \ldots\right] F_1(X_1)\, dX_1 \qquad (13)$$

where $h_c = h+a$, head measured from the crest.

For large heads, X_1/h_c and its higher powers may be neglected so that Q_b is approximately proportional to the square root of the head. Hence,

As $\quad h \rightarrow \infty \quad , \quad h_c \rightarrow \infty$

$$Q_b \rightarrow C(h_c)^{1/2}$$

This is physically obvious, as when the head increases, the velocity is proportional to $\sqrt{2gh}$, and area being constant, the discharge is proportional to the square root of the head.

Let $\dfrac{dQ_b}{dh} = \sigma$

σ is finite at $h = 0$,

$\sigma = 0$ at $h \rightarrow \infty$

Hence, ' σ ' is positive throughout $0 \leq h \leq \infty$. Since ' σ ' is a single valued function of 'h', it is a monotonically decreasing function of 'h'. Hence, $\dfrac{2\sigma}{dh} = d^2Q_b/dh^2$ is negative throughout $0 \leq h \leq \infty$ and from Eq. 12 $\phi'(h) = 2b - d^2Q_b/dh^2$ is positive in $0 \leq h \leq \infty$. Therefore, the function $f(x)$ can be interpreted as the slope of the discharge curve for a notch whose profile is defined $2b - (d^2Q_b/dh^2)$, which is always positive, and hence $f(x)$ is always positive in $0 \leq h \leq \infty$.

2. $f(x) \rightarrow \infty$, as $x \rightarrow \infty$:

Assuming $f(x)$ and $f'(x)$ are of exponential order and at least piecewise continuous, the final value theorem of Laplace transform (15) gives,

$$\lim_{x \to \infty} f(x) = \lim_{S \to 0} SL\{f(x)\} \tag{15}$$

where 'L' refers to the Laplacian Operator defined by

$$L\,f(t) = \int_0^{\infty} e^{-st} f(t)dt$$

Taking Laplace Transform on either side of Eq. 12, we get

$$L\{f(x)\} = \frac{1}{\pi}\{f(x-h)^{-1/2}\,\phi'(h)dh\} \tag{16}$$

Applying the Borel's theorem /15/ of the convolution integral to Eq. 16, we have,

$$L\{f(x)\} = \frac{1}{\pi}\{x^{-1/2}\}\; L\{\phi'(x)\} \tag{17}$$

Since, $L\{\phi'(x)\} = SL\{\phi(x)\} - \phi(0)$ in which $\phi(0) = 0$ (Slope-discharge continuity theorem) Eq. 17 reduces to,

$$L\{f(x)\} = \frac{1}{\pi} L\{x^{-1/2}\} \cdot SL\{\phi I(x)\}$$

$$= \frac{1}{\pi}\sqrt{\frac{\pi}{S}} \cdot S\left[L\left\{\frac{4b}{K}(h+\lambda a) - \frac{2}{K}Q_b'\right\}\right] \tag{18}$$

where $Q_b' = \dfrac{dQ_b}{dh}$

$$= \sqrt{\frac{S}{\pi}}\left[\frac{4b}{K}\left(\frac{1}{S^2} + \frac{\lambda a}{S}\right) - \frac{2}{K} L\{Q_b'\}\right]$$

$$\lim_{S \to 0} SL\{f(x)\} = f(\infty) \lim_{S \to 0} \frac{4b}{K\sqrt{\pi}}\left(\frac{1}{S^{1/2}} + \lambda a\, S^{1/2}\right) - \lim_{S \to 0} \frac{2}{K}\sqrt{\frac{S}{\pi}} \lim_{S \to 0} S\,L(Q_b')$$

$$= \lim_{S \to 0} \frac{4b}{K\sqrt{\pi}}\left(\frac{1}{S^{1/2}} + \lambda a S^{1/2}\right) - \lim_{S \to 0} \frac{2}{K\sqrt{\pi}} S^{1/2}\, Q_b'(0) \tag{19}$$

$f(\infty) = \infty$ as $Q_b'(0)$ is finite.

Hence the width of the weir tends to infinity as the depth increases without limit.

Evaluation of Critical 'λ' for equal slope

In general, there will be a kink at the junction of base weir and the complementary weir. The condition of equal slope at the junction will overcome this lacuna and ensure a smooth transition of flow facilitating easy cutting and improving the possibilities of higher coefficient of discharge. It is not always possible to achieve this condition for all bases, e.g., for the base $Y_1 = C_1 + C_2 X^{1/2}$ 'λ' is imaginary for this condition. However, for the two bases $Y_1 = C_1 + C_2 {}^{3/2}$ and $Y_1 = C_1 + C_2 X^2$, critical values of 'λ' have been obtained for the above condition.

Following the same procedure detailed before in this article, the complementary weir for the base $Y_1 = C_1 + C_2 X^{3/2}$ in terms of 'λ' can be obtained as:

$$\frac{Y}{W} = 1 - \frac{2}{\pi}\tan^{-1}\sqrt{\frac{x}{a}} + \frac{16}{3\pi}\frac{(4-3\lambda)}{(3\lambda-2)}\left[(1+\frac{x}{a})^{3/2} + (\frac{x}{a})^{3/2} - \frac{3}{2}(\frac{x}{a})^{1/2}\right] + \\ + \frac{8}{\pi}\frac{\sqrt{x/a}}{\lambda(3\lambda-2)} \qquad (20)$$

$$\text{with } \frac{C_2}{C_1} = \frac{16}{3\pi}\frac{(4-3\lambda)}{(3\lambda-2)}\frac{1}{a^{3/2}}$$

Hence the equation of the base weir can be written as:

$$\frac{Y_1}{W} = 1 + \frac{16}{3\pi}\frac{(4-3\lambda)}{(3\lambda-2)}(\frac{x}{a})^{3/2} \qquad (21)$$

Differentiating Eqs (20) and (21), with respect to X and X_1, respectively, and enforcing the condition of equal slope, at x = 0,

$$\text{i.e.,} \quad \left.\frac{dY_1}{dX_1}\right|_{X_1 = a} = \left.\frac{dY}{dX}\right|_{X = 0}$$

results in,

$$9\lambda^2 - 14\lambda + 4 = 0$$

Solving we get,

$$\lambda = 0.38 \text{ or } 1.18$$

$\lambda = 0.38$, results in the base weir having negative coordinates which is physically unrealizable and hence this value is neglected. $\lambda = 1.18$ gives the ordinates of proportional parabolic weir with equal slope at the junction.

Proportional parabolic weir with the base $Y_1 = C_1 + C_2X^2$ can be designed in a similar manner. It can be shown that the condition of equal slope results in,

$$21\ \lambda^2 - 32\lambda + 8 = 0$$

solving we get, $\lambda = 0.31$ or 1.21 .

However, only for $\lambda = 1.21$, positive coordinates can be obtained for the above condition. The profiles of these weirs are shown in Fig. 5(a) and 6(a), respectively.

(a) Equal slope

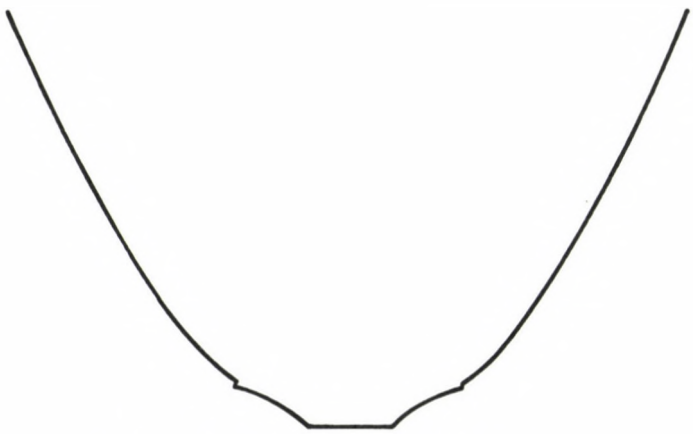

(b) Constant indication accuracy

Fig. 5. Profiles of proportional parabolic weir for base $Y_1 = C_1 + C_2X^{3/2}$

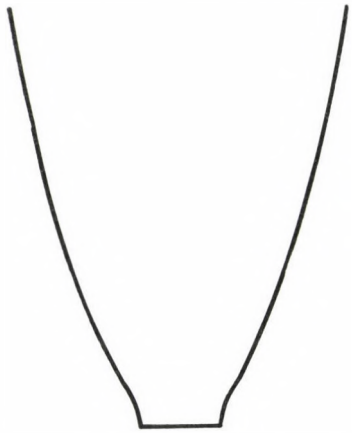

(a) Equal slope

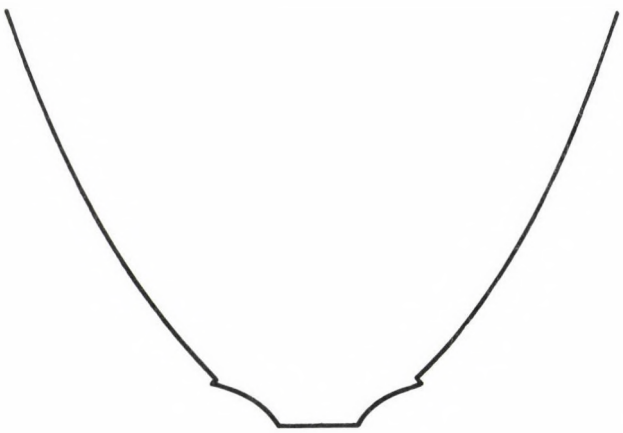

(b) Constant indication accuracy

Fig. 6. Profiles of proportional parabolic weir for base $Y_1 = C_1 + C_2 X^2$

Constant Indication accuracy

When the reference plane coincides with the crest, the head can be measured from the crest as in conventional weirs. Further, it ensures Constant Indication Accuracy /8/ (explained later in this paper). This is achieved by putting $\lambda = 1$ in the profile equations of the weir. However, this advantage cannot be incorporated for all the bases. For proportional parabolic weir having the base $Y_1 = C_1 + C_2 X^{3/2}$ and $Y_1 = C_1 + C_2 X^2$, the above condition has been achieved with $C_2/C_1 = 16/3\pi a^{3/2}$ and $35/24a^2$, respectively. These are shown in the Figs 5(b) and 6(b), respectively.

Condition of Equal Slope with Constant Indication Accuracy

These conditions enable the head to be measured directly from the crest in addition to having a smooth transition at the junction of base weir and the complementary weir. It also ensures constant Indication Accuracy. These conditions are simultaneously achieved for the base weir of the form $Y_1 = C_1 + C_2 X^{3/2} + C_3 X^2$ in which $C_2/C_1 = 64/3\ a^{3/2}$ and $C_3/C_1 = -35/8a^2$. This is shown in Fig. 7.

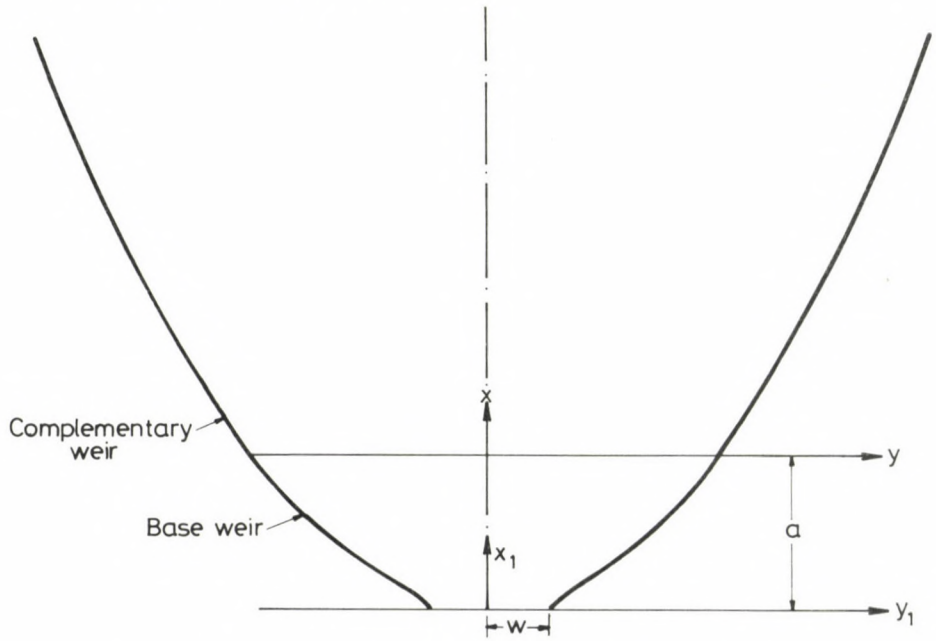

Fig. 7. Profile of proportional parabolic weir for base $Y = C_1 + C_2 X^{3/2} + C_3 X^2$

Indication Error

Indication Error is the error in the measurement of discharge for a known error in the measurement of head /16/.

The indication error or relative error, e_Q, in measuring the rate of flow with a weir depends mainly on the error (e_h) in the measurement of head (h_c) over the weir. For a given discharge-head relationship, $Q = f(h)$, the relative error in discharge (e_Q) and relative error in head (e_h) may be mathematically expressed as:

$$e = me \quad Q \quad h(22)$$

where m is the power of head in the discharge-head relationship.

A weir giving lesser error in the computed discharge for the same error in the measurement of the head is said to have higher indication accuracy over the other weir.

Comparison of indication accuracies

(a) Conventional Parabolic Weir:

Assuming the coefficient of discharge to be the same for a given weir, the discharge equation is

$$Q = bh_c^2 \tag{23}$$

where

$b = \frac{C\pi}{2} \sqrt{2g} \sqrt{2P}$

C = discharge coefficient, and

P = parametric constant of parabola $Y^2 = \sqrt{2p}\, x$.

Differentiating Eq. 23 with respect to h_c, we get

$$dQ = 2bh_c\, dh_c$$

$$\text{Relative error} = e_q = \frac{dQ}{Q} = 2\left(\frac{dh_c}{h_c}\right)$$

$$eQ = 2e_{hc} \tag{24}$$

It can be clearly seen that for 1% error in the measurement of head over a parabolic weir causes 2% error in the measurement of discharge.

(b) Modified proportional parabolic weir:

The discharge equation is,

$$Q = b(h + \lambda a)^2$$
$$= b(h_c + a(\lambda - 1)^2) \tag{25}$$

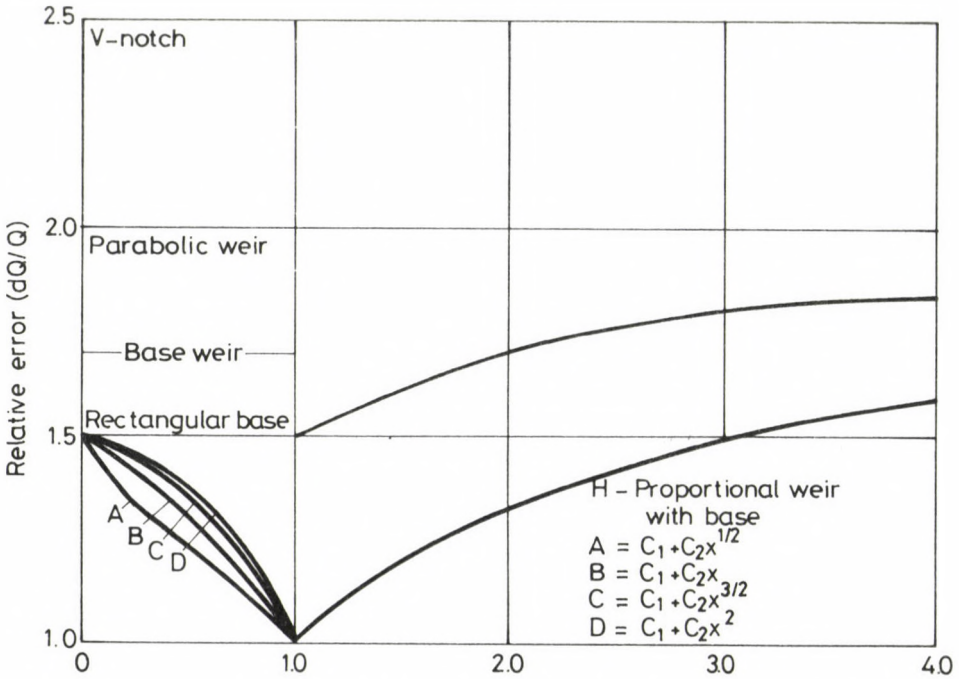

Fig. 8. Non-dimensional head (Hc/a)

Differentiating Eq. 24, with respect to h_c and simplifying

$$e_Q = \frac{dQ}{Q} = 2\,\frac{dh_c}{(h_c + a(\lambda - 1))} = \frac{2e_{hc}}{\left(1 + \frac{(\lambda - 1)}{(h_c/a)}\right)} \qquad (26)$$

It is clearly seen that the relative error for the proportional parabolic weir varies with the non-dimensional head (h_c/a). As $\lambda < 1.0$ in several cases (1 and 5 to 9 of Table 1) the relative error will be low at lower heads and is always less than that of conventional parabolic weir. Fig. 8 shows the variation of relative error (e_Q) with the (h_c/a) for conventional as well as for the modified parabolic weir. Since $\lambda = 2$, for weir types 4-8 (Table 1), the relative error in discharge varies from 1% at the minimum head to 2% at the infinite head assuming e_{hc} = 1%. Hence the sensitivity /16/ of these weirs is higher than that of the conventional parabolic weir.

Table 4 Details of the complementary weir profiles with co-ordinate points

x/a	$(Y/W)^2/(x + \lambda a)$ Weir type number								
	1	2	3	4	5	6	7	8	9
0.5	0.0898	0.0565	0.1272	0.07098	1.4849	1.1544	0.09880	0.1289	0.0722
1.0	0.0907	0.0563	0.1267	0.0707	1.4875	1.1538	0.09899	1.1284	0.0721
1.5	0.0910	0.0563	0.1266	0.0706	1.4880	1.1532	0.0990	0.1282	0.0721
2.0	0.0911	0.0563	0.1266	0.0706	1.4883	1.1530	0.0991	0.1282	0.0721
2.5	0.0911	0.0563	0.1266	0.0706	1.4885	1.1529	0.0991	0.1281	0.0721
3.0	0.0911	0.0563	0.1266	0.0706	1.4885	1.1529	0.0991	0.1281	0.0721
3.5	0.0911	0.0563	0.1266	0.0706	1.4886	1.1529	0.0991	0.1281	0.0721
4.0	0.0911	0.0563	0.1266	0.0706	1.4886	1.1529	0.0991	0.1281	0.0721
4.5	0.0911	0.0563	0.1266	0.0706	1.4886	1.1528	0.0991	0.1281	0.0721
5.0	0.0911	0.0563	0.1266	0.0706	1.4886	1.1528	0.0991	0.1281	0.0721
6.0	0.0911	0.0563	0.1266	0.0706	1.4886	1.528	0.0991	0.1281	0.0721

Experiments

Experiments were conducted on five proportional parabolic weirs (Table 3). As shown in Table 4, the tests were conducted on symmetrical notches, with all but one having horizontal base to check the theory. Experimental set up is shown in Fig. 9. The weirs were cut in 0.65 cm (6.5 mm) mild steel plates. The boundary of the weir was carefully marked by a scratch awl. The weir had a sharp edge of 0.15 cm (1.5 mm) with a 45% chamfer. The weir was fixed at the end of a rectangular channel 19.2 m long, 1.2 m wide and 1.1 m deep with its crest 23 cm above the bed of the channel. The water was fed through a head tank measuring 2.25 m x 2.25 m x x 1.8 m, to which water was supplied by two pumps, having a combined capacity of 7.0 cfs ($\simeq 0.2\ m^3/s$). The head over the weir was measured with an electronic point gauge having a least count of 0.0025 cm set 1.8 m apart upstream of the weir section. The discharges were measured volumetrically in a tank measuring 4.52 m x 4.52 m x 1.5 m, through readings in a persplex tube of 2 cm internal diamter, connected to the bottom at one end. They were measured by finding the time taken for the water to raise from one indicator fixed in the persplex tube to another fixed exactly at a height

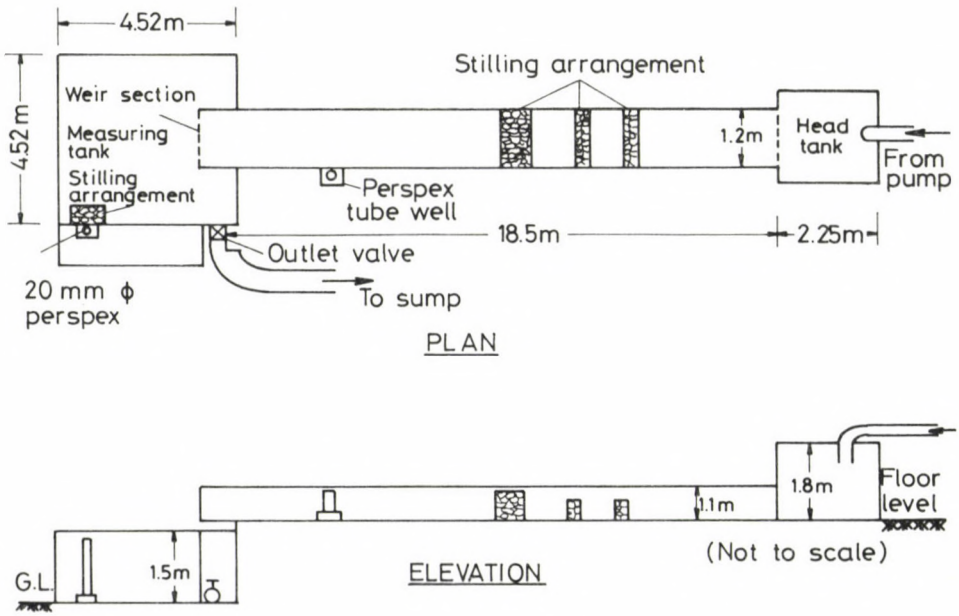

Fig. 9. Experimental set-up

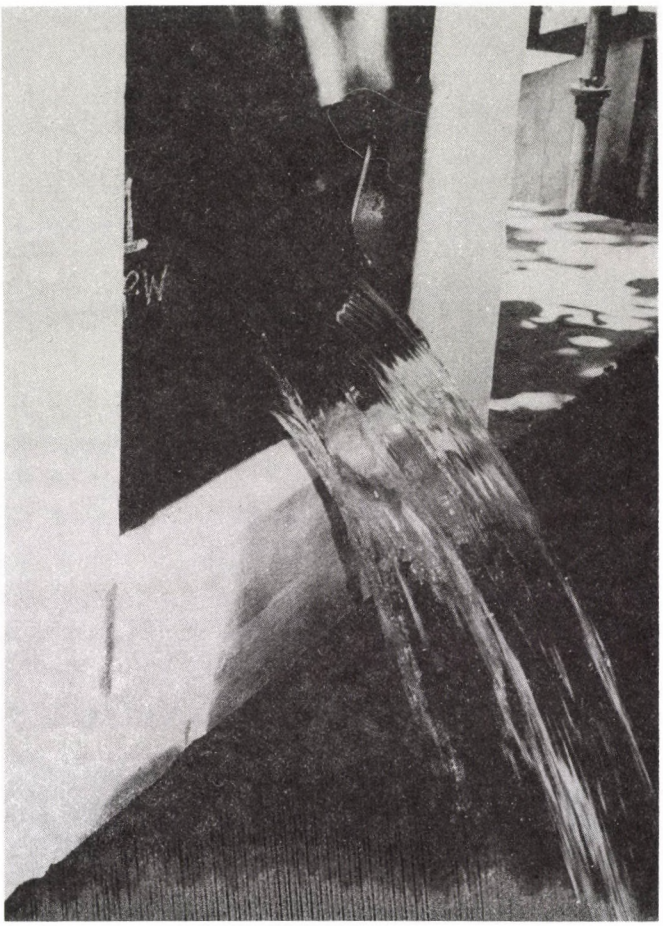

Fig. 10a. Side-views of flow through proportional weir of Fig. 3a

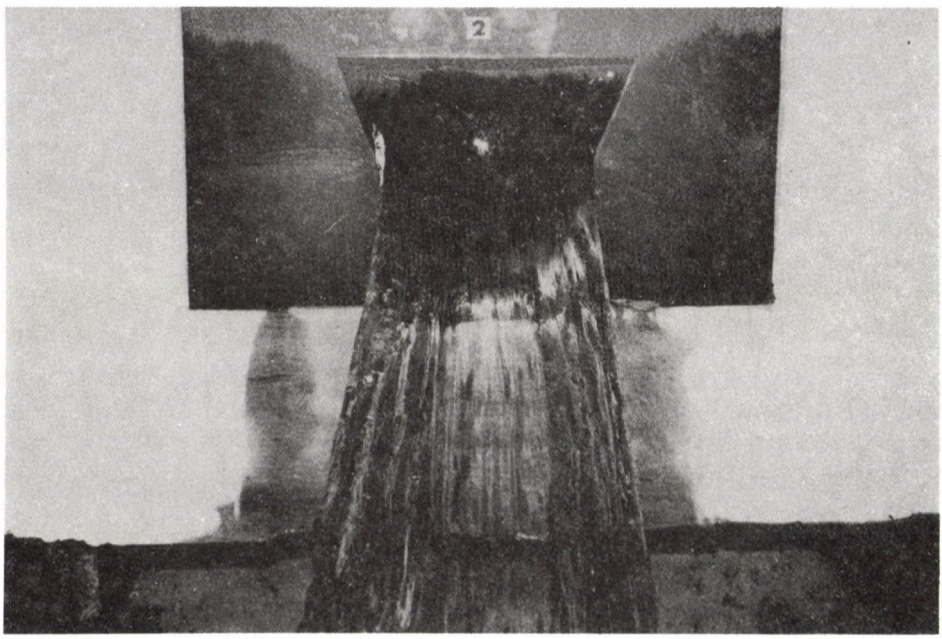

Fig. 10b. Front-views of flow through proportional weir of Fig. 3a

of 0.92 m. The indicator points were connected to the leads of an electronic timer through the start and stop mechanism. As soon as the water touched the lower indicator the timer was started and automatically stopped when the water touched the upper indicator. The time to collect the fixed volume of water was recorded with an accuracy of 0.01 sec for each discharge. Each experiment was repeated thrice to ensure accuracy. At least 15 min were allowed between the two sets of experiment to allow for the water level to stabilize. The experimental details are shown in Figs 10a, 10b, and Fig. 11 shows the plot of the $(h+\lambda a)^2$ versus actual discharge of the five weirs tested. It is seen that the experimental set up shows a remarkable agreement with theory by giving a constant coefficient of discharge.

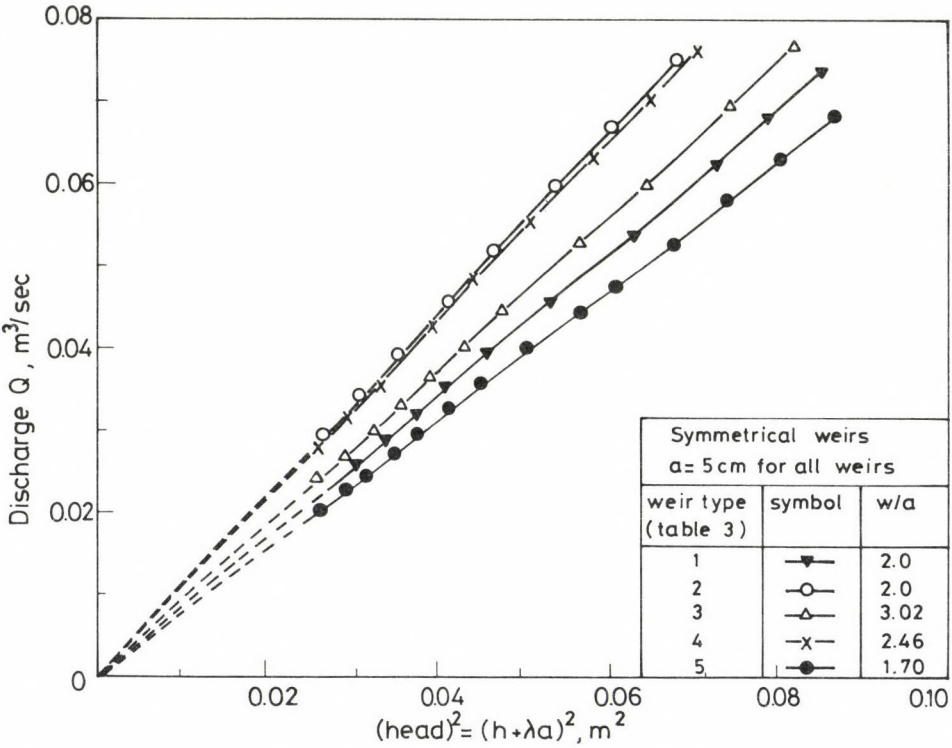

Fig. 11. Discharge versus head above datum

Table 5 Base weir dimensions of tested weirs

Sl No.	Weir type No. (Table 3)	Top half width base weir 'W' cm (mm)	Depth of base weir 'a' cm (mm)	Coeff. of discharge C_d	Remarks
1	1	10(100)	5(50)	0.584	Sym
2	3	10(100)	5(50)	0.615	Sym
3	7	15.1(151)	5(50)	0.610	Sym
4	8	12.3(123)	5(50)	0.613	Sym
5	9	8.5(85)	5(50)	0.602	Sym

Conclusions

A new design of proportional weir having bases producing a discharge proportional to the square of the head measured above a reference plane is given. Some of the weirs have a horizontal base thus overcoming the inherent difficulty of fixing and finding the initial level of the conventional parabolic weir. The indication accuracies of these weirs are found to be higher than the conventional weir. For the weir having the rectangular base, it is seen that the value of $\lambda = 4/3$, so that the reference plane is situated at 1/3 the depth of base weir below the crest. Further, it is significant to note that the profile of all these weirs rapidly approach the shape of the conventional weir even above a small height thus very much retaining the simplicity of the conventional weir.

The designs are further improved by incorporating the additional features viz.; (1) equal slope at the junction of base weir and complementary weir which ensures smooth transition of flow from base weir to the upper curved weir and (2) Constant indication accuracy (by making the reference plane coincide with the crest, i.e., $\lambda = 1$). These are achieved independently for the bases in the form of $Y_1 = C_1 + C_2X^{3/2}$ and $Y_1 = C_1 + C_2X^2$. Further, the above two conditions are simultaneously achieved by for the base in the form of $Y_1 = C_1 + C_2X^{3/2} + C_3X^2$.

It is significant that the parabolic weir having rectangular base can be utilised even in the rectangular base weir portion as the indication accuracy in the base weir portion is higher than the parabolic weir. A theorem on the realizability of the parabolic weir has been enunciated and proved which should prove useful to the designers.

Hydraulic tests on five designed weirs show excellent agreement with the theory by giving a constant average coefficient of discharge which varies for different weirs from 0.602 to 0.613.

Acknowledgements

The authors thank Mr. D.P. Giridhar for his help in coducting the experiments. They express their thanks to the authorities of the Indian Institute of Science for providing the necessary facilities for conducting the work.

REFERENCES

1. Chandrashekhara, D. - Lakshmana Rao, N.S.: Increased logarithmic weir profiles, Journal of Hydraulics Division, ASCE, Vol. 100, No. 11, HY11, Proc. Paper 10946, Nov. 1974, 1583-1599
2. Cowgill, P.: The Mathematical weir forms, Quart. of Appl. Math., Vol. 11, No. 2, (1944), 142
3. Govinda Rao, N.S. - Keshava Murthy, K.: On the design of logarithmic weirs, Journal of Hydraulic Research, Vol. 4, No. 1, (1966), 51-59
4. Greve, F.W.: Parabolic weirs, Transactions, ASCE, Paper No. 1473, (1921), 487-51
5. Haszpra, O.: The problem of quadratic weirs, Acta Technica, Hungary, Vol. 51, No. 1, 121-122
6. Hilderbrand, F.B.: Method of applied mathematics, Prentice Hall, Inc., (1952), 440
7. Keshava Murthy, K.: On the design of quadratic weirs, Journal of Franklin Institute, Vol. 287, No. 2, Feb. 1969, 159-174
8. Keshava Murthy, K. - Gopalakrishna Pillai, K.: Design of constant accuracy linear proportional weir, Journal of Hydraulics Division, ASCE, Vol. 104, No. HY4, Proc. Paper 13705, April 1978, 527-541
9. Keshava Murthy, K. - Gopalakrishna Pillai, K.: Modified proportional V-notch weirs, Journal of Hydraulic Division, ASCE, Vol. 104, No. HY5, May 1978, 715-791
10. Keshava Murthy, K. - Gopalakrishna Pillai, K.: Some aspects of quadratic weirs, Journal of Hydraulic Division, ASCE, Vol. 103, No. HY9, Sept. 1974, 1059-1076
11. Keshava Murthy, K. - Seshagiri, N.: A generalized mathematical theory and verification of proportional notches, Journal of Franklin Institute, Vol. 286, No. 5, May 1968, 347-363
12. Keshava Murthy, K.: A generalised mathematical theory of proportional weirs, Ph.D. thesis, Indian Institute of Science, Bangalore, October 1967
13. Lakshmana Rao, N.S.: Theory of weirs, Chapter in 'Advances in Hydrosciences', V.T. Chow, (ed.), Academic Press, Inc., New York, N.Y. Vol. 10, 1975, 309-406
14. Reddick, H.W. - Miller, F.W.: Advanced mathematics for engineers, John Wiley and Sons, Inc., New York, 1957, p. 263, 174
15. Thomson William, T.: Laplace transformation, Prentice Hall, Inc., 1960, p. 40
16. Troskolansky, A.T.: Hydrometry, 2nd edition, Pergamon Press, Inc., New York, N.Y., 1960, 301-306

Acta Technica Acad. Sci. Hung., 103(2-3), pp. 171-189 (1990)

BUCKLING OF GENERALLY ANISOTROPIC (AEOLOTROPIC) SHALLOW SHELLS

KOLLÁR, L.P.*

(Received: 28 March 1989)

The paper deals with the stability analysis of doubly curved aeolotropic shallow shells. The governing equation system of buckling is derived for the general case of anisotropy (aeolotropy) and a closed form solution is shown for the buckling load which can be applied for a wide range of cases, among others for orthotropic shells. The results can be applied for laminated (composite), corrugated, folded, and eccentrically rib-stiffened shells as well.

1. Introduction

The buckling analysis of isotropic shells of different shapes can be find in the literature e.g. [10, 11, 12]. The stability of anisotropic shells were treated by several authors [17 - 22, 13], and there are works on their post-buckling behaviour and on the effect of initial inperfections as well [14-16]. The authors used different assumptions for the middle surface of the shell, for the buckling shape and for the characteristics of anisotropy.

Orthotropic shallow shells were also treated by several authors, e.g. in [10, 1, 2, 3, 4, 6]. Dulácska has dealt in his paper [2] with the buckling of shallow orthotropic hyperbolic paraboloidal shells provided that the principal axes of orthotropy are parallel with the generatrices. The same case was investigated in [1, 4, 6]. Dulácska assumed that the buckling shape is given by a trigonometrical function which satisfies the differential equation but not the boundary conditions, and derived an equation from which the critical load can be calculated minimizing with respect to two parameters. The results of Gergely [6] are similar, but Gergely took into consideration a buckling shape which satisfies the boundary conditions in one direction, and the differential equation approximately only, making use of the energy principles. In papers [1, 4]

*Kollár, László P., H-1122 Budapest, Karap u. 9, Hungary

Akadémiai Kiadó, Budapest

numerical analysis can be found.

Dulácska also investigated the stability of shallow orthotropic shells with arbitrary shapes assuming that the stiffness matrix of the constitutive equation system contains non-zero elements only in the main diagonal [3]. He derived an equation on the basis of which the buckling load can be determined provided that the equation of the middle surface of the shell is $z = ax^2+by^2$, the principal axes of the orthotropy are x and y and the buckling shape is given by the function $w = W \sin\alpha x \sin\beta y$, which contains two parameters α and β . The buckling load can be calculated minimizing with respect to these parameters.

As far as we know, the stability of generally anisotropic (aeolotropic) shallow shells was not yet investigated. The aim of this paper is to generalize the previous results [2, 3, 6, 13] for these structures. We derive analytical solution for the buckling load if the equation of the middle surface of the shell is an arbitrary function of the second order, assuming that the buckling shape is given by double trigonometrical functions in a skew co-ordinate system.

In our derivations we shall use operator matrices, which results a relatively simple procedure that can be checked easily [8].

2. Basic assumptions and notations

The buckling load is considered to be the load which belongs to the bifurcation point of the load-displacement function.

We assume that the displacements are small and the material of the shell is homogeneous and linearly elastic. The middle surface of the shell is shallow, consequently, we can use the assumptions of shallow shell theory [5]. The equation of the surface is denoted by

$$z = z(x,y) \quad .$$

where x and y are the cartesian co-ordinates of the ground plane.

The internal forces acting on a shell element are shown in Fig. 1. These constitute the force vector

$$\mathbf{n} = \begin{bmatrix} n_x \\ n_y \\ n_{xy} \\ m_x \\ m_y \\ m_{xy} \end{bmatrix} . \qquad (2.1)$$

The external loads acting on a shell element are p_1, p_2 and p_3 (Fig. 1). It should be noted that the components of the load do not follow the co-ordinate axes x, y and z, but are tangents to the middle surface in planes parallel to the co-ordinate planes (p_1, p_2) and normal to the surface (p_3).

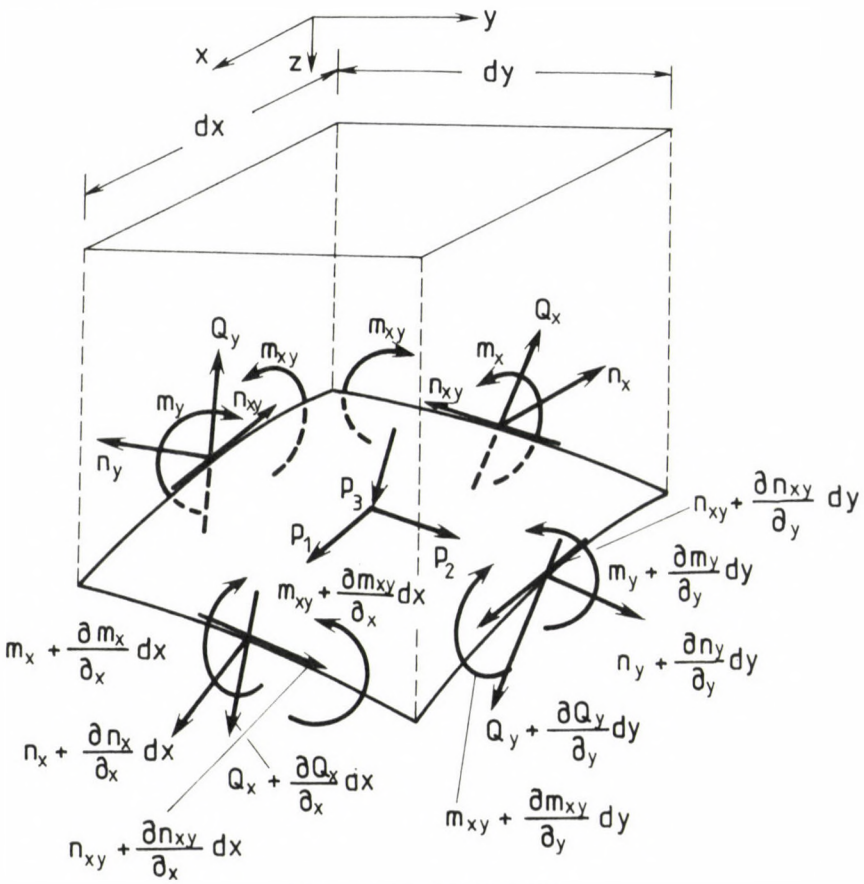

Fig. 1. Shell element

The displacements of an arbitrary point of the middle surface is described by the components u, v and w, which have the same directions as the load components p_1, p_2 and p_3.

We shall use the load vector $\mathbf{p}$ and the displacement vector $\mathbf{u}$ defined by the expressions :

$$\mathbf{p} = \begin{bmatrix} p_1 \\ p_2 \\ p_3 \end{bmatrix} , \qquad \mathbf{u} = \begin{bmatrix} u \\ v \\ w \end{bmatrix} . \tag{2.2a,b}$$

We denote the in-plane deformations by ε_x, ε_y and γ_{xy}, and the changes in curvature and twist of the middle surface by κ_x, κ_y and κ_{xy}. These constitute the deformation vector

$$\mathbf{e} = \begin{bmatrix} \varepsilon_x \\ \varepsilon_y \\ \gamma_{xy} \\ \kappa_x \\ \kappa_y \\ \kappa_{xy} \end{bmatrix} . \tag{2.3}$$

The connection between the internal forces and deformations is

$$\mathbf{n} = \mathbf{M}\,\mathbf{e} , \tag{2.4}$$

where $\mathbf{M}$ is the stiffness matrix which is (even in the case of *aeolotropic* material) symmetrical :

$$\mathbf{M} = \begin{bmatrix} T_{11} & T_{12} & T_{13} & C_{11} & C_{12} & C_{13} \\ T_{12} & T_{22} & T_{23} & C_{21} & C_{22} & C_{23} \\ T_{13} & T_{23} & T_{33} & C_{31} & C_{32} & C_{33} \\ C_{11} & C_{21} & C_{31} & B_{11} & B_{12} & B_{13} \\ C_{12} & C_{22} & C_{32} & B_{12} & B_{22} & B_{23} \\ C_{13} & C_{23} & C_{33} & B_{13} & B_{23} & B_{33} \end{bmatrix} .$$

If the shell is *orthotropic* and the principal axis of orthotropy are x and y, than

$$\mathbf{M} = \begin{bmatrix} T_{11} & T_{12} & & C_{11} & C_{12} & \\ T_{12} & T_{22} & & C_{21} & C_{22} & \\ & & T_{33} & & & C_{33} \\ C_{11} & C_{21} & & B_{11} & B_{12} & \\ C_{12} & C_{22} & & B_{12} & B_{22} & \\ & & C_{33} & & & B_{33} \end{bmatrix} . \tag{2.5}$$

Here T_{ij} are the extensional (tensile) stiffnesses, B_{ij} are the flexural (bending) stiffnesses and C_{ij} are the bending-stretching coupling stiffnesses of the shell [13].

A special case of orthotropy is when the stiffness matrix has the form

$$\mathbf{M} = \begin{bmatrix} T_x & & & & & \\ & T_y & & & & \\ & & T_{xy}/2 & & & \\ & & & B_x & & \\ & & & & B_y & \\ & & & & & B_{xy}/2 \end{bmatrix}. \tag{2.6}$$

This case was treated by Dulácska [2, 3, 10]. In the case of *isotropic shells*

$$\mathbf{M} = \begin{bmatrix} T & \nu T & & & & \\ \nu T & T & & & & \\ & & T(1-\nu)/2 & & & \\ & & & B & \nu B & \\ & & & \nu B & B & \\ & & & & & B(1-\nu)/2 \end{bmatrix}, \tag{2.7}$$

where

$T = Et/(1-\nu^2)$	the tensile stiffness of the shell,
$B = Et^3/\left[12(1-\nu^2)\right]$	the bending stiffness of the shell,
E	Young's modulus,
ν	Poisson's ratio,
t	the shell thickness.

3. Differential equations of aeolotropic shallow shells

The equilibrium equations of shallow shells can be found e.g. in [5]. Eliminating the transverse shearing forces, three equations are obtained

which can be written in matrix form :

$$\mathbf{p} = \Theta\,\mathbf{n} \quad , \tag{3.1}$$

where Θ is an operator matrix as follows :

$$\Theta = \begin{bmatrix} -\frac{\partial}{\partial x} & 0 & -\frac{\partial}{\partial y} & 0 & 0 & 0 \\ 0 & -\frac{\partial}{\partial y} & -\frac{\partial}{\partial x} & 0 & 0 & 0 \\ -\frac{\partial^2 z}{\partial x^2} & -\frac{\partial^2 z}{\partial y^2} & -\frac{2\partial^2 z}{\partial x \partial y} & -\frac{\partial^2}{\partial x^2} & -\frac{\partial^2}{\partial y^2} & -\frac{2\partial^2}{\partial x \partial y} \end{bmatrix} . \tag{3.2}$$

The connection between the displacements and deformations, i.e. the kinematic relations of the shallow shells are, according to [5]:

$$\mathbf{e} = \Theta^{*}\,\mathbf{u} \quad , \tag{3.3}$$

where

$$\Theta^{*} = \begin{bmatrix} \frac{\partial}{\partial x} & 0 & -\frac{\partial^2 z}{\partial x^2} \\ 0 & \frac{\partial}{\partial y} & -\frac{\partial^2 z}{\partial y^2} \\ \frac{\partial}{\partial y} & \frac{\partial}{\partial x} & -\frac{2\partial^2 z}{\partial x \partial y} \\ 0 & 0 & -\frac{\partial^2}{\partial x^2} \\ 0 & 0 & -\frac{\partial^2}{\partial y^2} \\ 0 & 0 & -\frac{2\partial^2}{\partial x \partial y} \end{bmatrix} \tag{3.4}$$

is the adjoint of Θ [8].

(3.1), (3.3) and (2.4) constitute the differential equation system of the eight order of shallow shells. Eliminating the stresses and deformations, we obtain :

$$\mathbf{p} = \Theta\,\mathbf{M}\,\Theta^{*}\,\mathbf{u} \quad . \tag{3.5}$$

4. Governing equations of buckling

For the investigation of stability the change in geometry has to be taken into account.

The vector of internal forces before buckling is denoted by $\mathbf{n}_0$, and the middle surface of the shell is given by the function z_0, which contains the deformations due to $\mathbf{n}_0$ as well. The displacements, deformations and internal forces during buckling are denoted by $\mathbf{u}_B$, $\mathbf{e}_B$ and $\mathbf{n}_B$ respectively.

The shell is shallow, consequently, the function of the middle surface of the shell can be written in the following way :

$$z = z_0 + w_B \quad , \tag{4.1}$$

where w_B is the third element of $\mathbf{u}_B$.

Operator matrices Θ and Θ^* depend on z. Splitting them into two parts, equations (3.1) and (3.3) become

$$\mathbf{p} = [\Theta_1 + \Theta_2(z)]\,\mathbf{n} \quad , \tag{4.2}$$

$$\mathbf{e} = [\Theta_1^* + \Theta_2^*(z)]\,\mathbf{u} \quad , \tag{4.3}$$

where

$$\Theta_1 = \begin{bmatrix} -\frac{\partial}{\partial x} & 0 & -\frac{\partial}{\partial y} & 0 & 0 & 0 \\ 0 & -\frac{\partial}{\partial y} & -\frac{\partial}{\partial x} & 0 & 0 & 0 \\ 0 & 0 & 0 & -\frac{\partial^2}{\partial x^2} & -\frac{\partial^2}{\partial y^2} & -\frac{2\partial^2}{\partial x \partial y} \end{bmatrix}, \tag{4.4a}$$

$$\Theta_2(z) = \begin{bmatrix} 0 & 0 & 0 & 0 & 0 & 0 \\ 0 & 0 & 0 & 0 & 0 & 0 \\ -\frac{\partial^2 z}{\partial x^2} & -\frac{\partial^2 z}{\partial y^2} & -\frac{2\partial^2 z}{\partial x \partial y} & 0 & 0 & 0 \end{bmatrix}, \tag{4.4b}$$

$$\Theta_1^* = \begin{bmatrix} \frac{\partial}{\partial x} & 0 & 0 \\ 0 & \frac{\partial}{\partial y} & 0 \\ \frac{\partial}{\partial y} & \frac{\partial}{\partial x} & 0 \\ 0 & 0 & -\frac{\partial^2}{\partial x^2} \\ 0 & 0 & -\frac{\partial^2}{\partial y^2} \\ 0 & 0 & -\frac{2\partial^2}{\partial x \partial y} \end{bmatrix}, \quad \Theta_2^*(z) = \begin{bmatrix} 0 & 0 & -\frac{\partial^2 z}{\partial x^2} \\ 0 & 0 & -\frac{\partial^2 z}{\partial y^2} \\ 0 & 0 & -\frac{2\partial^2 z}{\partial x \partial y} \\ 0 & 0 & 0 \\ 0 & 0 & 0 \\ 0 & 0 & 0 \end{bmatrix}. \qquad (4.5a,b)$$

The internal forces in the shell are

$$\mathbf{n} = \mathbf{n}_0 + \mathbf{n}_B \quad , \qquad (4.6)$$

where $\mathbf{n}_B$ can be expressed by $\mathbf{u}_B$, using equations (2.4) and (4.3) :

$$\mathbf{n}_B = \mathbf{M} [\Theta_1^* + \Theta_2^*(z_0 + w_B)] \mathbf{u}_B \, . \qquad (4.7)$$

In the equilibrium equation we do not take into consideration the change of the external loads during buckling. Introducing (4.1) and (4.6) into (4.2), and making use of the linearity of operator Θ_2, we obtain

$$\begin{aligned} \mathbf{p} &= [\Theta_1 + \Theta_2(z_0 + w_B)] (\mathbf{n}_0 + \mathbf{n}_B) = \\ &= [\Theta_1 + \Theta_2(z_0)] \mathbf{n}_0 + \Theta_2(w_B) \mathbf{n}_0 + \\ &\quad + [\Theta_1 + \Theta_2(z_0 + w_B)] \mathbf{M} [\Theta_1^* + \Theta_2^*(z_0 + w_B)] \mathbf{u}_B . \end{aligned} \qquad (4.8)$$

The shell is in equilibrium before buckling, hence

$$\mathbf{p} = [\Theta_1 + \Theta_2(z_0)] \mathbf{n}_0 \, .$$

Omitting these terms from Eq. (4.8) we obtain :

$$\begin{aligned} &\Theta_2(w_B) \mathbf{n}_0 + [\Theta_1 + \Theta_2(z_0)] \mathbf{M} [\Theta_1^* + \Theta_2^*(z_0)] \mathbf{u}_B \\ &\quad + \Theta_2(w_B) \mathbf{M} [\Theta_1^* + \Theta_2^*(z_0)] \mathbf{u}_B + [\Theta_1 + \Theta_2(z_0)] \mathbf{M} \Theta_2^*(w_B) \mathbf{u}_B + \\ &\quad + \Theta_2(w_B) \mathbf{M} \Theta_2^*(w_B) \mathbf{u}_B = 0 \, . \end{aligned} \qquad (4.9)$$

This is a Donnell-type equation for the equilibrium of aeolotropic shells.

The last three terms in this equation contain the second and third power terms of the displacements, which are negligible in the analysis of the bifurcation load. The first term in Eq. (4.9) can be written in the following form

$$\Theta_2(w_B)\,\mathbf{n}_0 = \Theta_3\,\mathbf{u}_B \quad , \tag{4.10}$$

where

$$\Theta_3 = \begin{bmatrix} 0 & 0 & 0 \\ 0 & 0 & 0 \\ 0 & 0 & \left(-n_{x0}\frac{\partial^2}{\partial x^2} - n_{y0}\frac{\partial^2}{\partial y^2} - n_{xy0}\frac{2\partial^2}{\partial x \partial y}\right) \end{bmatrix} , \tag{4.11}$$

and n_{x0}, n_{y0} and n_{xy0} are the elements of $\mathbf{n}_0$.

Now we can obtain a homogeneous linear differential equation system from (4.9), on the basis of which the buckling load can be calculated :

$$\left[[\Theta_1 + \Theta_2(z_0)]\,\mathbf{M}\,[\Theta_1^* + \Theta_2^*(z_0)] + \Theta_3 \right] \mathbf{u}_B = 0 \, . \tag{4.12}$$

5. Determination of bifurcation load for aeolotropic shallow shells

We have determined the equation system (4.12) of buckling. This is a differential equation system of the eight order with variable coefficients. As a rule we can solve this equation only numerically as is usual in the literature e.g. [1, 4, 12, 17, 22].

The coefficients of the differential equation system become constant if the membrane forces are constant and if the function of the middle surface is of the second order, i.e.

$$z_0 = ax^2 + by^2 + cxy \tag{5.1}$$

Let us introduce the following notations :

$$\frac{1}{R_x} = -\frac{\partial^2 z_0}{\partial x^2} \quad , \quad \frac{1}{R_y} = -\frac{\partial^2 z_0}{\partial y^2} \quad , \quad \frac{1}{R_{xy}} = -\frac{2\partial^2 z_0}{\partial x \partial y} \, . \tag{5.2a-c}$$

Introducing them into (4.12) we obtain

$$\left\{\begin{bmatrix} -\frac{\partial}{\partial x} & 0 & -\frac{\partial}{\partial y} & 0 & 0 & 0 \\ 0 & -\frac{\partial}{\partial y} & -\frac{\partial}{\partial x} & 0 & 0 & 0 \\ \frac{1}{R_x} & \frac{1}{R_y} & \frac{1}{R_{xy}} & -\frac{\partial^2}{\partial x^2} & -\frac{\partial^2}{\partial y^2} & -\frac{2\partial^2}{\partial x \partial y} \end{bmatrix} \mathbf{M} \begin{bmatrix} \frac{\partial}{\partial x} & 0 & \frac{1}{R_x} \\ 0 & \frac{\partial}{\partial y} & \frac{1}{R_y} \\ \frac{\partial}{\partial y} & \frac{\partial}{\partial x} & \frac{1}{R_{xy}} \\ 0 & 0 & -\frac{\partial^2}{\partial x^2} \\ 0 & 0 & -\frac{\partial^2}{\partial y^2} \\ 0 & 0 & -\frac{2\partial^2}{\partial x \partial y} \end{bmatrix} + \right.$$

$$\left. + \begin{bmatrix} 0 & 0 & 0 \\ 0 & 0 & 0 \\ 0 & 0 & \left(-n_{x0}\frac{\partial^2}{\partial x^2} - n_{y0}\frac{\partial^2}{\partial y^2} - n_{xy0}\frac{2\partial^2}{\partial x \partial y}\right) \end{bmatrix} \right\} \mathbf{u}_B = 0 \,. \qquad (5.3)$$

We assume the displacement functions in the following form in the skew co-ordinate system ξ, η (Fig.2):

$$u_B = u_1 \cos\frac{\pi}{l_\xi}\xi \sin\frac{\pi}{l_\eta}\eta - u_2 \sin\frac{\pi}{l_\xi}\xi \cos\frac{\pi}{l_\eta}\eta \,,$$

$$v_B = v_1 \sin\frac{\pi}{l_\xi}\xi \cos\frac{\pi}{l_\eta}\eta - v_2 \cos\frac{\pi}{l_\xi}\xi \sin\frac{\pi}{l_\eta}\eta \,,$$

$$w_B = w_1 \sin\frac{\pi}{l_\xi}\xi \sin\frac{\pi}{l_\eta}\eta + w_2 \cos\frac{\pi}{l_\xi}\xi \cos\frac{\pi}{l_\eta}\eta \,,$$

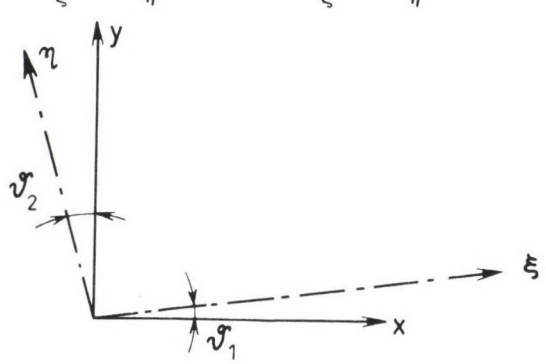

Fig. 2. The co-ordinate system

where l_ξ and l_η are the half wavelengths of buckling in the ξ and η directions respectively. These functions can be written with our cartesian co-ordinates, x and y as follows:

$$u_B = u_1 \cos\alpha(x+c_1y)\ \sin\beta(y+c_2x) - u_2 \sin\alpha(x+c_1y)\ \cos\beta(y+c_2x), \qquad (5.4a)$$

$$v_B = v_1 \sin\alpha(x+c_1y)\ \cos\beta(y+c_2x) - v_2 \cos\alpha(x+c_1y)\ \sin\beta(y+c_2x), \qquad (5.4b)$$

$$w_B = w_1 \sin\alpha(x+c_1y)\ \sin\beta(y+c_2x) + w_2 \cos\alpha(x+c_1y)\ \cos\beta(y+c_2x), \qquad (5.4c)$$

where α, β, c_1 and c_2 are constants which can be calculated from l_ξ, l_η, ϑ_1 and ϑ_2.

These functions can be used for the investigation of local buckling of shallow shells, nevertheless, they satisfy the boundary conditions in several cases as well.

Let us introduce functions (5.4a-c) into (5.3). These satisfy the differential equation system only if the coefficients of each trigonometrical function vanish. Hence, we obtain from (5.3) six linear equations, which can be written in the following hypermatrix form :

$$\left\{ \begin{bmatrix} \mathbf{A} & \mathbf{C} \\ \mathbf{C} & \mathbf{A} \end{bmatrix} \begin{bmatrix} \mathbf{M}_o & \mathbf{M}_n \\ \mathbf{M}_n & \mathbf{M}_o \end{bmatrix} \begin{bmatrix} \mathbf{A}^T & \mathbf{C}^T \\ \mathbf{C}^T & \mathbf{A}^T \end{bmatrix} - \begin{bmatrix} \lambda_1\mathbf{B} & \lambda_2\mathbf{B} \\ \lambda_2\mathbf{B} & \lambda_1\mathbf{B} \end{bmatrix} \right\} \mathbf{U} = \mathbf{0} \qquad (5.5)$$

where

$$\mathbf{A} = \begin{bmatrix} -\alpha & 0 & \beta & 0 & 0 & 0 \\ 0 & -\beta & \alpha & 0 & 0 & 0 \\ \dfrac{1}{R_x} & \dfrac{1}{R_y} & 0 & \alpha^2+\beta^2c_2^2 & \beta^2+\alpha^2c_1^2 & -2\alpha\beta(1+c_1c_2) \end{bmatrix}, \qquad (5.6a)$$

$$\mathbf{C} = \begin{bmatrix} \beta c_2 & 0 & -\alpha c_1 & 0 & 0 & 0 \\ 0 & \alpha c_1 & -\beta c_2 & 0 & 0 & 0 \\ 0 & 0 & \dfrac{1}{R_{xy}} & -2\alpha\beta c_2 & -2\alpha\beta c_1 & c_1\alpha^2+c_2\beta^2 \end{bmatrix}, \qquad (5.6b)$$

$$\mathbf{B} = \begin{bmatrix} 0 & 0 & 0 \\ 0 & 0 & 0 \\ 0 & 0 & 1 \end{bmatrix} . \qquad (5.7)$$

$\mathbf{A}^T$ and $\mathbf{C}^T$ are the transposes of $\mathbf{A}$ and $\mathbf{C}$. The set-up of $\mathbf{M}_o$ is identical with (2.5) and that of $\mathbf{M}_n$ is the following :

$$\mathbf{M}_n = \begin{bmatrix} & & T_{13} & & & C_{13} \\ & & T_{23} & & & C_{23} \\ T_{13} & T_{23} & & C_{31} & C_{32} & \\ & & C_{31} & & & B_{13} \\ & & C_{32} & & & B_{23} \\ C_{13} & C_{23} & & B_{13} & B_{23} & \end{bmatrix} , \tag{5.8}$$

provided that the stiffness matrix is

$$\mathbf{M} = \mathbf{M}_o + \mathbf{M}_n \quad . \tag{5.9}$$

Further

$$\lambda_1 = -n_{x0}(\alpha^2+\beta^2 c_2^{\,2}) - n_{xy0}2(\alpha^2 c_1+\beta^2 c_2) - n_{y0}(\beta^2+\alpha^2 c_1^{\,2}) \tag{5.10a}$$

$$\lambda_2 = 2\alpha\beta\left[n_{x0}c_2 + n_{xy0}(1+c_1c_2) + n_{y0}c_1\right] \tag{5.10b}$$

and

$$\mathbf{U} = \begin{bmatrix} u_1 \\ v_1 \\ w_1 \\ u_2 \\ v_2 \\ w_2 \end{bmatrix} \quad .$$

We can obtain the buckling (bifurcation) load from the condition of singularity of the coefficient matrix in Eq. (5.5) :

$$\det \left\{ \begin{bmatrix} \mathbf{A} & \mathbf{C} \\ \mathbf{C} & \mathbf{A} \end{bmatrix} \begin{bmatrix} \mathbf{M}_o & \mathbf{M}_n \\ \mathbf{M}_n & \mathbf{M}_o \end{bmatrix} \begin{bmatrix} \mathbf{A}^T & \mathbf{C}^T \\ \mathbf{C}^T & \mathbf{A}^T \end{bmatrix} - \begin{bmatrix} \lambda_1\mathbf{B} & \lambda_2\mathbf{B} \\ \lambda_2\mathbf{B} & \lambda_1\mathbf{B} \end{bmatrix} \right\} = 0 \ . \tag{5.11}$$

The buckling load calculated from (5.11) depends on four parameters : α, β, c_1 and c_2. For the determination of buckling load we have to minimize it with respect to these four parameters.

6. Special cases of anisotropy

6.1. Orthotropic shells

The investigation of orthotropic shells becomes relative simple if the surface is translational, the membrane shear force is zero and the principal axes of orthotropy are x and y. In this case

$$\mathbf{M}_n = \mathbf{0} \quad , \tag{6.1a}$$

$$\frac{1}{R_{xy}} = 0 \quad , \qquad n_{xyo} = 0 \quad . \tag{6.1b,c}$$

Assuming

$$c_1 = c_2 = 0 \quad , \tag{6.1d,e}$$

condition (5.11) becomes

$$\det \left[\mathbf{A}\, \mathbf{M}_o \mathbf{A}^T - \lambda_1 \mathbf{B} \right] = 0 \quad . \tag{6.2}$$

From this expression we obtain:

$$\lambda_1 = \frac{\det \begin{bmatrix} D_{11} & D_{12} & D_{13} \\ D_{12} & D_{22} & D_{23} \\ D_{13} & D_{23} & D_{33} \end{bmatrix}}{\det \begin{bmatrix} D_{11} & D_{12} \\ D_{12} & D_{22} \end{bmatrix}} \quad , \tag{6.3}$$

where

$$D_{11} = T_{11}\alpha^2 + T_{33}\beta^2 \tag{6.4a}$$

$$D_{12} = T_{12}\alpha\beta + T_{33}\alpha\beta \tag{6.4b}$$

$$D_{13} = -T_{12}\frac{\alpha}{R_y} - C_{11}\alpha^3 - C_{12}\alpha\beta^2 - 2C_{33}\alpha\beta^2 - T_{11}\frac{\alpha}{R_x} \tag{6.4c}$$

$$D_{22} = T_{22}\beta^2 + T_{33}\alpha^2 \tag{6.4d}$$

$$D_{23} = -T_{12}\frac{\beta}{R_x} - C_{22}\beta^3 - C_{21}\beta\alpha^2 - 2C_{33}\beta\alpha^2 - T_{22}\frac{\beta}{R_y} \tag{6.4e}$$

$$D_{33} = B_{11}\alpha^4 + B_{22}\beta^4 + 2(B_{12} + 2B_{33})\alpha^2\beta^2 +$$

$$+ \frac{1}{R_y}\left[T_{22}\frac{1}{R_y} + 2C_{22}\beta^2 + (C_{12}+C_{21})\alpha^2 + T_{12}\frac{1}{R_x}\right] +$$

$$+ \frac{1}{R_x}\left[T_{11}\frac{1}{R_x} + 2C_{11}\alpha^2 + (C_{12}+C_{21})\beta^2 + T_{12}\frac{1}{R_y}\right] \qquad (6.4f)$$

(We can apply these formulas for an axially compressed cylindrical shell (Fig.3) introducing $n_y=0$ and $1/R_x=0$ into the expressions. In so doing, these results become identical with those of Jones [19, 20].)

We can derive a simple closed formula if in (2.5)

$$C_{ij} = 0 \quad , \quad i,j = 1,2,3 \ .$$

After a lengthy but straightforward algebraic procedure we obtain from (6.3):

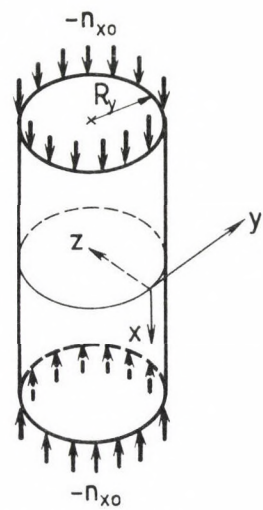

Fig. 3. Cylinder

$$\lambda_1 = \frac{\left(\frac{\alpha^2}{R_y} + \frac{\beta^2}{R_x}\right)^2\left(1 - \frac{T_{12}^2}{T_{11}T_{22}}\right)}{\frac{\alpha^4}{T_{22}} + \alpha^2\beta^2\left(\frac{1}{T_{33}} - \frac{T_{12}\left(T_{12}+2T_{33}\right)}{T_{11}T_{22}T_{33}}\right) + \frac{\beta^4}{T_{11}}} +$$

$$+ \alpha^4 B_{11} + \alpha^2\beta^2(4B_{33}+2B_{12}) + \beta^4 B_{22} \qquad (6.5)$$

In the special case, if the stiffness matrix has non-zero elements only in the main diagonal (2.6), this result becomes more simple. Introducing

$$T_{11} = T_x \ , \quad T_{22} = T_y \ , \quad T_{12} = 0 \ , \quad T_{33} = T_{xy}/2 \ ,$$

$$B_{11} = B_x \ , \quad B_{22} = B_y \ , \quad B_{12} = 0 \ , \quad B_{33} = B_{xy}/2$$

into (6.5) we obtain :

$$\lambda_1 = \frac{\left[\frac{\alpha^2}{R_y} + \frac{\beta^2}{R_x}\right]^2}{\frac{\alpha^4}{T_y} + \alpha^2\beta^2 \frac{2}{T_{xy}} + \frac{\beta^4}{T_x}} + \alpha^4 B_x + 2\alpha^2\beta^2 B_{xy} + \beta^4 B_y , \qquad (6.6)$$

which is identical with the result of Dulácska [10. Eq.(7.7)].

Let us consider an orthotropic hyperbolic paraboloidal shell assuming that the principal axes of orthotropy are parallel with the generatrices. If we use simplifications in our Eq. (5.11) which can be found in [2], we obtain the result of Dulácska exactly [2, Eq. (18)].

6.2 Isotropic shells

Our results are obviously valid for isotropic shells as well. Assuming (6.1a-e) we can use formula (6.3), provided that

$$T_{11} = T_{22} = T , \quad T_{12} = \nu T , \quad T_{33} = T(1-\nu)/2 ,$$
$$B_{11} = B_{22} = B , \quad B_{12} = \nu B , \quad B_{33} = B(1-\nu)/2 .$$

Introducing them into (6.3) we obtain, after arranging ,

$$\lambda_1 = -n_{x0}\alpha^2 - n_{y0}\beta^2 = T(1-\nu^2) \frac{\left[\frac{\alpha^2}{R_y} + \frac{\beta^2}{R_x}\right]^2}{\left(\alpha^2+\beta^2\right)^2} + B\left(\alpha^2+\beta^2\right)^2 . \qquad (6.7)$$

This expression becomes identical with formula (9.3) of Dulácska [3] in the case of $\nu=0$.

On the basis of (6.7) we can derive easily formulas for some cases which are well known in the literature.

Let us consider as an example an *axially compressed cylinder* shown in Fig.3. Here $n_y=0$ and $1/R_x=0$, consequently we obtain from (6.7)

$$-n_{x0} = \frac{T(1-\nu^2)}{\pi^2 R_y^2} \frac{\frac{1}{l_x^2}}{\left[\frac{1}{l_x^2} + \frac{1}{l_x^2}\right]^2} + B\pi^2 \frac{\left[\frac{1}{l_x^2} + \frac{1}{l_x^2}\right]^2}{\frac{1}{l_x^2}} . \qquad (6.8)$$

Let us minimize $-n_{x0}$ with respect to the expression

$$\frac{\frac{1}{l_x^2}}{\left(\frac{1}{l_x^2} + \frac{1}{l_x^2}\right)^2}$$

After arranging we obtain

$$-n_{x0} = \frac{2}{R_y}\sqrt{B\,T(1-\nu^2)} = \frac{Et^2}{R_y}\,\frac{1}{\sqrt{3\;\;B\,T(1-\nu^2)}}\,. \qquad (6.9)$$

Eqs. (6.8) and (6.9) are identical with the expressions (2.8) and (2.11) of [10].

The buckling load of spherical and hyperbolic paraboloidal shells can be similarly determined from (6.7).

6.3 Laminated (composite) plates

We can apply our results for aeolotropic plates as well. Let us consider as an example an antisymmetric cross-ply laminate consists of an even number of orthotropic laminae laid on each other with principal material directions alternating at 0° and 90° to the laminate axes as in the simple example of Fig.4. The replacement stiffness matrix of the plate has a special form [9. Eq.4.51 and 4.52]:

$$\mathbf{M} = \begin{bmatrix} T_{11} & T_{12} & & C_{11} & & \\ T_{12} & T_{22} & & & -C_{11} & \\ & & T_{33} & & & \\ C_{11} & & & B_{11} & B_{12} & \\ & -C_{11} & & B_{12} & B_{22} & \\ & & & & & B_{33} \end{bmatrix} \,. \qquad (6.10)$$

Consider a rectangular plate that is simply supported along edges $x=0$, $x=a$, $y=0$, $y=b$ and subjected to uniform in plane forces $-n_{x0}$ and $-n_{y0}$. In this case the differential equation of the buckling and the boundary conditions can be satisfied with the functions (5.4a-c) provided that

$$c_1 = c_2 = 0\,, \quad u_2 = v_2 = w_2 = 0\,,$$

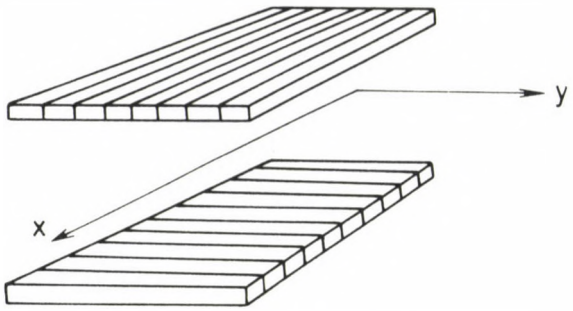

Fig. 4. Exploded (unbonded)
view of a two-layered regular antisymmetric cross-ply laminate

$$\alpha = \frac{\pi}{l_x} = \frac{\pi m}{a} \quad , \qquad m = 1,\ 2,\ \ldots\ ,$$

$$\beta = \frac{\pi}{l_y} = \frac{\pi n}{b} \quad , \qquad n = 1,\ 2,\ \ldots\ .$$

From Eq, (6.3) the following equation can be derived (provided that $1/R_x = 1/R_y = 0$) :

$$-n_{x0}\alpha^2 - n_{y0}\beta^2 = \alpha^4 B_{11} + \alpha^2\beta^2 (4B_{33}+2B_{12}) + \beta^4 B_{22} +$$

$$+ C_{11}^2 \frac{\alpha^6\left[\beta^2 T_{22}+\alpha^2 T_{33}\right]+2\alpha^4\beta^4\left[T_{12}+T_{33}\right]+\beta^6\left[\alpha^2 T_{11}+\beta^2 T_{33}\right]}{\alpha^2\beta^2\left[T_{12}^2+2T_{12}T_{33}-T_{11}T_{22}\right] - T_{33}\left[\alpha^4 T_{11}+\beta^4 T_{22}\right]}. \qquad (6.11)$$

These expression becomes identical with formula (5.81) of [9], if $n_{y0}=0$, $T_{11}=T_{22}$ and $B_{11}= B_{22}$. The last term in (6.11) shows the effect of coupling stiffness.

7. Possibilities of further applications

The main result of our paper is that we can take into consideration the coupling stiffnesses, i.e. the elements of the stiffness matrix out of the diagonal blocks (the C_{ij} elements in (2.5)). The effect of these elements can be significant naturally in the case of *laminated* shells, but in the case of some other engineering structures as well, e.g. in the

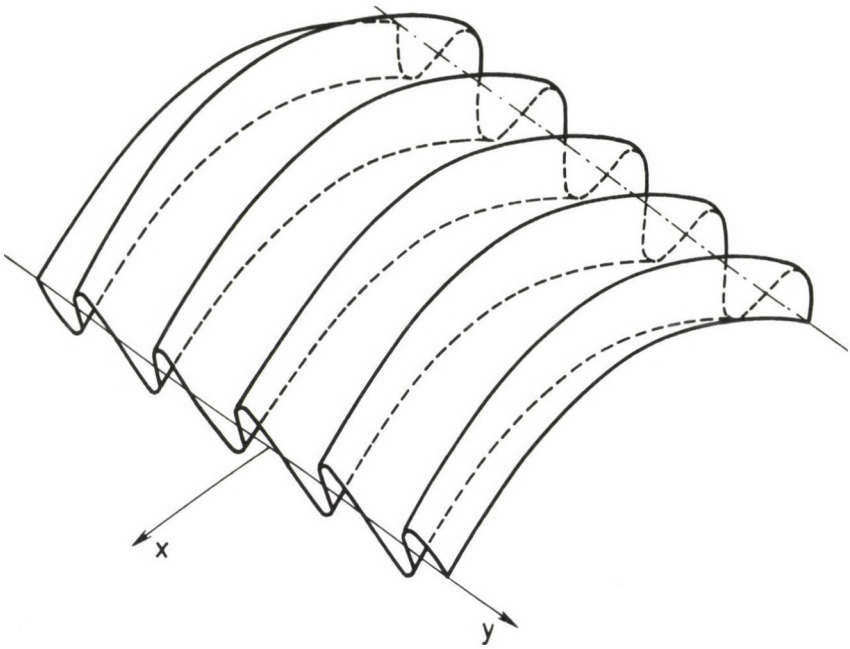

Fig. 5. Corrugated shell

investigation of *eccentrically stiffened shells*, when ε_x (or ε_y) causes n_x and m_x (or n_y and m_y) [7]; or that of *corrugated* (Fig.5) and *folded shells*, when ε_y causes not only n_y but m_x as well.

References

1. Banavalkar, P. V. and Gergely, P. : Analysis of Thin-Steel Hyperbolic Paraboloid Shells. Proc. ASCE **98.** (1972), Structural Division, 2605-2621.

2. Dulácska, E. : Stability of anisotropic hyperbolic paraboloidal shells. Acta Techn. Hung. **59.** (1967), 123-130.

3. Dulácska, E. : Vibration and stability of anisotropic shallow shells. Acta Techn. Hung. **65.**, (1969), 225-260.

4. Fischer, M. : Das Beulproblem der flachen, orthotropen, hyperbolischen Paraboloidschale. Der Stahlbau. **43.** (1974), 52-61.

5. Flügge, W.: Stresses in Shells . 2nd edition. Springer, Berlin etc. 1973.

6. Gergely, P. : Buckling of Orthotropic Paraboloid Shells. Proc. ASCE **98.** (1972), Structural Division, 395-398.

7. Giencke, E. : Die Grundgleichungen für die orthotrope Platten mit excentrishen Steifen. Stahlbau. **24.**, (1955), 128-129.

8. Kollár, L and Hegedűs, I. : Analysis and Design of Space Frames by the Continuum Method. Elsevier Science Publishers, Amsterdam. 1985.

9. Jones, R. M. : Mechanics of Composite Materials. McGrow-Hill, NewYork etc., 1975.

10. Kollár, L. and Dulácska, E. : Buckling of Shells for Engineers. J. Whiley & Sons, Chichester etc. and Akadémiai Kiadó, Budapest, 1984.

11. Ralston, A. : On the Problem of Buckling of Hyperbolic Paraboloidal Shell Loaded by Its Own Weight. Journ. Math. Phys. **35.** (1956), 53-59.

12. Reissner, E.: On some Aspects of the Theory of Thin Elastic Shells. Journal Boston Soc. of Civ. Eng. **42.** (1955), 100-133.

13. Vinson, J. R. and Sierakowski, R. L. : The behaviour of structures composed of composite materials. Martinus Nijhoff Publishers, Dordrecht etc., 1986.

14. Abu-Farsakh, G. A. F. R. and Lusher, J. K. : Buckling of Glass-Reinforced Plastic Cylindrical Shells Under Combined Axial Compression and External Pressure. AIAA Journal, **23.** (1985), 1946-1951.

15. Simitses, G. J., Shaw, D. and Sheinman, I. : Stability of Imperfect Laminated Cylinders : A Comparison Between Theory and Experiment. AIAA Journal, **23.** (1985), 1086-1092.

16. Simitses, G. J. and Shaw, D. : Imperfection Sensitivity of Laminated Cylindrical Shells in Torsion and Axial Compression. Composite Structures. **4.** (1985), 335-360.

17. Bauchau, O. A., Krafchack, T. M. and Hayes, J. F. : Torsional Buckling Analysis af Graphite/Epoxy Shafts. Journal of Composite Materials. **22.** (1988), 258-270.

18. Hirano, Y. : Buckling of Angle-Ply Laminated Circular Cylindrical Shells. Journal of Applied Mechanics. **46.** (1979),233-234.

19. Jones, R. M. : Buckling of Circular Cylindrical Shells with Multiple Orthotropic Layers and Eccentric Stiffeners. AIAA Journal, **6.** (1968), 2301-2305.

20. Jones, R. M. and Morgan, H. S. :Buckling and Vibration of Cross-Ply Laminated Circular Cylindrical Shells. AIAA Journal, **13.** (1975), 664-671

21. Tasi, J. : Effect of Heterogenity on the Stability of Composite Cylindrical Shells under Axial Compression. AIAA Journal, **4.** (1966), 1058-1061.

22. Whitney J. M. : Buckling of Anisotropic Laminated Cylindrical Plates. AIAA Journal, **11.** (1984), 1641-1645

Acta Technica Acad. Sci. Hung., 103(2-3), pp. 191-202 (1990)

DETERMINATION OF THE ERECTION SHAPE FOR A SINGLE-MAST ROTATIONALLY SYMMETRICAL CABLE NET IN CASE OF A SPECIFIC VARIATION OF THE TENSILE FORCE

KOLLÁR, P.W.*

(Received: 3 February 1989)

In this paper, the erection shape of structures, consisting of rotationally symmetrical, meridional and annular cables, is determined for values specified either for the meridional or for the annular cable tension. It is also demonstrated between what limits the given structures can be constructed with constant meridional or annular cable tension. Further on, a simple variation in the annular specific forces is described, the use of which enables to construct a tent with an arbitrary boundary point. Finally, the possibility is pointed out that the calculation of compressed membrane shells is also rendered possible with the use of this method.

Introduction

When designing suspended prestressed cable nets, the problem arises whether a structure with a prescribed variation of the cable force could be designed. The fulfilment of this condition can be advantageous from the aspect of both design and erection. This condition can be specified only for either the meridional or for the annular cables of the tent. If the variation in the tensile force is prescribed for the cables in one direction, then the forces arising in the cables in the other direction can no longer be specified. A prescribed variation of the tensile force can require different tent-shapes depending on the loads acting upon the different tents. In the following, only the erection shape of the tent will be dealt with, on which only the prestressing forces act.

*Kollár, Péter W., H-1026 Budapest, Sodrás u. 17, Hungary

Akadémiai Kiadó, Budapest

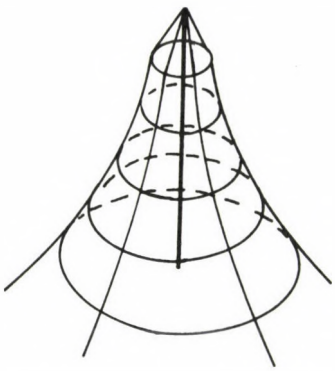

Fig. 1.

Basic assumptions

Let the structure in Fig. 1 consisting of rotationally symmetrical, meridional and annular cables be examined first. The cables are assumed to be ideally elastic, but no pressure is permitted to arise within them. The behaviour of the structure is described by the membrane theory, and as a load, only the prestressing force $P = 2 \cdot \pi \cdot C$ acts. According to our notations in Fig. 2, if the specific meridional force is denoted by N_m, and that in the annular direction by N_a, then, on the basis of /1/, the following equations are obtained:

$$(r \cdot N_a) - r_1 \cdot N_m \cdot \cos\varphi = -p_m \cdot r \cdot r_1$$

$$N_a(r_2 + N_m)r_1 = p_r \qquad (2)$$

where p_r = surface load in normal direction, and

p_m = surface load in meridional direction.

With N_m expressed from equation (2) and introduced into (1), after rearranging, the following relationship is obtained:

$$N_m = \frac{1}{r_2 \cdot \sin^2\varphi}\left[\int r_1 \cdot r_2(p_r \cdot \cos\varphi - p_m \cdot \sin\varphi)\sin\varphi \, d\varphi + C\right] \qquad (3)$$

Since, according to our basic assumption, $p_r = 0$ and $p_m = 0$, therefore

$$N_m = \frac{C}{r_2 \cdot \sin^2\varphi} = \frac{C}{r \cdot \sin\varphi}, \qquad (4)$$

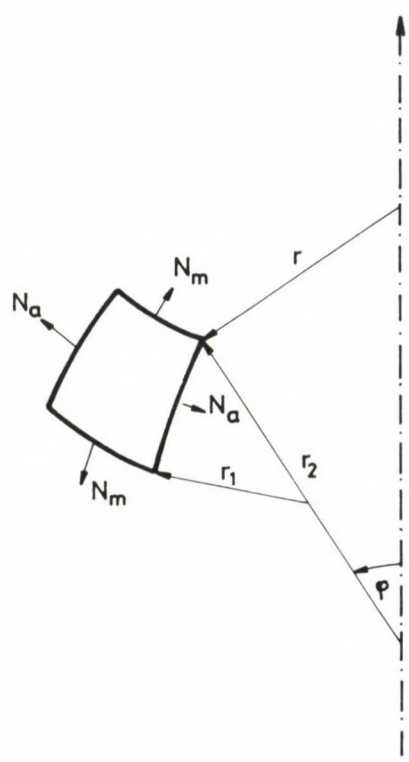

Fig. 2.

and on the basis of (4) and (2)

$$N_a = - N_m \frac{r_2}{r_1} \tag{5}$$

Mathematical solutions

a) First, the cables of meridional direction are examined. If constant forces are supposed to act along these cables, then the following equation can be written on the basis of (4):

$$C = N_m \cdot 2 \cdot \pi \cdot r = \frac{2 \cdot \pi \cdot P \cdot r}{2 \cdot \pi \cdot r \cdot \sin\varphi} = \frac{P}{\sin\varphi} \quad .$$

This expression shows that the given condition can be satisfied only by forces the slope of which is identical in each point, i.e., $\sin\varphi = \frac{P}{C}$. Consequently, this rotationally symmetrical surface will be a normal cone with a vertex angle of $\alpha = 90^{\circ} - \varphi$.

b) As a second case, the condition is examined when the specific annular forces are constant, $N_a = C_a$. With the introduction of (4) into (5), and after simplifying, the following relation is arrived at:

$$C_a = N_a = - \frac{P}{2 \cdot \pi \cdot r_1 \cdot \sin^2 \varphi}$$

Hence:

$$r_1 \cdot \sin^2 \varphi = - \frac{P}{2 \cdot \pi \cdot C_a} = - \frac{1}{K_1} \qquad (6a)$$

According to the relationships obtained above

$$r_1 = (1 + z'^2)^{3/2} / z'' \quad ; \quad \sin^2 \varphi = z'^2 / (1 + z'^2) \quad .$$

Introducing these into (6a), and rearranging, the following differential equation is obtained:

$$z'' / \left[z'^2 \cdot \sqrt{(1 + z'^2)} \right] = -K_1 \qquad (6b)$$

With the substitutions: $z' = u$ and $z'' = u'$, we obtain:

$$u' / \left[u^2 \cdot \sqrt{(1 + u^2)} \right] = -K_1 \quad .$$

Since $u' = du/dx$, after separating the variables, the equation can be integrated as follows:

$$\int \frac{1}{u^2 \cdot \sqrt{1 + u^2}} \, du = - \int K_1 \, dx \quad .$$

After performing the integration, the following equation is arrived at:

$$- \sqrt{(1 + u^2)} / u = - (K_1 \cdot r + C_1) \quad .$$

Hence, after solving the equation for u, the following relationship is obtained:

$$u = \frac{1}{\left[(K_1 \cdot r + C_1)^2 - 1 \right]^{1/2}} \quad .$$

Since u = dz/dr, therefore, after separating the variables again and performing the integration of the equation, the following solution for z will be obtained:

$$z = \pm \frac{1}{K} \ell n \left[K_1 \cdot r + C_1 + \sqrt{(K_1 \cdot r + C_1)^2 - 1} \right] + C_2 \qquad (7a)$$

The domain of definition of the function is not the full domain of r, but it is limited by two conditions:

1) it is required that $\sqrt{(K_1 \cdot r + C_1)^2 - 1}$ should be real, i.e.: $(K_1 \cdot r + C_1)^2 - 1 \geq 0$, which yields the condition: $|K_1 \cdot r + C_1| \geq 1$.

2) it is required that the inequality: $K_1 \cdot r + C_1 + \sqrt{(K_1 \cdot r + C_1)^2 - 1} > 0$ holds.

From the diagram of this function, plotted in Fig. 3, it can be seen that, with the condition: $K_1 \cdot r + C_1 \geq 1$ fulfilled, criteria 1 and 2 are satisfied simultaneously.

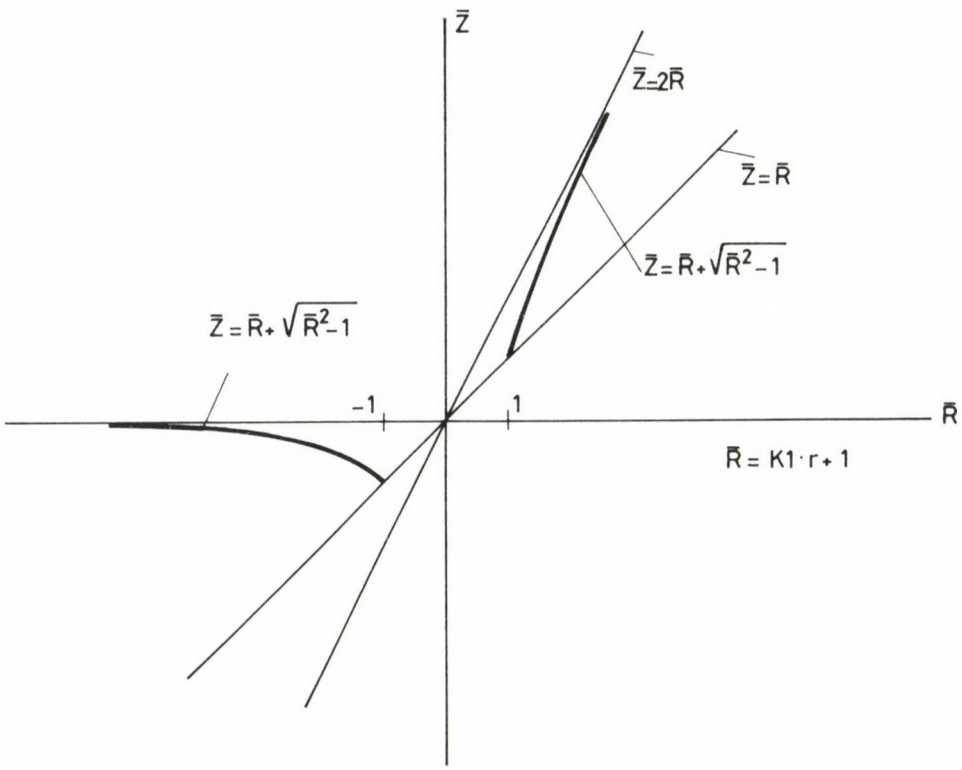

Fig. 3.

The question emerges whether, in this limited domain of values, there exists any solution in the case of point pairs R_1; Z_1 and R_2; Z_2, defining an arbitrary boundary condition, if $K = K_1 = \text{constant}$ is given. Introducing the given boundary conditions into (7a), the following equation system of two unknowns is obtained:

$$Z_1 = \pm \frac{1}{K} \ln \left[K R_1 + C_1 + \sqrt{(K R_1 + C_1)^2 - 1} \right] + C_2 \qquad \text{(I)}$$

$$Z_2 = \pm \frac{1}{K} \ln \left[K R_2 + C_1 + \sqrt{(K R_2 + C_1)^2 - 1} \right] + C_2 \qquad \text{(II)}$$

Substracting (II) from (I) yields following:

$$Z_1 - Z_2 = \pm \frac{1}{K} \left[\ln (K R_1 + C_1 + \sqrt{(K R_1 + C_1)^2 - 1} - \right.$$
$$\left. - \ln (K R_2 + C_1 + \sqrt{(K R_2 + C_1)^2 - 1} \right] ,$$

and, hence,

$$e^{\pm K(Z_1 - Z_2)} = \frac{K R_1 + C_1 + \sqrt{(K R_1 + C_1)^2 - 1}}{K R_2 + C_1 + \sqrt{(K R_2 + C_1)^2 - 1}} \qquad \text{(7b)}$$

The left-hand side of equation (7b) is a concrete number depending on the fixed data, while its right-hand side is a function of C_1. However, it can be seen that this function cannot take an arbitrary value, because the constant C_1 has only a limited domain of definition due to conditions 1 and 2 mentioned above. The two limit points, as degenerated cases, are dealt with in detail in connection with a numerical example.

c) In the third case to be examined, the specific annular force varies according to the function $K_2 = K_1 (1 + z'^2)$. This variation of the tensile force, as it will be seen later, results in a solution which - contrary to the examined case b) - permits to construct a tent-shape fitting two arbitrary boundary points.

Starting from (6a), the differential equation can be written in the following form:

$$z'' \left(\frac{1}{z'^2} + 1 \right) = - K_1 \qquad \text{(8a)}$$

This differential equation can be solved in a way analogous to that used in the solution of Eq. (6b). The solution is given by the function:

$$Z = \pm \frac{(K_1 r + C_1)^2}{4K_1} \pm \frac{1}{4K_1} \left[(K_1 r + C_1) \sqrt{(K_1 r + C_1)^2 + 4} + \right.$$
$$\left. + 4 \operatorname{en} (K_1 r + C_1 + \sqrt{(K_1 r + C_1)^2 + 4}) \right] + C_2 \qquad (8b,c)$$

where (8b) is the solution belonging to the positive sign, while (8c) is the solution belonging to the negative sign. As it can be seen, the domain of definition of the function is subject to no limitation, since condition $(K_1 r + C_1)^2 + 4 \geq 0$ is always satisfied, and, at the same time, it is true that

$$\sqrt{(K_1 r + C_1)^2 + 4} > | K_1 r + C_1 | \ .$$

It is advisable to find the solution in a numerical way, due to the difficult treatability of the function.

Numerical examples

1) Determine the equation of the tent whose top boundary ring of a diameter 2 m is situated 12 m high, while its bottom ring of a dimater 22 m is 2 m high above the ground level (see Fig. 4). The specific annular forces should vary according to the following law:

$$C = \frac{P}{2\pi} (1 + z'^2)^{3/2} \text{ (case c)} \ .$$

The boundary conditions are:

$$R_1 = 1 \quad \text{and} \quad Z_1 = 12$$

$$R_2 = 11 \quad \text{and} \quad Z_2 = 2$$

$$K_1 = -1 \ .$$

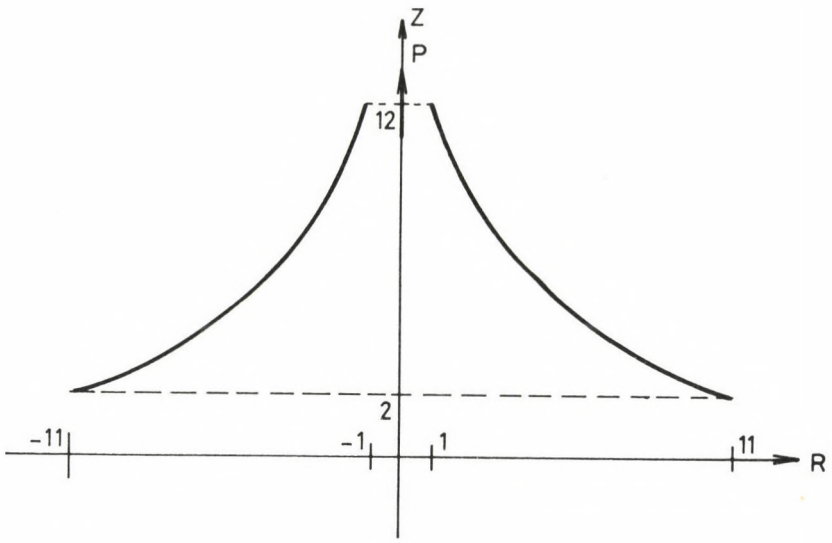

Fig. 4.

Consequently, the differential equation takes the form of (8a):

$$z''\left(\frac{1}{z'^2} + 1\right) = 1$$

Its solution is yielded by equations (8b) or (8c), respectively. The integration constants C_1 and C_2 are determined from a non-linear equation system with the aid of a computer. Eq. (8c) has no solution for the given points, while two constants can be calculated from (8b):

$$C_1 = 4.4164123$$

$$C_2 = 3.7027119$$

The shape of the tent is shown in Fig. 5.

2) The boundary conditions of numerical example No. 1 were assumed arbitrarily in the positive domain. We could have also assumed the number pairs.

$$R_1 = -1 \quad Z_1 = 12$$

$$R_2 = -11 \quad Z_2 = 2 \quad ,$$

which are situated symmetrically the previous point pairs with respect to axis z.

This boundary condition is satisfied by equation (8c), and, of course, the tent-shape obtained is identical with the mirror-image of the shape shown in Fig. 5 with respect to axis z.

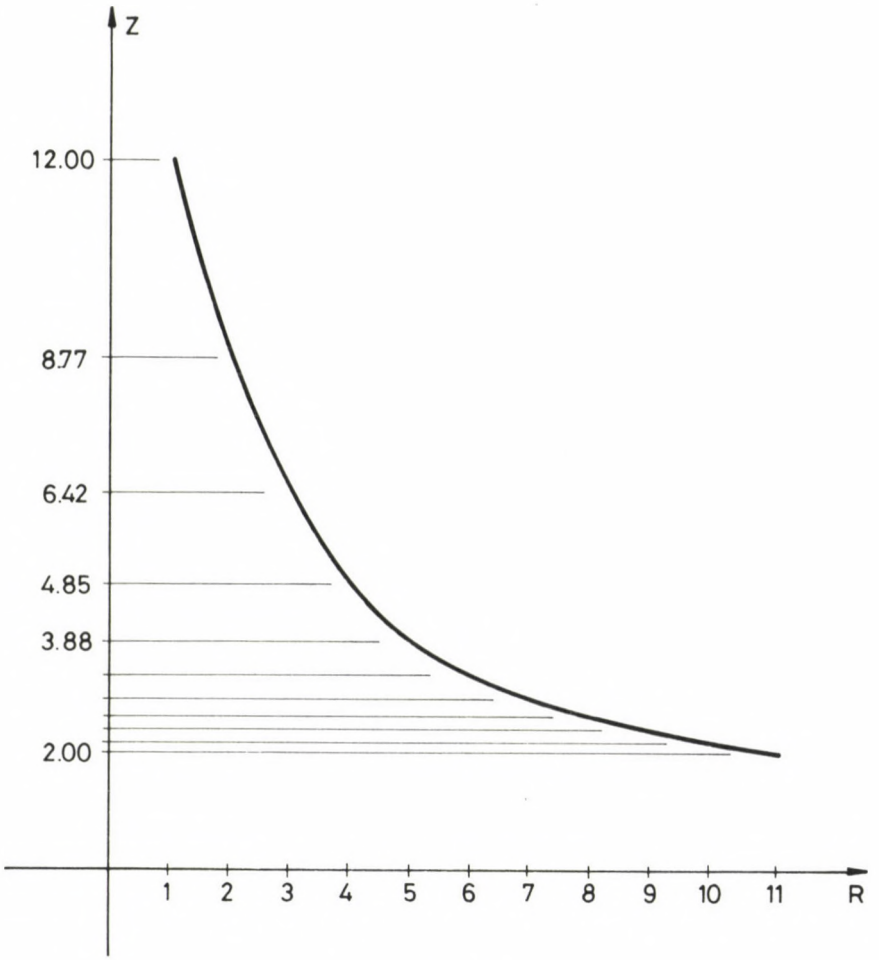

Fig. 5.

3) Let us reduce the annular forces of the given tent. Let it be $K^{*} = K.\alpha$, where $\alpha < 1$. The solutions for the tent-shape satisfying this condition are represented in Fig. 6.

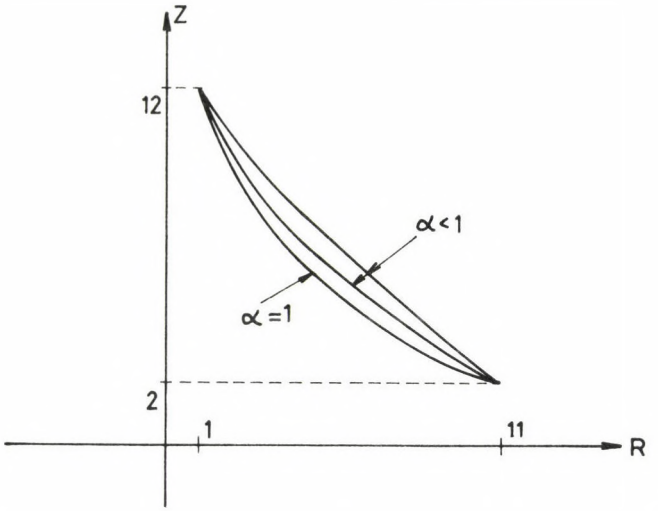

Fig. 6.

What result is yielded if $\alpha = 0$? If constant $K_1 = 0$ is substituted into (8a), the following relation is obtained:

$$z''\left(\frac{1}{z'^2} + 1\right) = 0 \quad .$$

A product is equal to zero only if at least one of its factors is zero, i.e.:

a., $\frac{1}{z'^2} + 1 = 0$; $\qquad z'^2 = -1$.

This equation has no real solution.

b., $z'' = 0$; $z' = C_1$; $z = C_1 r + C_2$.

Consequently, the solution will be given by a straight line passing through the two boundary points.

The correctness of this solution can be easily checked even by visual inspection, since there occurs no annular force if the meridional curve has no curvature, but this can be encountered only with a straight line. But, at the same time, this includes that the meridional cable tension will be constant only if the annular force is zero. Naturally, this yields a cone. This is in accordance with the result of our assumption examined first.

4) In the basic assumptions we allowed only structures in tension, according to the users' aspects. However, from the theoretical aspect, the examination of structures in compression is not limited at all either. Since, in the basic relations, neither the tension nor the compression of the structures was made use of anywhere, therefore the shape of the structure will depend only on the sign of the constant meridional or annular forces, respectively. Due to this, e.g. even the variation of the specific annular compressive force can be specified in a membrane shell, and, depending on the specified variation, the solutions yielded and examined in cases 2 and 3, respectively, can also be obtained. Naturally, the structures in compression show a curvature "in the opposite direction" as compared to those in tension, i.e. the former ones will have a concave shape from underneath.

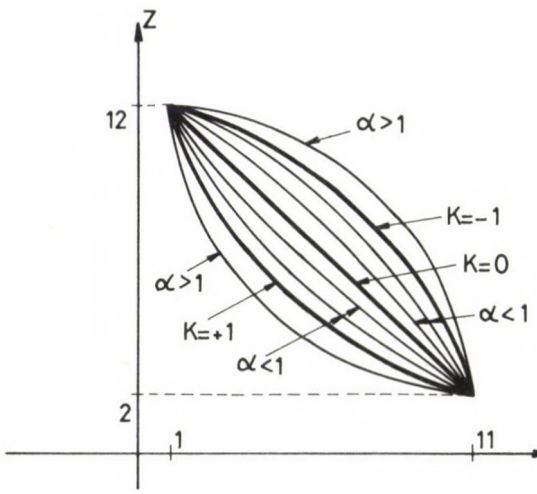

Fig. 7.

In Fig. 7, the shapes belonging to both the structures in tension and in compression are shown.

5) What can be the "height" of the structures constructed if, in the above example, a constant value of the specific annular prestressing force is specified, and the radii of the top and bottom rings of the tent, and condition K = constant = 1 are prescribed? Introducing the given values into (7b), we obtain the following:

$$e^{\mp(Z_1-Z_2)} = \frac{1 + C_1 + \sqrt{(1 + C_1)^2 - 1}}{11 + C_1 + \sqrt{(11 + C_1)^2 - 1}} \quad .$$

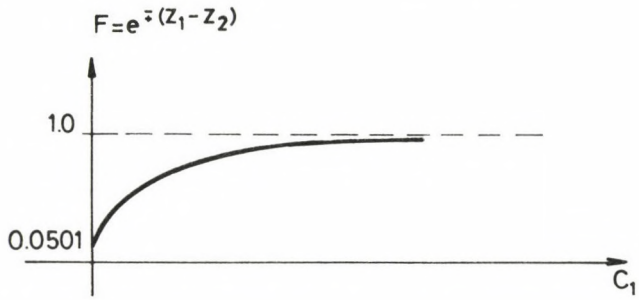

Fig. 8.

The function on the right-hand side is plotted in Fig. 8. It can be seen that the function takes its maximum or minimum values, respectively, in points $C_1/1/ = 0$ and $C_1/2/ = \infty$. Hence, tent-heights Z_1 and Z_2 can be calculated. If Z_2 is assumed to $Z_2 = 2$ encountered in the given example, then $Z_1 max = 5.088971$, and $Z_2 min = 2$ m are yielded. Consequently, the "height" points of our structure are marked by these two limits. In the first case, the slope of the tangent belonging to the curve increases infinitely, while in the second case the tangent remains horizontal all along. However, in both cases, the sepcific meridional force increases infinitely, and, consequently, these extreme points can be taken into consideration only as mathematical solutions.

However, those said above involve the fact that if the positions of the top and bottom boundary rings of the tent are fixed as initial conditions, then the value of the annular, constant prestressing force can be specified only within a determined range. Similarly to the case introduced in numerical example No. 4, structures in compression can be calculated also in the case of constant specific forces.

The character of the functions obtained as solutions is very close to that of the curves shown in Fig. 7.

REFERENCES

1. Flügge, W.: Statik und Dynamik der Schalen, Springer-Verlag, Berlin 1962

2. Csonka, P.: Theory and Practice of Membrane Shells, Akadémiai Kiadó, Budapest, and VDI-Verlag, Düsseldorf, 1987

3. Korn, G.A. - Korn, T.M.: Mathematical Handbook for scientists and Engineers, McGraw-Hill Book Company, 1968

Acta Technica Acad. Sci. Hung., 103(2-3), pp. 203-224 (1990)

NEW ASPECTS OF DRIP IRRIGATION HYDRAULICS

SHARAF, A.G.*

(Received: 14 July 1990)

The implementation of drip irrigation technology requires three stages: design, installation and management. The design and management stages are intensive in numerical calculation. The purpose of this paper is to assemble the last information available as a technical tool and reference source, dealing with frictional head losses in multiple-outlet irrigation lines, including the primary losses caused by pipe friction and minor losses caused by emitter barbs, pressure variation along the irrigation line, energy gradient along the lateral, emitter flow variation and uniformity of emitter flow. The paper does not address all aspects of drip irrigation hydraulics but includes a lot of common techniques and models used.

NOTATION

List of frequantly used symbols and units

Symbols	Explanation	Units
C	Hazen Willims roughness coefficient of pipe	-
D	Inside pipe dimater	mm
e	Number of emitters per emitter group	-
EU	Emission uniformity	%
EUa	Absolute emission uniformity	%
f	Pipe friction factor	-
fe	Emitter connection loss as an equivalent length	m
F	Reduction coefficient for friction loss in multiple outlet pipe	-
g	Acceleration of gravity	m/s^2
H	Pressure head at the emitter	m

*Sharaf, A. Gamal, GATE Vízgazd. és Meliorációs Tnsz., H-2103 Gödöllő, Nyisztor tér 1, Hungary

Akadémiai Kiadó, Budapest

Symbols	Explanation	Units
HFe	Emitter connection pressure loss	m
Hi	Pressure head at a given length ratio i	m
Hmax	Maximum pressure head in line	m
Hmin	Minimum pressure head in line	m
Ho	Pressure head at the head of the lateral line	m
Hvar	Pressure head variation	m
H'	Total energy	m
HF	Pressure head loss due to friction in lateral	m
HFi	Pressure head loss due to friction at a given length ratio i	m
HFx	Pressure loss due to friction from X to the closed end	m
HF'	Pressure head gain or loss by slopes	m
HF'i	Pressure head gain or loss by slopes at a given length ratio i	m
i	Length ratio (l/L)	-
J	Pressure head loss gradient of lateral	m/100
J'	Pressure head loss gradient of lateral with emitters	m/100
k	Constant of proportionality of emitter flow	-
ℓ	Given length measured from head end of the line	m
L	Total lateral line length	m
m	Flow rate exponent in friction equation	-
n	Number of emitters	-
q	Emitter flow rate	(l/h)
qavg	Average emitter flow	(l/h)
qi	Emitter flow rate at a given length ratio i	(l/h)
qmax	Maximum emitter flow rate	(l/h)
qmin	Minimum emitter flow rate	(l/h)
qvar	Variation of lateral line flow	%
q'var	Statistical definition of qvar	%
qx	Average of the highest 1/8 of emitter flow rates	(l/h)
q'	Mean emitter discharge	(l/h)
Q	Lateral flow rate	(l/h)
Re	Reynolds number	-
Ri	Friction energy drop ratio	-
R'i	Elevation energy gain or loss ratio	-
se	Emitter spacings on lateral line	m
Sj	Slope of the j section along the line	m
Sm	Standard deviation of emitter flow due to manufacturing	(l/h)
Sq	Standard deviation of emitter flow due to hydraulics	(l/h)

Symbols	Explanation	Units
Uc	Chritiansen's uniformity	%
Us	Statistical uniformity	%
v	Flow velocity	m/s
Vm	Coefficient of manufacturing variation	-
Vq	Coefficient of variation of emitter flow due to hydraulics	-
Vt	Total coefficient of variation of emitter flow along the lateral line	-
x	Emitter discharge exponent	-
X	Given length, measured from the closed end of the line	m
y	Irrigation depth	m
y'	Mean irrigation depth	mm
dy'	Mean deviation of irrigation depth	mm
z	Elevation	m

Introduction

Drip irrigation is a relatively new method that has developed mainly over the last decade. Water is applied by means of mains, manifolds and plastic laterals, usually laid on the ground surface. Equally spaced along the laterals are emitters, operating at low inlet pressure head (roughly 10 m) and small discharges (for example 2, 4 and 8 l/h). The water trickling onto the ground surface enters the soil profile and percolates downwards and outwards. The result is a limited cone shaped volume of moist soil surrounding the plant root zone.

Current trickle irrigation design practice has evolved from methods and relationships were developed for design of other types of irrigation systems. Similar principles apply in the design of both trickle and sprinkler irrigation. In both methods water is applied by means of a network of pipes and heads, placed at desired spacings and discharging given flow rates at selected pressure head. The differences lie in the length of the spacings, the sizes of the discharges and operating pressure heads, and the duration of water application and irrigation intervals.

Development of drip irrigation

Originally, drip irrigation was developed as a subsurface irrigation. The first such experiment began in Germany in 1869 where clay pipes were used in a combination of irrigation and drainage. The first reported work in the U.S.A. was made in Colorado in 1913 indicated that the concept was expensive to use. Subsequent to 1920 perforated pipe was used in Germany which made the concept feasible. Since then, various experiments have been started (Jensen, 1980).

Drip irrigation system components

The drip irrigation system consists of emitters, lateral lines, main lines, and the head of control station as shown in Fig. 1.

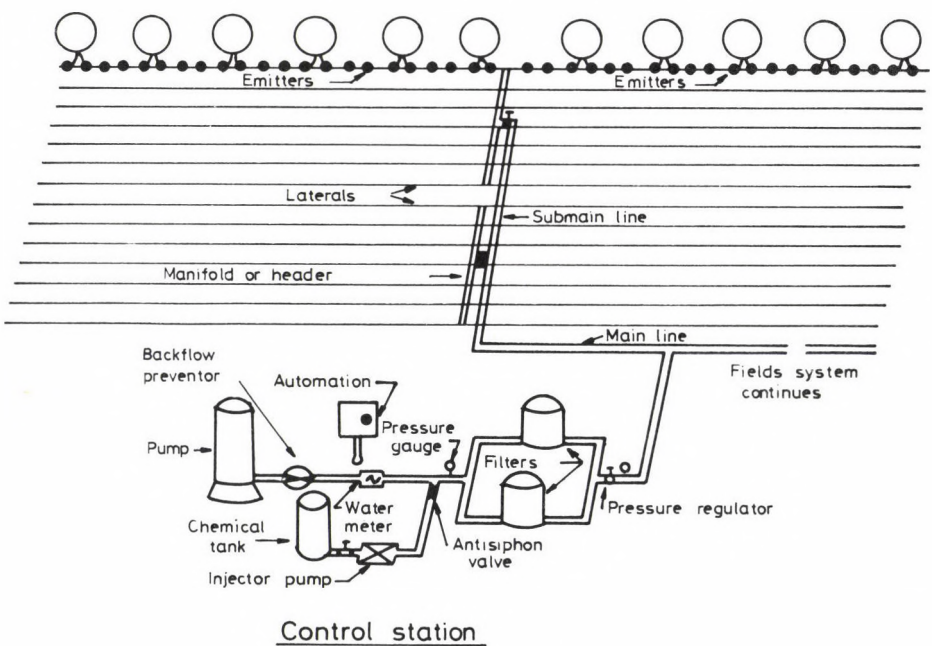

Fig. 1. Typical drip irrigation system

1 - Emitters: they are mechanical devices located at selected points along the water delivery lines to control the flow and decrease the water pressure head.

2 - Lateral lines: they are the hydraulic link between the supply lines and the emitters, have diameter of (9-19 mm) and usually made of plastic.
3 - Main lines: for carrying water to the lateral lines from the head.
4 - Control station: is located where the water is measured, filtered or screened, treated, and regulated as to pressure and timing of application.

Hydraulics of emitters

The hydraulics characteristics of emitters are directly related to the mode of fluid motion (flow regime) inside the emitter as characterized by the Reynolds number Re (Jensen, 1980). The flow regimes are usually characterized as (a) laminer $Re < 2000$; (b) instable $2000 < Re <= 4000$; (c) partially turbulent $4000 < Re <= 100.000$; (d) fully turbulent $100.000 < Re$. Keller and Karmeli, 1974 classified emitter characteristics by flow regime, pressure dissipation, lateral connection, water distribution, flow cross-section, cleaning characteristics, pressure compensation, and construction material.

In general, characteristics of most drip emitters can represented in the emitting flow regime by an exponential equation of the form.

$$q = k H^{x} \tag{1}$$

where q is the emitter discharge (l/h), k is proportionality factor that characterized the emitter dimension, x is emitter discharge exponent, and, H is the operating pressure head (m).

The coefficient k is the intercept on a log - log plot of q versus H and the coefficient x is the slope of the line. It is also possible to estimate x from the discharges from two different operating pressures as follow

$$x = \frac{\ln(q_1/q_2)}{\ln(H_1/H_2)} \tag{2}$$

where q_1 and q_2 are the emitter flows at pressure H_1 and H_2, respectively (Balogh and Gergely, 1985; Nakayama, 1986).

The magnitude of x characterizes the discharge versus pressure relationship. It is the measure of how sensitive the discharge is to pressure. The value of x will typically fall between 1.0 and 0.1 depending on the design of the emission device (Braud and Soon, 1979).

The orifice and nozzel type usually have fixed area (Benami and Ofen, 1984). The flow and hydraulic pressure relation is shown to be

$$q = k\, H^{0.5} \tag{3}$$

This means that the discharge varies with the square root of the pressure head. Pressure compensating emitters are designed so that the flow area changes with respect to pressure (Nakayama and Bucks, 1986). The flow area and the hydraulic pressure are related by

$$A = b\, H^{-y} \tag{4}$$

where A is the orifice area and b, y are constants in power function and combining equation (3) and (4) the resultant emitter flow function becomes

$$q = k\, H^{0.5-y} \tag{5}$$

this shows that x value in the power function can be less than 1.5. If y value is 0.5, the emission exponent will be zero and thus means that the emitter is fully pressure compensating to give a constant flow rate even the hydraulic pressure changes.

The long flow path type can be represented by the flow of a small microtube (Balogh, 1985). If the area of the flow path is fixed, the emitter flow function can be given as a simple power function

$$q = k\, H^{x} \tag{6}$$

in which x = 1 for laminar flow, x = 0.75 when the flow is considered as turbulent flow in smooth pipe, and x = 0.5 when the flow is considered full turbulent in a small tube (Nakayama, 1986).

Hydraulics of drip irrigation lines

Drip irrigation lines made of plastic are usually considered as smooth pipe. Both the Darcy - Weisbach equation for pipe flow and Hazen-Willims empirical equation can be used to determine friction loss along the lateral line and submain. Friction loss is usually evaluated using

Hazen-Willims equation with c value equal to 150, due to its simplicity (Meshkat, 1985)

$$HF = K(Q/C)^{1.852} D^{-4.87} L \quad (7)$$

in which HF is pipe friction head loss (m), L is pipe length (m), K is a constant 1.21E10, D is the inside pipe diameter (mm), C is the Hazen - Willims friction coefficient, and Q is the flow rate (l/s).

Many pipe manufacturers recommend a maximum velocity of 1.5 m/s in plastic pipe. At this velocity the value of C that compares best to the Blasius equation will depend on pipe diameter, with C = 130 for 14 to 15 mm pipe, C = 140 for 18 to 19 mm pipe, and C = 150 for 25 to 27 mm pipe (Jensen, 1980).

Hazen-Willims equation was originally developed for flow of water in water distribution network where Reynolds numbers were greater than 100.000. In trickle irrigation systems, particularly in small emitter tubes and lateral hoses, flow ranges from the laminar region up to Reynolds number of only 20,000 to 40,000 (Watters and Keller, 1978).

The Darcy-Weisbach equation along with the Moody diagram for determining the friction factor is the most universally applicable formula commonly used for computing friction head loss in trickle irrigation pipes

$$HF = f \left(\frac{L}{D}\right) \left(\frac{v^2}{2g}\right) \quad (8)$$

where f is the friction factor from the Moody diagram, v is the velocity in the pipe (m/s), and g is the acceleration of gravity.

The Moody diagram Fig. 2 permits finding f values when the Reynolds number of the flow and the pipe roughness are known. The friction factor f can also be found for the flow regime expected in trickle irrigation through use of the Reynolds number, Re from the following equations (Meshkat and Warner, 1985)

Hagen-Poiseuille	$f = 64/Re$	$Re < 2000$	(9)
Blasius	$f = 0.316/Re^{0.25}$	$2000 < Re < 10^5$	(10)
Nikuradse	$f = 0.13/Re^{0.172}$	$10^5 < Re < 10^7$	(11)

In general, the friction losses for pipe flow have a simple form

$$HF = k\, Q^m\, L \quad (12)$$

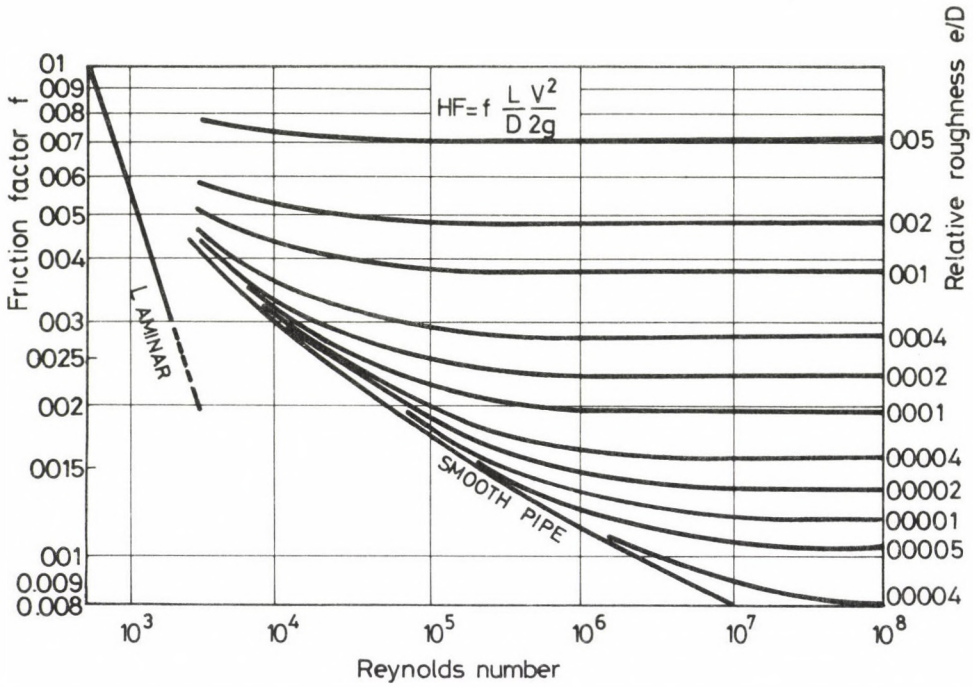

Fig. 2. Moody diagram with Darcy-Weisbach friction factor vs. Reynolds number

In case of using Darcy-Weisbach equation:

$K = 4 \cdot 10^3/D^4$ m = 1 $Re < 2000$

$K = 7.89 \cdot 10^5/D^{4.75}$ m = 1.75 $2000 < Re < 10^5$

$K = 9.47 \cdot 10^5/D^{4.825}$ m = 1.825 $10^5 < Re < 10^7$

In case of using Hazen-Willims equation with c coefficient 150:

$K = 1.135 \cdot 10^6/D^{4.871}$ m = 1.852 $Re > 10^5$

where HF is the pipe friction head (m), Q is the total flow rate (1/s), D is the inside pipe diameter (mm), and L is total pipe length (m).

Head losses in laterals and mainfolds with evenly spaced outlets each with uniform discharge must include a reduction coefficient F necessary to compensate the discharge along the line (Watters and Keller, 1978). F values for different numbers of outlets along the line are given in Table 1 or can be estimated by the following formula

$$F = (1/(m+1) + (1/2n) + ((m-1)^{0.5}/6n^2) \quad (13)$$

where m is the flow rate exponent and n is the number of emitters.

Table 1 Reduction coefficient F for multiple-outlet pipeline friction loss computations

No. of outlets	F-values	No. of outlets	F-values
1	1.00	9	0.42
2	0.65	10-11	0.41
3	0.55	12-15	0.40
4	0.50	16-20	0.39
5	0.47	21-30	0.37
6	0.45	31-70	0.37
7	0.44	70	0.36
8	0.43		

Emitters connection losses (minor losses) in laterals

The emitter connector barb projects into flow in lateral hose causes additional turbulence over the above normal pipe friction turbulence. The additional head loss must be computed and combined with the pipe friction head loss to represent the total head loss along the lateral. Karmeli and Keller, 1974 give two methods for calculating emitter friction loss, one being an equivalent increase of roughness (c value) in the pipe and the other being the determination of equivalent additional lateral length.

If the spacing of the emitters is se (m), then for purpose of computing head loss, the length of the lateral L (m) should be increased to Le, and can be expressed as

$$Le = \frac{se + fe}{se} L \quad (14)$$

where Le is the equivalent length of the lateral with emitters (m), fe is the emitter connection loss as an equivalent length of lateral (m).

Values of fe for different size emitter barbs and various pipe sizes can be obtained from Fig. 3 which is based on laboratory studies presented by Watters and Keller, 1978. The fe can also be estimated according to the following formulas, as given by De Paco, 1985.

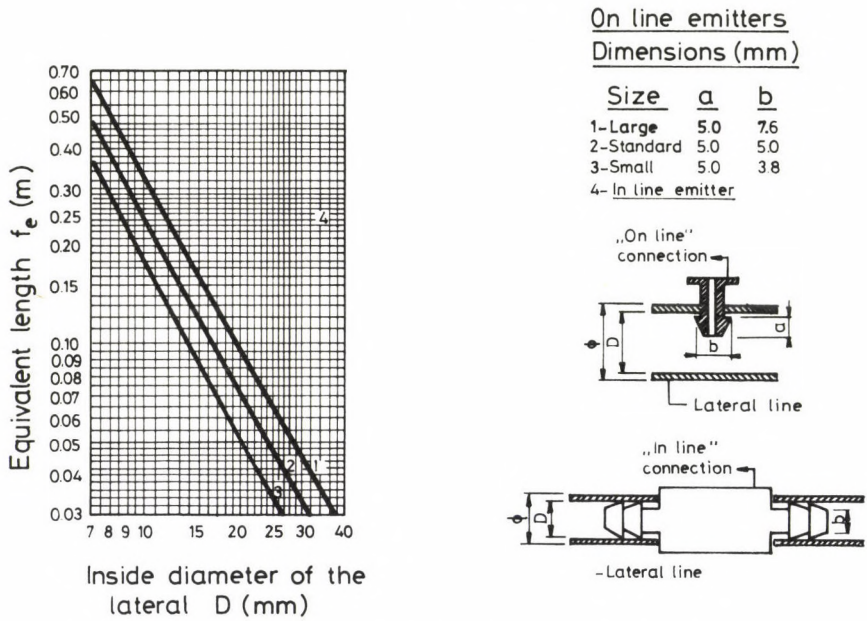

Fig. 3. Equivalent length of pipe

1- On-line large size connection

$$fe = 23.04/D^{1.84} \quad (15)$$

2- On-line standard size connection

$$fe = 18.91/D^{1.87} \quad (16)$$

3- On-line small size connection

$$fe = 14.38/D^{1.89} \quad (17)$$

4- In-line connection

$$fe = 0.23$$

where fe is the equivalent length (m); and D is the inside diameter (mm).

Terryan and Forilan, 1978 estimated the friction losses due to emitter connection across seven types of emitters by using Hazen-Willims equation with c value 140 and pipe internal diameter 14.7 mm.

The Hazen-Willims equation after reduction and rearrangement becomes

$$fe = 0.384\ HFe\ Q^{-1.852} \quad (18)$$

where HFe is the emitter connection pressure loss (m), and Q is the discharge (l/s).

The values of fe were plotted versus Q on log - log paper, after determining HFe. A power function was fit to the data for the emitter with the form

$$fe = Ce\ Q^{M} \tag{19}$$

where Ce and M are the intercept and slope, respectively. The results are represented in Fig. 4.

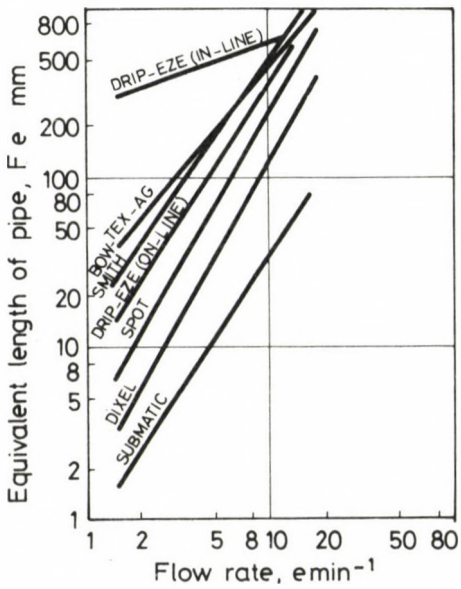

Fig. 4. Pressure losses across on-line emitters expressed as equivalent length of pipe

General friction curve for drip irrigation lines

The head loss along any multiple - outlet pipe line with uniform outlet spacing and discharge can be represented by a single line on a dimensionless plot of the relative haed loss and the position (Wu and Gitlin, 1974).

Watters and Keller, 1978 have shown that for the small diameter smooth pipes used in trickle laterals, the Darcy-Weisbach equation (18) combined with the Blasius equation (10) for F gives accurate predictions of friction head loss, as follow.

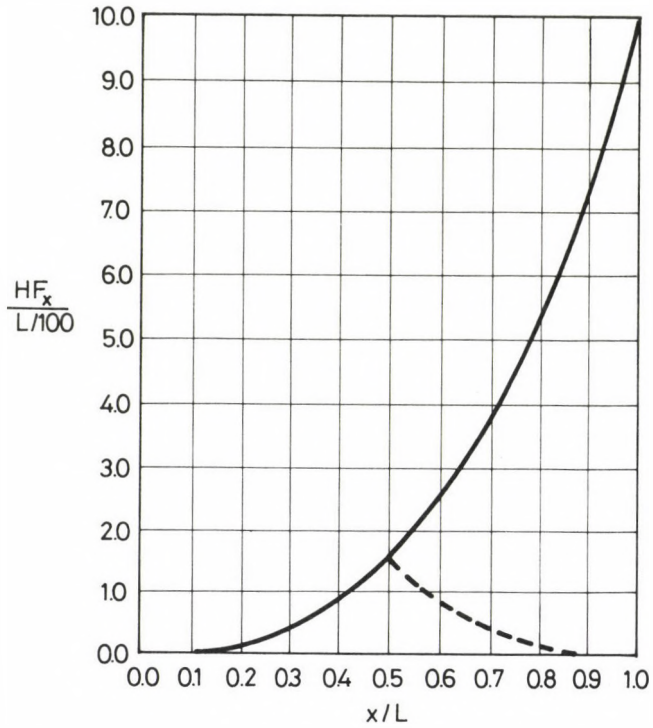

Fig. 5. General friction curve for a multi-outlet pipeline with uniform pipe size, spacing between outlets and flow per outlet

$$J = 100\ HF/L = K(Q^{1.75}/D^{4.75}) \tag{20}$$

Where J is the head loss gradient (m/100m), K is constant 7.89E7.

Using the equivalent length method to estimate the additional head loss due to emitter connections along the irrigation line

$$J' = J\,\frac{se + fe}{se} \tag{21}$$

where J' is the equivalent head loss gradient of lateral with emitters, se is the spacing between emitter connections (m), and fe is the equivalent length of emitter connection loss.

Then, head loss computation in laterals which have evenly spaced outlets with uniform discharge from each outlet can be estimated by

$$HF = J'FL/100 \tag{22}$$

combining equations 20, 21 and 22 yields

$$\frac{HFX}{L/100} = J'F\left(\frac{X}{L}\right)^{2.75} \qquad (23)$$

where X is the distance from the lateral closed end (m), HFX is the head loss from X to the closed end, and L is the total length of the lateral.

Equation (23) defines the general friction curve Fig. 5, which is useful for graphical solutions to such problems as: locating the optimum manifold positions on sloped fields; determining the emitter pressure profile along downhill laterals; and selecting optimum sets of pipe sizes for tapered manifolds on sloping fields (Keller and Radrigo, 1979).

The shape of the general friction curve can be plotted from an outlet by outlet analysis of a typical multiple outlet line.

Energy gradient line for drip irrigation lines

The total specific energy at any section of a trickle line can be expressed by the energy equation

$$H' = z + H + \frac{v^2}{2g} \qquad (24)$$

where H' is the total energy (m), z is the potential head (m), H is the pressure head (m), and $(v^2/2g)$ is the velocity head (m).

As the flow rate in the line decreases with respect to length, the energy gradient line will not be a straight line but exponential type curve. The shape of the energy gradient line for level irrigation lines Fig. 6 can be expressed by a dimensionless pressure gradient line, since velocity head changes are negligible, as derived by Wu and Gitlin, 1974

$$Ri = \ell_m\,(1-i)^{m+1} \qquad (25)$$

where Ri is energy drop ratio (HFi/HF), m is the exponent of the flow rate in the friction equation, HFi is the pressure drop (m) at a length ratio i ($i = \ell/L$), HF is the total energy drop at the end of the line, L is the total length and ℓ is a given length measured from the head end of the line.

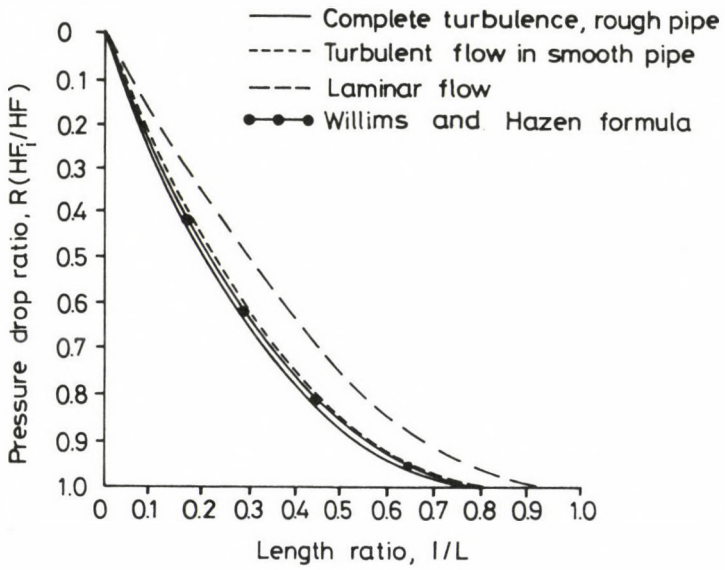

Fig. 6. Dimensionless curves showing the friction drop pattern caused by laminar flow in smooth pipe, and complete turbulent flow in the lateral line

The dimensionless energy gradient line will serve to determine the energy gradient curve (pressure gradient curve) when the total energy drop is known.

Pressure variation along a drip irrigation line

Jensen, 1980 indicated that the pressure distribution along a drip irrigation line is a linear combination of the line slope and energy slope.

With the knowledge of length and slope of a line, the pressure head gain or drop can be determined. The friction drop at any given length of line can be determined when a total pressure drop (HF) is known. The pressure distribution along a drip irrigation lateral if an initial pressure is given can be determined as shown in Figs 7, 8.

The pressure variation along a lateral can be expressed mathematically as follow

$$Hi = Ho - HFi \pm HF'i \qquad (26)$$

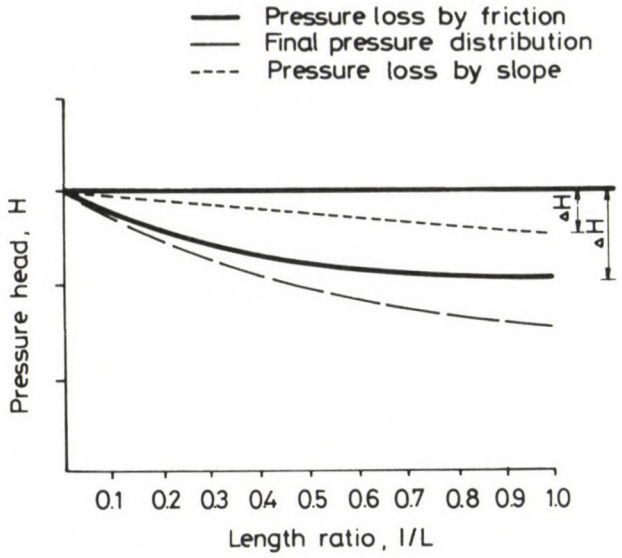

Fig. 7. The pressure distribution along a drip irrigation line (upslope)

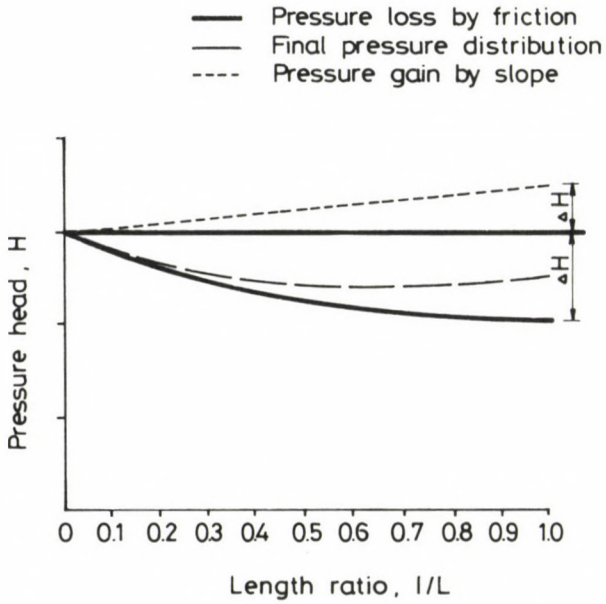

Fig. 8. The pressure distribution along a drip irrigation line (downslope)

where Hi is the pressure head at a given length ratio i, Ho is the input pressure, H'Fi is the pressure head gain or loss by slopes ("+" sign for downslope, "-" sign for upslope) at a given length ratio i, and HFi is the total friction drop at a given length ratio i.

Equation (26) can be expressed by using the pressure drop ratio Ri from the dimensionless pressure (energy) gradient line and pressure head gain or loss ratio by slopes, R'i (Wu and Gitlin, 1974)

$$Hi = Ho - Ri\ HF \pm R'i\ HF' \tag{27}$$

where Ri is pressure drop ratio by friction = HFi/HF, and R'i is the pressure drop (or gain) ratio by slopes = HF'i/HF'.

Equation (26) can be used for both uniform and non-uniform slopes, for uniform slopes, the R'i is the same as the length ratio i. The pressure along the drip irrigation line will then be given by

$$Hi = Ho - Ri\ HF \pm i\ HF' \tag{28}$$

In the case where the trickle irrigation line is laid on non-uniform slopes the pressure along the irrigation line can be expressed as

$$Hi = Ho - Ri\ HF + \left(\frac{L}{n}\right) \text{sum } Sj \tag{29}$$

where Sj is the slope of the j section along the line using "+" sign for downslope (energy gain) and "-" for upslope (energy loss).

Emitter flow variation and uniformity of emitter flow

The following is a brief review of some of the more commonly used measures for irrigation uniformity and emitter.

As shown in eq. (1) the emitter flow is determined by the hydrostatic pressure H at the emitter. This means whenever there is a pressure variation Hvar in the drip irrigation line there will be an emitter flow variation qvar.

Flow variation with suggested modifications for statistically based calculations summarized by Barlts and Wu, 1979 in Table 2.

Table 2 Uniformity and emitter flow variation equations

Common name	Original form	Statistical form	
Chirstiansen's Uniformity (Uc)	$Uc = 100\ (1-dy'/y')$	$Ucm = 100(1-.798Vq)$	(30)
Statistical Uniformity (Us)	$Us = 100\ (1-Vy)$	$Us = 100\ (1 - Vq)$	(31)
Emission Uniformity (EU)	$EU = 100\ (1 \frac{1.27}{e^{0.5}} Vm) \frac{qmin}{qavg}$	same	(32)
Emitter Flow Variation (qvar)	$qvar = 100\ (\frac{qmax - qmin}{qmax})$	$q'var = 100\ (1 - (\frac{1-2Vq}{1+2Vq}))$	(33)

where qmin, qavg, and qmax are the minimum, average, and maximum emitter flow, respectively, Vm is the coefficient of manufacturer's variation, Vq is the coefficient of variation of emitter flow, Vy is the coefficient of variation of irrigation depth, dy' is the mean deviation of irrigation depth and y' is mean irrigation depth, along the irrigation line. The relationship between pressure and emitter flow variation are related by the x value in equation (1) expressed by Keller and Karmeli, 1974 as follow

$$qvar = 1 - (1-Hvar)^{x} \tag{34}$$

and

$$Hvar = \frac{Hmax - Hmin}{Hmax} \tag{35}$$

The relationship between qvar and Hvar for different x values is plotted in Fig. 9.

The emitter flow at any point qi along the lateral can be estimated by substituting equation (26) into emitter flow equation (1) as indicated by Wu and Gitlin, 1975

$$qi = k\ (Ho - Ri\ Hf \pm R'i\ HF')^{x} \tag{36}$$

Removing k by dividing by the emitter flow at Ho yields

$$qi = qo\ (1- \frac{Ri\ HF}{Ho} \pm \frac{R'i\ HF'}{Ho})^{x} \tag{37}$$

where qi is the emitter flow at a given length ratio i, Ho is the operation (input) pressure, and qo is the emitter flow at input pressure Ho.

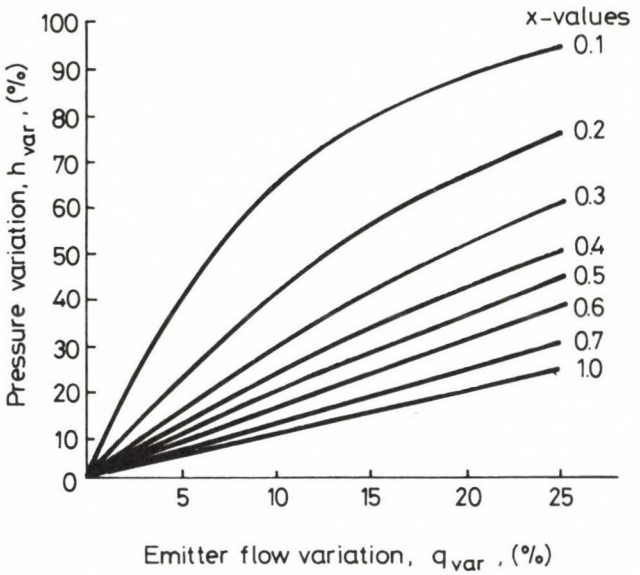

Fig. 9. The relationship between emitter flow variation and pressure variation for x values

Equation (37) used by Barlts and Wu, 1979 to develop the coefficient of variation of emitter flow due to hydraulics Vq as follow

$$Vq = \frac{Sq}{q'} \tag{38}$$

and

$$Sq = (\frac{1}{n} \text{ sum } (gi - q')^2)^{0.5} \tag{39}$$

where Sq is the standard deviation of emitter flow rate due to hydraulics (1/h), q' is the mean emitter discharge (1/h), and n is the number of emitters.

Since no two emitters devices can be identically manufactured, some variation will exist from emitter to emitter. Solomon, 1977 recommended adopting a measure of this variation called the coefficient of manufacturing variation Vm given by the following relationship

$$Vm = \frac{Sm}{q'} \tag{40}$$

where Sm is the standard deviation of the flow rate due to manufacturing (1/h).

Barlts et al., 1981 introduced the following equation to estimate the statistical uniformity Us for laterals or submains

$$Us = 100\ (1-Vt) \tag{41}$$

and

$$Vt^2 = (Vq^2 + Vm^2) \tag{42}$$

where Vt is the total coefficient of variation of emitter flow along the lateral or submain.

The advantage of the above equation over the other presently used uniformity measures is that additional factors such as emitter plugging, lateral line temperature and other variations can also be included in the final uniformity coefficient which is the quantitative evaluation of the emitter flow variation. The relationship between the amitter flow variation and uniformity coefficient is represented in Fig. 10.

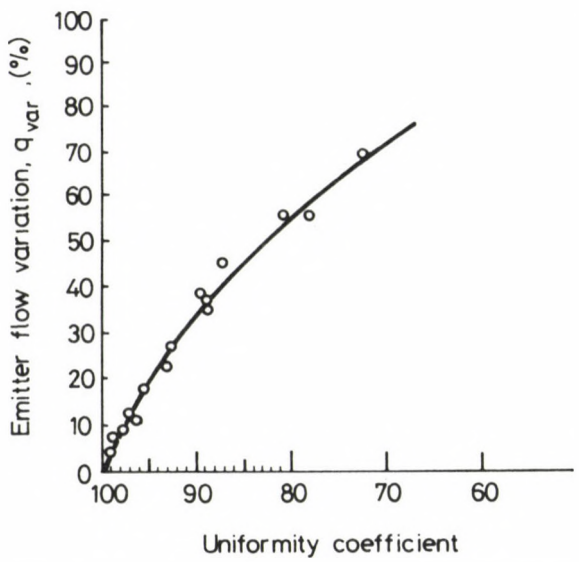

Fig. 10. Relationship between emitter flow variation and uniformity coefficient

Field uniformity estimation

Several methods are used for estimating field uniformity. A modified form of equation (32) is to consider the absolute emission uniformity EUa as follow

$$EUa = 100 \left(\frac{qmin}{qavg} + \frac{qavg}{qx}\right) \left(\frac{1}{2}\right) \quad (43)$$

where qx is the average of the highest 1/8 of emitter flow rates.

For this method at least 8 pressure and 32 discharge volume readings are recommended. The general criteria for EUa values are: 90% or greater, excellent; 80 to 90% good; 70 to 80% fair; and less than 70% poor (Barlts and Donald, 1985).

Another simple method for field evaluation of emitter emission uniformity based on estimating emitter flow variation (Wu and Gitlin, 1975). In this approach the evaluation consists in finding the maximum and minimum

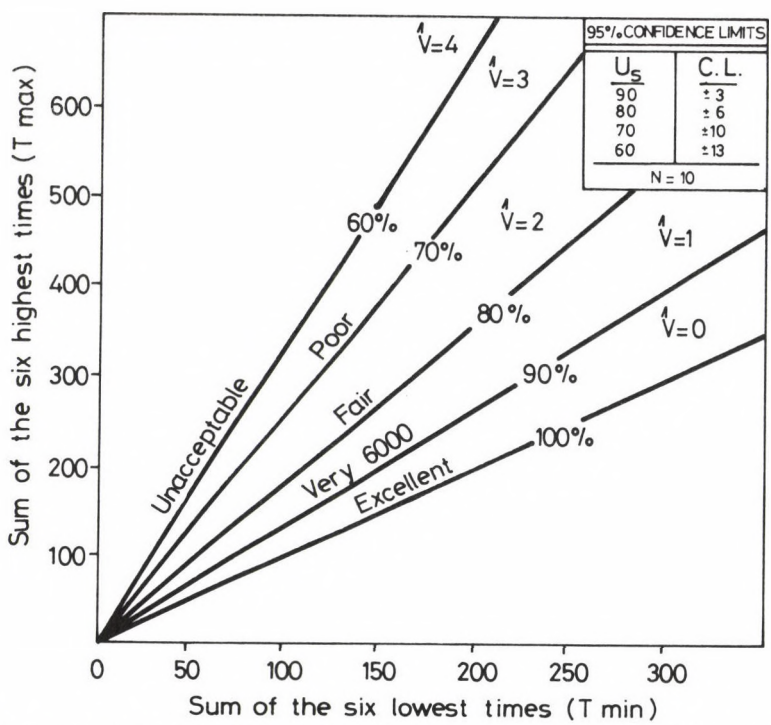

Fig. 11. Nomograph for estimating statistical uniformity based on emitter discharge rates

pressure in the submain unit and then calculating qvar (emitter flow variation) as given in equations (34) and (35). The general criteria for qvar values are 10% or less, desirable; 10 to 20%, acceptable; and greater than 20% not acceptable.

A third method for estimating system uniformity is based upon the statistical uniformity coefficient given by equation (31). This method assumes that the distribution of emitter flow is normal. It uses the highest one-sixth and lowerst one-sixth of the time needed to fill 18 containers from 18 emitters selected randomly in the submain unite (Bralts and Kenser, 1982) and by using Fig. 11 the statistical uniformity can be estimated.

Conclusions

In drip irrigation water is carried in pipe network to the points where it infiltrates into the soil. A primary objective of good drip irrigation system design and management is to provide sufficient system flow capacity to adequately irrigate all the plants. Uniformity of application depends on the uniformity of emitter discharge. Non uniformity of discharge is caused primarily by pressure differences due to friction loss and elevation, variation between emitters due to manufacturing tolerance, water temperature changes, and clogging.

Acknowledgment

The author wishes to thank Dr. László Vermes head of Department of Water management and Land Reclamation, Gödöllő University for his assitance and his continuous encouragement.

REFERENCES

1. Balogh, J. - Gergely, I.: Basic aspects of tricking irrigation, VIZDOK, Budapest, 1985
2. Barlts, F.V. - Wu, I.P.: Emitter flow variation and uniformity of drip irrigation, ASAE paper No. 79-2099, st. Joseph, Michigan 49085, 1979
3. Barlts, F.V. - Wu, I.P. - Gitlin, M.H.: Manufacturing variation and drip irrigation uniformity, Transactions of the ASAE, 24 (1) (1981), 113-119
4. Barlts, F.V. - Kenser, C.D.: Drip irrigation field uniformity estimation, ASAE paper No. 83-2590, st. Joseph, Michigan 49085, 1983

5. Barlts, F.V. - Donald, M.E.: Field evaluation of drip/trickle irrigation submain units. Drip/trickle irrigation in action, ASAE Proceedings of the third international drip/trickle irrigation congress, volume I (1985), 275-280

6. Benami, A. - Ofen, A.: Irrigation engineering, IESP, Haifa, Israel, 1984

7. Braud, H.J. - Soon, A.M.: Trickle irrigation design for improved application uniformity, ASAE paper No. 79-2571, St. Joseph, Michigan 49085, 1979

8. De Paco, J.L.: Lengths of sections in lateral of two diameters. Drip/trickle irrigation in action, ASAE Proceedings of the third international drip/trickle irrigation congress, volume I (1985), 410-415

9. Jensen, M.E.: Design and Operation of farm irrigation system, ASAE, St. Joseph, Michigan 49085, 1980

10. Keller, J. - Karmeli, D.: Trickle irrigation design parameters, Transactions of the ASAE, 17 (4) (1974), 678-684

11. Keller, J. - Radrigo, J.: Trickle irrigation lateral design, ASAE paper No. 79-2570, St. Joseph, Michigan 49085, 1979

12. Meshkat, M. - Warner, R.C.: A user friendly interactive trickle irrigation design model. Drip/trickle irrigation in action, ASAE Proceedings of the third international drip/trickle irrigation congress, volume I (1985), 439-451

13. Nakayama, F.S. - Duck, D.A.: Trickle irrigation for crop production, Elsevier, Amsterdam. 1986

14. Solomon, K.: Manufacturing variation of emitters in trickle irrigation system, ASAE paper No. 77-2009, st. Joseph, Michigan, 49085, 1977

15. Terry, A.H. - Forilan, A.B.: Pressure losses across trickle irrigation fittings and emitters, ASAE papr No. 78-2014, st. Joseph, Michigan 49085, 1978

16. Watters, G.S. - Keller, J.: Trickle irrigation tubing hydraulics, ASAE Technical paper No. 78-2015, St. Joseph, Michigan 49085, 1978

17. Wu, I.P. - Gitlin, H.M.: Drip irrigation design based on uniformity, Transactions of the ASAE 17 (3) (1974)

18. Wu, I.P. - Gitlin, H.M.: Energy gradient line for drip irrigation laterals, Journal of irrigation and drainage division, ASCE, 101 (IR4) (1975), 321-326

PRINTED IN HUNGARY

Akadémiai Kiadó és Nyomda Vállalat, Budapest

NOTICE TO CONTRIBUTORS

Papers in English* are accepted condition that they have not been previously published or accepted for publication.

Manuscripts in two copies (the original type-written copy plus a clear duplicate one) complete with figures, tables, and references should be sent to

Acta Technica
Nádor u. 7. I. 118
Budapest, Hungary
H-1051

Although every effort will be made to guard against loss, it is advised that authors retain copies of all material which they submit. The editorial board reserves the right to make editorial changes.

Manuscripts should be typed double-spaced on one side of good quality paper with proper margins and bear the title of the paper and the name(s) of the author(s). The full postal address(es) of the author(s) should be given in a footnote on the first page. An abstract of 50 to 100 words should precede the text of the paper. The approximate locations of the tables and figures should be indicated on the margin. An additional copy of the abstract is needed. Russian words and names should be transliterated into English.

References. Only papers closely related to the author's work should be referred to. The citations should include the name of the author and/or the reference number in brackets. A list of numbered references should follow the end of the manuscript.

References to periodicals should mention: (1) name(s) and initials of the author(s); (2) title of the paper; (3) name of the periodical; (4) volume; (5) year of publication in parentheses; (6) numbers of the first and last pages. Thus: 5. Winokur, A., Gluck, J.: Ultimate strength analysis of coupled shear walls. American Concrete Institute Journal 65 (1968) 1029-1035

References to books should include: (1) author(s)' name; (2) title; (3) publisher; (4) place and year of publication. Thus: Timoshenko, S., Gere, J.: Theory of Elastic Stability. McGraw-Hill Company, New York, London 1961.

Illustrations should be selected carefully and only up to the necessary quantity. Black-and-white photographs should be in the form of glossy prints. The author's name and the title of the paper together with the serial number of the figure should be written on the back of each print. Legends should be brief and attached on a separate sheet. Tables, each bearing a title, should be self-explanatory and numbered consecutively.

Authors will receive proofs which must be sent back by return mail.

Authors will receive 50 reprints free of charge.

*Hungarian authors can submit their papers also in Hungarian.

Periodicals of the Hungarian Academy of Sciences are obtainable at the following addresses:

AUSTRALIA
C.B.D. LIBRARY AND SUBSCRIPTION SERVICE
39 East Splanade
P.O. Box 1001, Manly N.S.W. 2095

AUSTRIA
GLOBUS, Höchstädtplatz 3, *1206 Wien XX*

BELGIUM
OFFICE INTERNATIONAL DES PERIODIQUES
Avenue Louise, 485, *1050 Bruxelles*
E. STORY-SCIENTIA P.V.B.A.
P. van Duyseplein 8, *9000 Gent*

BULGARIA
HEMUS, Bulvar Ruszki 6, *Sofia*

CANADA
PANNONIA BOOKS, P.O. Box 1017
Postal Station "B", *Toronto, Ont. M5T 2T8*

CHINA
CNPICOR, Periodical Department, P.O. Box 50
Peking

CZECH AND SLOVAK FEDERAL REPUBLIC
MAD'ARSKA KULTURA, Národni třida 22
115 66 Praha
PNS DOVOZ TISKU, Vinohradská 46, *Praha 2*
PNS DOVOZ TLAČE, *Bratislava 2*

DENMARK
EJNAR MUNKSGAARD, 35, Nørre Søgade
1370 Copenhagen K

FEDERAL REPUBLIC OF GERMANY
KUNST UND WISSEN ERICH BIEBER
Postfach 10 28 44
7000 Stuttgart 10

FINLAND
AKATEEMINEN KIRJAKAUPPA, P.O. Box 128
00101 Helsinki 10

FRANCE
DAWSON-FRANCE S.A., B.P. 40, *91121 Palaiseau*
OFFICE INTERNATIONAL DE DOCUMENTATION ET LIBRAIRIE, 48 rue Gay-Lussac
75240 Paris, Cedex 05

GREAT BRITAIN
BLACKWELL'S PERIODICALS DIVISION
Hythe Bridge Street, *Oxford OX1 2ET*
BUMPUS, HALDANE AND MAXWELL LTD.
Cowper Works, *Olney, Bucks MK46 4BN*
COLLET'S HOLDINGS LTD., Denington Estate,
Wellingborough, Northants NN8 2QT
WM DAWSON AND SONS LTD., Cannon House
Folkstone, Kent CT19 5EE

GREECE
KOSTARAKIS BROTHERS INTERNATIONAL BOOKSELLERS, 2 Hippokratous Street, *Athens-143*

HOLLAND
FAXON EUROPE, P.O. Box 167
1000 AD Amsterdam
MARTINUS NIJHOFF B. V.
Lange Voorhout 9–11, *Den Haag*
SWETS SUBSCRIPTION SERVICE
P.O. Box 830, 2160 Sz Lisse

INDIA
ALLIED PUBLISHING PVT. LTD.
750 Mount Road, *Madras 600002*
CENTRAL NEWS AGENCY PVT. LTD.
Connaught Circus, *New Delhi 110001*
INTERNATIONAL BOOK HOUSE PVT. LTD.
Madame Cama Road, *Bombay 400039*

ITALY
D. E. A., Via Lima 28, *00198 Roma*
INTERSCIENTIA, Via Mazzé 28, *10149 Torino*
LIBRERIA COMMISSIONARIA SANSONI
Via Lamarmora 45, *50121 Firenze*

JAPAN
KINOKUNIYA COMPANY LTD.
Journal Department, P.O. Box 55
Chitose, *Tokyo 156*
MARUZEN COMPANY LTD., Book Department
P.O. Box 5050 Tokyo International, *Tokyo 100-31*
NAUKA LTD., Import Department
2-30-19 Minami Ikebukuro, Toshima-ku, *Tokyo 171*

KOREA
CHULPANMUL, *Phenjan*

NORWAY
S.A. Narvesens Litteraturjeneste
Box 6125, Etterstad
1000 Oslo

POLAND
WĘGIERSKI INSTYTUT KULTURY
Marszalkowska 80, *00-517 Warszawa*
CKP I W, ul. Towarowa 28, *00-958 Warszawa*

ROUMANIA
D. E. P., *Bucuresti*
ILEXIM, Calea Grivitei 64–66, *Bucuresti*

SOVIET UNION
SOYUZPECHAT — IMPORT, *Moscow*
and the post offices in each town
MEZHDUNARODNAYA KNIGA, *Moscow G-200*

SPAIN
DIAZ DE SANTOS Lagasca 95, *Madrid 6*

SWEDEN
ESSELTE TIDSKRIFTSCENTRALEN
Box 62, *101 20 Stockholm*

SWITZERLAND
KARGER LIBRI AG, Petersgraben 31, *4011 Basel*

USA
EBSCO SUBSCRIPTION SERVICES
P.O. Box 1943, *Birmingham, Alabama 35201*
F. W. FAXON COMPANY, INC.
15 Southwest Park, *Westwood Mass. 02090*
MAJOR SCIENTIFIC SUBSCRIPTIONS
1851 Diplomat, P.O. Box 819074,
Pallas, Tx. 75381-9074
REDMORE PUBLICATIONS, Inc.
22 Cortlandt Street, New York, N.Y. 1007

YUGOSLAVIA
JUGOSLOVENSKA KNJIGA, Terazije 27, *Beograd*
FORUM, Vojvode Mišića 1. *21000 Novi Sad*

HU ISSN 0864-8085

Index: 26.025

ACTA TECHNICA

ACADEMIAE SCIENTIARUM HUNGARICAE

EDITOR-IN-CHIEF: P. MICHELBERGER

VOLUME 103
NUMBER 4

ENERGY ENGINEERING — E/2

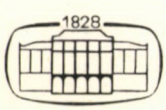

AKADÉMIAI KIADÓ, BUDAPEST 1990

ACTA TECHNICA

A JOURNAL OF THE HUNGARIAN ACADEMY OF SCIENCES

CENTRAL EDITORIAL BOARD

T. CZIBERE, K. GÉHER, L. KOLLÁR, P. MICHELBERGER (EDITOR-IN-CHIEF), A. LÉVAI, J. PROHÁSZKA, K. REMÉNYI, J. SZABÓ, GY. CZEGLÉDI (MANAGING EDITOR)

EDITORIAL COMMITTEE FOR ENERGY ENGINEERING (SERIES E)

G. BÜKI, GY. CSOM, K. GÉHER, T. JÁSZAY, I. KRÓMER, I. NÉVERY, K. REMÉNYI (CHAIRMAN), G. SZABOLCS

Acta Technica publishes original papers, preliminary reports and reviews in English, which contribute to the advancement of engineering sciences.
Acta Technica is published by

AKADÉMIAI KIADÓ
Publishing House of the Hungarian Academy of Sciences
H-1117 Budapest, Prielle K. u. 19—35.

Subscription information

Orders should be addressed to

KULTURA Foreign Trading Company
H-1389 Budapest P.O. Box 149

or to its representatives abroad

Acta Technica is abstracted/indexed in Applied Mechanics Reviews, Current Contents–Engineering, Technology and Applied Sciences, GeoRef Information System, Science Abstracts.

© *Akadémiai Kiadó, Budapest*

CONTENTS

Besze, J. - Mrs. Sándor, Gy.: Coupling elements of audio-frequency central control systems 225

Paláncz, B.: Simulation of power plant circuits and equipment state estimation I. - Simulation 249

Paláncz, B.: Simulation of power plant circuits and equipment state estimation II. - State estimation 263

Reményi, K.: Development of fluidized-bed firing technology in the Institute for Electric Power Research 279

Szergényi, I.: The bases of the prognosis of energy demand within the renewing Hungarian economy in the mirror of the 14th Energy World Congress 299

Tersztyánszky, T.: Probability distribution of random load of electric power system inter-ties 319

BOOK REVIEW

Frigyes, I. - Szabó, Z. - Várnyai, P.: Digital microwave transmission (Berczeli, T.) 329

Acta Technica Acad.Sci.Hung., 103(4), pp. 225-248 (1990)

COUPLING ELEMENTS OF AUDIO-FREQUENCY CENTRAL CONTROL SYSTEMS

BESZE, J.* - Mrs. SÁNDOR, GY.**

(Received: 20 December 1988)

This paper describes a 120 kV, 160 MVA coupling developed by VEIKI, the first developed and manufactured in Hungary, serving to couple audio-frequency signals with the high-voltage electric energy distribution system. After description of the serial coupling circuit, the most important problems of rating and practical application - including the effect of different loads occurring simultaneously, to be taken into consideration in determination of the capacitor rating - are discussed in detail.

Couplings are an important element of audio-frequency central control systems. The coupling is a dual-function element. On the one hand, it serves to couple audio-frequency signals supplied by the transmitter, usually signals below 1000 V, with the high-voltage power-frequency system for signal transmission with minimum energy loss after the signals have been transformed to the required voltage level. On the other hand, power-frequency interference signals fed back from the high-voltage system are suppressed by the coupling so that they will not result in operating troubles of the transmitter.

Described in this paper are the circuit configurations that can be taken into account for the functions outlined above and also the problems of rating and practical realization are discussed. Efforts to develop a 120 kV serial coupling by VEIKI, the first developed and manufactured in Hungary, are discussed in detail.

These efforts included a complex work from investigation of the theoretical problems through selection of the appropriate characteristics, determination of the dimensions and rating as well as design and construction of the different elements to testing. The result is important in that

*Besze, Jenő, H-1111 Budapest, Budafoki u. 10/B, Hungary

**Sándor, Györgyné, H-1141 Budapest, Paskálmalom u. 7, Hungary

Akadémiai Kiadó, Budapest

the coupling developed and manufactured in Hungary substitutes for import. Namely, licences purchased to contribute to a wide use of audio-frequency central control, an important step towards economically efficient energy distribution, included only the system configuration as well as the transmitter and receiver but nothing about coupling.

1. Basic types of coupling

Audio-frequency signals can be coupled with the high-voltage system capacitively or inductively. In case of capacitive coupling, the coupling element is a suitably selected capacitor while one of the windings of a transformer of suitable rating is connected to the system in case of inductive coupling where coupling takes place thus magnetically.

Figures 1 and 2 show the operation of the two types of coupling in respect of the system to be supplied, illustrating also the schematic arrangement and substitution circuit.

Capacitive coupling is shown in Fig. 1. It is called parallel coupling because according to Fig. 1/a (substitution circuit), the generator supplying the audio-frequency signal is connected in parallel with the

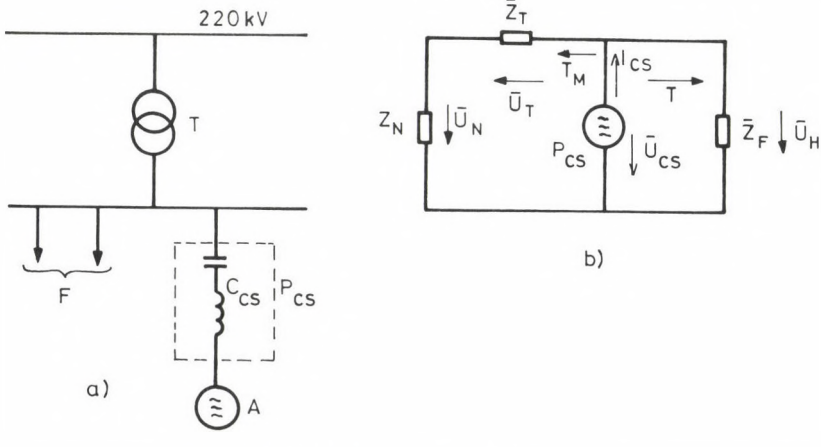

Fig. 1. Block Diagram of parallel coupling
(T: 220/120 kV power transformer, F: 120 kV consumer lines, P_{CS}: Parallel coupling, C_{CS}: Coupling capacitor, A: Audio-frequency transmitter, Z_F: Impedance of controlled system, Z_T: Impedance of transformer T, Z_N: Impedance of high-voltage system behind the coupling)

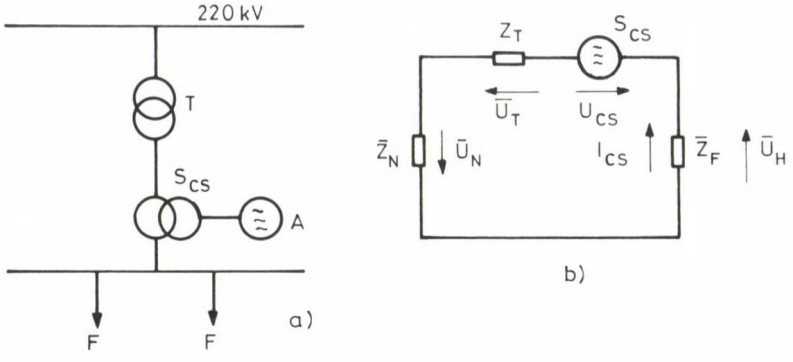

Fig. 2. Block Diagram of serial coupling
(S_{CS}: Serial coupling, T: 220/120 kV power transformer, F: 120 kV consumer lines, A: Audio-frequency transmitter, $\bar{Z}_F$: Impedance of controlled system, $\bar{Z}_T$: Impedance of transformer T, $\bar{Z}$: Impedance of high-voltage system behind the coupling)

impedance of the system to be controlled as well as with the impedance of the feeding system and of the transformer connected in series with it. Hence, in case of parallel coupling, the signal level of the controlled system (U_H) complies with the terminal voltage of coupling while the coupling current is determined by the parallel resultant of impedances $\bar{Z}_F$ and $\bar{Z}_T + \bar{Z}_N$ for given terminal voltage.

The so-called serial coupling unit shown in Fig. 2 results in inductive coupling through the coupling transformer connected in series with the current path of the power transformer. In this case, the impedance of the system to be controlled ($\bar{Z}_F$) is connected in series with the impedance of the feeding system and that of the power transformer as well as with the generator supplying the audio-frequency signal. Accordingly, signal level $\bar{U}_H$ of the system to be controlled lies always below terminal voltage $\bar{U}_{CS}$ of the coupling depending on the ratio of impedances $\bar{Z}_F$ and $\bar{Z}_T + \bar{Z}_N$, coupling current $\bar{I}_{CS}$ being determined by the sum of the above impedances.

Complicated calculations using both technical and economic parameters of a large number are required to decide which type of coupling should most reasonably be used for given supply point. Factors affecting the decision are the impedance relations of the system to be controlled and of the feeding system, control frequency, required inverter power, conditions of operation, investment costs etc., problems that would require another paper to discuss them and not analyzed therefore in detail in this work.

The first 120 kV system for which audio-frequency central control shall be provided is the Budapest network of the Electricity Works. Preliminary network calculations as well as economic considerations suggested to decide for serial coupling for most of the supply points as the best practice at the selected frequency of 216 2/3 Hz. Accordingly, development in this field has been focussed first on serial coupling in the country. This development work is discussed in detail below.

2. Principle of operation of serial coupling

The audio-frequency signal is applied by means of magnetic coupling to the network to be supplied when serial couplings are used. Therefore, the basic element of serial coupling is a suitably designed so-called coupling transformer the function of which is to galvanically isolate the high-voltage network from the audio-frequency equipment of lower voltage by means of suitable insulation.

One of the high-voltage windings of the coupling transformer is connected in series with the current path of the power transformer or transmission line for energy supply of the network. Accordingly, a fundamental requirement imposed upon coupling is that, in respect of the 50 Hz network, the equipment act like a low impedance resulting in a voltage drop below 0.5 to 1.5% of mains phase voltage even in case of rated operating load current. That is the 50 Hz impedance of coupling measurable on the high-voltage side shall meet the following requirement:

$$\overline{Z}_{CS} \leq \frac{U_{VN}^2}{S_N} \frac{f}{100} \quad , \tag{1}$$

where

f permissible voltage drop, %

U_{VN} rated line voltage of the network supplied, kV

S_N rated power of the power transformer or transmission line co-operating with the coupling, MVA.

It follows from the principle of operation of serial coupling that the coupling forms an integral unit with the power transformer or transmission line connected in series with it. Therefore multiple current as compared with the rated current (10 to 25 times as much) is following in the high-voltage winding of the coupling in case of a short circuit of the

50 Hz high-voltage network, depending on the place of the short circuit as well as on the impedance voltage of the power transformer. Mechanical load is applied to the high-voltage winding by this short-circuit current on the one hand while the voltage and current of any element of the coupling is increased by it significantly as compared with the rated operating values on the other hand, the extent of voltage and current increase depending on the selected impedance. Accordingly, another fundamental requirement the coupling has to meet is that any overload resulting from short-circuit current at the place of installation be endured by the coupling without breakdown from both a mechanical and an electrical point of view.

Hence, the higher the output (S_N) and the short-circuit current expectable at the place of installation at given mains voltage, the lower impedance shall be selected for the coupling to be used. However, the equipment supplied by the audio-frequency transmitter shall act at the same time as a transformer suited for signal transmission with the loss remaining within reasonable limits.

Depending on the method used to meet the above requirements, distinctions shall be made between two basic types of serial couplings that is between current transformer type and transformer type coupling.

2.1 Current transformer type serial coupling

The equipment is schematically illustrated in Fig. 3. In this case, the coupling transformer has three windings and a serial oscillating circuit tuned to 50 Hz, consisting of elements L_S - C_S and representing at this frequency an impedance corresponding to the loss resistance is connected to the terminals of one of these windings, the so-called short-circuited winding. Hence, the coupling transformer operating as a transformer suited for signal transmission due to the audio-frequency winding and the high-voltage winding, acts at the same time as a current transformer terminated by the low loss resistance of the oscillating circuit in respect of 50 Hz. Suitable rating of the equipment will result in an impedance for the 50 Hz energy transmission permitting the voltage drop to remain within the permissible limits.

In respect of the audio-frequency transmitter, oscillating circuit L_S - C_S acts like inductance constituting a parallel oscillating circuit tuned to audio frequency with compensating capacitor C_K connected in parallel with it and thus no load is applied to the transmitter by the impedance of the oscillating circuit.

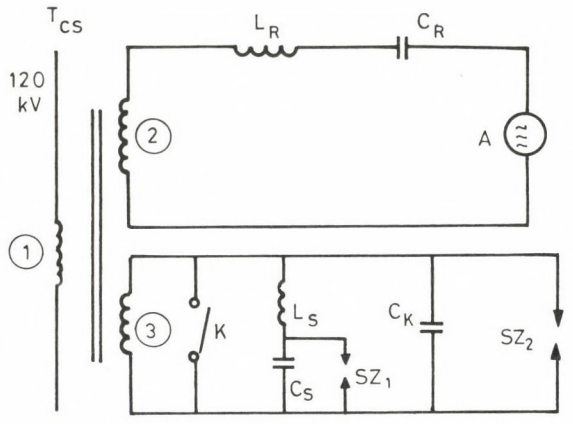

Fig. 3. Block Diagram of serial current transformer type coupling
(T_{CS}: Current transformer type coupling transformer, 1: High-voltage winding, 2: Audio-frequency winding, 3: Short-circuited winding, L_S, C_S: 50 Hz serial oscillating circuit, elements, C_K: Compensating capacitor bank, K: Short-circuiting switch, L_R, C_R: Audio-frequency serial oscillating circuit elements, SZ_1, SZ_2: Protective spark gaps)

In the intervals between transmissions, the terminals of the short-circuited winding are closed by switch K and thus the transformer actually acts as a current transformer and in the short-circuited winding flows a constant 50 Hz current corresponding to the transformation ration. This current shall be taken as a basis for rating of the winding. At the same time, it is only the currents of intermittent operation occurring at the time of audio-frequency transmission that shall be taken into consideration for the elements of the 50 Hz serial oscillating circuit and thus an economically more efficient structure can be developed.

The 50 Hz current flowing through the coupling results in voltage drop also in the audio-frequency winding, the magnitude of which depends on the transformation ratio and on the loss resistance of the serial oscillating circuit. If the load resulting in the transmitter from this so-called parasitic current exceeds the permissible value, the serial oscillating circuit tuned to audio-frequency, denoted by L_R - C_R in the figure, shall be built in. In respect of 50 Hz, this circuit acts like a high impedance and sets thus limits to parasitic current loads acting upon the transmitter.

In case of a short circuit of the high-voltage network, current of a value corresponding to the transformation ratio is forced to flow also

through the short-circuited winding by the short-circuit current flowing in the high-voltage winding of the current transformer type coupling independently of whether the switch is on or off. Should the short-circuit take place during audio-frequency transmission, significant overvoltages will occur both in the capacitor of the 50 Hz serial oscillating circuit and the compensating capacitor. Spark gaps SZ_1 and SZ_2 provide protection against overvoltages of this type. Spark gap SZ_1 is the first to respond and as a result, tuning of the serial oscillating circuit is discontinued. Then spark gap SZ_2 responds and as a result, short-circuit current depending on the transformation ratio is flowing through it until it short-circuited by switch K actuated by the overcurrent protection of the power transformer.

According to literature /1/, current transformer type coupling is used, for economic reasons, only for medium-voltage equipment of a relatively lower output. Namely, high-voltage units (e.g. 120 kV) of an output above 100 MVA in general need large and expensive equipment for coupling (including the coupling transformer and inductance L_S of the serial oscillating circuit for 50 Hz termination), the costs and size of which are compatible with the transformer type serial coupling.

On the other hand, because of the transformation conditions of the coupling transformer, the use of a filter circuit (L_R - C_R) can not be avoided either. In this case, a so-called transformer coupling discussed below seems to be an economically feasible choice.

2.2 Transformer type serial coupling

The equipment is schematically illustrated in Fig. 4. An air-gap choke coil is provided for coupling transformer T_{CS} and, dissimilarly to the usual iron-core transformers, an a priori low magnetic reactance is selected for it so that 50 Hz voltage drops of the coupling on the high-voltage side will not exceed the permissible value.

A compensating capacitor bank (C_K) is connected in parallel with the low-voltage, so-called audio-frequency, winding of the coupling circuit, constituting a parallel oscillating circuit tuned to audio-frequency with the reactance of the coupling transformer. Thus no load is applied to the transmitter by the high magnetizing current of the coupling transformer, resulting from the necessarily low impedance.

50 Hz voltage the magnitude of which depends on 50 Hz mains current, impedance of the transformer and selected transformation ratio appears on

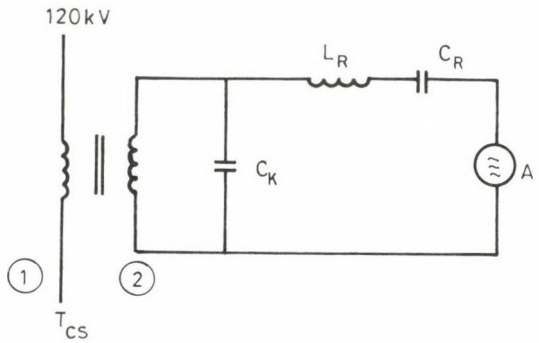

Fig. 4. Block Diagram of serial transformer type coupling
(T_{CS}: Serial coupling transformer, 1: High-voltage winding, 2: Audio-frequency winding, C_K: Compensating capacitor, L_R, C_r: Serial filter circuit, A: Audio-frequency transmitter)

the audio-frequency winding of the coupling transformer. For the transmitter, this voltage could represent a significant parasitic current load. Therefore, a serial oscillating circuit (L_R - C_R) tuned to audio-frequency, already mentioned in par 2.1, shall be built into the transformer type coupling in any case with a view to provide the required filtration.

Hence, in respect of the 50 Hz network, the transformer type coupling acts as a series reactor. As compared with rated voltage, the short-circuit current flowing through the high-voltage winding in case of a short-circuit of the high-voltage network results in significant overvoltage in the compensating capacitor bank connected to the audio-frequency winding. Overvoltage protection is possible in two ways. On the one hand, spark-gap shall be provided for the terminals of the compensating capacitor similarly to the method described in par 2.1. In this case, the short-circuit current is deflected to the audio-frequency winding of an otherwise lower current rating. On the other hand, the impedance of the coupling transformer and the rated capacitor voltage shall be selected in such a way that overloads due to short-circuit will not result in breakdown.

Two 120 kV BBC couplings of this type, with an output of 260 MVA each, are operated by the Electric Works at an OVIT substation near Budapest. The units have been supplied under a BBC-VBKM contract for production of central control devices on the basis of BBC licence.

Demand has arisen that coupling units be produced in Hungary for the central control system to be developed in the country. On the basis of a contract concluded with VBKM, VEIKI has undertaken to develop, and manu-

facture as a general contractor, 120 kV coupling units for the system. The first step had been the development of 160 MVA serial units and the prototype was manufactured in 1983. Additional two units were put into service in 1985. Problems in relation to development, rating and dimensions as well as construction of this equipment are discussed below in detail.

3. Development, rating and construction of the 120 kV coupling unit of an output rating of 160 MVA developed in Hungary

3.1 Requirements for the dimensioning

According to the principles outlined in Chapter 2, the parameters of serial coupling units and the requirements imposed upon them are fundamentally determined by the parameters of the 50 HZ energy transmission system for which the coupling is designed. These data have been taken as a basis for development of the coupling units, taking into consideration the signal level to be provided by the coupling as well as the characteristics of the transmitter to be built in.

3.1.1 Energy transmission system characteristics

A 220/120 kV OVIT substation in Zugló district of Budapest has been selected for installation of the first coupling units developed in Hungary in the 1980 system plan of the Budapest HKV system. Three coupling units have been installed at the substation, each connected in series with the 120 kV winding of a GVM transformer of a rated power of 160 MVA. The rated current of this transformer is 733 A, the rated short-circuit voltage being 9.85%.

Maximum three-phase short-circuit power of the 120 kV busbar is 5000 MVA with a short-circuit current of 23 kA. Because of the effective earthing of the Hungarian 120 kV system, the frequency single-phase and the less frequent three phase short-circuit current values are considered to be approximately identical.

For determination of short-circuit current to be taken into consideration in calculating for the rating of the coupling units see Fig. 5. As can be seen, short-circuit current flowing through the coupling depends on the point of substation where short-circuit has taken place. Should a short-circuit take place at point A, I_A = 23 kA current associated with

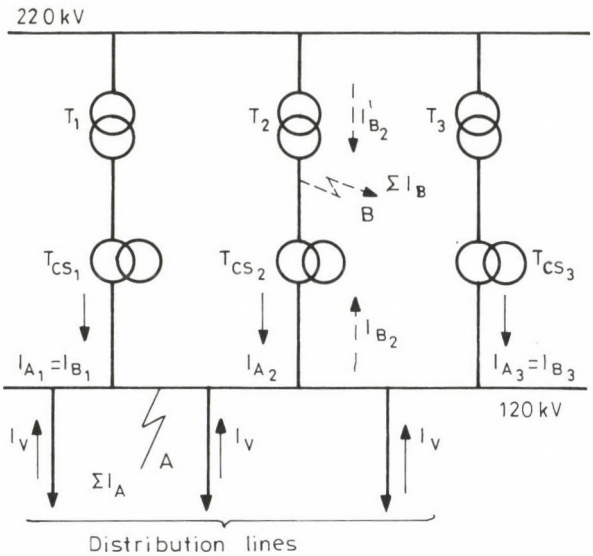

Fig. 5. Calculation of short-circuit current of coupling transformer (T_1, T_2, T_3: Power transformers, T_{CS1}, T_{CS2}, T_{CS3}: Coupling transformers)

5000 MVA will appear at point A only while through the coupling transformers, current distributed in accordance with the short-circuit impedances that is $I_{A1} = I_{A2} = I_{A3} = 7.5$ kA will be flowing. Case A is called external short-circuit.

Short-circuit current critical in respect of coupling rating will flow through the coupling if a short-circuit takes place e.g. at point B. Case B is called internal short-circuit. In this case, current according to formula $I_{B2} = \Sigma I_B - I'_{B2}$ is flowing through coupling transformer T_{CS2} the value of which must not exceed 17.4 kA even in the worst case. For T_{CS1} and T_{CS2}, $I_{B1} = I_{B3}$ is approximately identical with the previous case.

For the sake of increased safety, a short-circuit current exceeding the calculated value, that is 20 kA, has been specified for the couplings. However, considering that a dangerous busbar section is only that between coupling and power transformer and thus the probability of an internal short-circuit is minimum, use of loads occurring in case of external short-circuits as a basis for determining safe dimensions for the entire equipment instead of this critical value may require consideration from an economic point of view in future development. Namely, the price of the coupling is significantly affected by the short-circuit current rating as will be outlined later in detail.

3.1.2 Audio-frequency system characteristics

On the basis of calculations of the 1980 system plan, the following data have been available for the design of the coupling units:

- transmission frequency 216 2/3 Hz ~ 217 Hz,
- busbar signal level 2.5%,
- expectable load current 54 A (requiring a terminal voltage of 2540 V at the 120 V end of the coupling),
- the final configuration includes two transmitters of a unit capacity of 375 kVA, a max. phase voltage of 550 V and a max. load current of 300 A for each coupling to supply them,
- relative duty time of audio-frequency transmission: 5%/1 hour.

3.2 Rating and construction of the coupling units

The single-phase circuit diagram of the transformer type coupling unit of a rating and construction according to data given in par 3.1 is shown in Fig. 6. The function of the different elements in the Figure is described below:

The function of coupling transformer T_{CS} and compensating capacitor C_K has been described in par 2.2.

Switch K is designed to galvanically isolate the capacitor and the equipment behind it from the transformer terminals if necessary (e.g. in case of breakdown or maintenance etc.). Hence it is neither designed to

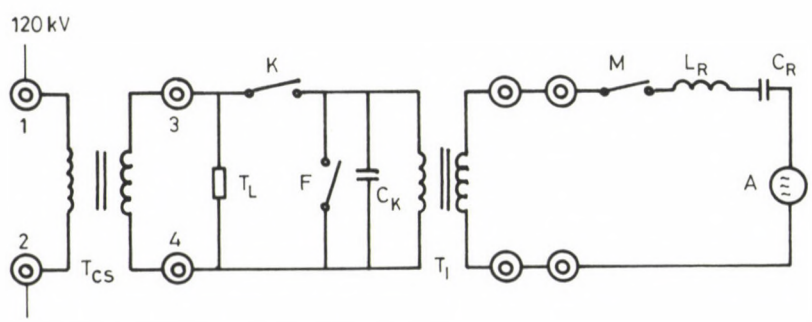

Fig. 6. Single-phase circuit diagram of 160 MVA serial transformer type coupling unit (T_{CS}: Coupling transformer, TL: Overvoltage arrester, C_K: Compensating capacitor bank, K: Isolating switch, F: Earthing isolating switch, T_I: Matching transformer, L_R, C_R: Inductance and capacitance of serial filter circuit, M: Low-voltage switch, A: Audio-frequency transmitter)

switch audio-frequency current on or off nor to disconnect 50 Hz short-circuit current resulting from short-circuits of the coupling unit.

Matching transformer T_1 serves to match the transmitter voltage with the transformation ratio of the coupling transformer, to set limits to surge current occurring when the coupler is switched on and to reduce overvoltage in case of short-circuits of the 120 V system to protect the transmitter.

The function of serial filter circuit L_R - C_R is well known. It is essentially an accessory of the inverters supplying the coupling and thus independent of the coupling unit.

The overvoltage arrester provided for the audio-frequency end of the coupling transformer serves to protect the audio-frequency winding of the transformer against atmospheric overvoltage.

Discussed below are the most important parameters of the different elements of the coupling unit as well as some problems relevant to development and design.

3.2.1 Coupling transformer and compensating capacitor: design directives

The key problem of the design of the coupling unit is to select optimum values for inductance of the coupling transformer and/or capacity and/or rated voltage of the capacitor bank because the dimensions and thus also the price of the equipment are fundamentally determined by these parameters.

Let first the 50 Hz impedance of the coupling, measurable at the high-voltage end, be determined in such a way that the requirement according to relationship (1) will be met. Assuming an ideal that is lossless transformer with zero short-circuit impedances, 50 Hz reactance of the circuit shown in Fig. 6, measurable in the direction of terminals 1-2, disregarding the detailed derivation, will be

$$X_{CS50} = \frac{j \omega_{50} L_1 a^2}{a^2 - \omega_{50}^2 L_1 C_K} , \qquad (2)$$

where

$a = \sqrt{\frac{L_1}{L_2}} = \frac{N_1}{N_2}$ transformation ratio,

L_1 and L_2 no-load inductance of the coupling transformer measurable between terminals 1-2 and 3-4, respectively.

Since C_K forms a parallel oscillating circuit tuned to audio-frequency with inductance L_2 of the transformer,

$$C_K L_2 = C_K \frac{L_1}{a^2} = \frac{1}{\omega^2 H} \tag{3}$$

from which

$$C_K = \frac{a^2}{L_1 \omega^2 H} \quad . \tag{4}$$

With (4) substituted into (2) and reduced, we obtain

$$X_{CS50} = \frac{j \omega_{50} L_1}{1 - k^2} \quad , \tag{5}$$

where

$$k = \frac{\omega 50}{\omega H} \quad ,$$

that is the reactance of the coupling depends on inductance L_1 between terminals 1 - 2 and on the ratio between 51 Hz and audio-frequency exclusively independently of the transformation ratio and size of the compensating capacitor.

Taking into consideration relationships (1) and (5) as well as the permissible voltage drop of f = 0.5 - 1.5% for the coupling, the reactance limits can be determined for the high-voltage end of the coupling transformer. In the present case where U_{VN} = 126 kV, S_N = 160 MVA, k = 0.23,

$$\omega_{50} L_1 = 0.47 \ldots 1.4 \text{ ohm}$$

is obtained for reactance.

Should a transformation ratio of 1:1 be selected on economic considerations not discussed here in detail, also the capacity limits of the compensating capacitor can be determined on the basis of relationship (3).

Considering the selection of capacitors available, the question is now what a rated voltage and capacity of the capacitor is required. To answer the question, let us see the loads to be taken into consideration for the compensating capacitor.

3.2.1.1 Constant voltage stress acting upon the capacitor bank

Under rated operating conditions, 50 Hz (U_{C50}) voltage that can be calculated on the basis of the coupling parameters appears continuously while audio-frequency voltage (U_{CH}) depending on transmission time intermittently on the capacitor bank.

In case of a selected transformation ratio of 1:1 and audio-frequency parameters according to par 3.1.2,

$$U_{C50} = I_{1N} X_{CS50} = 364 - 1092 \text{ V} \quad ,$$

$$U_{CH} = 2640 \text{ V} \quad , \tag{6}$$

$$\varepsilon = 4\%/1 \text{ hour},$$

where $I_{1N} = 733$ A is the rated primary current of the coupling.

The compensating capacitor bank is usually set up of so called phase-correction capacitors designed for a constant 50 Hz rated voltage and current. In case of the above combined (continuous-intermittent or 50 Hz-audio-frequency, respectively) operation, the effective value of voltage to be taken into consideration in respect of capacitor insulation is

$$U_K = \sqrt{U_{C50}^2 + U_{CH}^2} \quad , \tag{7}$$

the effective value of current to be taken into consideration in respect of thermal load being

$$I_{Ke} = \sqrt{I_{C50}^2 + I_{CH}^2} \quad , \tag{8}$$

where

$I_{C50} = U_{C50} \omega_{50} C$,

$I_{CH} = U_{CH} \omega_H C$,

ε relative duty time,

C capacity of the capacitor.

Given phase-correction capacitor of rated voltage U_{N50}, rated current I_{N50} and capacity C will meet the requirements of continuous operation if

$$U_{N50} \geq U_K = U_{CH} \sqrt{k_1^2 + 1} \tag{9}$$

and

$$I_{N50} \geq I_{Ke} = U_{CH} \quad \omega_H \, C \sqrt{\varepsilon + k^2 \, k_1^2} \quad , \tag{10}$$

where

$$k = \frac{\omega_{50}}{\omega_H} \quad ,$$

$$k_1 = \frac{\omega_{50}}{CH} \quad .$$

Since

$$I_{N50} = U_{N50} \quad \omega_{50} \, C \quad , \tag{11}$$

this can be substituted into (10) to obtain the second condition

$$U_{N50} \geq \frac{CH}{k} \sqrt{\varepsilon + k^2 \, k_1^2} \quad . \tag{12}$$

With the highest value, $U_{C50} = 1092$ V, selected from relationship (6) and taking into consideration that $k = 0.23$, $k_1 = 0.43$, $\varepsilon = 0.04$ in this case,

$$UN_{50} \geq 2764 \text{ V and } U_{N50} \geq 2463 \text{ V}$$

will be obtained for the rated voltage of the capacitor bank on the basis of relationship (9) and (12), respectively.

In respect of continuous loads in operation, the adequate capacitor bank can be obtained if a rated voltage of 3.15 V as usually in case of phase-correction capacitors, best approximating the numerical values obtained, is selected.

3.2.1.2 Transient voltage stress acting upon the capacitor bank

In the course of development of the coupling unit, the rated voltage defined by relationships (9) and (12) alone was found to be insufficient as a voltage rating specified for the compensating capacitor bank. Namely, significant transient overvoltages and overcurrents appear on the capacitors in case of a short-circuit of the 120 kV system and these loads shall be taken into consideration.

As has been described in par 3.1, current of an amperage 10 to 25 times as much as the rated current is flowing in the high-voltage winding of the transformer in case of a short-circuit of the 120 V system, depend-

ing on the place of short-circuit. As a result, the voltage of the audio-frequency winding and thus also the voltage appearing at the capacitor poles increase considerably as compared with operating voltage.

As a result of the high current intensity, the iron core of the coupling transformer is saturated in a way depending on the magnetizing curve. Thus the voltage appearing on the transformer would be strongly distorted if the capacitor were not connected to the audio-frequency winding. Such an oscillogram is shown in Fig. 7/a, obtained on the occasion of short-circuit current flowing through the 120 kV winding of the coupling transformer while U_{3-4} the voltage of the audio-frequency winding.

The impedance of the high-voltage network is much higher than that of the coupling. Therefore, in respect of the coupling, this high impedance acts like a quasi-ideal current generator. Hence, in spite of saturation, the theoretical maximum of the voltage illustrated in the figure is given by the following relationship:

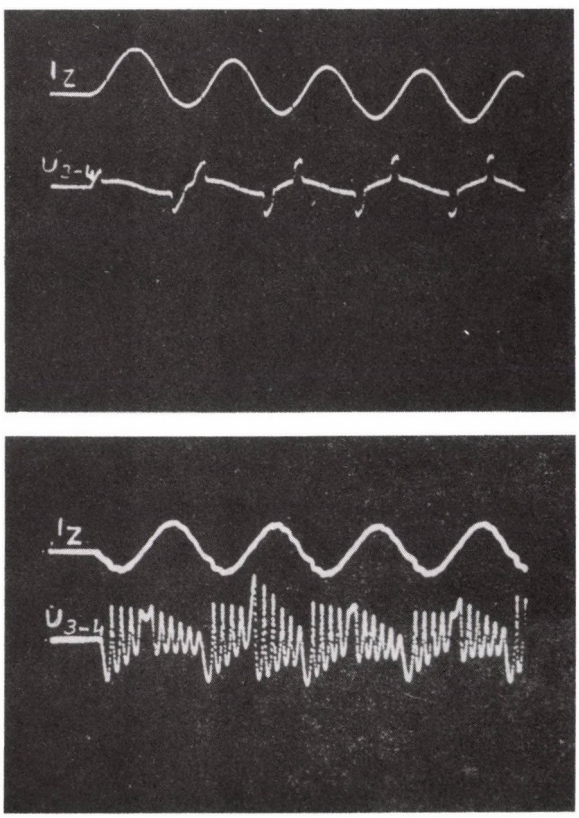

Fig. 7. Short-circuit test of 160 MVA coupling unit

$$U_T = \sqrt{2I_Z}\ \omega_{50}\ L_1 \quad , \tag{13}$$

where

I_Z effective value of short-circuit current,

L_1 initial value of non-linear inductance of the coupling transformer, associated with the range of rated currents.

If the network acts like an other than ideal current generator, the voltage according to (13) will be somewhat lower.

When the capacitor bank is connected to the coupling transform, the non-linear inductance of the transformer and the capacity of the capacitor bank form an oscillating circuit the inductance of which varying as a function of the relative permeability of the iron core at every instant. This system is generated by short-circuit current in such a way that a transient oscillation takes place twice within every half-period of 50 Hz that is when the system becomes saturated and when saturation discontinues, this transient oscillation being superimposted on the 50 Hz constant voltage associated with the non-saturated state. The amplitude and frequency of the oscillation vary depending on the magnitude of short-circuit current. As a result of this complicated non-linear process, the voltage increases on the terminals of the capacitor bank as compared with the measurable no-load voltage while the high-frequency component results in a capacitor bank current higher than what would be obtained in case of a sinusoidal voltage of identical maximum.

An oscillogram obtained on the occasion of a short-circuit test of a coupling made in Hungary is given in Fig. 7/b, the construction and lay-out of the coupling being illustrated in Fig. 6. The oscillograms according to Figs 7/a and 7/b have been recorded for the same winding of the coupling transformer subjected to short-circuit test, the effective value of current being 15 kA in both cases and also the scale is identical. After the initial transients, values of 8 kV and 12.6 kV have been obtained for voltage U_{3-4} as a maximum incase a) and b), respectively. That is the increase in voltage has been 1.57 fold as compared with the measurable value of no-load voltage.

During the test, switch M has been off and thus filter circuit L_R - C_R and the transmitter have not been tested. The inductance of matching transformer T_1 being no load because of the break on transmitter side is higher than the inductance of the coupling transformer, the difference

being about three orders of magnitude and thus it has not affected the phenomenon presented.

Because of non-linearity as well as the large number of parameters affecting the phenomenon, use of a computer is necessary for calculation of the capacitor voltage. However, difficulties are faced due to the fact that the magnitude of voltage is strongly influenced by the attenuation of the oscillating circuit consisting of the three-phase coupling transformer and the capacitor bank, which is frequency dependent and non-linear depending presumably also on current. No results of measurements required to determine the values of attenuation are available for the time being. Therefore, the capacitor voltage resulting from short-circuit current can be only estimated at present on the basis of measurement results obtained so far in short-circuit tests.

Two tests of this type have been carried out so far, the first including a coupling unit of an output of 360 MVA while the second a 160 MVA equipment. The results of both tests are tabulated in Table 1, indicating the maximum value of the short-circuit voltage of the capacitor as a function of the ratio of short-circuit current I_Z and rated current I_N as compared with the maximum value of non-load voltage measurable for the same current.

Table 1

360 MVA coupling			160 MVA coupling		
I_Z (kA)	$\frac{I_Z}{I_N}$	$\frac{U_{CZ}}{U_{Ü}}$	I_Z (kA)	$\frac{I_Z}{I_N}$	$\frac{U_{CZ}}{U_{Ü}}$
2	1.15	1.09	2	2.73	1.1
5	2.89	1.11	10	13.69	1.52
10	5.77	1.8	15	20.46	1.57
20	11.54	1.37	20	27.3	1.74

As seen in the Table, short-circuits result in a different voltage increase for either of both equipment but the increase is less than 1.8 fold in both cases.

According to what has been said above, rated voltage U_{N50} of the capacitor bank shall be selected in such a way that even overvoltages of shortest time (some tenths of a second), resulting from maximum short-

circuit current, will not exceed the value of maximum test voltage specified for the capacitor.

Two different test voltages are specified for capacitors in the relevant standards, depending on whether the test takes place at 50 Hz or d.c. voltage. The effective value of test voltage in case of 60 Hz tests is

$$U_{p50} = 2.15\ U_{N50} \tag{14}$$

while in case of d.c. voltage tests

$$U_{pe} = 4.3\ U_{N50} \quad . \tag{15}$$

Assuming a maximum value of 1.8 for ratio $\frac{U_{CZ}}{U_T}$ taking relationship (15) as a criterion, then

$$1.8\ \sqrt{2 I_Z}\ \omega_{50}\ L_1 \quad \omega 4.3\ U_{N50} \quad . \tag{16}$$

With U_{N50} calculated from (16) we obtain

$$U_{N50} \geq 0.59\ I_Z\ \omega_{50}\ L_1 \tag{17}$$

as a rated voltage for the capacitor to be selected.

In turn, for a capacitor of given rated voltage, the reactance of the coupling transformer can be determined in accordance with the following relationship:

$$\omega_{50}\ L_1 \leq \frac{U_{N50}}{0.59\ I_Z} \quad . \tag{18}$$

As is well known, the price of the capacitor bank depends on the installed reactive power: the higher the reactive power, the higher is the price of the capacitor bank. Using relationship (17),

$$P_C = U_{N50}^2 \quad \omega_{50}\ C = 0.59^2\ I_Z^2\ (\ \omega_{50}\ L_1)^2\ \omega_{50}\ C \quad . \tag{19}$$

Making use of

$$CL_1 = \frac{1}{\omega^2_H} \quad \text{and} \quad k = \frac{\omega_{50}}{\omega_H}$$

the following relationship is obtained for the capacity of the capacitor bank:

$$P = 0.59^2\ k^2\ I_Z^2 \quad \omega_{50}\ L_1 \quad . \tag{20}$$

As obviously shown by relationship (20), the price of the capacitor bank increases quadratically with increasing effective short-circuit current while linearly with increasing impedance of the coupling transformer. The impedance of the coupling shall therefore reasonably be selected at a value falling within the limits given in par 3.2.1, possibly close to the lower range.

Since the coupling transformer has to be capable at the same time of transmitting given audio-frequency voltage and/or power, limits are set to reduction of the reactance by the fact that, below given reactance, the transformer dimensions and prices quite irrational. Therefore, the parameters shall be co-ordinated so as to result in an economically relatively favourable compromise. However, reduction of the effective value of short-circuit-current within reasonable limits after careful consideration of the probability of short-circuits of different type will definitely result in lower equipment prices.

3.3 Most important parameters of the equipment constructed

Based on the above considerations, the following basic parameters have been selected for the coupling of an output of 160 MVA developed in Hungary:

- 50 Hz reactance of coupling in relation to audio-frequency winding 0.65 ohm $\pm$ 10%
- capacitor bank: rated voltage 4.71 kV; associated test voltage 25.25 kV; capacitance 240 μF $\pm$ 10%
- transformation ratio of coupling transformer about 1:1 suited for transmission of power supplied by two 375 kVA inverters at audio-frequency, including also coupling losses.

The above values would result in a maximum theoretical capacitor voltage of 12.4 V in case of so-called external short-circuits, 28 V in case of short-circuits of extremely low probability, resulting in 17.5 kA while 33 kV in case of the specified short-circuit current of 20 kA.

Thus, on the basis of criterion (17), a rated capacitor voltage of 7.67 kV should have been selected. Since the original, installed power of the capacitor is 1.7 MVAr per phase, any further increase of the rated voltage of the capacitor bank seemed to be unreasonable considering that a voltage rating of 3.15 kV would meet the requirements.

It was therefore decided to build in special spark gaps connected in parallel with the audio-frequency winding to protect the capacitor bank

if the capacitor voltage exceeded the value of test voltage in the course of actual short-circuit tests while the impedance of the transformer and the response voltage of the spark gap were determined in such a way that a response could not take place below a short-circuit current of 10 kA even in the most unfavourable case.

However, the capacitor voltage did not exceed the specified value of test voltage even in case of a short-circuit current of 20 kA in the course of the short-circuit tests of the coupling unit. Therefore, it was unnecessary to build in spark gaps and thus not only the costs of the equipment could be reduced but, by eliminating a possible source of faults, also the safety of operation was increased.

3.3.1 Most important characteristics of other components of the coupling unit

Notation of the block diagram of Fig. 6 is used. In accordance with the transmission voltage supplied and the output signal level, the transformation ratio of coupling transformer T_I is 5:1. The transformer windings have been designed for a relative duty time of 4%, the audio-frequency short-circuit voltage drop being about 37% with a view to reduce the short-circuit current of the transmitter.

Switch K is an encapsulated isolating switch of a rated voltage of 12 kV and a rated current of 800 A for indoor use, suited to break 50 Hz capacitive current of the built-in capacitor bank of the coupling at given voltage.

TL is a built-in overvoltage arrester of a rated voltage of 10 kV and a rated discharge current of 5 kA. The 50 Hz spark-over voltage of TL has been selected so as to prevent the overvoltage arrester from operating even in case of an overvoltage resulting from a short-circuit current of 20 kA.

The capacitor bank switch, the coupling transformer and the overvoltage arrester form an integral unit with the compensating capacitor bank, called compensating-matching unit.

The coupling unit consisting of coupling transformer and compensating unit can be seen in a photograph (Fig. 8) taken from the equipment on the site of erection.

Serial filter circuit $L_R - C_R$ called otherwise coupling matching unit has been constructed as an independent unit the inductance of which being provided by a three-phase air-gap iron-core where the different phase

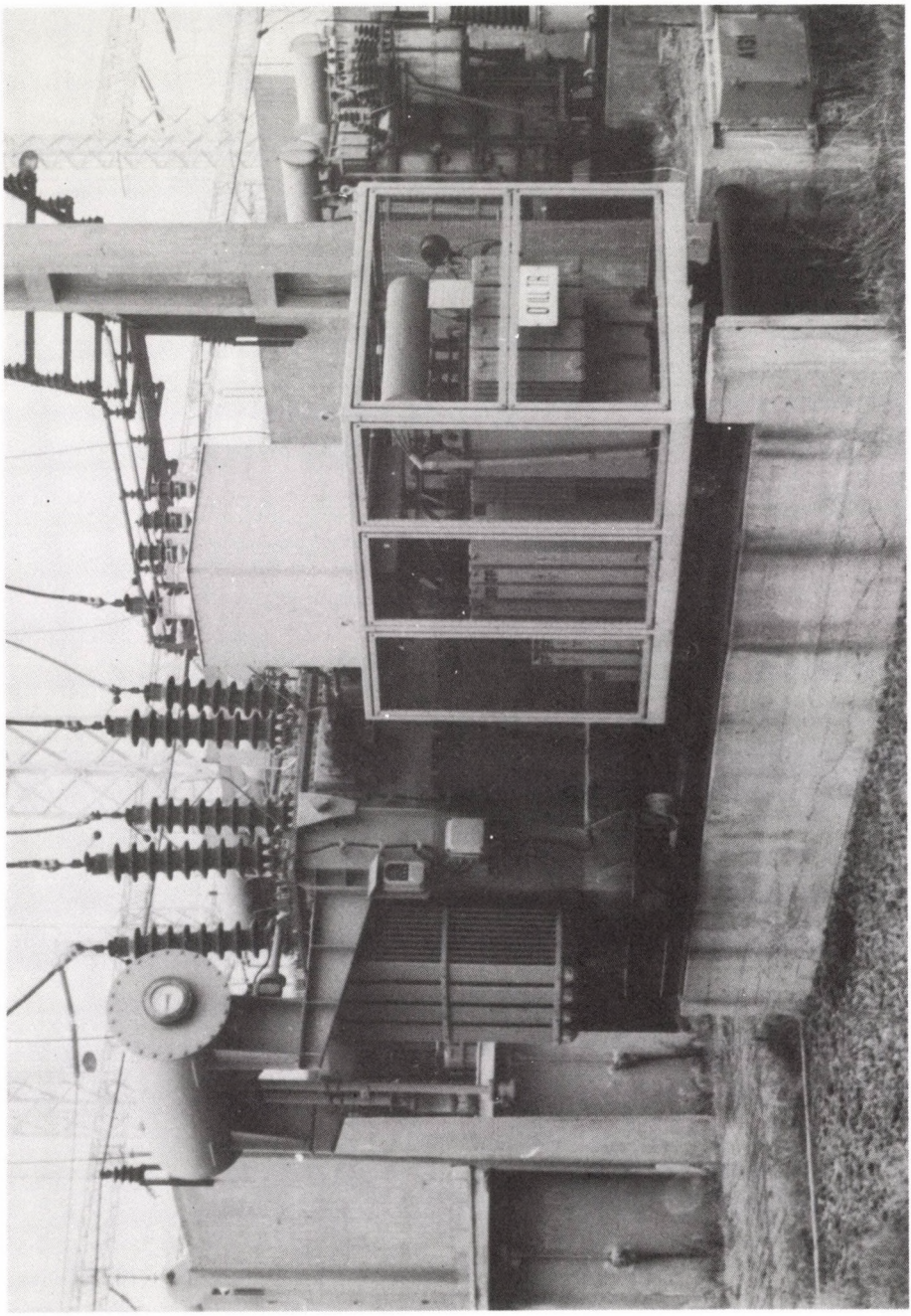

Fig. 8. Audio-frequency coupling unit

windings are electrically independent of each other. The unit is disconnected from the coupling by a magnetic switch in the intervals between transmissions and thus the transmitter is connected to the coupling for the time of transmission only.

The coupling matching unit is suited for transmission of current supplied by an inverter and it is therefore erected as an indoor unit near the inverter.

Finally, manufacturers of the different elements of the equipment are listed below:

GANZ Villamossági Művek:
coupling transformer
Csepeli Transzformátorgyár:
matching transformer
Dunakanyar Co-operative:
choke-coil of serial filter circuit
KAPSCH, Austria:
capacitors for compensating capacitor bank and coupling matching unit.

4. Summary

As has been said introductorily, development of the coupling elements of audio-frequency central control devices in Hungary had been necessary because of unavailability of licence or know-how concerning the construction of such elements.

Therefore, first thing to do was to clear up the theoretical problems. The results of thorough theoretical investigations were then taken as a basis for development of the first Hungarian coupling unit, a serial coupler.

The results described here obviously reflect the nature and depth of works in the different fields in relation to the problem.

With full knowledge of the circuit problems, it was possible as early as in the design phase to calculate for dimensions and rating resulting in best economies of scale for the entire coupling, based on data of the audio-frequency system (network data, signal level, relative duty time, etc.) and taking into consideration the interactions between the different coupling elements.

The combined load resulting from high-frequency and audio-frequency voltages, acting upon the capacitors designed normally as phase-correction capacitors, had to be paid special attention. Additional problems resulted from transients due to audio-frequency pulses in the oscillating circuit brought about by the coupling elements.

The coupling transformer design had to meet complex requirements considering the load resulting from two different voltages the two different types of power transmission. Because of the special mode of operation, the coupling transformer has to endure also the short-circuit current of the high-voltage network. Therefore, works in relation to design of the coupling transformer were focussed on proper selection of the parameters as well as on short-circuit tests where the transformer was subjected to the same load as under operating conditions.

LITERATURE

1. Junior, H. - Müller, K.P.: Aufbau und Betrieb von Rundsteueranlagen mit 110 kV Einspeisung. Elektrizitätswirtschaft 75 (1976), Heft 18

2. Neese, H. - Will, K.: Eine Tonfrequenzsteueranlage mit 110 Hz Steuerfrequenz. Elektrizitätswirtschaft 77 (1978), Heft 5

Acta Technica Acad.Sci.Hung., 103(4), pp. 249-261 (1990)

SIMULATION OF POWER PLANT CIRCUITS AND EQUIPMENT STATE ESTIMATION

(Part I)

SIMULATION

PALÁNCZ, B.*

(Received: 20 December 1988)

Presented in this work is a module oriented simulation process for calculation of power plant heat-flow diagrams. A characteristic feature of the procedure is that, dissimilarly to first-generation modular procedures where a module stands for a device or equipment /3/, the modules of this procedure represent an elementary heat or material flow conversion process each. In this sense, MODSIM can be considered a second-generation procedure suited for generation of any arbitrary flow diagram. Since the program consists of a small number of elements of different type, the memory demand is small. A modified version of the multivariable Wegstein method is used, a robust method resulting in good convergence and requiring a short running time.

The typical running time is 5-8 minutes in case of an IBM-PC AT machine that is the time required for computation of a flow diagram consisting of 60 modules and 100 streams and having 20 iteration variables.

The interactive version of MODSIM offers convenient and simple program handling for the user and the LOTUS compatibility permits the results of computation to be displayed descriptively and processed in accordance with different requirements.

NOTATION

F_i — i-th nonlinear balance equation of the flow-diagram model

mod/a,b/ — module function

s_i — relaxation factor

x_i^k — value of i-th flow variable in k-th iteration step

*Páláncz, Béla, H-1085 Budapest, Salétrom u. 9, Hungary

Akadémiai Kiadó, Budapest

Introduction

A procedure to simulate the steady state of a power plant heat-flow diagram can be used for different problems such as e.g. for detection of the reasons of a reduction in electricity generation, monitoring of the thermodynamic state of power plant equipment, optimum selection of operating parameters of the power plant and for determination of the starting values of dynamic simulation /1/.

Although different simulation computer codes are known /2—4/, almost every code has certain deficiencies, including cumbersomeness in producing a new version of flow diagram, significant memory demand, uncertainty of convergence, long running time etc.

The modular simulator described here tries to reduce or eliminate all these disadvantages. The principle adopted that is modular description of complex systems where a transformation of heat and material flow is taking place is not new as it was successfully applied to modelling of systems of chemical industry long before /5/.

The MODSIM system

The different modules represent balance equations describing the different elementary material and energy transformation processes. Accordingly, the modular representation of a complex heat-flow diagram includes only a small number of elements of different type with, however, these elements repeated many times. Typically, the following elements are included in the MODSIM process:

SPLIT for decomposition of the material flow and for use as a liquid separator,

MIX for mixing of two streams and for pump and throttle valve modelling,

TURB for simulation of expansion processes taking place in turbine stages,

CSHE1 for heat exchange between two streams without change of the phase,

CSHE2 for heat exchange with change of the phase,

PCOND for simulation of processes taking place in the steam condenser.

The relation between the modules is determined by the knowledge of the input and output streams of the modules. Computation takes place in a specified sequential order with the output streams calculated on the basis of the input streams. Components of the different stream vectors are mass

flow, steam content, temperature, pressure and enthalpy. The module parameters including capacity of heat transmission (kF), thermodynamic efficiency and Stodola number of the turbine stages are constant and/or specified function of some stream component.

Because of recirculation streams like e.g. extraction streams of turbine stages, the sequential computation can not be carried out directly in general. Therefore, these recirculation streams shall be cut up and the deviation between the (estimated and calculated) values associated with the places of cut shall be reduced below a specified limit using some iteration method. The MODSIM process uses the multivariable Wegstein method /6/, a robust method of good convergence.

Let x_i^k be the value of i-th stream variable in k-th iteration step. Then the value associated with the next iteration step will be:

$$x_i^{k+1} = t_i F_i (x_1^k, x_2^k, \ldots x_m^k) + (1 - t_i) x_i^k \quad . \tag{1}$$

Calculation of relaxation factor t_i:

$$t_i = \frac{1}{1 - s_i} \tag{2}$$

where

$$s_i = \frac{F_i(x_1^k, x_2^k, \ldots x_m^k) - F_i (x_1^{k-1}, x_2^{k-1}, \ldots x_m^{k-1})}{x_i^k - x_i^{k-1}} \tag{3}$$

On the basis of experience gained in numerical investigations, the following choice shall reasonably be for the relaxation factor:

$$t_i = \begin{cases} 6 \text{ if } t_i > 6 \\ \\ 0.5 \text{ if } t_i > 0.5 \end{cases} \quad . \tag{4}$$

Introduction of the following algorithm increases the stability of the iteration process considerably:

$$x_i^{(k)} = (x_i^{(k)} + x_i^{(k-1)})/2 \qquad \text{mod } (k,3) = 0 \quad . \tag{5}$$

Convergence condition specified for the different stream components:

$$\left| \frac{x_i^{(k+1)} - x_i^{(k)}}{x_i^{(k+1)} + x_i^{(k)}} \right| < 10^{-3} \quad . \tag{6}$$

The procedure described above is realized by WEGSTM convergence module. The special feature of the MODSIM code is that instead of a specified value, it uses a condenser pressure depending on the conditions of condenser and cooling water. A special Newton iteration algorithm, realized by NEWT convergence module, is used to determine the ultimate state of throttling for the stage before the first turbine stage in this case.

A method consisting of rather efficient fast algorithms is used for computation of the thermodynamic variable /7/.

Application example

The relatively simple heat-flow diagram of the old block No. 2 of Tisza Thermal Power Station has been simulated to illustrate how the procedure can be applied. The Block Diagram is given in Fig. 1 while the appropriate modular diagram can be seen in Fig. 2.

The first iteration setup of computation is, as follows:

a Recording of extraction values

b Recording of the value of pressure of the stream entering the first turbine stage

c Calculation of heat-flow diagram up to condenser

d Testing whether the outlet pressure of the last stage complies with condenser pressure

e If not, modification of pressure according to b)

f If the values of pressure comply with each other, the flow rate of the medium leaving the first high-pressure preheater to enter the deaerator shall be recorded at the preheater jacket

g Calculation for preheaters

h Testing whether the value according to f) is correct. If it differs from the modified values, repeat g).

i If the value is correct, test whether the values of extraction are correct.

k If these values differ from the recorded values, modify them and repeat the process from b).

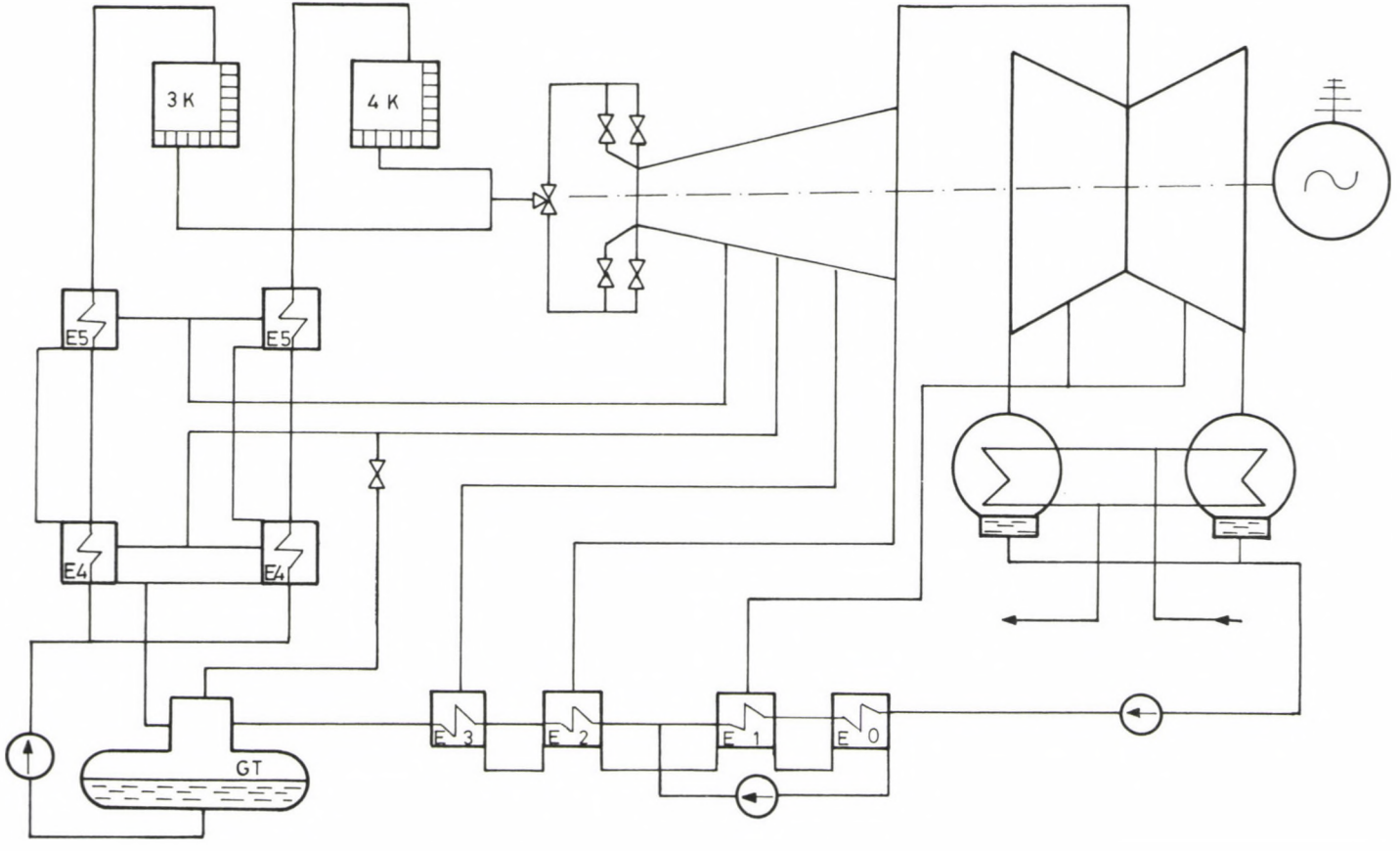

Fig. 1. Simplified Block Diagram of unit 2 of Tisza Thermal Power Station

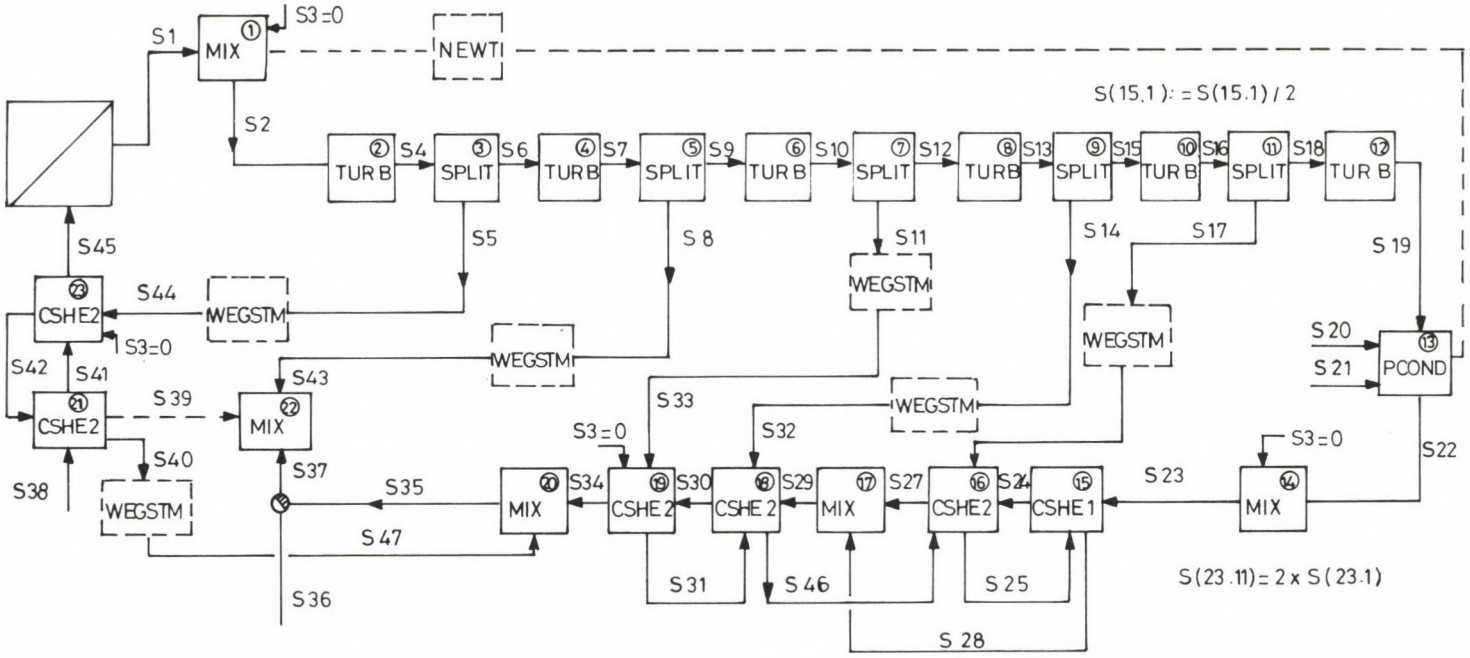

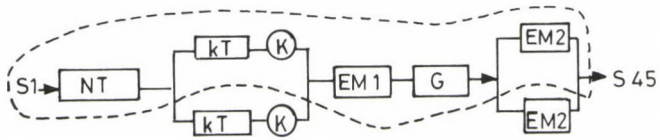

Fig. 2. Modular representation of the heat-flow diagram

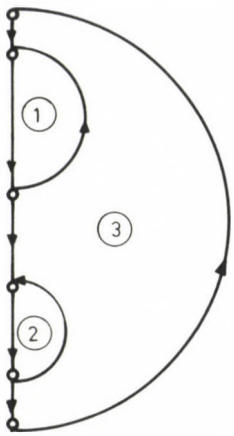

Fig. 3. Iteration cycles
(1 - iteration of the initial pressure of expansion, 2 - iteration of condensate returning from the first high-pressure preheater, 3 - iteration of expansions)

As compared with a simultaneous iteration of every unknown value, the above iteration process is advantageous in that it offers high stability concerning convergence.

However, a disadvantage of the process is that, because of repeated calculation of the heat-flow diagram, it might be quite slow.

The iterative cycles are shown in Fig. 3.

Figure 4 shows the changes of condenser pressure and outlet steam pressure of the last stage as a function of the number of iterations for constant extraction.

Interactivity

The wide use of personal computers resulted in a significant change of the man-machine system with an interactive system of dialogues, a question-answer system becoming increasingly predominant over so-called batch processing methods that have been used so far. Also MODSIM tries to meet this up-to-date requirement. It permits any arbitrary heat-flow diagram to be simply generated and/or modified in an interactive way. Figure 5 shows the graphic record of the Block Diagram for the above example, appearing on the computer screen.

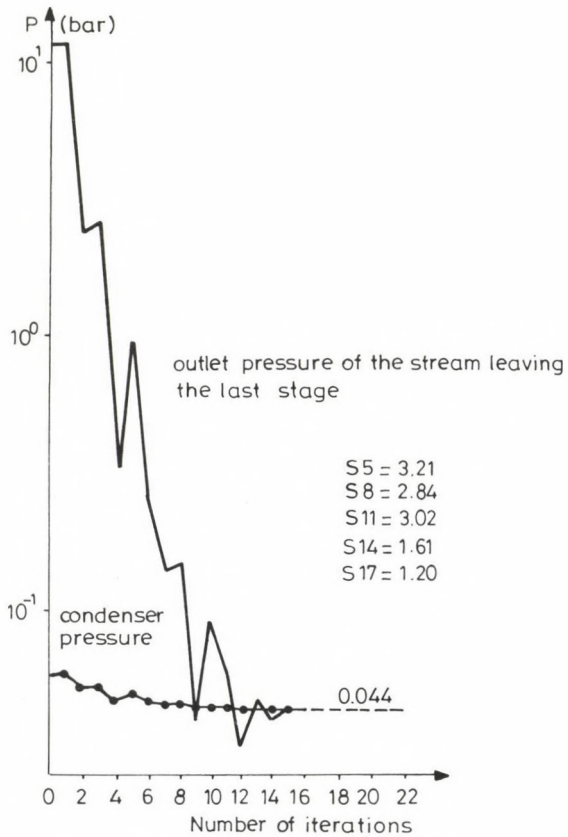

Fig. 4. Changes of condenser pressure and outlet pressure of steam leaving the last stage as a function of the number of iterations

The MODSIM menus permit the actual user demands to be met. The Information Menu shown in Fig. 6 allows to display the results of simulation in different forms. MODSIM is compatible with LOTUS 1-2-3, a product of Lotus Development Corporation, which permits the results of program running to be interpreted in different ways graphically or in the form of charts (see Figs 7 through 9).

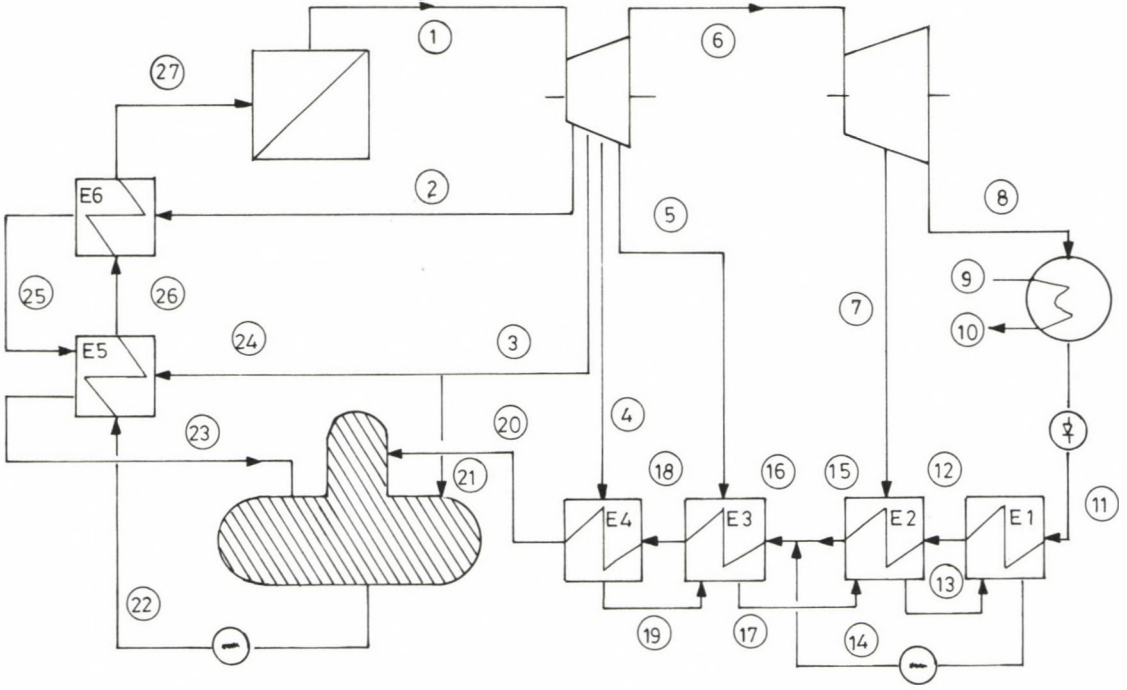

Fig. 5. MOSIM heat-flow diagram of unit 2 of Tisza Thermal Power Station

Information Menu

Options

1. Values of all Streams on Screen
2. Values of all Streams on Hard Copy
3. Evaluated Data of the Plant Process
4. Expansion Line
5. Temperature Elevation in Preheaters
6. General Report
7. Return to Operation Menu

Enter Number ===>

Fig. 6. MODSIM Information Menu

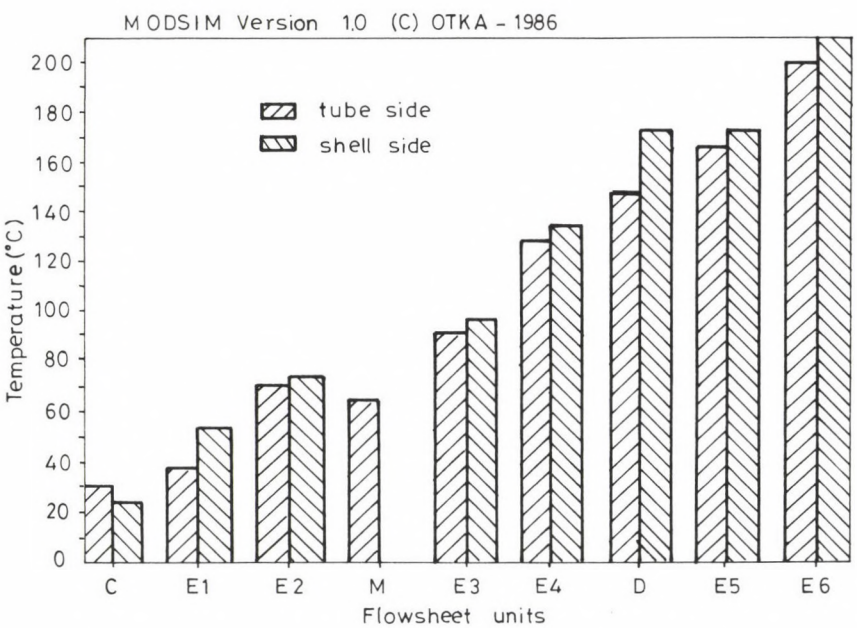

Fig. 7. Change of feed water temperature in preheaters, MODSIM - LOTUS output

Temperature Elevation in Preheaters:

Unit	Label	Tube Side	Shell Side
Condensator	C	30.84	24.33
Heater 1	E1	38.74	54.39
Heater 2	E2	71.04	73.81
Mixing	M	64.04	
Heater 3	E3	90.91	97.09
Heater 4	E4	128.82	134.93
Deaerator	D	147.01	174.16
Heater 5	E5	167.96	174.16
Heater 6	E6	201.69	209.05

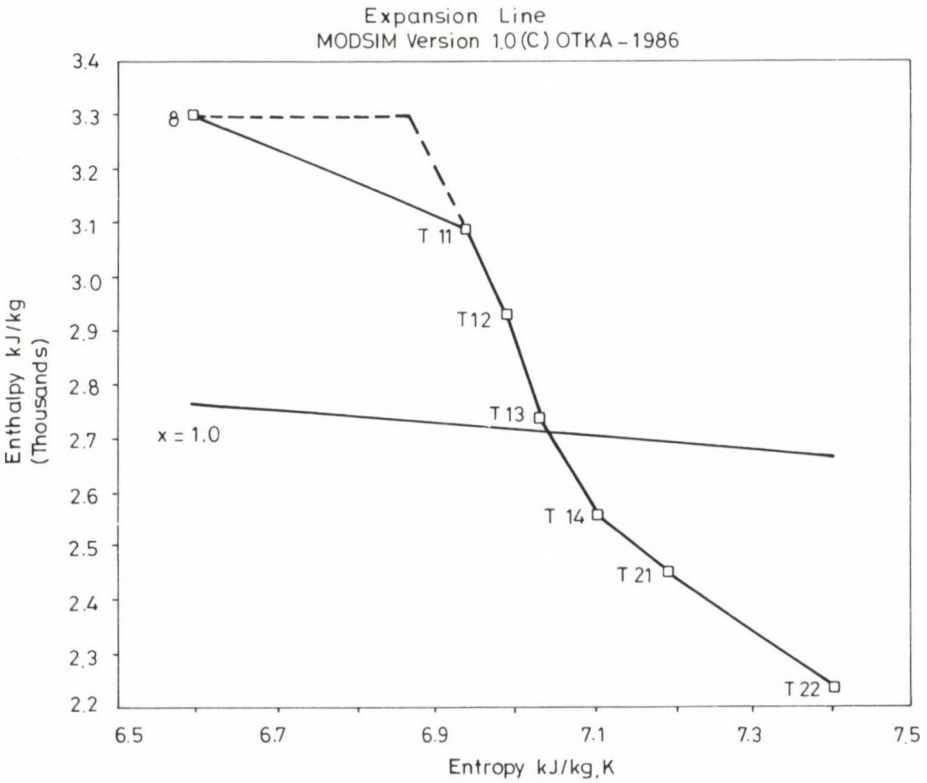

Expansion Line

P: Pressure in decibar TURB1: High Pressure Turbine
T: Temp. in Celsius TURB2: Low Pressure Turbine
x: Vapor ratio in gr/kg

	Unit	Label	P	T	x
Boyler		B	882.5	520.01	1000
TURB1	Stage 1	T11	187.19	332.66	1000
	Stage 2	T12	87.47	247.02	1000
	Stage 3	T13	31.23	145.81	1000
	Stage 4	T14	9.13	97.09	953
TURB2	Stage 1	T21	3.67	73.81	922
	Stage 2	T22	0.44	30.91	870
Condenser		C	0.44	30.91	0

Fig. 8/a.

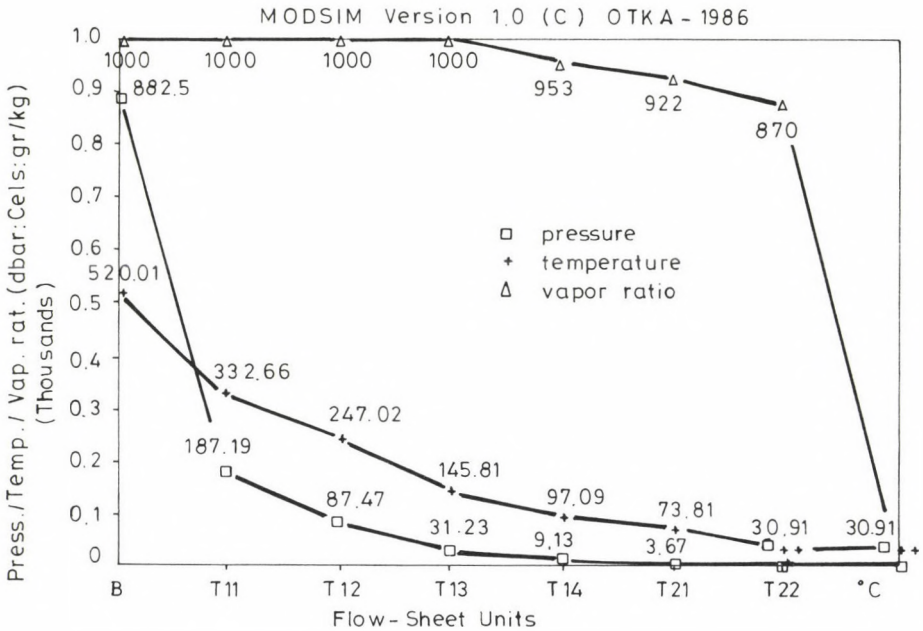

Fig. 8/a., 8/b. Expansion process in the turbine stages, MODSIM - LOTUS output

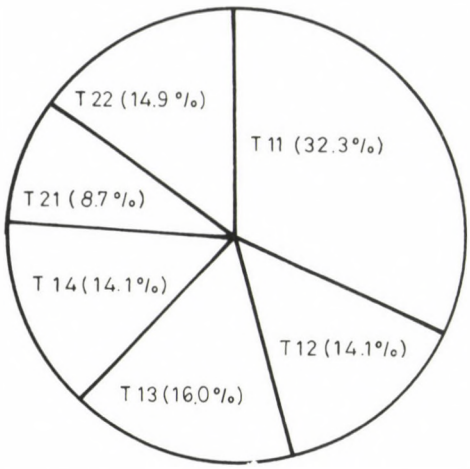

Evaluated Plant Data

1. Output Power of Turbines

TURB1: High Pressure Turbine
TURB2: Low Pressure Turbine

		Label	Power (MW)
TURB1	Stage 1	T11	16.3
	Stage 2	T12	7.1
	Stage 3	T13	8.1
	Stage 4	T14	7.1
TURB2	Stage 1	T21	4.4
	Stage 2	T22	7.5
Total:			50.4

Fig. 9. Output of the different turbine stages, MODSIM - LOTUS output

LITERATURE

1. Mackenzie, J. - Reason, J.: Monitoring Power Plant Performance, Power (1984), Sept., S1-S24

2. Fuller, L.C.: User's Introduction for ORCENT-II, a Digital Computer Program for the Analysis of Steam Turbine Cycles Supplied by LWR's, ORNL-TM-6525, Oak Ridge National Lab. (1979)

3. Sonnenschein, H.: Eine modulare Kraftwerkskreislauf-Berechnungsmethode zur Optimierung von Energiebalanz und Anlagenwirkungsgrad, VGB Kraftwerkstechnik, Vol. 61. No. 7. (1981), 547-554

4. Sandner, Th.: Verfahren zur Berechnung von thermodynamischen Kreisprozessen in Dampfkraftanlagen, VGB Kraftwerktechnik, Vol. 63. No. 1. (1983), 1-7

5. Franks, R.G.E.: Modelling and Simulation in Chemical Engineering, Wiley - Interscience, New York (1972)

6. Kehat, E., Scacham, M.: Solution of System of Nonlinear Equations, Process Technology Ints., Vol. 15, No. 4/5 (1973), 181-184

7. Rivkin, S.L., Kremenvskaia, E.A.: State Equations of Water and Steam suitable for Computer Calculation (in Russian), Teploenergetika, No. 3. (1976), 69-73

Acta Technica Acad.Sci.Hung., 103(4), pp. 263-278 (1990)

SIMULATION OF POWER PLANT CIRCUITS AND EQUIPMENT STATE ESTIMATION

(Part II)

STATE ESTIMATION

PALÁNCZ, B.*

(Received: 20 December 1988)

This work describes a method to estimate the state of major equipment of power plant circuits based on balance equalization and parameter estimation. The method permits the acceptability of the results of measurements to be investigated and to identify the changed model parameters and thus the state of equipment of the circuit to be estimated, using a linearized circuit model.

A practical example, a block of Tisza Power Plant, is used to illustrate application. The method has been used also for the 440 MW blocks of Paks Nuclear Power Station.

NOTATION

A — Jacobi matrix for linearized system variables

B — Jacobi matrix for linearized system parameters

F — nonlinear functional connection, vector-vector function

I — unit matrix

J — weighted residual in parameter estimate

kF — thermal transmission factor, $kW/^{O}C$

P — vector of parameters

Q — weighted residual in balance equalization

x — state vector of input variables

y — state vector of output variables

χ^2 — Chi-square distribution

σ^2 — mean square deviation

Indices:

o — place of linearization

p — parameter estimate

*Palánczy, Béla, H-1085 Budapest, Salétrom u. 9, Hungary

Akadémiai Kiadó, Budapest

1. Introduction

Reliability and efficiency range among the most important criteria of up-to-date operation of plants where technological processes of industrial chemistry and energy production are taking place. Of course, reliability and efficiency are closely interrelated as a reduction in the efficiency of major equipment, losses in production due to unforeseen breakdown and increased costs of repair affect the economic efficiency equally unfavourably. Figure 1 shows the theoretical relationship between maintenance costs and availability. In the Figure, preventive maintenance is minimum along section 'A' and thus availability in terms of percentage of actual hours of operation as compared with the planned hours reduces due to frequently occurring breakdowns, accompanied with increasing costs resulting from subsequent repairs. The correct preventive maintenance schedule along section 'B' results in increasing availability with also the costs of preventive and subsequent maintenance lying well below the costs according to strategy 'A'. At the same time, an over-estimated preventive maintenance demand like in strategy 'C' results in increasing standstill that is in reducing availability /1/. Hence, in fact, the relationship between availability and maintenance costs can be optimized although in practice it is difficult to express this optimum numerically.

The close correlation between reliability and efficiency of operation comes in focus especially if reliability implies not only unforeseen

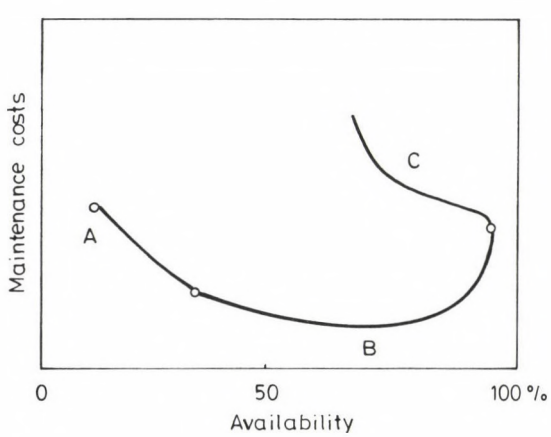

Fig. 1.

standstill prevention but also control of disorders in major equipment which, although not preventing the equipment from operating at given instant, may reduce the efficiency of operation considerably and result sooner or later in a temporary and partical reduction in performance due to inevitable repair /2/.

Measurements alone are not enough to determine reduction in the efficiency of power plant operation. Use of a mathematical model describing given process, usually together with material and energy balances, is therefore necessary /3/.

2. State estimation

The energetic efficiency of certain equipment like turbines and heat exchangers may reduce during operation as a result of leakage, contamination etc. These changes are typically slow and they have no direct drastic effect upon operation.

A mathematical model describing the process is used on the basis of measurement of certain typical operating variables to investigate the state that is to answer the question whether the difference between the measured values and those supplied by the model resulted from erroneous measurements or the state of some major equipment changed so that the model parameters characteristic of that equipment were no longer valid. What we want to know is what kind of change has occurred or is about to develop in which of the equipment.

The model parameters characteristic of the energetic state of the equipment like stage efficiency or thermal transmission factor etc. are based essentially on parameter estimation. However, balance equalization is necessary to decide whether new parameters have to be determined that is parameter estimation has to be carried out or the significant difference between the calculated and measured values resulted from erroneous, failing measurements only /4/.

3. Linear balance equalization

Values measured in the course of operation include pressure, differential pressure, temperature etc. For different reasons (instability in

time, error of measuring device, recurrent measuring error etc.), the values so obtained are more or less erroneous. A condition for acceptability of the measurements is that they satisfy the material and energy balances describing the process. The process is usually described by the following nonlinear input-output model:

$$y = F(p, x) \quad . \tag{1}$$

Linearized in the environment of the state of operation according to input variables of the model:

$$\begin{aligned} y &= F(P_o, x_o) + \left[\frac{DF}{DX}\right]_{p_o,\, x_o} (x-x_o) \ , \\ y &= y_o + A(x-x_o) \quad . \end{aligned} \tag{2}$$

Essentially, equalization is a correction of the values less deviating from the measured values in a certain sense and satisfying at the same time the heat and material balances constituting the heat-flow diagram model. It is usually minimization in a weighted quadratic sense where the weight matrix is a reciprocal of the diagonal matrix set up of mean square deviations.

New variables are introduced for the linearized model in order to use the usual relationships:

$$Y = \begin{bmatrix} x \\ y \end{bmatrix} \quad \text{and} \quad b = y_o - Ax_o \quad . \tag{3}$$

Thus the original linear model can be written in the following form:

$$WY - b = 0 \tag{4}$$

where

$$W = [A \,\vdots\, -E] \quad . \tag{5}$$

Let

$$Y_m = \begin{bmatrix} x_m \\ y_m \end{bmatrix} \tag{6}$$

be the vector of measurement results.

Now quadratic form

$$Q(Y) = (Y - Y_m)^* \, V^{-1} \, (Y - Y_m) \tag{7}$$

is minimized by linear balance equalization, where on the basis of variation in relation to measurement of input and output variables, the weight matrix will be

$$V=\begin{bmatrix} \delta^2_{x_{m1}} & & \\ & \ddots & \\ & & \delta^2_{y_{mn}} \end{bmatrix} . \qquad (8)$$

4. Filtering out of failing measurements

On certain assumptions, the measurements will be acceptable if

$$Q_{min} = Q(Y_{min}) < \chi^2_{0.95}(n) \qquad (9)$$

holds for the residual associated with the result vector.

If not, this means that the measurements are recurrently erroneous or a change occurred in the state of major equipment which made the value of parameter vector p_0 used questionable.

Almásy's gamma index /4/ can be used to test whether or not a recurrent major error is existing. Accordingly, measurement results for which the absolute value of Almásy's gamma lies in the vicinity of 1 are suspect of error.

5. Linear parameter estimation

Hence, if the χ^2 Test is negative but a value near 1 of Almásy's gamma is not obtained for any of the measured variables, it can be rightly assumed that a change has taken place in the state of the equipment, resulting in a new state that can not be represented by the value of model parameter associated with the old state. E.g. also model parameter kF characteristic of the value of the thermal transmission factor for given heat exchanger shall be reduced accordingly for the sake of appropriate modelling in case of contaminated heat transfer surfaces.

Since the changes are slow and thus difficult to detect, a linear-

ized model is used again where linearization according to the model parameters is also carried out now. That is

$$y = y_o + A\,(x-x_o) + B(p-p_o) \tag{10}$$

where

$$B = \left[\frac{DF}{Dp}\right]_{p_o,x_o} . \tag{11}$$

Taking into consideration identity

$$x = x_o + I\,(x-x_o) \tag{12}$$

and introducing variables

$$Y_p = \begin{bmatrix} \Delta x \\ \Delta y \end{bmatrix} \quad X_p + \begin{bmatrix} \Delta x \\ \Delta p \end{bmatrix} \quad \text{and} \quad M = \begin{bmatrix} I & 0 \\ A & B \end{bmatrix} , \tag{13}$$

where

$$\begin{aligned} \Delta x &= x-x_o \\ \Delta y &= y-y_o \\ \Delta p &= p-p_o \quad , \end{aligned} \tag{14}$$

model

$$Y_p = MX_p \tag{15}$$

is obtained. As the layout of the variables shows (13), now not only parameter vector p but also the input vector are present on the right side that is also the input vector shall be determined in the course of the estimation process.

With matrix V used again as a weight matrix, the expression to be minimized will be

$$J(X_p) = (Y_p - MX_p)\, V^{-1}\, (Y_p - MX_p) \quad . \tag{16}$$

Note that in practice, use of an arbitrary domain for minimization of (16) is usually not permissible. Namely, an unconditional linear parameter estimation can yield also a solution resulting in minimum value for J with, however, the physically optimum values of X_p falling within the inadmissible domain (e.g. the active heat transfer coefficient increases).

Therefore, it is necessary that

$$(X_p)_{min} \leq X_p \leq (X_p)_{max} \tag{17}$$

be stipulated for the minimization of (16).

6. Application example

Consider unit II of Tisza Thermal Power Plant again. In the simplified Block Diagram given in Figure 2, the points of measurement of the state variables that is temperature, pressure and mass flow have been indicated (see Fig. 2).

Temperatures were measured by means of a Rosemount 78 S resistance thermometer. The error of temperature measurement was $\pm$ 0.15%. A pressure transmitter of a cell factor of 1 mV/V was used for pressure measurements while the measuring orifices used in normal operation served for mass flow measurements. The pressure difference signals proportional to mass flow were fed to the data collecting units by a Rosemount C.719 transmitter. Mass flow figures were calculated in accordance with DIN1952-82.

An AOTT Kempton flowmeter of an accuracy of $\pm$ 2% as compared with the rated value, supplying a digital output signal, was used for measurement of the condenser coolant flow. A calibration type electric consumption meter was used to measure the wattage and the wattless component of the generator output power. By means of this measuring device, each phase can be measured independently in case of the three-phase system and the results can be summed to an accuracy of 0.2.

To obtain reliable information about the steady state, the measured characteristics were collected by means of 2 portable HP 2141 data collecting units controlled by a small HP 75 computer. This computer is capable of evaluating the measured signals immediately. Measurements were made under the conditions of rated electricity production, maximum electricity production and electricity production corresponding to 50% of the rated output.

On the basis of the measured input variables in case of rated load (Table 1), the rest of measured values has been determined by means of MODSIM /5/.

The relative difference between measured and calculated values is illustrated in Fig. 3. Although the difference is insignificant in general,

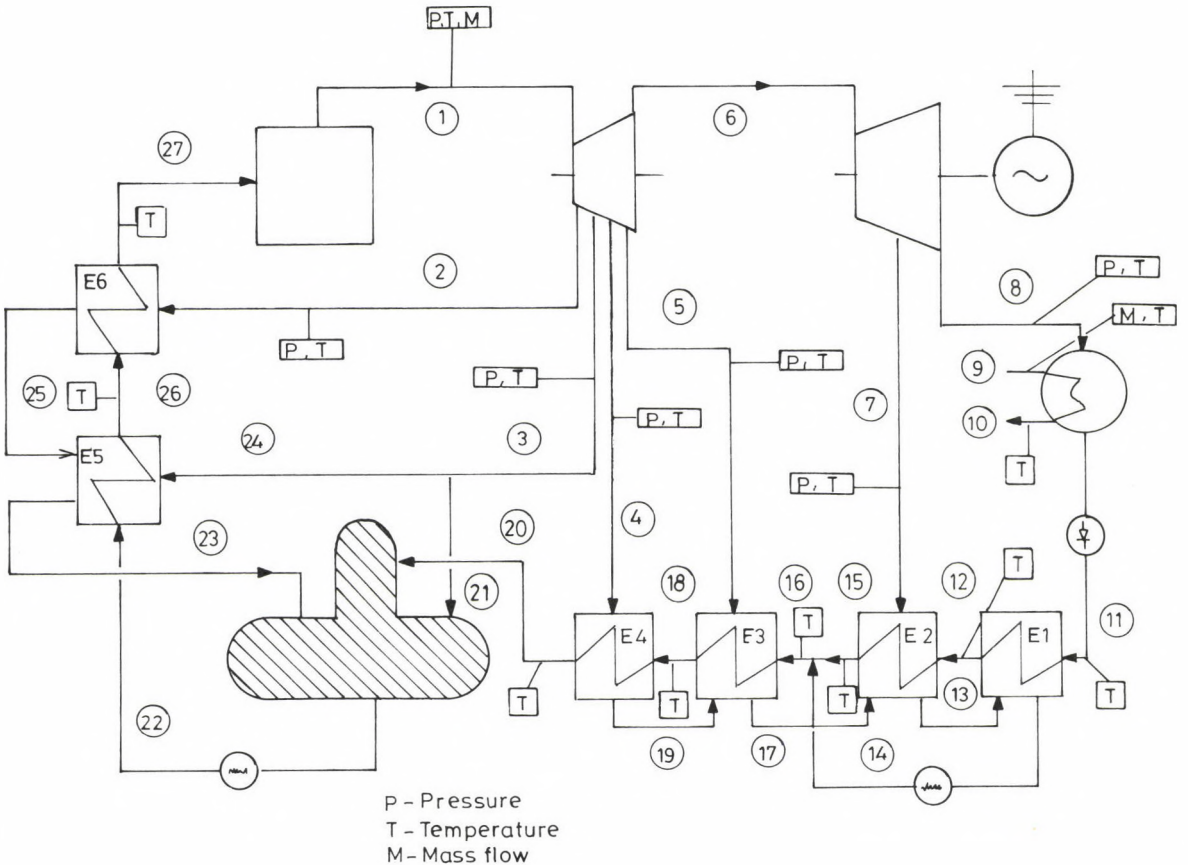
P,T,M
1
2
3
4
5
6
7
8
9
10
11
12
13
14
15
16
17
18
19
20
21
22
23
24
25
26
27
E6
E5
E4
E3
E 2
E1
P , T
M , T
T
P - Pressure
T - Temperature
M - Mass flow

Fig. 2.

Table 1

Variable	Measured values	Calculated value	Variation of measurement	Instrument error	Overall variation
1 Live steam flow rate, kg/s	48.180	input	0.520	0.480	0.708
2 Live steam pressure, bar	88.250	input	0.910	0.880	1.266
3 Coolant flow rate, kg/s	1006.320	input	10.200	10.000	14.284
4 Coolant inlet temperature, ^{o}C	15.600	input	1.100	0.500	1.208
5 Live steam temperature, ^{o}C	520.500	input	6.270	1.000	6.349
6 Bleed 1 temperature, ^{o}C	332.200	337.590	2.300	1.000	2.508
7 Bleed 1 pressure, bar	18.200	18.850	0.310	0.500	0.588
8 Bleed 2 temperature, ^{o}C	251.000	253.750	2.100	1.000	2.326
9 Bleed 2 pressure, bar	8.760	8.890	0.210	0.500	0.542
10 Bleed 3 temperature, ^{o}C	149.900	152.400	2.000	1.000	2.236
11 Bleed 3 pressure, bar	3.080	3.190	0.120	0.300	0.323
12 Bleed 4 temperature, ^{o}C	95.500	97.770	1.300	0.500	1.393
13 Bleed 4 pressure, bar	0.921	0.935	0.080	0.100	0.128
14 Bleed 5 temperature, ^{o}C	72.600	74.390	1.100	0.500	1.208
15 Bleed 5 pressure, bar	0.365	0.379	0.020	0.100	0.102
16 Condensate temperature, ^{o}C	30.200	31.590	0.900	0.500	1.030
17 Condensate pressure, bar	47.100	46.430	2.000	5.000	5.385
18 Coolant outlet temperature, ^{o}C	23.700	24.520	1.100	0.500	1.208
19 Preheater 1 inlet temperature, ^{o}C	30.600	31.420	1.080	0.500	1.190
20 Preheater 1 outlet temperature, ^{o}C	39.200	39.530	1.300	0.500	1.393
21 Preheater 2 outlet temperature, ^{o}C	70.300	71.350	1.810	0.500	1.878
22 Preheater 3 inlet temperature, ^{o}C	65.200	65.160	1.920	0.500	1.984

Table 1 (cont.)

Variable	Measured values	Calculated value	Variation of measurement	Instrument error	Overall variation
23 Preheater 3 outlet temperature, °C	89.600	91.760	1.500	0.500	1.581
24 Preheater 4 outlet temperature, °C	127.01	129.400	2.000	1.000	2.236
25 Preheater 5 outlet temperature, °C	164.3	167.800	2.100	1.000	2.326
26 Preheater 6 outlet temperature, °C	194.9	201.470	1.850	1.000	2.103
27 Electric power, MW	50.23	51.570	0.780	0.915	1.202

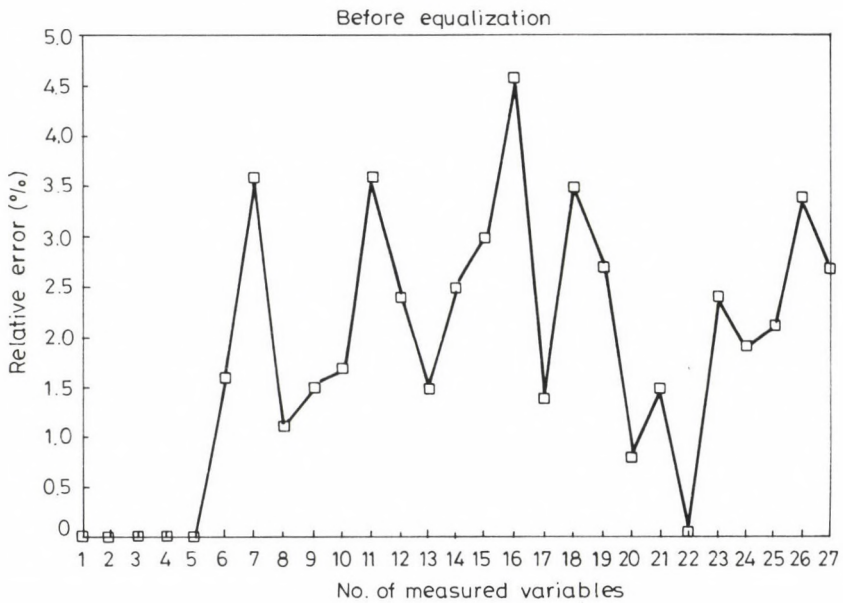

Fig. 3. Model error

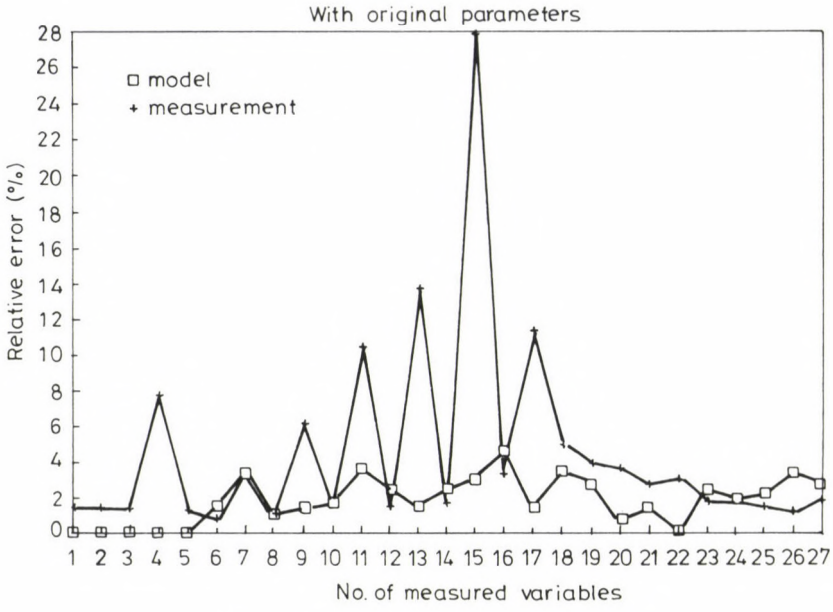

Fig. 4. Measurement error and model error

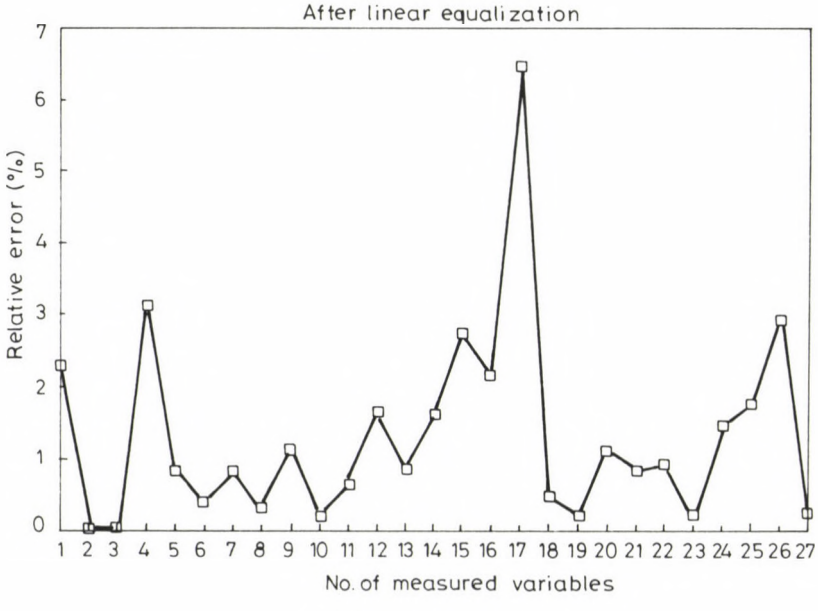

Fig. 5. Model error

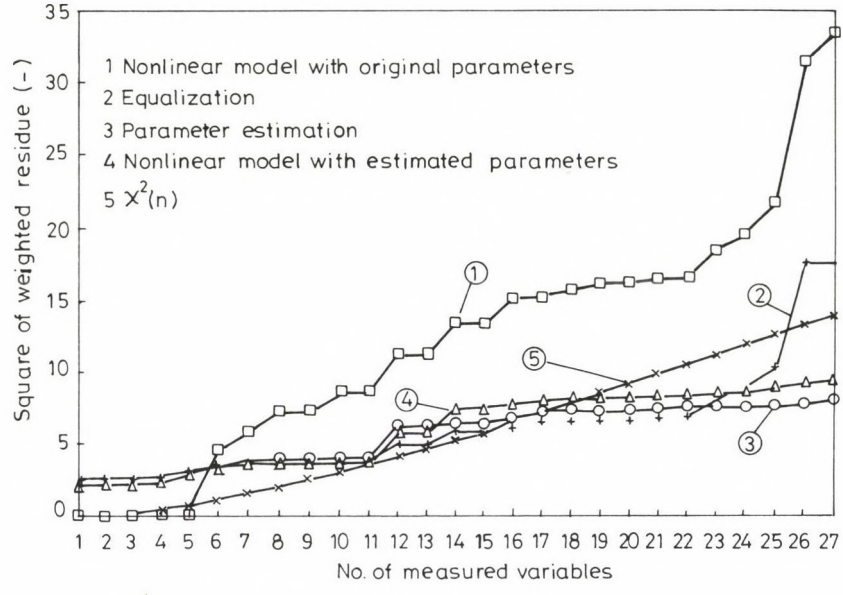

Fig. 6. Result of state estimation

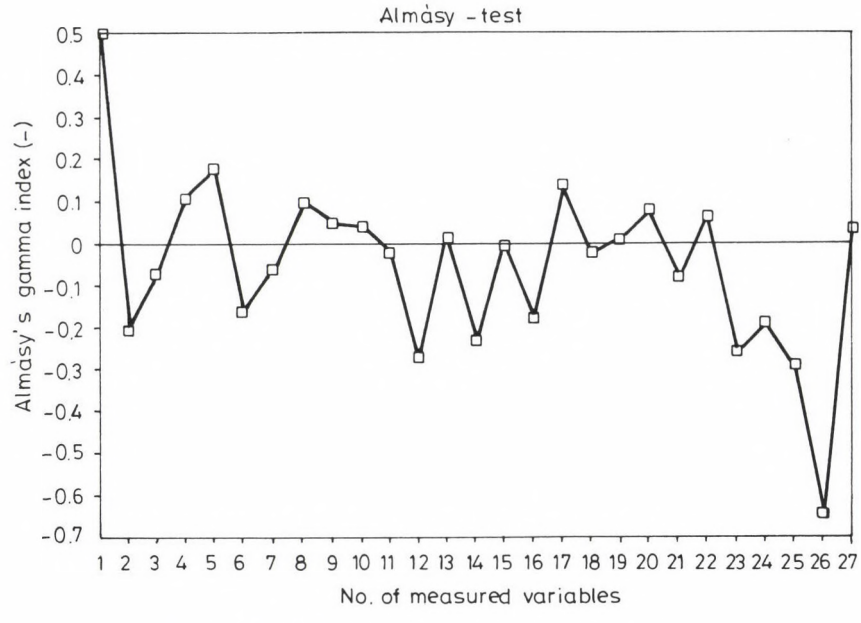

Fig. 7. Detection of failing measurements

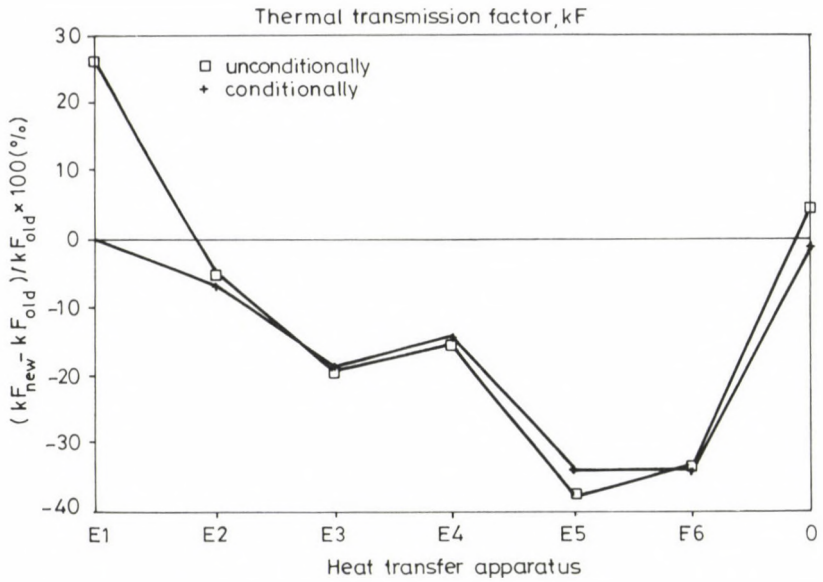

Fig. 8. Result of parameter estimation

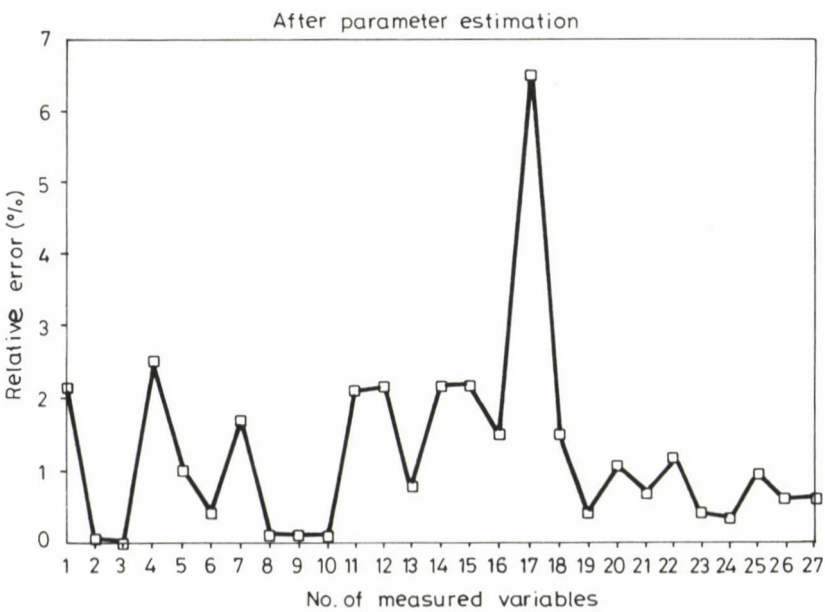

Fig. 9. Model error

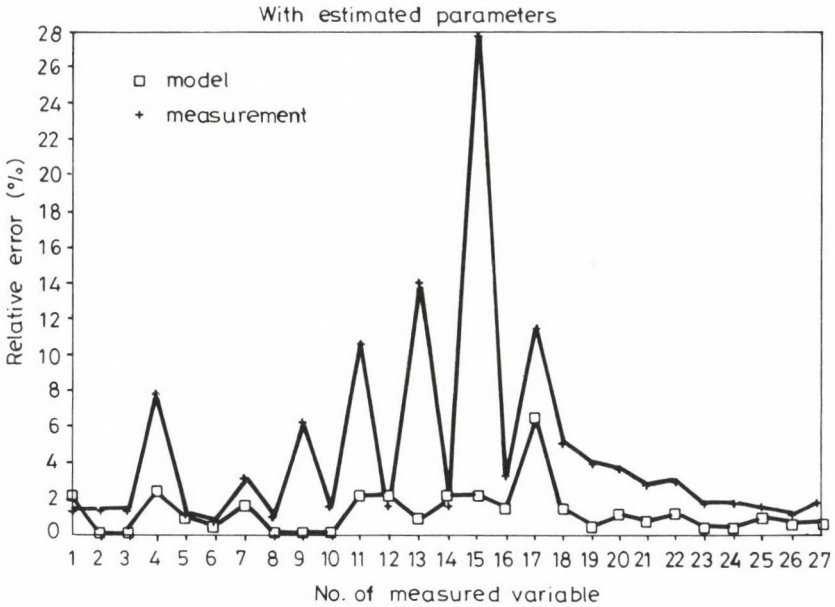

Fig. 10. Measurement error and model error

the error of the model was found to lie above the error of measurement for some variables in a comparison of the measured and simulated values (Fig. 4). The differences after linear equalization can be seen in Fig. 5. The χ^2 test was positive for the residuum of equalization (see Fig. 6). Therefore, Almásy's gamma index was calculated for every variable as shown in Fig. 7 to see whether the positive χ^2 can be attributed to failing measurements or not.

No failing measurements could be detected. Hence, linear parameter estimation was used as an additional possibility of reduction of the residuum. The values of kF for the different preheaters and the condenser were considered as a parameter. The results of parameter estimation are shown in Fig. 8, indicating the values obtained for the parameter both unconditionally and conditionally (permitting reduction only). The model error obtained in calculation with the new parameters is shown in Fig. 9. As can be seen in Fig. 6, the differences between measurement and calculation reduced after parameter estimation in spite of the fact that the linearized model had been used for parameter estimation and thus the nonlinear model had resulted in a somewhat greater residuum.

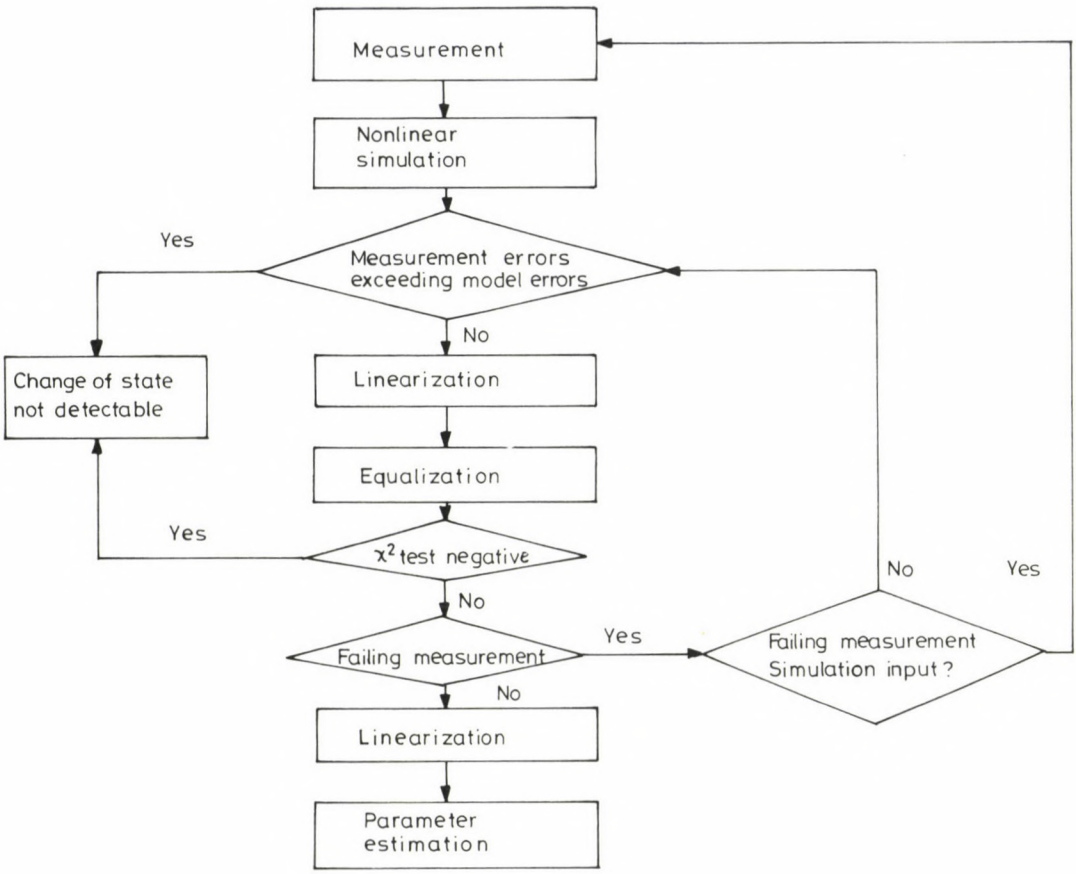

Fig. 11. State estimation process

Finally, Fig. 10 shows that after parameter estimation, the error of measurement exceeds the error of the model for almost every variable.

ACKNOWLEDGEMENT

The useful advices of Prof. Dr. Gergely Büki have significantly contributed to the professional value of this work. I feel therefore indebted to Professor Büki and express my sincere thanks for his contribution.

LITERATURE

1. Davis, D.A. et al.: Availability of Thermal Generating plant Proceedings of the 13rd World Energy Conference, Working Group 1, Cannes, France (1986), 287-295

2. Chiv, C.: Identify Electric Output Losses of PWR Nuclear Plants. Power, Sept. (1986), 35-39

3. Gilles, E.D. - Nicklaus, E. - Palke, M.: Sensortechnik in der Chemie - Status und Trend Chem. Ing. Techn. 58 (1986), 557-564

4. Almásy, G.: Balance equations and measuring errors (in Hungarian) Doctor's Thesis (1980)

5. Paláncz, B.: A Modular Approach to the Simulation of Steam Turbine Cycles. Applied Energy 30 (1988), 147-152

Acta Technica Acad.Sci.Hung., 103(4), pp. 279-297 (1990)

DEVELOPMENT OF FLUIDIZED-BED FIRING TECHNOLOGY IN THE INSTITUTE FOR ELECTRIC POWER RESEARCH

REMÉNYI, K.*

(Received: 20 February 1991)

A new firing technology has been developed by the Institute of Electric Power Research (VEIKI). The new technology can be realized on the basis of a fluidized-bed combustion system with cooled combustion chamber surfaces using a specially designed, aerodynamically favourable free-board geometry permitting the entire volume of the combustion chamber to be utilized as well as a simple but efficient wall cooling system.

In the quick bed, a simple injection system can be used due to the good mixing conditions and favourable partial load conditions. The required temperatue of 800 to 900 °C can be reached even without the use of cooling surfaces and the space above the layer can be used for combustion of the coal particles blown into the chamber separately.

A so-called "hybrid" fluidized-bed/pulverized coal firing technology where 30-70% of the heat input enters the combustion chamber through mills without separator and pulverized coal burners has also been tested in practice. To reduce the sulphure dioxide emission, pulverized limestone or dolomite can be fed to the fluidized bed. This technology can be ideally used for soft or hard brown coals or waste materials.

Introduction

The Institute for Electric Power Research (VEIKI) has been dealing with the development of coal firing — including both conventional (pulverized-coal firing) and new (fluidized-bed firing) techniques — for decades.

Experimentation in the Institute includes both laboratory and industrial scale experiments.

*Reményi, Károly, H-1014 Budapest, Úri u. 38. II/I. 10, Hungary

Akadémiai Kiadó, Budapest

Laboratory experiments

Experimental equipment:

Three-draft forced-circulation hot-water boiler of individual design with atmospheric fluidization for pilotscale experiments (Figs 1 and 2).

Boiler specifications:

effective heat output	0.5 MW
fluidized-bed temperature	750-900 ^{o}C
grain size of bed material	0.8-1.2 mm
max. grain diameter	6 mm
cooling water flow rate	4 kg/s
average bed cross section	0.49 m^2
bed cooling surface	1.39 m^2

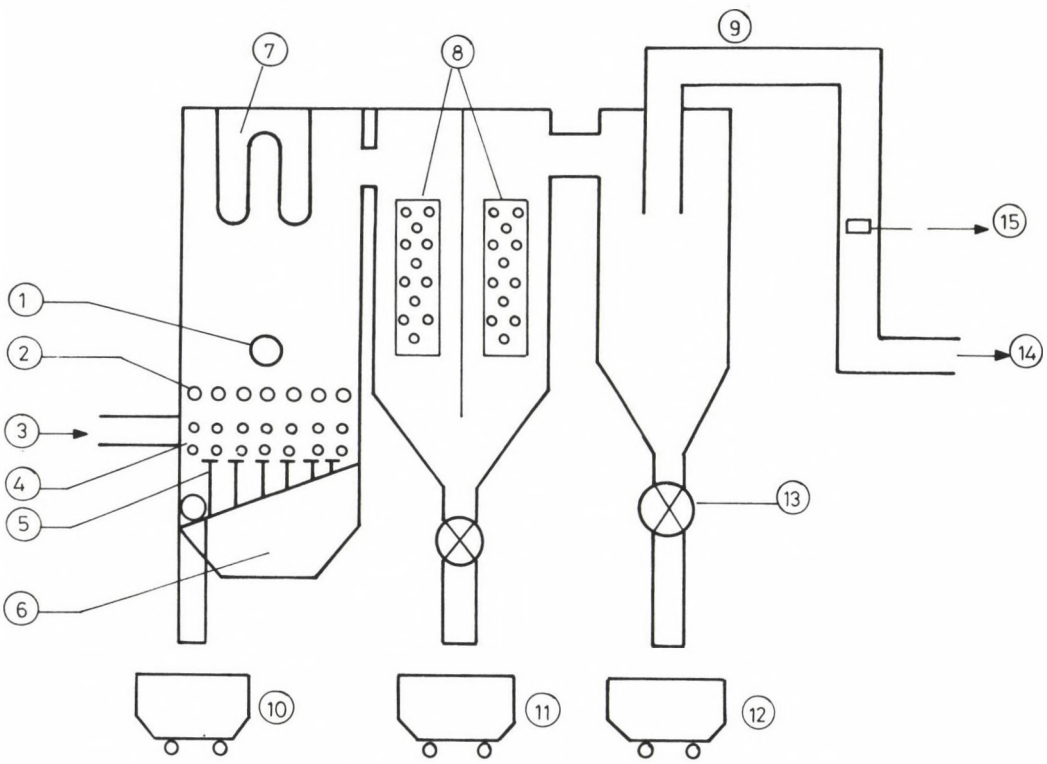

Fig. 1. Laboratory experimental set-up for fluidization experiments
(1 - starting burner, 2 - secondary air, 3 - coal, 4 - bed cooling pipes, 5 - air nozzles, 6 - air box, 7 - combustion chamber pipes, 8 - heat exchanger, 9 - cyclone, 10 - bed material discharge, 11 - coarse fly-ash, 12 - cyclone fly-ash, 13 - cell-type feeder, 14 - flue-gas exhaust, 15 - gas analyzer)

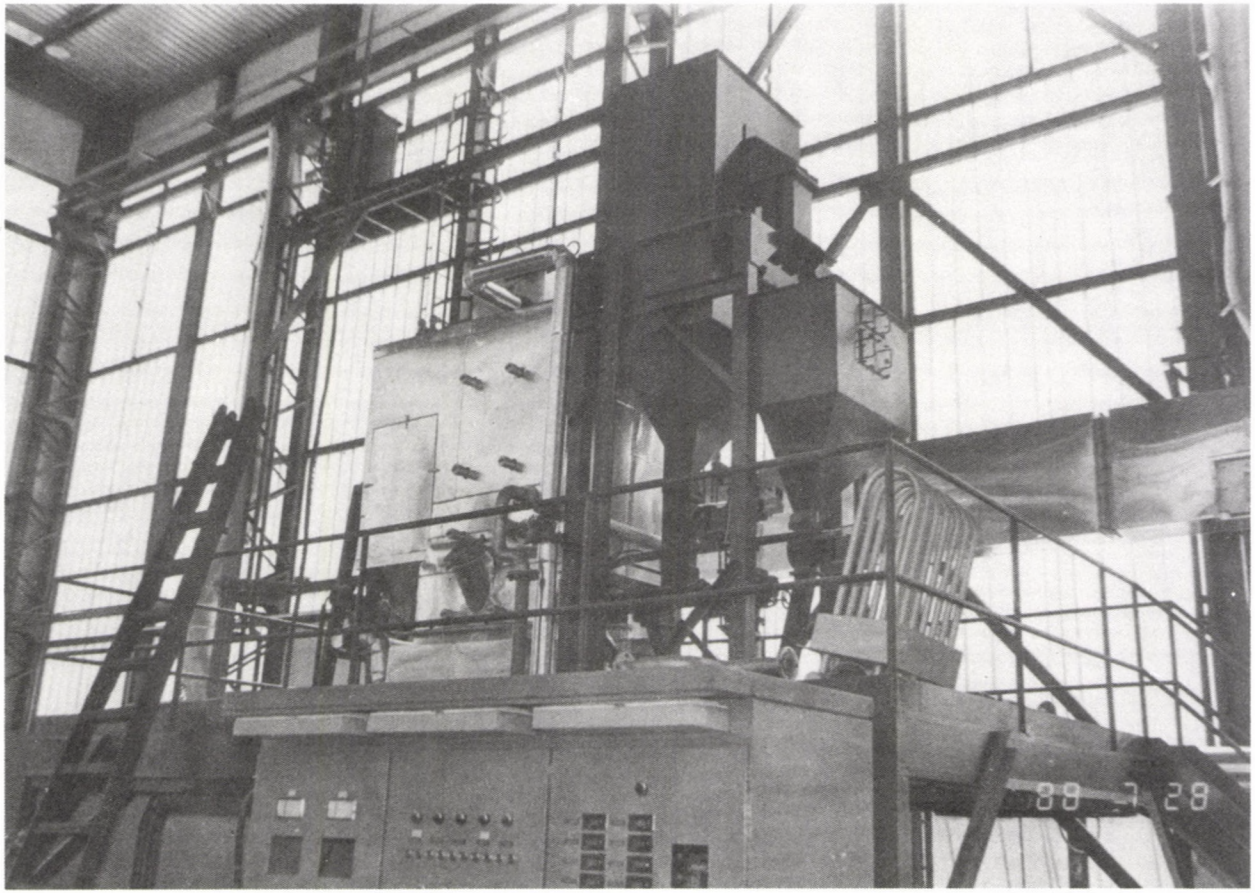

Fig. 2. Photograph of experimental boiler

convective heating surface	4.83 m^2
outdoor cooling surface	0.628 m^2
height of bed material	0.4-0.6 m
rate of fluidization	1.5-2.3 m

Combustion air supply takes place through the nozzles in majority while a minor part, the so-called "secondary air", enters the combustion chamber through holes somewhat above the bed surface at a similarly controllable rate. Secondary air supply is necessary first of all because of burning of carbon monoxide.

The fuel supply system has a bin for coal and a bin for additives. The required feed rate and mixing ratio can be adjusted by means of a cell-type feeder of regulatable speed provided for the bottom of either bin. From the cell-type feeders, the coal and additives get through descent pipes onto a worm conveyor which feeds the coal and the mixture to the combustion chamber at about half height of the bed.

A cyclone and a filter with teflon bag, arranged after the flue gas outlet, provide for fly-ash separation.

Three finned aluminium coolers serve for recooling of the output water stream as required.

No automatic control is provided for the equipment for the time being.

Results

Our investigations included two main fields, such as

— environmental problems (e.g. SO_2, NO_x emissions and their parameter dependence and optimization, experiments with additives etc.),

— operating and constructional problems to work out recommendations (such as e.g. cold starting and emergency shutdown strategy etc.).

Crushed coal from Ajka and Tatabánya has been used for the firing experiments.

SO_2 emission

The temperature dependence of specific sulfur dioxide emission (related to total sulfur) is shown in Figs 3 and 4. It can be seen that maximum sulfur separation (minimum emission) takes place at a temperature of 820 ^{o}C that is below 880 ^{o}C, first of all because the equilibrium carbondioxide point is shifted by fluidization air. In the range of higher temperatures, less sulfur can be absorbed by the so-called "overburnt" calcium oxide.

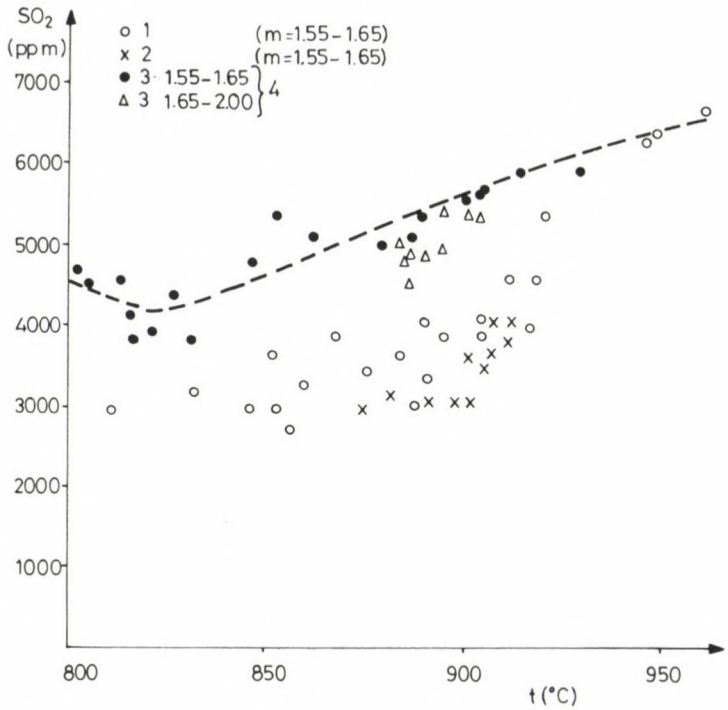

Fig. 3. SO_2 temperature dependence (for coal from Tatabánya)
(1 - with limestone feed, 2 - with dolomite feed, 3 - excess air, 4 - without additive)

As suggested by the process, the bed temperature shall be adjusted to a value of about 820 ^{o}C if energetically and economically reasonable.

NO_x emission

For structural reasons and with respect to slag melting, the bed temperature had to be kept below 900 ^{o}C. Therefore, thermal and spontaneous NO_x were present in spots only.

In the course of investigations, no clear, significant relationship could be detected between NO_x emission and bed temperature or if indeed at all, the effect was insignificant as compared with changes due to other parameters.

There is a close and definable relationship between nitrogen oxide emission and carbon monoxide developing in the combustion chamber. For coal from Ajka, this relationship is illustrated in Fig. 5 (assuming excess air of m = 1).

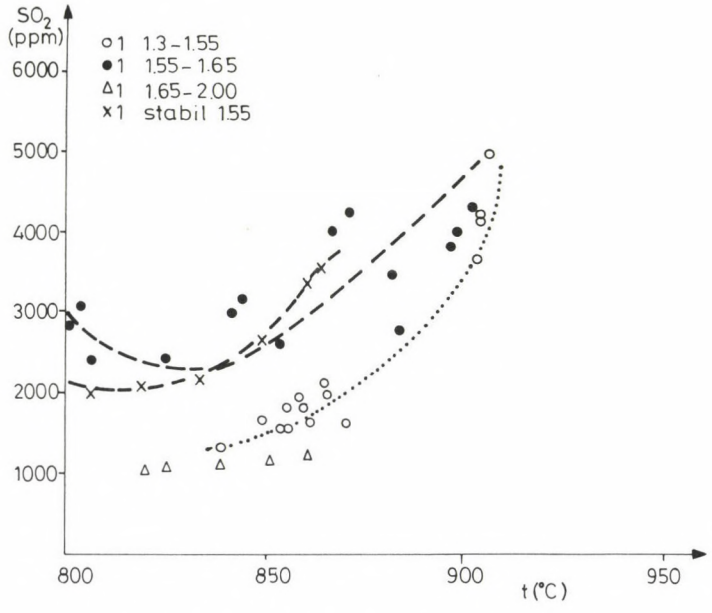

Fig. 4. SO_2 temperature dependence (for coal from Ajka)
(1 - excess air)

The high CO is not appearing at the flue-gas outlet of the boiler because it can be burnt with secondary air in the upper region of the combustion chamber without increase in NO_x content.

The above relationship suggests that, in respect of NO_x, the combustion will be optimum if maximum CO, still safely burnt with secondary air, is developing in the combustion chamber. This requirements is in agreement with experience in relation to NO_x reduction in case of vacuum firing.

New fluidized-bed firing equipment

Considering how long the principle of fluidized-bed firing has been available, the technology itself is finding use at a surprisingly slow rate. However, in addition to advantages of quite a number offered by fluidized-bed firing, there are problems of a similarly large number which explain the limits set to the wide use of the technology. One of these problems, perhaps the most important one, is the unpredictably low rate of

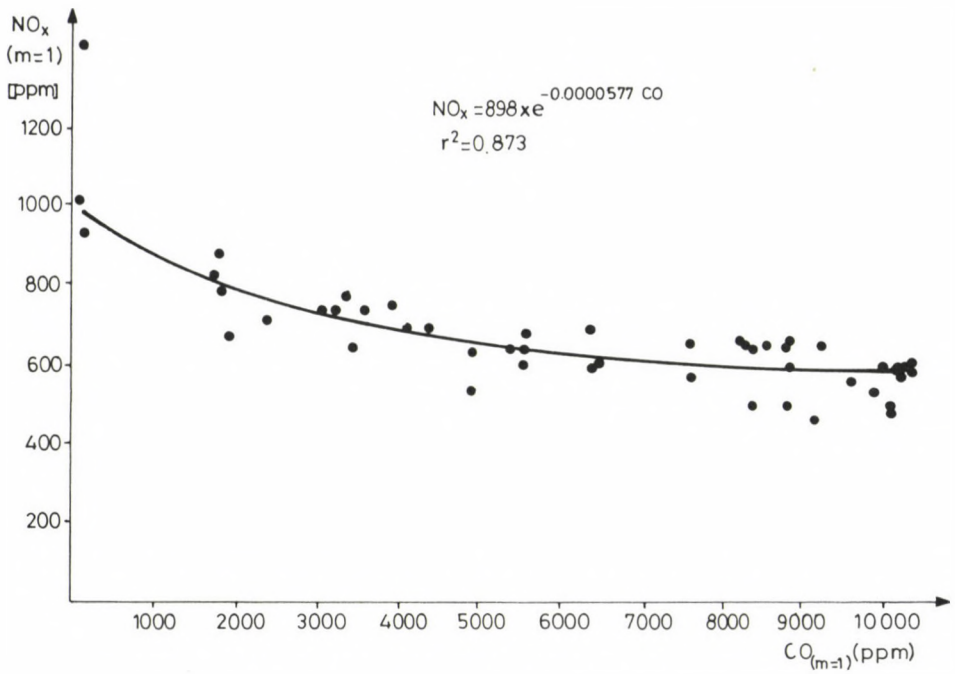

Fig. 5. Relationship between combustion chamber CO and specific NO_x

increase in energy demand. Other problems are encountered in relation to the boiler for fluidized-bed firing. The desirable high power station unit capacities have not been available yet. At the same time, in spite of a substantial reduction in size, the equipment prices have not reduced proportionally as compared with the conventional equipment furnished with SO_2 and NO_x separators. No appropriate equipment is available for utilization of the extremely high rate of heat transfer inherent in the fluidized bed. Essentially, two major types of equipment have been used so far for atmospheric fluidized-bed combustion techniques, such as

— bubbling-fluidized-bed firing (BFB) plant and

— circulating-fluidized-bed firing (CFB) plant.

In case of bubbling-bed firing, limits are set to unit capacity by the bed size. In case of circulating-bed firing, the capacity can be increased but generating sets (precipitators, feeders, conveyors baffles) of a special design shall be used.

Environmental considerations rage at first place among factors contributing to a wide use of fluidized-bed combustion technology. Note that

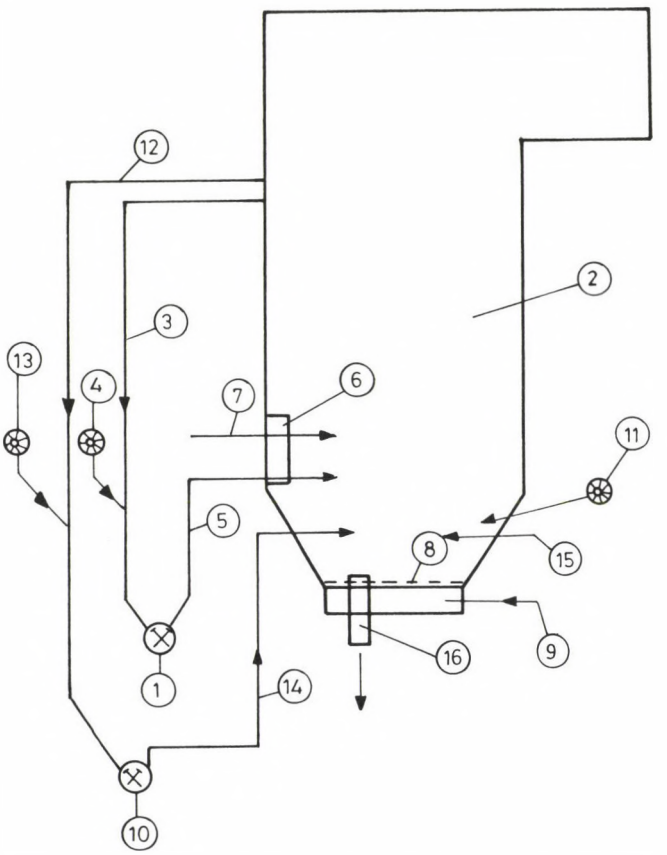

Fig. 6. Schematic illustration of fluidized-bed firing using the VEIKI process
(1 - fan-mill with separator, 2 - combustion chamber, 3 - flue gas resuction, 4 - coal-feeder, 5 - PC-ducts, 6 - coal burner, 7 - secondary air duct, 8 - wind box, 9 - main air ducts, 10 - fan mill without separator, 11 - spreader, 12 - flue gas resuction, 13 - coal-feeder, 14 - PC-duct, 15 - seconder air, 16 - bottom ash removal)

the competition between conventional steam boilers with SO_2, NO_x separators and fluidized-bed boilers is still in the balance.

At the same time, elimination of environmental pollution by old plants representing a substantial part of the energy system remains a problem to be solved. That means that SO_2 and NO_x separators shall be provided for the old plants.

In the Institute for Electric Power Research (VEIKI), Hungary, a so-called hybrid fluidized-bed combustion technology has been developed with a view to reduce environmental pollution by old pulverized-coal fired

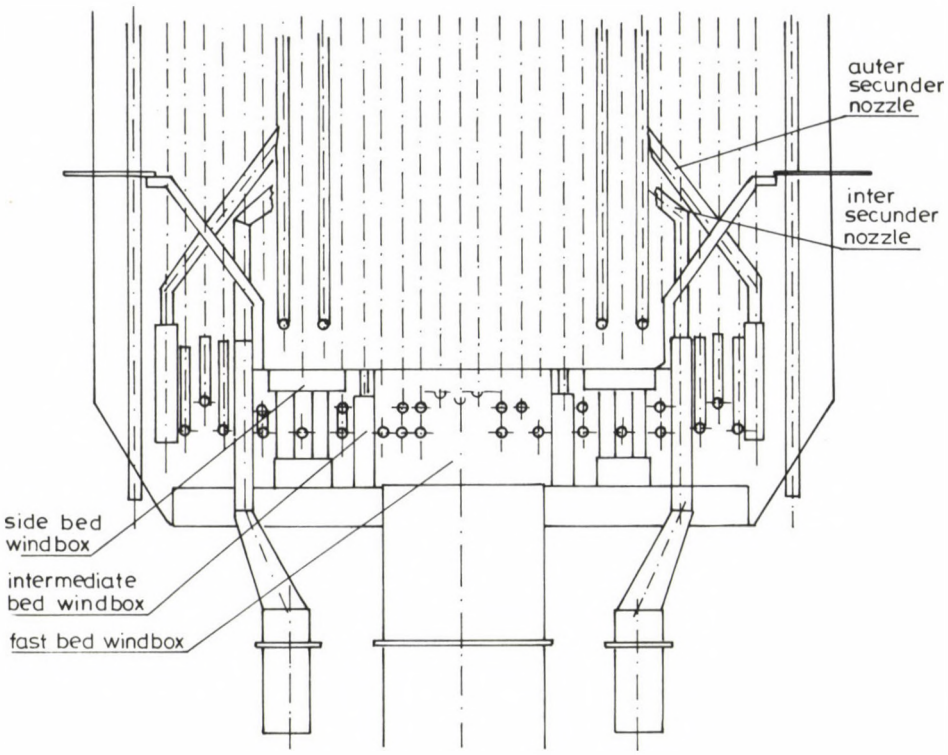

Fig. 7. Air distribution according to the VEIKI process

boilers and, on the other hand, to develop new boiler types (Figs 6 and 7).

The most important objects of the R&D program have been

— improvement of the conditions of combustion when coals of variable quality (7-12 MJ/kg, 35-50% ash content) are burnt,

— utilization of by-products of coal mining (interts, tailings),

— utilization of the benefits of fluidized-bed combustion technology in respect of environmental protection (reduction of SO_2 and NO_x emissions) and

— use of the new technology with existing boilers.

In the course of design of the equipment for fluidized-bed combustion, the following problems had to be solved:

— starting of fluidized-bed firing,

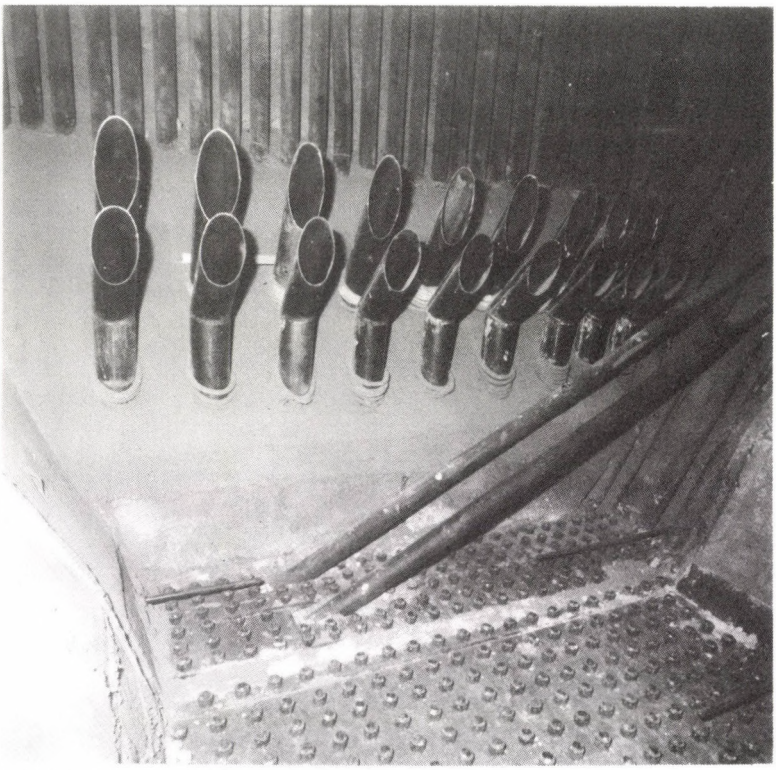

Fig. 8. Photograph of VEIKI fluid-bed combustion at the Thermal Power Plant of Tatabánya

-- coal feed,

-- appropriate air injection and distribution

-- removal of excess material from the bed.

An oil-fired flue-gas generator was used to start the process (that is to heat primary air to a temperature of approx. 400 ^{o}C) and an oil-jet lance was directed down-ward to the bed.

Implementation at the Thermal Power Plant of Tatabánya

The first boiler to be reconstructed had been equipped originally with four blowers of which two blowers had been used to support pulverized-coal firing in the boiler of original construction while two blowers served to feed the fluidized bed after reconstruction. The system is schematically illustrated in Fig. 8 (VEIKI patent).

Introduction of the fluidized-bed technology at the Thermal Power Plant of Tatabánya resulted in an advanced technological process at an existing old power station. Attempts have been made all over the world to utilize low-grade coal but no success in balance with the expenditure has been achieved so far. Some sophisticated, rather expensive, methods to utilized low-grade coal are available, however. In case of the equipment developed by VEIKI, the specific (cross-sectional) heat release increased two-to-threefold as compared with other equipment in operation in the world. The new practice is unique also in that it offers a technology that can be used either independently for fluidized-bed firing or pulverized-coal firing or for both in combination. The technology can be ideally used for burning of by-products of coal mining and lignites and it helps to meet the environmental requirements even in case of existing old boilers.

The rate of so-called internal and external secondary air supply can be regulated separately.

Operating experiences, experimental results

Experimental operation and testing in September–October 1986:

In case of continuous operation, 40-70% of the coal enters the combustion chamber through mills without separator while the rest through mills equipped with separator.

This "hybrid" combustion resulted from operation with at least one mill without air separator and the steam output was less than 40 t/h. Most successful operation resulted from use of mill No. 2 (without separator) and mill no. 3 (with separator). Other mills were also operated. Due to the fluidized bed, the combustion chamber temperatures were lower and more homogeneous and the combustion itself was stabler than in case of coal firing.

In case of operation with one mill without separator, the steam output ranged between 12 and 28 t/h (max. 18-24 MW in terms of coal-heat conversion) as a result of combustion in fluidized bed, equalling a specific heat release of 4-5 MW/m^2 from the bed. This value exceeds the typical value of 1.5-2 MW/m^2 for conventional fluidized-bed firing considerably. The value includes also the effect of after-firing above the bed but the contribution of this effect has a theoretical significance only.

Temperatures below 850 ^{o}C were measured in the upper part of the combustion chamber by means of two temperature sensors. These temperatures are very close to bed temperatures, which means that the technology used resulted in so-called "cold burning", a process rather favourable in respect of environmental protection.

The boiler operation was easy to control. Thus the adequate method was used for temperature regulation.

Independently of the number of mills used, the operation was stable, backfires did not occur during combustion. Except for the starting process, use of oil to support combustion was not necessary. The capacity could be increased as compared with coal firing, a significant advantage in case of heating power stations.

In case of two-mill operation including mill No. 3 (with separator), a steam output as high as 42-48 t/h could be achieved. At the same time, temperatures of about 950 ^{o}C were measured in the higher section of the combustion chamber. In the 1986/1987 winter period, the steam output was stabilized at 35-40 t/h to avoid possible adverse effects of undesirably high temperatures.

Using the same coal of an ash content of 38-50% for both equipment, the VEIKI equipment proved to be more reliable as compared with some imported equipment for fluidized-bed combustion which had to be shut down after two or three days of operation because of accumulation of the bed material.

As compared with conventional boilers, the efficiency of combustion increased by 2-4%. At the same time, the flue gas losses were by about 0-1% higher. Accordingly, the actual increase in efficiency is 1.5-2.5%. By use of a method based on in-depth analysis developed by VEIKI, the efficiency of fluidized-bed boilers can be further improved.

After successful accomplishment of development in the year 1986, the boiler for fluidized-bed combustion was put into service and operated continuously at the Thermal Power Station of Tatabánya during the winter. In this period, the steam output did not exceed a value of 40 t/h in accordance with the contract concluded between VEIKI and the power station.

Mills No. 2 and 4 were operated without separator (the latter having been connected to the original burner).

To complete the program and upon request of the power plant management, also full-capacity boiler operation had to be investigated. For this purpose, the boiler has been operated as the only steam generating unit of

the power station continuously for a week (steam output: 25-58 t/h). The boiler efficiency was about 86% and the losses in both combustion and flue gas reduced as compared with low-capacity operation.

Research is continued. Within the framework of the National Scientific Research Fund (OTKA), several problems of a great importance from both a theoretical and a practical point of view (aerodynamics, heat exchange) have been investigated and, on the basis of a contract concluded between VEIKI and MVMT (Hungarian Electricity Board), research to optimize the sulfur-dioxide retention by limestone is going on.

Modification of the boilers of Ajka Thermal Power Plant

International commitments (reduction of SO_2 and NO_x emissions) and the increasingly strict national environmental regulations necessitate that new technologies resulting in reduction of damages to the environment be widely used. The fuel used for the steam generators of 100 t/h operated at the Ajka Power Plant and especially the high CaO typical of the ash content of the coal used offer a firm basis for reduction of the significant sulfur emission. Preparatory series of experiments run by VEIKI proved that as a result of appropriate co-ordination of luidized-bed firing and conventional pulverized-bed firing, 55 to 75% of the sulfur could be absorbed that is, both sulfur-dioxide and, to a reduced extent, nitrous gas emissions could be significantly reduced.

In order to achieve the above results, the construction and the control system of the boiler as well as the firing process have to be modified fundamentally for the first time in the country.

Modification of boiler construction

The bottom of the boiler shall be reshaped to permit a new air distribution system, the key element in fluidization, to be developed. A membrane bottom connected to the circulation system is provided for the membrane-walled boiler of natural circulation, a perfectly new design which provides continuous safe cooling for the bottom and, due to the air-right construction, reduces false air intrusion considerably resulting in the last analysis in improvement of the boiler efficiency. Thus also the fuel consumption reduces and as a result, harmful emissions reduce as well.

To improve the conditions of combustion and to increase the residence time of fuel in the combustion chamber so that the necessary reactions between calcium oxide and sulfure dioxide will take place, vertical recirculation has been introduced in the combustion chamber with different air blow rates. Air blow rates of 5-7 m/sec and 2-3 m/sec can be adjusted for the central layer and outermost layers, respectively. According to preliminary calculations, the additional fuel load in the combustion chamber due to the two vertical recirculation zones results in a much more homogeneous vertical temperature distribution along the combustion chamber and in a maximum combustion chamber temperature of 1050 ^{o}C. This means a temperature reduction of 300 ^{o}C as compared with the present value, an obvious advantage in respect of reduction of nitrous gas emission.

Another advantage is that no slagging, typical of boiler operation at the Ajka Power Plant, is required at that temperature. Thus use of the equipment for slagging as well as shoot pipes can be avoided and the boiler jacket can be made perfectly air tight.

Fluidized-bed and conventional pulverized-coal firing can be used in combination for boilers of a rated capacity of 100 t/h. In this case, the pulverized-coal burners are rearranged that is removed from the corners and arranged along the front wall and rear wall of the boiler to supply both the fluidized bed and the layer above it. The new firing process requires that also the air system be modified by introduction of delayed air feed in accordance with the recent results of research, another contribution to reduction of nitrogen oxide formation.

Modification of firing techniques

As compared with conventional pulverized-coal firing, coarser coal grains are required for fluidized-bed combustion. Therefore, two of the coal mills shall be adjusted to coarse grinding and thus the component for fine grinding, the so-called air separator, becomes unnecessary. In this way, not only energy can be saved but also the service life of the mills increases four-to-fivefold and, in the last analysis, the reliability and availability of the boiler itself increase.

In case of fluidized-bed combustion, a minimum boiler load of 40 t/h can be guaranteed without the use of oil to support combustion. Thus also the oil system becomes unnecessary.

For starting of a cold boiler, use of a flue-gas generator with its own oil burner and automatic control system is planned. By means of the flue-gas generator, the mixture of air and flue-gas entering the boiler at the bottom is heated to a temperature of 450 ^{o}C together with the bed material fed to the boiler earlier. Two oil burners provide for additional heat required to reach ignition temperature depending on the quality of coal available. According to calculations, ignition takes place at a temperature of 650-700 ^{o}C. After coal feed has been started, the bed temperature shall be stabilized at 850 ^{o}C. Then the burners used for starting can be switched off.

The low-grade coal from Ajka can be burnt in the fluidized bed without any difficulty for electricity generation at the Ajka Power Plant. Use of a mixture of coals of different grade is also possible, a practice finding increasing use in the Hungarian power system.

Coal specifications

The ash of coals from Ajka has a typically high CaO, MgO, K_2O and Na_2O content. This composition is advantageous in that much of the sulfur is absorbed by the ash itself but at the same time disadvantageous because the heating surfaces are contaminated by the alkali components. Namely, the alkali results in formation of eutectic mixtures of low melting temperatures which, after sublimation, condensate on the afterheating surfaces. The deposition process has been simulated in laboratory. It was found that deposition started at temperatures above 950 ^{o}C and the rate of deposition on the surface of the probe of a temperature of 300 ^{o}C was maximum at temperatures of about 1000 ^{o}C. No ash deposits on the heating surfaces have been detected so far in the course of pilot-scale experiment or normal operation with coal from Ajka in the fluidized bed.

Coal specifications (design values):

W^r	18.8%
A^r	34.9%
C	29.83%
H	1.4%
S_c	3.17%
O	11.4%
N	0.4%
Heat value	9.643 MJ/kg

Boiler specifications:

Outlet pressure of steam (after superheater)	74 atg	73.6 bar
Outlet temperature of steam (after superheater)	500 °C	
Feed water temperature	190 °C	
Maximum output (for 190 °C feed water)	100 t/h	27.8 kg/s
Peak output	120 t/h	33.3 kg/s
Air preheating	260 to 305 °C	

Design data of boiler reconstruction:

	Alternative A	Alternative B
Maximum output (for 190 °C feed water)	120 t/h 33.3 kg/s	100 t/h 27.78 kg/s
Heat demand of steam (2596 kJ/kg)	86.533 MW	72.111 MW
Fuel heat (for 85% boiler efficiency)	101.7 MW	84.82 MW
Coal based heat for flue-gas generation (for 89% heat transfer efficiency)	97.228 MW	81.024 MW
Fuel flow rate for coal of a heat value of 9.643 MJ/kg	37.97 t/h 10.55 kg/s	31.67 t/h 8.8 kg/s

On the fuelling process

The quick bed of small cross-section results in increased pulverized coal and gas circulation within the combustion chamber. At the same time, the flue-gas temperature is homogenized at a low value and the increased pulverized-coal concentrations and the resultant increased heat transfer result in a heat absorption corresponding to the evaporation heat of steam at the walls. Not only should the technology be suited for use with low-grade coals and for increased output but it should be optimum also in respect of reduction of sulfure dioxide emission. It is therefore necessary that

— as much as possible coal and combustible sulfur content of coal be released in the bed,

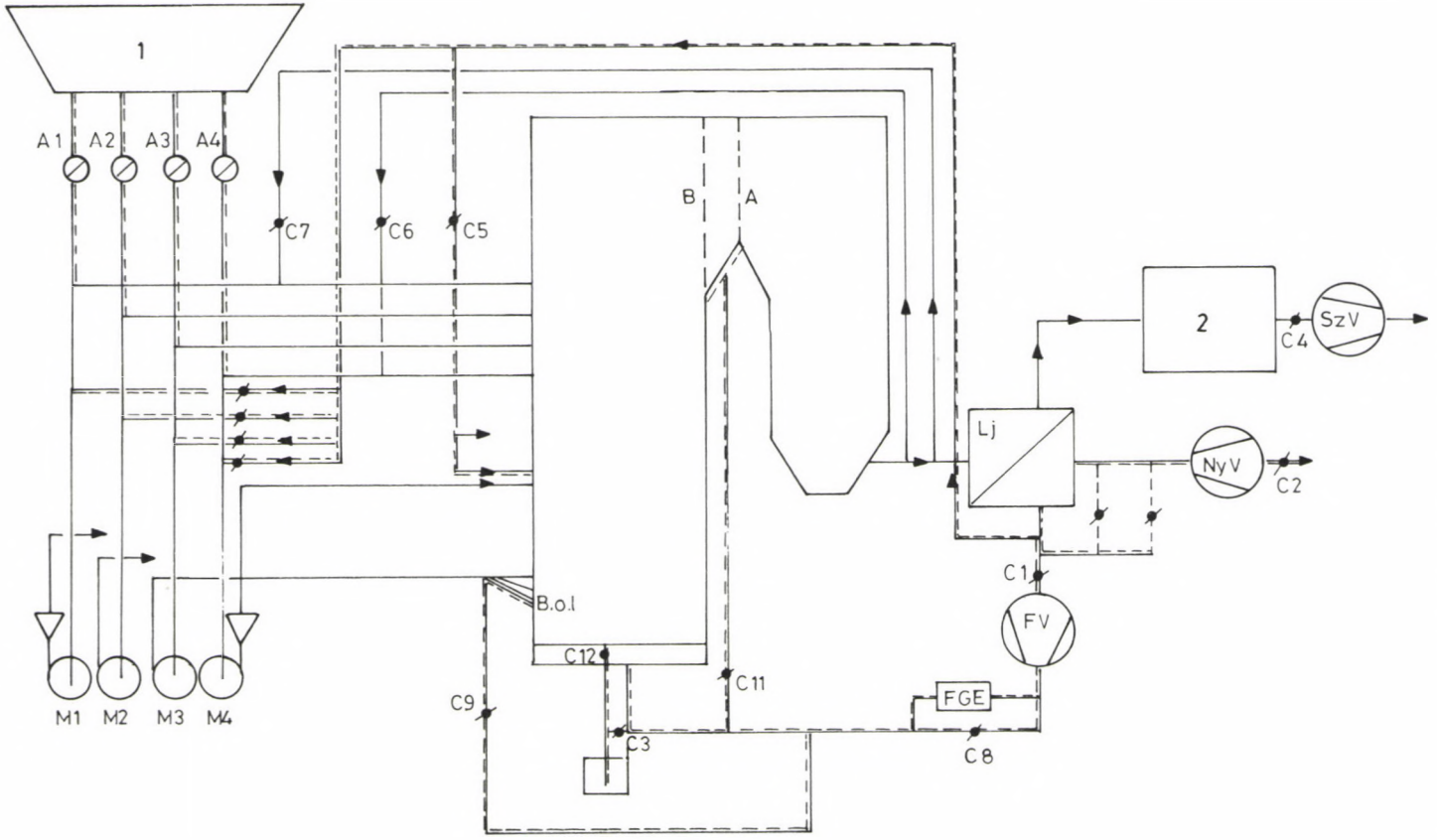

Fig. 9. Block Diagram of VEIKI fluid-bed firing at the Thermal Power Plant of Ajka
(1 - coal bin, 2 - electric fly-ash precipitator, A1, A2 - coal feeders, M1, M2 - mills, FV - fluidization blower)

— the maximum temperatures in the space above the bed be reduced as far as possible and stabilized at a uniform value below 880 ^{o}C,

— circulation of pulverized coal in the combustion chamber be speeded up and

— the thickness of the bed be increased if combustion in the bed can be intensified.

The above requirements are mutually dependent and thus intensified combustion in the bed requires that also the cooling and the circulation of pulverized coal in the combustion chamber be intensified.

According to the schematic diagram given in Fig. 9, operation of the existing mills without air separator results in a bed of coal grains of sufficient size.

Two mills are usually suited for grinding of the coal passed through them to supply the fluidized bed.

The majority of combustion air gets under the fluidization air distributors while the rest enters the combustion chamber as secondary air and through the mills provided they are operated.

From among the four mills, two mills are operated without air separator while the air separator of the other two mills is adjusted to maximum coarseness. One mill can be operated without while another mill with air separator in case of any coal grade, e.g. in case of a grain size of 0 to 20 mm or, in case of an output of 100 t/h, two mill can be operated without air separator. Exhaust of the drying gas of the front mills from the combustion chamber takes place in the same way as earlier. The temperature before and after the mill is regulated by means of hot air admixture. As compared with the earlier setup, a flue-gas exhaust pipe has been provided for the section after the economizer at the rear mills.

At the Thermal Power Plant of Ajka, the first boiler of a steam output of 100 t/h was put into service in October 1990. Since that time, the boiler has been operating to full satisfaction of the user in accordance with the expectations. The preliminary measurements detected a reduction in sulfur and nitrogen oxide emissions. Evaluation of the process is based on comparison of the values of SO_2 and NO_x measured for the conventional boiler and for the modified boiler.

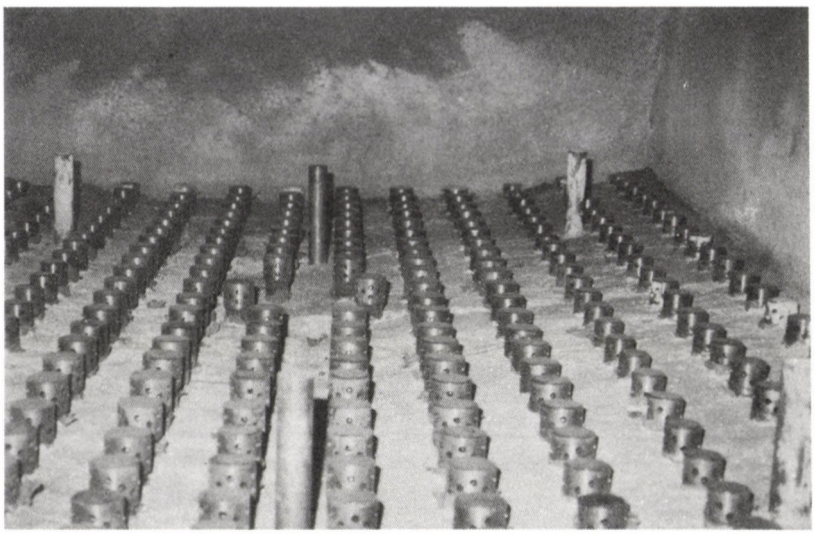

Fig. 10. Photograph of 100 t/h boiler fo Thermal Power Plant of Ajka

		Modified boiler	Conventional boiler
Boiler load	t/h	60	60
SO_2	mg/Nm^3	2020	5050
NO_x	mg/Nm^3	230	500
Boiler load	t/h	100	100
SO_2	mg/Nm^3	2640	5540
NO_x	mg/Nm^3	360	520

Note that the above results have been obtained without the use of additives. Increase of the Ca/S ratio that is use of additives and adjustment of the combustion process result in further reduction of the pollutants.

LITERATURE

1. Porkoláb, L.: Fluidization experiments to reduce SO_2 and NO_x formation. VEIKI report, Budapest 1990

2. Reményi, K. - Boross, L. - Gerlai, T.: New fluidized-bed firing equipment. 9th Int. Symp. Miedzyzdroie, Poland 1989

3. Boross, L. - Maráz, T.: Modification of a 100 t/h boiler of the Thermal Power Plant of Ajka to make it suitable for fluidized-bed firing. Feasibility study. VEIKI report, Budapest 1988

Acta Technica Acad.Sci.Hung., 103(4), pp. 299-317 (1990)

THE BASES OF THE PROGNOSIS OF ENERGY DEMAND WITHIN THE RENEWING HUNGARIAN ECONOMY IN THE MIRROR OF THE 14TH ENERGY WORLD CONGRESS*

SZERGÉNYI, I.**

(Received: 12 February 1990)

The author's publications appeared in the last years as well as the lectures at the 14th Energy World Congress made it clear that the energy demand and its changing pace characterizes well the relations between the formation of economy and energy consumption. The author of this article presents the home experiences within this branch on the basis of his contribution published at the above Congress.

In addition to the experiences the publication implies the method of the author concerning demand prognoses.

In such an economy, which renews in its bases as Hungary, where contrary to the practice of the earlier decades no producing activity directed centrally will define the formation of future energy consumption, there even the energy planners must seek for some new methods in order to notify better the probable energy demands and the tasks in its connection.

It is all the more necessary because the opinions of energy prognosis producers and reviewers seems to move in vacuum, in the same way more or less, this time rather than formerly. Apart from the uncertainty of the international comparedness of our nation-wide energy effectivity/energy intensity[1] (considered differently by several experts) some new difficulties has namely emerged. Partly by concluding the extensive development and starting the market economy, respectively, the concrete reducing ideas of energy consumers are no more known and the pace of the future economy growth has become uncertain. On the other hand, one has not sufficient information on the speed of modernization which reduce the growth of demands,

---

*The present publication has been made on the basis of the author's contribution handed down at the 14th Energy World Congress in Montreal, to which he also used the lectures delivered by other authors at the same place like supplements.

**Szergényi, István, H-1125 Budapest, Zalatnai u. 5, Hungary

[1]Energy intensity means the necessary energy consumption for the production value of one unit. Energy efficacy is the reciprocal of energy intensity.

Akadémiai Kiadó, Budapest

and energy intensity depends to a high extent on it, surely it depends in the highest degree on the exterior factors. It does in the first line on that in which degree and which pace "the acting capital"[2] which is essential in acclimation of the up-to-date technology, will participate in the renewal of economy.

These factors influence basicly the scope of action of energy demands. Therefore it is practical to form the prognosis of demand formation by means of the variation coming up concerning the speed of modernization and economical growth, which must be really combined.

To judge our possibilities of modernizing, one must also know our present effectivity of energy consumption, at least approximately. Out of it one can namely get to know if the present level of energy consumption presents any reserves (and how large ones) for the growth of economy. But here one must remark that any access to the reserves is more difficult than one would think in the first moment. The meloriation of energy efficacy of production means namely a complex problem, and spectacular results can be achieved only by long-lasting efforts. Its understanding is the basic condition of being able to speak well-foundedly on energy demands and energy policy.[3]

---

[2] Here the functioning capital means so much that it should not enter this country in the form of current currencies but as up-to-date techniques.

[3] In the opinion of the author the energy policy means the accepted principle and scientific basis of action program-in smaller countries mainly at government level-which through the series of part decisions ensures to have the indispensable energy for the undisturbed functioning of the society and economy at disposal.

During its formation one must also consider economical, environmental, security, production and international cooperating respects. As starting out factors must be considered the energy demands to be expected. Its volume depends in the first line on the growth of production, on the possibilities of energy intensity decrease connected even with the structure change of production, however, the population's consumption, the formation of infrastructural demands as well mean important factors. Such a role is also played by the success of energy saving measures to be done in every branch.

The energy policy may involve, because of the complexity of energy question outlined above, only the most fundamental objects. It must be defined the necessary conduct for solving the problems regarding smaller or bigger energy questions arising among numerous, operative circumstances. To form the energy policy the most important respects are as follows:

- within the assurance of energy sources the defining principle of the measure of energy dependence or the volume of production level of home energy,
- provision of sharing (diversification) of energy imports among the branches,
- long-term program of building up power plants,
- system of means ensuring the prevailing harmony between demands and sources, included the energy prices as well,
- consideration of respects of society and environment as well as of international experiencies and circumstances.

Beyond the above-mentioned questions the ensurance of harmony and "system of means" as the marked economy goes forward in the direction of automatism. So this term as an energetic question may lose something of its importance in the course of future happenings.

The creation of energy resources must be adjusted to the demands which is one of the most responsible questions of the energy policy, but for the sake of defining the demands, it is necessary to know the connection of changing paces among energy consumption, energy growth and energy intensity in an up-to-date comprehension. But for the latter one the effect of modernization in every sphere (production, infrastructure, etc.) must be considered in the first place.

Therefore — after having compared the summarizing indices of the Hungarian (energy) economy with the international data -- we shall deal in an extra chapter with the connection between modernization and energy intensity decrease as well. Only then we intend to pass over onto making known the idea concerning the bases of prognostization of the energy demands. Up to that point we draw the attention of the readers to understand also modernization figuratively under this concept, and mutually, whenever we speak on energy intensity decrease.

1. Comparison between the energy intensity of Hungary and the developed industrial countries

The absolute level of energy intensity in the developed industrial countries is essentially more favourable (lower) than that in Hungary (or those of the other "ex-socialist" countries). According to several experts it makes nonsense to compare them, however, others draw a parallel willingly between the Hungarian and the developed cuntries' energy intensity. Those belonging to the first group, refer to those possible uncertainties which can arise partly by probably different GDP reckoning of certain countries, partly by error sources of conversion of different national currencies to dollar as to the uniform basis of reference.

The author belongs rather to the second group just for the sake of at least approximate appreciation of the measure of the potential energy intensity decrease. He remarks, of course, that there are limits of comparativeness regarding the precision of numerical values. Especially then the comparativeness exists if the pace of changes of energy intensity is considered. But it is an indicator of direction concerning the absolute numerical values as well because the difference among the indices of Hungary and the developed countries is so big that it can be hardly traced back to any methodical causes.

According to the methodology of UNO International Comparison Project (ICP) which expresses the comparison of GDP on the basis of purchasing power parity, the total energy intensity of Hungary's economy is about the double of the developed countries, however, in the case of comparison at official rate is surpasses even its quadruple (Table 1). Regarding the electric energy intensity the differences are somewhat more moderate.

The comparison by both methods, which singles the extreme values of the uncertainty, too, proves the high state of the Hungarian energy intensity. The reality of comparativeness between these two values is to be found near the data calculated by the ICP-like index. It is especially true if one thinks that our efforts toward convertibility — in long term — move away the energy intensity calculated on the basis of GDP according to the rate into the direction of that calculated in accordance with ICP.

Table 1. Hungary's energy intensity in international comparison

	Total energy falling on one unit of GDP (Consumption in % of the Hungarian index (1985)+)		Electric energy falling on one unit of GDP (Consumption in % of the Hungarian index (1985)+)	
	purchasing power on parity (ICP)	at official market price	purchasing power on parity	at official market price
Austria	50	24	76	36
United Kingdom	62	33	70	37
France	49	23	72	34
F.R.G.	65	30	81	37
United Nations of America	79	31	94	37
Japan	43	18	68	28
Hungary	100	100	100	100

Sources: /9/, /13/

Remarks to the table: In counting of energy intensity index/energy/GDP the uncertainty is caused by GDP value. Both methods applied to compare internationally the GDP standard, that is, the ICP comparison of U.N.O. and reckoning with rates of exchange give difference results. Both methods can give a distortion of opposite direction at the application of purchasing power parity (ICP), that is, overestimation of economy level of the less developed countries but underestimation of the more developed ones. - The application of rate of exchange distorts just in the opposite direction, moreover it is supposed in a greater degree. The reality is probably between the two methods, in addition in a territory near the ICP measure. The author considers the comparison according to ICP to be real.

Thus in the case of dynamic calculations which use the temporal pace of energy intensity change, the application of ICP-like method is more reasonable. (By the way, in the pace of energy intensity decrease calculated in two different ways it does not appear that big difference which can be experienced at the absolute level of energy intensity.)

The collective average energy intensity of the European Nine showed a slightly rising tendency from 1965 up to 1973 (Fig. 1). But within the general rising the indices of Great Britain, FRG and France decrease even then, too. Regarding it, see later the diagram 8 (but since the first oil crisis (1973) occurred a considerable decrease (in average 2.1% per year). This decrease within the average was more intensive during a few years, then it decreased up to 1979. But at that time the second oil crisis gave a newer impulse to the energy intensity decrease which was again followed by moderation in a few years (Fig. 1 does not show the absolute numbers but the values related by 1973). Whereas the effect of the first oil-price explosion (1973) did not appear in Hungary in the pace of energy intensity decrease.

On the contrary the "final" energy consumption[4] (-2%/year) projected for the GDP unit lessened quicker between 1965 and 1973 (-1.3% per

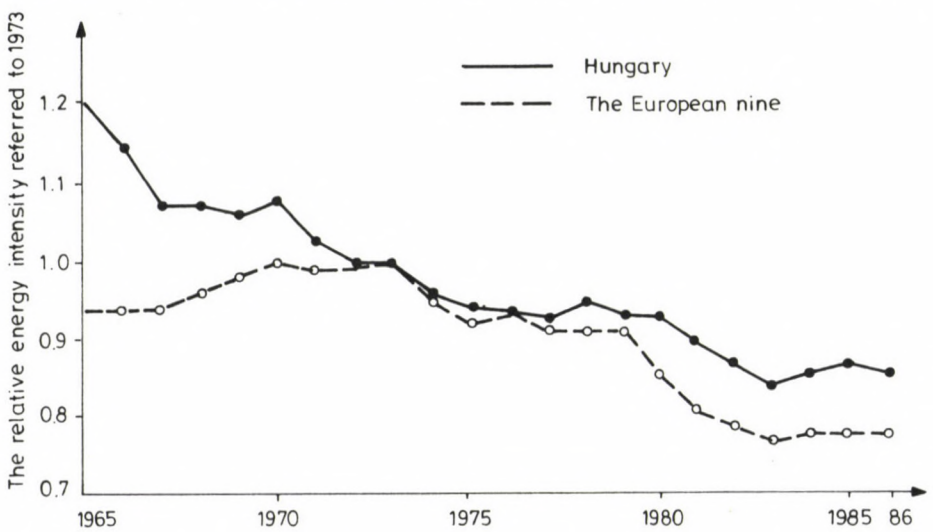

Fig. 1. Energy intensity change between 1965 and 1986 (1973: 100)

[4] In the so-called "final" energy consumption we do not consider the loss of transformation which arises in the course of electric energy production. Together with that the energy intensity decrease at the national economy level was still more moderate (1.1% per year).

Table 2. The formation of fuel-energy intensity of people'economy between 1973 and 1987

		GDP (price of the year 1981), GFt			Energy consumption, PJ			Energy intensity, kJ/Ft; kWh/Ft		
		1973	1980	1987	1973	1980	1987	1973	1980	1987
Indices of people's economy level projected on every energy (PJ)	PJ, GFt	566	751	866	1025	1260	1348	1810	1677	1566
	kJ/Ft									
	%/year		4.1	2.1		3.0	1.0		-1.1	-1.0
			3.1			2.0			-1.1	
Indices projected on final total energy consumption (PJ)**	PJ, kJ/Ft				845	1037	1084	1493	1381	1252
	%/year					3.0	0.6		-1.1	-1.4
						1.8			-1.3	
Indices projected on electric energy accounted at the level of people's economy (PJ)***	PJ, kJ/Ft				260	336	408	459	447	471
	%/year					3.7	2.8		-0.4	+0.8
						3.3			0.2	
Energy consumption without the practical heat value of electric energy (PJ)	PJ kJ/Ft				765	924	940	1351	1230	1085
	%/year					2.7	0.2		-1.3	-1.8
						1.5			-1.6	
Comsumption of electric energy accounted in kWh	10^9 kWh				22.3	31.1	40.0	39.4	41.7	46.2
	kWh/kFt									
	%/year					4.9	3.7		0.8	1.5
						4.3			1.1	

year — Table 2) than between 1973 and 1987. Thus market relations in this country did not influence the formation of index. In the earlier years the decrease of energy intensity was due to the change in energy structure which started more strongly in the middle of the sixties.

Probably without the spreading of carbohydrogen heating of better efficiency the formation of energy intensity of the period between 1965 and 1973 would not have been more favourable. Because of the general lack of COMECON price principle regarding the energy bearers and that of market economy, when the rearranging of energy structure was finished towards the energy sorts to be burned up with higher degree of efficiency, then the energy intensity decrease is losing its wind. This is just contrary to the wishes. Any improvement can be awaited only by the creation of market economy and by the essential change of production structure.

In Hungary the electric energy intensity grew in the whole period (1.1% per year) what was only so possible that the specific consumption of energy sorts outside of the electric energy lessened better than that of total energy (1.6% per year — Table 2).

It is to be remarked that concerning electric energy intensity a decrease of slight degree can be experienced even in the developed industrial countries only in the recent years (Fig. 2). This can be evidently attributed to the fact that the effect of modernization presents itself differently in the use of the fuel sorts and electric energy. One has to reckon with this phenomenon in Hungary as well.

One can learn some further information from those data which the energy intensity can be traced from (energy consumption and GDP). The formation of these indices (this time, too, regarding 1973 as comparing basis) can be seen in Fig. 3. According to these the growth of GDP and energy consumption of the developed European countries up to 1973 grew at nearly similar pace. From 1973 to 1979 there was a temporary decline, then the new boom was similarly almost parallel. In principle it must be esteemed as a new important phenomenon that since 1979 the energy consumption in these countries has not grown essentially but the production — es-

---

*The integrated time sequences at the price level of 1981 of the summarizing indices regarding the development of people's economy 1950 to 1987. Volume, 1, 1989

**The (final) energy consumption without the loss of transformation. In our case — for the sake of simplicity — only the biggest proposition, that is, the loss of electric energy transformation was subtracted from among the total energy.

***The heat quantity required for producing the electric energy.

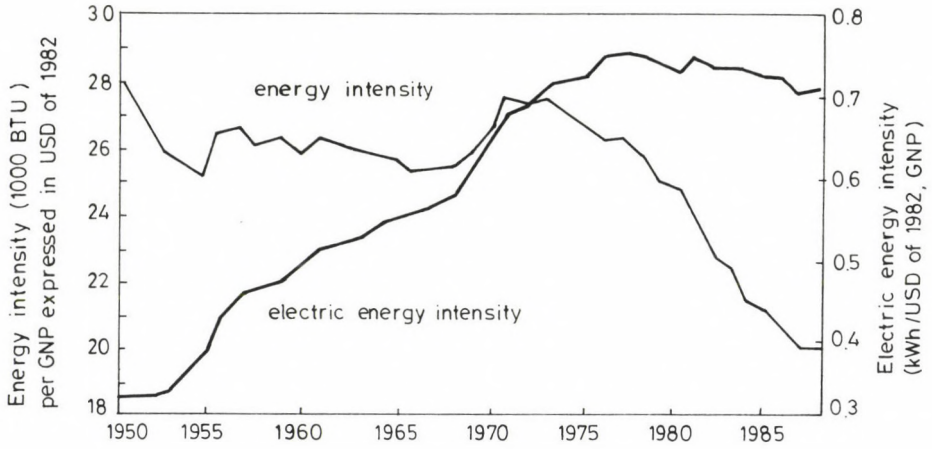

Fig. 2. The decrease of total energy intensity and that of electric energy in U.S.A.

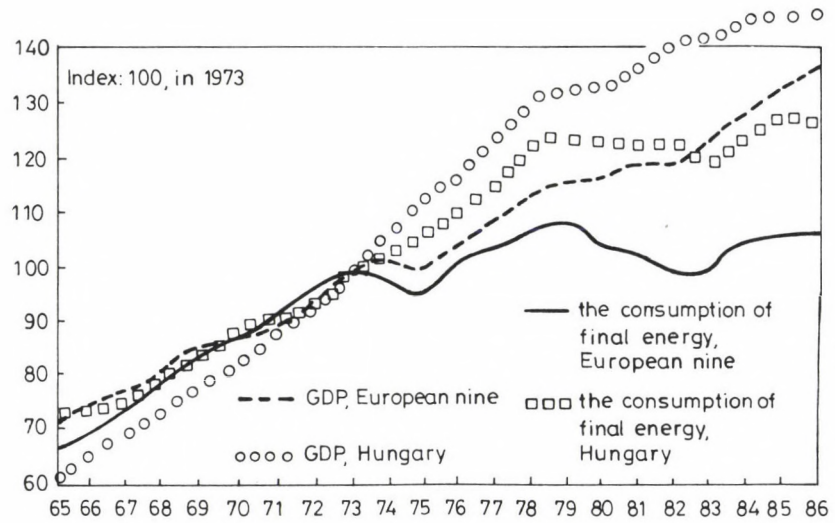

Fig. 3. The temporary change of GDP and energy consumption in Hungary and with the European nine

(Sources: Agence Française pour la Maitrise de l'Energie (AFME), 1989, The integrated time sequences at the price level of 1981 of indices summarizing the development of people's economy I, OT, IpM, 1989)

pecially from 1982 — has been again prospering. To the new energy situation these countries could conform within short time.

Contrary to it, the GDP grew with undiminished force in Hungary from 1965 to 1977 (mainly the extensive development went on), and although in a bit slower pace, but the growth of energy consumption was also continuous. But from 1977 on the GDP growth lessened durably, and in consumption of all-energies a stagnation diversified with fluctuation followed.

2. The effect of modernization on energy intensity

International comparisons show that there is a diverse ratio between energy intensity and efficiency of economy. As Fig. 4. shows on the basis of international comparisons it can be rendered probable that Hungary can decrease its total energy intensity to its half when the productivity of its economy increases approximately to its double and half. To reach this goal there are necessary 25-30 years even in the case of the economy growth of 3-4%. This time could be shortened, too, if one would go forwards in the modernization quicker than that was done by the countries considered today to be developed. To do so one ought to take over some ready technologies of little energy intensity in large numbers. So one could spare the developing which the leading countries had to invest in the innovating chain. This suppose a quick integration with the developed Western countries. By the way, just the same has been done by the "newly coming" industrializing developing countries. Contrary to them our disadvantage consists in the fact that we, who are developed in mediocre way, are burdened by an out-of-date industrial structure. In order to overcome all this it is necessary not only to introduce the new one, however, but to eliminate the out-to-date measures as well.

Expressing the modernization with pace of energy intensity decrease, Hungary should not only surpass, according to it, the dynamic experienced with us earlier, however, that of the developed countries as well. Just the success of our renewing could be expressed if a radical change happens in the pace of energy intensity change. Besides this index it could be an indicating number of our modernizing the rising share of informatics within the GDP. Both possibilities are similarly considered the measure of modernization as on it J. Bouvet reported /10/ at the 14th Energy World Congress (Fig. 5).

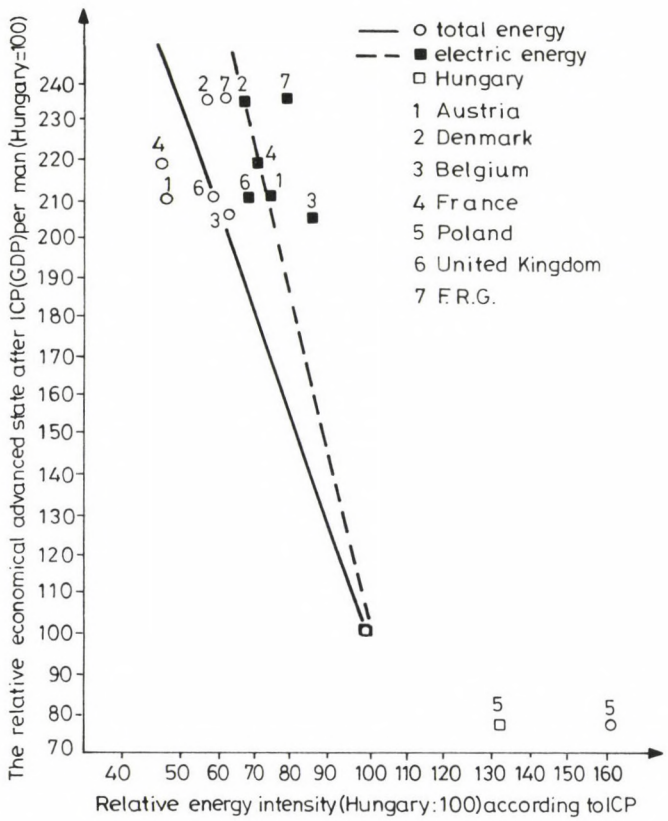

Fig. 4. The connection between the energy intensity and the advanced state of economy according to the data of 1985 (Source: /9/, /13/)

The following formula expresses the average year's pace of energy intensity improvement among the different points of time,

$$C_t = c_0\left(1 + \frac{r_c}{100}\right) t \qquad (1)$$

where

C_t = energy intensity of the period's end,

C_0 = energy intensity of the period's beginning,

r_0 = average year's pace of energy intensity,

t = duration of the examined period.

When one speaks on energy intensity decrease standing in front of us, one must consider or mention in the first place the industry. Partly because it consumes the most energy, partly the modernization in this branch is realized in the most quick way all over the world.

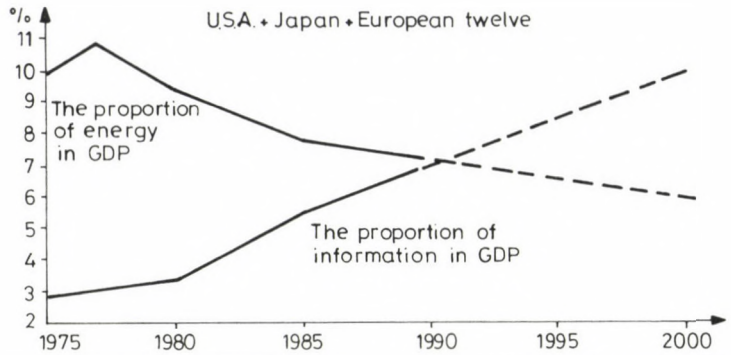

proportion	energy	9.8		9.4		7.8		7.1		6.5		6.0	
	infoma-tion	2.8		3.3		5.5		8.7		8.2		10.0	

Fig. 5. The proportion of the value of energy and informatics in the GDP production of the developed countries

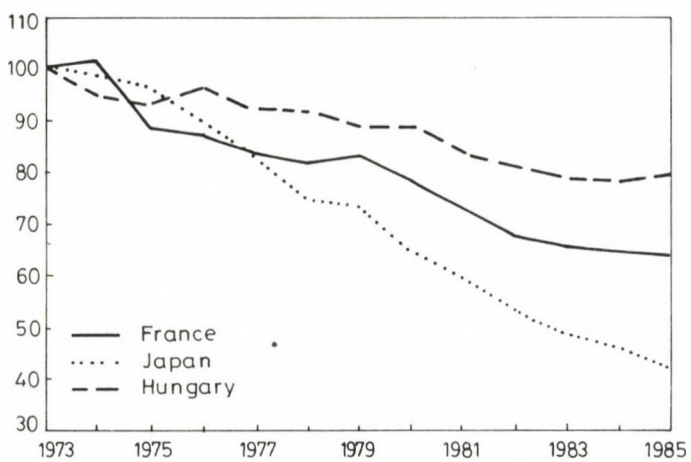

Fig. 6. The change of energy intensity of industrial GDP production between 1973 and 1985 (1973: 100)

Table 3. The formation of fuel-energy intensity of industry between 1973 and 1987

		GDP* (price of 1981), GFt			Energy consumption, PJ			Energy Intensity kJ/Ft; kwh/Ft		
		1973	1980	1987	1973	1980	1987	1973	1980	1987
Industrial indices projected on the final energy PJ**	PJ, GFt kJ/Ft	177	249	288	417	496	463	2356	1992	1676
	%/year	5.0	2.1		2.5	-1		-2.4	-2.4	
		3.5			+0.8			-2.4		
Industrial indices projected on energy consumption at the level of people's economy PJ PJ					541	637	615	3056	2558	2135
					2.4	-0.5		-2.5	-2.5	
					1.0			-2.5		
Indices projected on electric energy accounted at people's economy level*** (PJ)					160	186	203	90	75	70
					2.2	1.2		-2.6	-1.0	
					1.7			-1.5		
Energy consumption without the practical heat value of electric energy (PJ)					381	451	412	2152	1811	1431
					2.4	-1.3		-2.4	-3.3	
					0.6			-2.9		
Electric energy consumption accounted in kwh					10.0	12.4	14.1	56.5	49.8	48.9
					3.1	1.8		-1.8	-0.3	
					2.5			-1		

*, **, *** See the interpretation of indices projected on the whole of people's economy.

According to international comparisons, the energy intensity of industry of the more important Western countries of Europe decreased quicker than the national average, yearly between 2.5 and 4.5%, that measure of Japan did at the pace of 6.5% (Fig. 6). The Hungarian index met the most moderate West-European one (2.5% per year) (Table 3). But because our energy efficiency was even in the starting period out-of-date, the industrial energy intensity decrease must be considered as a very important concomitant phenomenon in the process of home modernization. In the following part we touch upon that.

There is the following connection between the energy intensity of the whole of industry and the industrial branches,

$$C_{ip} = \sum_{i=1}^{n} c_i \cdot q_i \quad , \tag{2}$$

where

C_{ip} = the energy intensity of the industry,
c_i = the energy intensity of the industrial branches
q_i = the participation of the single branches within the GDP.

In our standpoint we may reckon with two levels of modernization-in close connection of structure changes /8/. The higher level consists in the structure changes among the branches. The decrease in rate of producing activity of branches of higher energy intensity also leads itself to the improvement of industrial energy efficiency. For this very reason, among other things, the developed industrial countries strive to get free of industrial activities of energy intensity, and to get the productions of energy intensity possibly on foreign markets.

The deeper level consists in modernization of microstructure of economy which indirectly presents itself at the improving pace of the own energy intensity of the single branches. So, for example, the energy intensity (being favourable in advance) of machine industry improves at the biggest pace in Hungary, however, the chemical industry, too, proves similar experiences. In the case of the latter one experiences index-improvement of 5-6% per year in the first line by concluding the extensive development and the gradual spreading of processing activity /4/, /7/. With the effect of structure changes at these two levels B. Chateau and his co-authors dealt in the 14th Energy World Congress as well /6/. They named the higher level "structure effect", while the deeper one "intensity effect".

3. Estimation of future growth of energy demands Methodical recommendations and conclusions

As already mentioned, it is suitable so to prognosticate the energy demands that the prognosis should similarly involve the economy growth and energy intensity decrease to be expected from the modernization. In the following part we want to make known a method which is based on this double access.

The corresponding indices of energy intensity regarding the past can be reckoned out of the statistic data. But regarding the future -- alternative economy -- prognoses in different variations can be made by the use of considerations of structure policy both for the economical growth and the energy intensity decrease (modernization). By means of a proper connection, by the two kinds of prognoses the energy demand growth can be determined.

Among the change of economy growth, energy consumption and energy intensity the connection /3/ is valid. This is illustrated monographicly by the Fig. 7 /8/.

$$r_a = \frac{r_b - r_c}{1 + \frac{r_c}{100}} \qquad (3)$$

where

r_a, r_b and r_c mean, one after another, the average year's paces of the change of GDP, energy consumption and energy intensity, respectively.

The growing pace of energy consumption can be defined from /3/, in view of the relative low value of energy intensity change through the following approaching connection,

$$r_b \approx r_a + r_c \quad . \qquad (4)$$

Thus the growth of energy demands -- using contracted macroindices -- can be defined out of the growth of GDP and from energy intensity change with formula 4 (or by means of monogram of Fig. 6).[5]

[5] If, for instance, between 1989 and 2000 an energy growth of yearly 1.9% can be realized by energy intensity decrease of yearly 1.1% then the energy consumption-growth were yearly 0.8%. By considering the previous data of the year 1989/GDP is equal with 856 thousand million forint at price of 1981, 32 million ton of oil equivalent energy consumption), then the energy demand of the year 2000 were 35 million ton oil equivalent while the GDP would amount to 1053 thousand million of forint. With the same energy quantity 1210 thousand million forint (GDP) could be reached in the case of the modernization governing energy intensity decrease of yearly 2.5% in the year 2000.

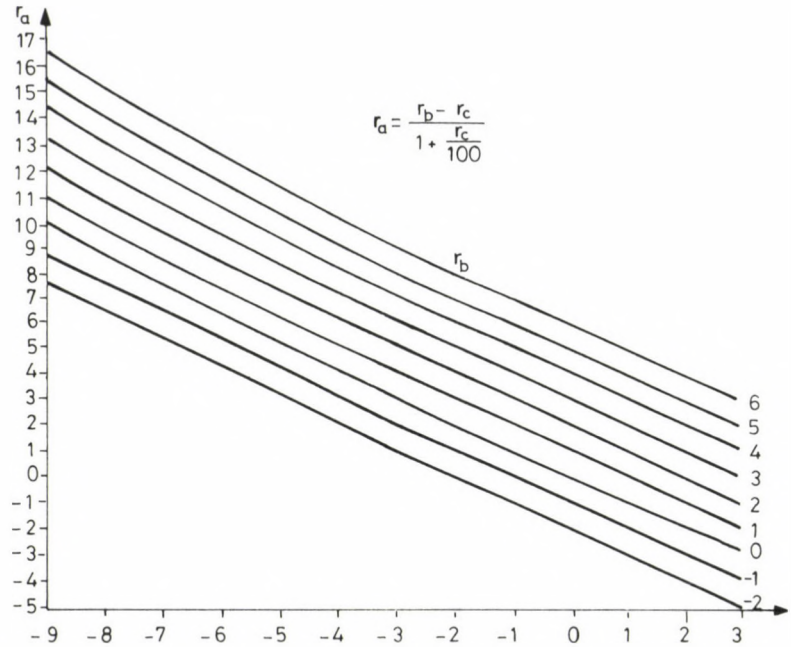

Fig. 7. The monographic connection of the changing paces of GDP, energy consumption and energy intensity

(r_a - the yearly average pace of change of GDP consumption, r_b - the yearly average pace of change of energy consumption, r_c - the yearly average change of energy intensity)

The most critical part of the method is the reflection what energy intensity decrease can be ordered rationally to the single economy growing alternatives. After all the variations arisen out of the combinations created in this way, form the probable zone of energy intensity growth.

Thus it is necessary to think over those processes what a basic change in the production will be caused by the Hungarian modernization to be carried out. In what proportion and pace the mortification of the technologies of out-of-date energy demands and introduction of up-to-date measures can be expected?

How can form the temporary change of GDP, the energy intensity in the function of producing structure change (2nd formula) — as its result? The publication does not become immersed in this question but it outlines, in three variations by means of the alternative formation of energy intensity change indicator, what chances we shall have in the case of different speeds of modernization to join up, to remain just on the surface or to get into danger concerning our competitiveness.

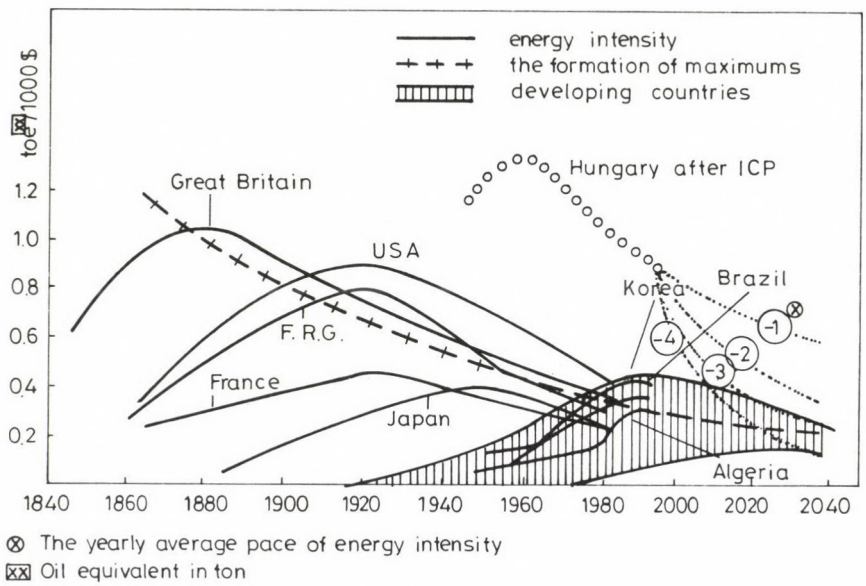

Fig. 8. The formation of energy intensity and the development
(Source: Revue de l'énergie, n° 415, novembre 1989)

On outlining the prognosis of formation of the future Hungarian energy intensity decrease, we set out from our present situation, experiences, the international comparisons and our European integration efforts. Let us look at Fig. 8 in which one compares the Hungarian energy intensity calculated by ICP method with those experienced in a few developed industrial countries and with those experienced in some newly industrializing countries, taking a longer space of time /14/. Fig. 8 shows that our energy efficiency would remain unfavourable in the case of pace of our energy intensity decrease up to the present, compared not only to the developed countries, but the newly industrialized ones as well.

It can be supposed that temporarily the high energy costs have been balanced in the competitiveness of several Hungarian wares by the low proportion of wages.

Keeping the pace of our up-to-now energy intensity decrease, in the case of home wage increase or unfavourable formation of some other producing factors would jeopardize even our competitiveness compared to the developing countries. Thus the yearly energy intensity improvement of

1-1.5% (first variation) were for our economy only the most pessimistic alternative. This ought to be avoided possibly!

More intensive -- yearly 1.5-2.4% — energy intensity decrease could be the sequence of processes of such real economy policy in which relatively rapid modernization starts. Finding position within the zone depends on the speed of modernization. But this variation /2/ would not assure more than so much that the distance among the developed countries and us should not increase. But this is only then valid if the upper part of the zone were realized. A more ambitious economy developing program should surpass even that if Hungary wants to approach the developed countries.

Although the probability of an energy intensity decrease overcoming the industrial countries, too, — thus about 3% or a bit more significant than that — is little, however, it is not totally impossible in the case of the possible quick integration of Hungary into the developed countries, moreover it were directly desirable. To accomplish this variation /3/ the whole arsenal of economy diplomacy and technical developing possibilities must be combined.

According to the author's judgement the middle variation has the greatest probability -- mainly for a middle horizont of time -- in which, of course, the upper limit of zone were desirable (2.5% per year) — this would mean the doubling of the pace of energy intensity decrease up to the present. It is reasonable to form also the energy zone corresponding to it. But it is recommendable to carry out this work consequently upon the methods put down above, and joined the economic development being formed actually (GDP growth). Thus one must make it running in order to be able to take into consideration the modernizing processes, that is, those otuside the energetics during "the maintenance" of energy demand prognosis. At the same time the information coming continuously will give instructions on the questions if the energy intensity decrease switches over indeed to an other course.

On counting the energy demand growth one must consider still one important factor so as to avoid a possible mistake in the course of adopting the formula /4/ mechanically, that is, the energy consumption per man. According to the international comparison (Table 4), except the indicator referring to the Japan specific total energy consumption, one always meets higher values of energy consumption per man everywhere in the developed industrial countries — particularly regarding the electric energy. From

Table 4. Hungary's energy consumption per man in international comparison

	Per one head	
	Total energy	Electric energy
	Consumption in % of the Hungarian index (1985) /9/	
Austria	105	159
United Kingdom	131	148
France	107	157
F.R.G.	173	190
United States of A.	255	305
Japan	99	158
Hungary	100	100

this fact one can draw the conclusion that it is not reasonable to disregard any — mainly electric-energy consumption growth even in the case of intensive modernization. We have already dealt with this question earlier, and the statement was also proved by means of Fig. 3.

Then a greater challenge of energy intensity decrease than the about 3% per year which could be ordered to the most intensive principle variation of modernization mentioned as the third one earlier, occurs if — for example — on the part of environmental protection a newer pressure would step up. This would mean tasks to the industrial countries, which participate in about three-quarters proportion out of the energy consumption of the world, corresponding to roughly 8 thousand million ton of oil. It could be imagined that these countries cannot use more energy for their future development, but they must decrease consumption. In this case some innovation waves can start from them out of which we cannot wriggle us. But its pondering exceeds the limits of this publication.

4. Summary

The functioning of the Hungarian economy is of very energy demand. The decrease of our energy bill is imperatively necessary both in respect of routine energy costs and energetic investments that our production should be and become competitive, even in the case of growth of probable cost shares regarding other production factors as well.

According to approximate calculations, the yearly average pace of

decrease of our energy intensity ought to be double compared to the home one experienced continuously up to the present (-1.3% per year) that the distance should not grow between the developed industrial countries and us — at least.

If we want to lessen the distance among the developed countries and us then we ought to experience about yearly 3% energy intensity decrease. But this wants the introduction of the new and not "the put off" technologies in Hungary, integrated into Western-Europe.

Considering that the decrease of energy intensity ensues mainly as result from modernization, therefore we must seek for the key of solution in the accelerated making of the production structure up-to-date. We must keep close watch on this process, and with the continuous maintenance of our energy prognoses we have to review the energetic consequences from time to time.

REFERENCES

1. Le Monde Diplomatique 1989. dec. p. 14
2. Statistiques energetiques. Ministere de l'Industrie et de l'Amenegement du territorie 1989
3. Futuribles 1989. June
4. Szergényi, I.: The challenge of energetics against the Hungarian economy (in Hungarian), Energia és Atomtechnika, August 1987, p. 348
5. Jean-Marie Martin: L'avenir du marché petrolière. Futuribles n. 122. June 1988
6. Chateau, B. - Coté, F. - Lapillone, B.: L'interpretation des changements dans l'intensité energetique de l'industrie, Lecture at the 14th World Congress of Energy in Montreal 1989
7. Szergényi, I. - Fölsz, A. - Faur, T.: The experiences of 25 years in energy intensity change of industry (in Hungarian), Energia és Atomtechnika vol. XLIII No. 2, p. 57
8. Szergényi, I.: Energy intensity decrease and economical growth (in Hungarian). Energiagazdálkodás, August 1989, p. 329
9. Department of Economics of Central Statistic Office in Hungary: The comparison of economical development level on the basis of GDP per man
10. Jacques Bouvet: Pour une société plus éfficace, Lecture at the 14th World Congress of Energy in Montreal 1989
11. Perspectives energetiques mondiales 2000-2020. At the above congress!
12. Szergényi, I.: Le developpement de la consommation d'energie en fonction du chamgenet de la structure de production at de l'augmentation économique, Revue d'études comparatives est-ouest (Paris, CNRS) juin. 1990. Vol. 31, No. 2, 107-116
13. Energy Statistics Yearbook 1985
14. Dessus, B.: Energy — developpement — environment, un enjeu planetaire au XXIe siècle. Revue de l'energie n° 415, novembre 1989, p. 978

Acta Technica Acad.Sci.Hung., 103(4), pp. 319-328 (1990)

PROBABILITY DISTRIBUTION OF RANDOM LOAD OF ELECTRIC POWER SYSTEM INTER-TIES

TERSZTYÁNSZKY, T.*

(Received: 12 November 1988)

The study investigates the resultant random load of the inter-ties between two electric power systems. First the distribution of random load is determined for the general case where power station units of a large number are in operation in both systems and then a method and a case study are presented for the case where the capacity of a 1000 MW power station unit exceeds 5-10% of the total system capacity.

1. Resultant random load of system inter-ties in case of power station units of a large number

The load of electric power system inter-ties is composed of deterministic loads and random loads, the random load being the resultant of power transfers of some hours (days) taking place for economic reasons and power transfers of some seconds (minutes) based on engineering. Because of a possible system disconnection and its consequences, the high values of power resulting from random loads endanger the security of interconnected system operation. Determined below are the characteristics of resultant load on the basis of probability theory for planning of a secure interconnected system operation.

In determining the resultant of random loads of shorter or longer time, the probability characteristics of both loads, e.g. variation, are assumed to be determined after matched averaging. Thus, if e.g. uncontrolled power oscillations are investigated on the basis of hour's average, also the characteristics of power transfer in case of a system disturbance and/or marginal energy exchange shall be calculated as an average on an hourly basis.

*Tersztyánszky, Tibor, H-1139 Budapest, Petneházy u. 35, Hungary

Akadémiai Kiadó, Budapest

The most convenient method is to determine the expectable value from among probability variables. If the same strategy can be assumed for both planning of power system reserves and power/frequency control, then it is only the change as compared with long-term planning that shall be taken into consideration (e.g. electricity purchase or sale as a result of a delay in power station construction as compared with the plan). If there is no change, the expectable value of short-term random load Z will be E (Z) = 0.

To calculate the resultant value of variation, let the number of values measured per hour (half-hour, quarter-hour etc.) be denoted by m while the number of measurements per hour (half-hour, quarter-hour etc. but definitely the same period as that used for m) by n. Thus the mean square deviation will be

$$\sigma_Z^2 = \frac{1}{n\,m} \sum_{i=1}^{n} \sum_{j=m}^{m} (Z_{ij} - \overline{Z})^2 \qquad (1)$$

where

Z_{ij} - resultant random load taking place at time j within hour (half-hour etc.) i,

$\overline{Z}$ - average of loads Z_{ij}.

Since the time intervals are matched in the investigation of the two different random loads as has been assumed, the above equation can be

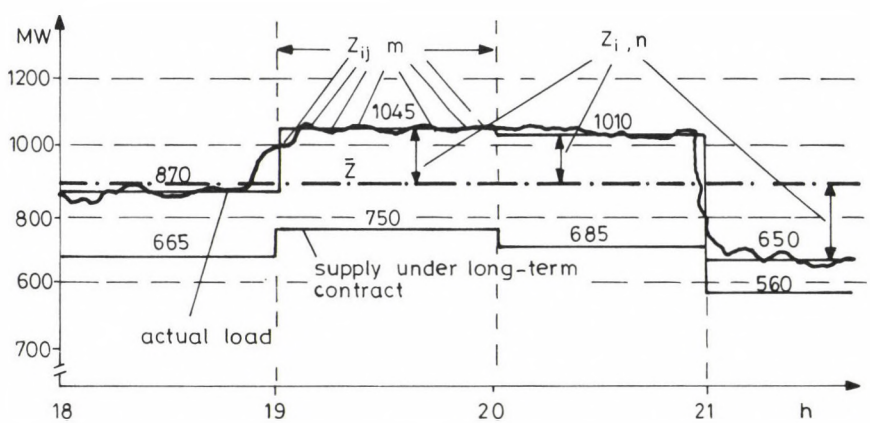

Fig. 1. Deterministic and random (longer and shorter) loads of inter-ties

divided in two parts:

$$\sigma_Z^2 = \frac{1}{n\,m} \sum_{i=1}^{n} \sum_{j=1}^{m} (Z_{ij} - Z_i)^2 + \frac{1}{m} \sum_{i=1}^{n} (Z_i - \overline{Z})^2 \qquad (2)$$

where

Z_i - average load in hour (half-hour etc.) i.

The first term of the expression is the variation of uncontrolled exchange power oscillation while the second term stands for the variation of substitution or marginal energy exchange in case of a system disturbance. Thus

$$\sigma_Z^2 = \sigma_o^2 + \sigma_p \qquad (3)$$

where

σ_o - variation of short-time uncontrolled power oscillation, assumed to be $(0.25\text{-}0.5)\sqrt{P_1}$ according to reference /1/,

σ_p - variation of mutual power transfer in case of operating troubles and of an economically favourable energy purchase, assumed to be $(1.3\text{-}1.7)\sqrt{P_1}$ according to investigation /2/,

P_1 - load of the smaller system of those interconnected by the system link investigated.

Hence, in case of power station units of a large number where the power of the largest unit lies at, or below, 5% of the installed system power, the resultant variation of random load can be calculated, using data from references, as follows:

$$\sigma_Z = (1.2 - 1.8)\sqrt{P_1} \qquad (4)$$

With the result obtained, the maximum values of different probabilities endangering the interconnected system operation can be determined on the basis of the method published in /3/.

2. 1000 MW unit is a small system

If, for different reasons, relatively large units, e.g. units of a power above 5% of the system capacity are built into a power station system, then the normal distribution based on the central limit theorem

will no longer be sufficient as an approximation of permanent (hourly average) random load of system links, representing mutual help in case of operating troubles. In this case, because of its magnitude, the effect of the power station unit of relatively high unit capacity shall be taken into consideration independently like in planning for the power station system /4/. A typical example is the Hungarian electric energy system at the turn of century when a 1000 MW nuclear power unit is expected to be commisioned in the system of a total capacity of about 8000 MW.

The random load of inter-ties is affected by the 1000 MW unit in that part of the lost power in case of an forced outage is replaced by the other power systems through the system interconnection lines at a rate depending of the parameters of the interconnected systems. In addition to what has been described in Chapter 1, the random load of system inter-ties may be affected also by two independent factors, namely by the availability of the unit and the ratio of system capacities.

In normal operation, the load of system inter-ties is not affected by the 1000 MW unit. However, in case of its forced outage, random load is appearing on the inter-ties at least temporarily as a substitution of the generator dropping. In this case a probability model is used for calculation, this effect can be approximated by binomial distribution. Probability of unavailability of units of number k from among units of number n:

$$P_{r_k} = \binom{n}{k} p^{n-k} q^k \tag{4a}$$

Distribution function of the probability of unavailability of the unit:

$$B(y) = Pr\ (\ \eta < y) = \sum_{i=0}^{k} \binom{n}{i}\ p^{n-i} q^i \tag{5}$$

where

$y = kP$,

P - capacity of 1000 MW units,

n - number of units,

k - number of unavailable unit investigated ($k = 0.1, \ldots, n$),

q - forced outage rate of the unit,

p - reliability of the unit.

Unavailability of the high-capacity 1000 MW unit and unavailability of the different machines from among units of a large number according to Chapter 1 are an independent event each and thus the rule of the sum of

dependent probability variables can be applied to resultant random load Z_y occurring on the system inter-ties in case of a coincidence /5/.

Using normal distribution, assumed and tested for random transfers of inter-tie in case of power station units of a large number and consumer load, denoted by D(Z), the distribution function of resultant random transfers of inter-tie, $G(Z_y)$, will be

$$G(Z_y) \equiv D(Z) * B(y) \quad . \tag{6}$$

However, in case of forced outage of the 1000 MW unit, the fact that the electric energy systems of parallel operation substitute for each other in the ratio of their capacity in the first instant shall also be taken into consideration /6/. This substitutional process may continue for a longer time if there is no significant reduction in frequency, there is no inter-tie is disconnection unless the power reserves are loaded or reductions are set to consumption in the system emergency. If a smaller system P_1 is connected in parallel with a larger system P_2, then the ratio of prompt substitution for a unit becoming unavailable in the smaller system will be

$$h = \frac{P_2}{P_1 + P_2} \quad . \tag{7}$$

Taking this into consideration a detailed expansion of the convolution for determination of the probability distribution of resultant random substitution load of the system link yields

$$G(Z_y) = \sum_{k=0}^{n} \binom{n}{k} p^k q^{n-k} \cdot \Phi\left(\frac{Z_y - h.k.}{Z} \right) \tag{8}$$

where

Φ - normal distribution function of values σ_Z and $E(z) = 0$,

P - $k \cdot P_{1000}$, total capacity of 1000 MW units,

Z_y - resultant random load of system inter-ties in case of unavailability of 1000 MW unit(s), taking into consideration also substitution.

A computer convolution program has been developed on the basis of equation (8) to calculate random load Z_y resulting from unavailability of the 1000 MW unit in an interconnected electric power system. The input data include essentially the following quantities:

1 Quantities describing the normal distribution representing mutual substitution in case of power station units of a large number that is variation σ_z and expectable value E(z) of the distribution.

2 Values describing binomial distribution that is the number of units as well as the forced outage rate q of the unit in respect of random load of the system intertie as well as capacity of the unit in MW.

3 Quantity describing the ratio of substitution, determined by the ratio of systems interconnected by the system links.

Index q expressing the forced outage rate of the unit in respect of random load of the system inter-tie shall be corrected because, even in case of unavailability of the unit for time $T_{üz}$, the time of random load of the system inter-ties is $T_{rö}$ only as a result of appropriate control measures to discontinue the overload of inter-ties. The corrected forced outaged rate

$$q^{*} = \frac{\sum T_{rö}}{\sum T_{üz}} \cdot q \qquad (9)$$

Use of a value of $q^{*} = 0.001 \ldots 0.01$ is recommended by the author in on the basis of data collected over years on unavailability of 800-1300 MW units of PWR nuclear power stations in the USA and France due to forced outages (7).

The following data have been used in a case study calculations for random load of system inter-ties, representing substitution without import in case of system disturbances:

Binomial distribution		Normal distribution		Substitution ratio	
		E(Z)	σ_Z		
P	1 x 1000 MW	0	150	h	1
	2 x 1000 MW		150		0.8
q^{*}	0.01				
	0.001				

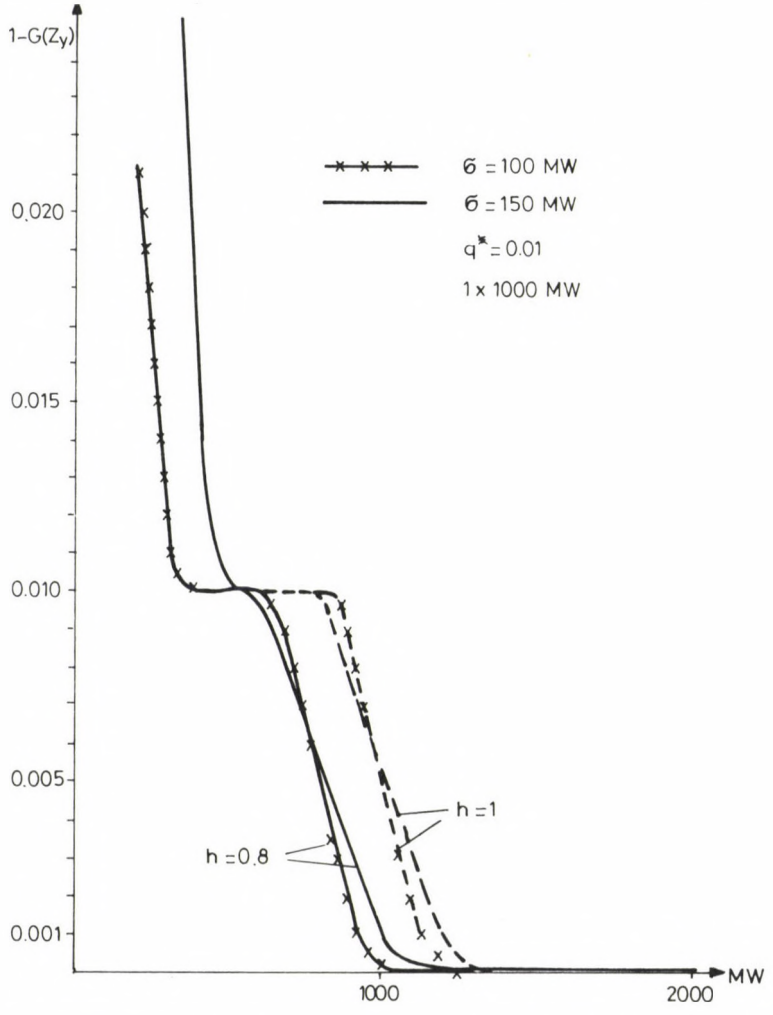

Fig. 2. Probability distribution of random load of system inter-ties in case of one 1000 MW power unit is added to a smaller system of 5000 MW and 10 000 MW interconnected with a larger system which is infinitely large or four times as large as the smaller system, respectively

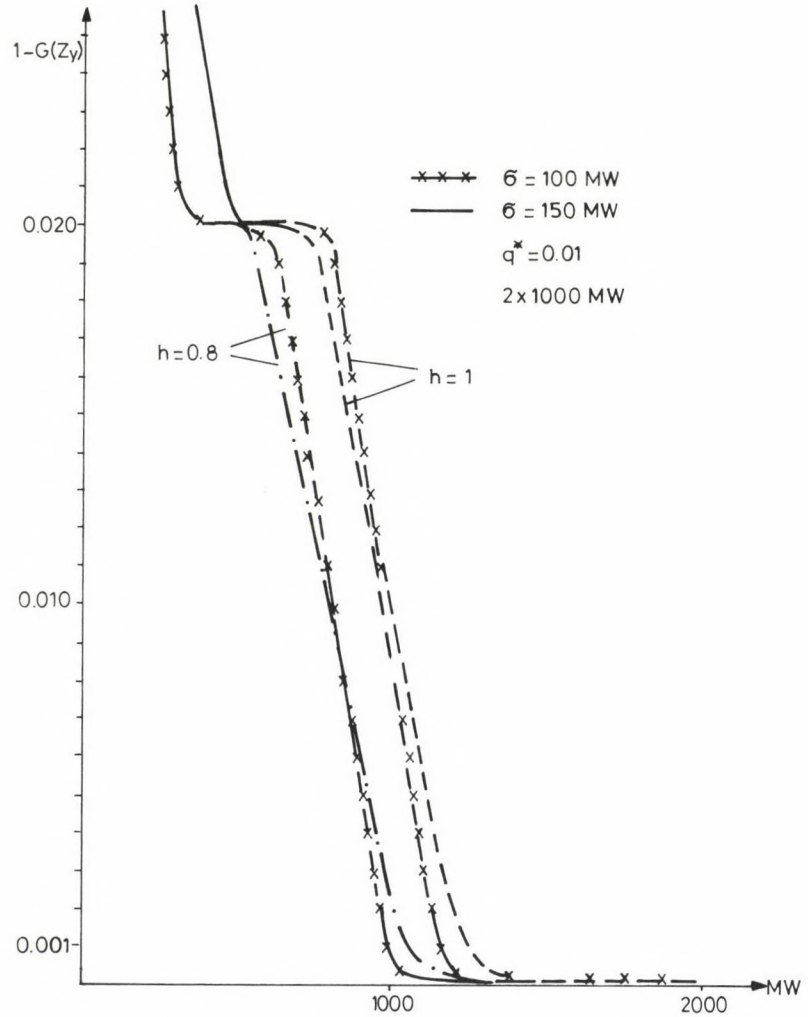

Fig. 3. Same as Fig. 2 but with two 1000 MW units added

The results of calculations are diagrammatically illustrated in Figs 2 thru 4. The diagrams show the probability of a load higher than the random load of a certain system inter-tie according to the approximate method used for calculation.

This case study permits different conclusions to be drawn. E.g. as seen in Fig. 2, the larger the smaller system, the less the probability of substitution in case of system disturbances and the probability of substitution will reduce also if there is not much difference in capacity between the interconnected systems.

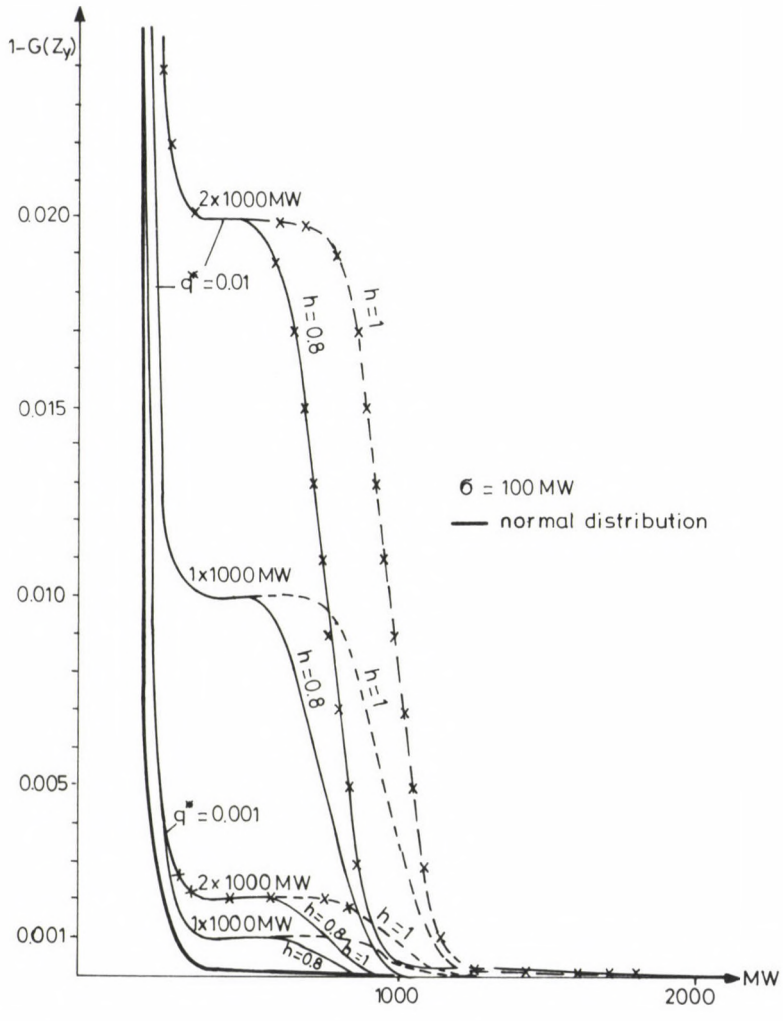

Fig. 4. Effect of probability of unit unavailability upon the probability distribution of random loads of system inter-ties in case of one or two 1000 MW unit(s) built into a 5000 MW system

The probability of load of inter-ties in case of breakdown of the system varies also as a function of the number of 1000 MW units built into the system (Fig. 4). Fig. 4 shows how do the different parameters affect each other. The significant effect of the availability of a unit (or units) on random load of system links is worthy of note.

REFERENCES

1. Timotshenko, V.F.: Kolebania nagrusok i obmennoi mosnosti energosystem - Moscow, Energia 1975 (in Russian).

2. Tersztyánszky, T.: Modelling of random loads of inter-ties - UNECE Seminar, Moscow 1987, EP (SEM 12) R. 23

3. Tersztyánszky, T. - Tusnádi, G.: An estimation of the maximum loads of interconnection - Acta Technica, Acad. Sci. Hung. 86 (1987), No. 1-2

4. Elek, J.: New method to calculate capacity reserves required in the system (in Hungarian)- ERŐTERV Publications No. 9 (1971)

5. Korn, G.A. - Korn, T.M.: Mathematical Handbook for Scientists and Engineers - McGraw-Hill Book 1970

6. UCPTE Jahresbericht 1986: Ausfälle von Kraftwerkseinheiten

7. Operating experience with nuclear power stations in member states in 1985 - IAEA, Vienna, 1986

Acta Technica Acad.Sci.Hung., 103(4), p. 329 (1990)

BOOK REVIEW

Frigyes, I. - Szabó, Z. - Várnyai, P.: Digital Microwave Transmission. Akadémiai Kiadó, Budapest, 1989

This book has been designed to provide information both for people who want to learn the fundamentals and for experts who are interested in details. Investigation of the technical problems if supported by an appropriate mathematical background. Thus the text is easy to read and understandable.

First the fundamentals of digital transmission are treated: vector representation, bit error probability, optimum receiver, multilevel encoding, band limiting, distortion equalization, spectral properties, nonlinearity, noise, interference, etc., followed by discussion of synchronization problems of microwave transmission: phase-locked loops, sequential filtering, carrier recovery, clock recovery.

Properties of the microwave transmission path are dealt with: sources of fading, selective multipath fading, outage probability, design for reliability, frequency re-use, satellite systems. Then multipath countermeasures are discussed: error correction encoding, adaptive equalization, multicarrier transmission, space diversity, frequency diversity.

In the second part of the book, details of the equipment are presented. Modulators, transmitter, demodulators, and receivers are dealt with. PSK, QAM, PRS, O-QPSK, MSK, ASK, and FSK modulators and demodulators are discussed in detail. Furthermore, the methods of baseband signal processing, including, encoding, decoding, scrambling, error detection, etc. are described. Finally, auxiliary equipment for continuous monitoring of transmission performance, transmission of service information, stand-by channel systems are discussed.

The book of 423 pages is rich in illustrations including figures, tables, and equations. The authors' intention that is to discuss the theoretical and practical problems encountered in digital microwave transmission in detail has been fully met by their work.

T. Berczeli

Akadémiai Kiadó, Budapest

PRINTED IN HUNGARY

Akadémiai Kiadó és Nyomda Vállalat, Budapest

NOTICE TO CONTRIBUTORS

Papers in English* are accepted condition that they have not been previously published or accepted for publication.

Manuscripts in two copies (the original type-written copy plus a clear duplicate one) complete with figures, tables, and references should be sent to

Acta Technica
Nádor u. 7. I. 118
Budapest, Hungary
H-1051

Although every effort will be made to guard against loss, it is advised that authors retain copies of all material which they submit. The editorial board reserves the right to make editorial changes.

Manuscripts should be typed double-spaced on one side of good quality paper with proper margins and bear the title of the paper and the name(s) of the author(s). The full postal address(es) of the author(s) should be given in a footnote on the first page. An abstract of 50 to 100 words should precede the text of the paper. The approximate locations of the tables and figures should be indicated on the margin. An additional copy of the abstract is needed. Russian words and names should be transliterated into English.

References. Only papers closely related to the author's work should be referred to. The citations should include the name of the author and/or the reference number in brackets. A list of numbered references should follow the end of the manuscript.

References to periodicals should mention: (1) name(s) and initials of the author(s); (2) title of the paper; (3) name of the periodical; (4) volume; (5) year of publication in parentheses; (6) numbers of the first and last pages. Thus: 5. Winokur, A., Gluck, J.: Ultimate strength analysis of coupled shear walls. American Concrete Institute Journal 65 (1968) 1029-1035

References to books should include: (1) author(s)' name; (2) title; (3) publisher; (4) place and year of publication. Thus: Timoshenko, S., Gere, J.: Theory of Elastic Stability. McGraw-Hill Company, New York, London 1961.

Illustrations should be selected carefully and only up to the necessary quantity. Black-and-white photographs should be in the form of glossy prints. The author's name and the title of the paper together with the serial number of the figure should be written on the back of each print. Legends should be brief and attached on a separate sheet. Tables, each bearing a title, should be self-explanatory and numbered consecutively.

Authors will receive proofs which must be sent back by return mail.

Authors will receive 50 reprints free of charge.

*Hungarian authors can submit their papers also in Hungarian.

Periodicals of the Hungarian Academy of Sciences are obtainable at the following addresses:

AUSTRALIA
C.B.D. LIBRARY AND SUBSCRIPTION SERVICE
39 East Splanade
P.O. Box 1001, Manly N.S.W. 2095

AUSTRIA
GLOBUS, Höchstädtplatz 3, *1206 Wien XX*

BELGIUM
OFFICE INTERNATIONAL DES PERIODIQUES
Avenue Louise, 485, *1050 Bruxelles*
E. STORY-SCIENTIA P.V.B.A.
P. van Duyseplein 8, *9000 Gent*

BULGARIA
HEMUS, Bulvar Ruszki 6, *Sofia*

CANADA
PANNONIA BOOKS, P.O. Box 1017
Postal Station "B", *Toronto, Ont. M5T 2T8*

CHINA
CNPICOR, Periodical Department, P.O. Box 50
Peking

CZECH AND SLOVAK FEDERAL REPUBLIC
MAD'ARSKA KULTURA, Národni třida 22
115 66 Praha
PNS DOVOZ TISKU, Vinohradská 46, *Praha 2*
PNS DOVOZ TLAČE, *Bratislava 2*

DENMARK
EJNAR MUNKSGAARD, 35, Nørre Søgade
1370 Copenhagen K

FEDERAL REPUBLIC OF GERMANY
KUNST UND WISSEN ERICH BIEBER
Postfach 10 28 44
7000 Stuttgart 10

FINLAND
AKATEEMINEN KIRJAKAUPPA, P.O. Box 128
00101 Helsinki 10

FRANCE
DAWSON-FRANCE S.A., B.P. 40, *91121 Palaiseau*
OFFICE INTERNATIONAL DE DOCUMENTATION ET LIBRAIRIE, 48 rue Gay-Lussac
75240 Paris, Cedex 05

GREAT BRITAIN
BLACKWELL'S PERIODICALS DIVISION
Hythe Bridge Street, *Oxford OX1 2ET*
BUMPUS, HALDANE AND MAXWELL LTD.
Cowper Works, *Olney, Bucks MK46 4BN*
COLLET'S HOLDINGS LTD., Denington Estate,
Wellingborough, Northants NN8 2QT
WM DAWSON AND SONS LTD., Cannon House
Folkstone, Kent CT19 5EE

GREECE
KOSTARAKIS BROTHERS INTERNATIONAL BOOKSELLERS, 2 Hippokratous Street, *Athens-143*

HOLLAND
FAXON EUROPE, P.O. Box 167
1000 AD Amsterdam
MARTINUS NIJHOFF B. V.
Lange Voorhout 9–11, *Den Haag*
SWETS SUBSCRIPTION SERVICE
P.O. Box 830, 2160 Sz Lisse

INDIA
ALLIED PUBLISHING PVT. LTD.
750 Mount Road, *Madras 600002*
CENTRAL NEWS AGENCY PVT. LTD.
Connaught Circus, *New Delhi 110001*
INTERNATIONAL BOOK HOUSE PVT. LTD.
Madame Cama Road, *Bombay 400039*

ITALY
D. E. A., Via Lima 28, *00198 Roma*
INTERSCIENTIA, Via Mazzé 28, *10149 Torino*
LIBRERIA COMMISSIONARIA SANSONI
Via Lamarmora 45, *50121 Firenze*

JAPAN
KINOKUNIYA COMPANY LTD.
Journal Department, P.O. Box 55
Chitose, *Tokyo 156*
MARUZEN COMPANY LTD., Book Department
P.O. Box 5050 Tokyo International, *Tokyo 100-31*
NAUKA LTD., Import Department
2-30-19 Minami Ikebukuro, Toshima-ku, *Tokyo 171*

KOREA
CHULPANMUL, *Phenjan*

NORWAY
S.A. Narvesens Litteraturjeneste
Box 6125, Etterstad
1000 Oslo

POLAND
WĘGIERSKI INSTYTUT KULTURY
Marszalkowska 80, *00-517 Warszawa*
CKP I W, ul. Towarowa 28, *00-958 Warszawa*

ROUMANIA
D. E. P., *Bucuresti*
ILEXIM, Calea Grivitei 64–66, *Bucuresti*

SOVIET UNION
SOYUZPECHAT — IMPORT, *Moscow*
and the post offices in each town
MEZHDUNARODNAYA KNIGA, *Moscow G-200*

SPAIN
DIAZ DE SANTOS Lagasca 95, *Madrid 6*

SWEDEN
ESSELTE TIDSKRIFTSCENTRALEN
Box 62, *101 20 Stockholm*

SWITZERLAND
KARGER LIBRI AG, Petersgraben 31, *4011 Basel*

USA
EBSCO SUBSCRIPTION SERVICES
P.O. Box 1943, *Birmingham, Alabama 35201*
F. W. FAXON COMPANY, INC.
15 Southwest Park, *Westwood Mass. 02090*
MAJOR SCIENTIFIC SUBSCRIPTIONS
1851 Diplomat, P.O. Box 819074,
Pallas, Tx. 75381-9074
REDMORE PUBLICATIONS, Inc.
22 Cortlandt Street, New York, N.Y. 1007

YUGOSLAVIA
JUGOSLOVENSKA KNJIGA, Terazije 27, *Beograd*
FORUM, Vojvode Mišića 1. *21000 Novi Sad*

HU ISSN 0864-8085

Index: 26.025